UNIVERSIDADE FEDERAL DO RIO GRANDE DO SUL
INSTITUTO DE GEOCIÊNCIAS
PROGRAMA DE PÓS-GRADUAÇÃO EM GEOCIÊNCIAS

SEQUÊNCIAS PORONGOS I E II: DEPÓSITOS EDIACARANOS SINOROGÊNICOS DO COMPLEXO PORONGOS (RS) E AS IMPLICAÇÕES PARA O SW GONDWANA

DAIANNE FRANCIS SILVA DA SILVEIRA

ORIENTADORA – Prof. Dra. Juliana Charão Marques

Volume I

Porto Alegre – 2017

UNIVERSIDADE FEDERAL DO RIO GRANDE DO SUL
INSTITUTO DE GEOCIÊNCIAS
PROGRAMA DE PÓS-GRADUAÇÃO EM GEOCIÊNCIAS

SEQUÊNCIAS PORONGOS I E II: DEPÓSITOS EDIACARANOS SINOROGÊNICOS DO COMPLEXO PORONGOS (RS) E AS IMPLICAÇÕES PARA O SW GONDWANA

DAIANNE FRANCIS SILVA DA SILVEIRA

ORIENTADORA : Prof. Dra. Juliana Charão Marques

BANCA EXAMINADORA

Dra. Andréia Oliveira Monteiro da Silva Gross – Companhia de Pesquisa de Recursos Minerais, Serviço Geológico do Brasil

Prof. Dra. Renata da Silva Schmitt – Instituto de Geociências, Universidade Federal do Rio de Janeiro

Prof. Dr. Léo Afraneo Hartmann – Instituto de Geociências, Universidade Federal do Rio Grande do Sul

Dissertação de Mestrado apresentada como requisito parcial para obtenção do Título de Mestre em Geociências.

Porto Alegre – 2017

CIP - Catalogação na Publicação

Silva da Silveira, Daianne Francis
Sequências Porongos I e II: Depósitos Ediacaranos sinorogênicos do Complexo Porongos (RS) e as implicações para o SW Gondwana / Daianne Francis Silva da Silveira. -- 2017.
153 f.

Orientador: Juliana Marques.

Dissertação (Mestrado) -- Universidade Federal do Rio Grande do Sul, Instituto de Geociências, Programa de Pós-Graduação em Geociências, Porto Alegre, BR-RS, 2017.

1. Complexo Porongos. 2. Antiforme Capané. 3. Cinturão Dom Feliciano. 4. Gondwana. 5. Pan-Africano–Brasiliano. I. Marques, Juliana, orient. II. Título.

Elaborada pelo Sistema de Geração Automática de Ficha Catalográfica da UFRGS com os dados fornecidos pelo(a) autor(a).

À minha família.

AGRADECIMENTOS

Agradeço ao Programa de Pós-graduação em Geociências da Universidade Federal do Rio Grande do Sul pela infraestrutura e ensino proporcionados ao longo do trabalho de mestrado.

Esse agradecimento é estendido à minha orientadora, Prof. Dra. Juliana Charão Marques, que me apoiou em todas as empreitadas durante a execução do mestrado e propiciou condições para a execução da presente pesquisa.

Ao Conselho Nacional de Desenvolvimento Científico e Tecnológico (CNPq), pela concessão da bolsa de mestrado, viabilizando meus estudos ao longo destes dois anos.

Meu mais profundo e sincero agradecimento é destinado a aqueles que me deram apoio, segurança, motivação, esperança, confiança e amor ao longo de toda a caminhada da minha vida: minha família. Vocês são minha inspiração, alegria e orgulho. Este trabalho não teria sido possível sem o apoio incondicional de vocês! Obrigada ao meu pai Antonio pelo exemplo de vida e garra, a minha mãe Silvéria pela torcida e ajuda constante, a minha irmã Hellen pela generosidade e carinho, e ao meu irmão Kaio pela companheirismo. Desculpe por todos os momentos de ausência, saudade apertada e essa vida tão intensa fora do ninho que a geologia proporciona!

Meu obrigado aos colegas e amigos, que me ajudaram ao longo do caminho até o fim da dissertação, fazendo de Porto Alegre um novo lar. Agradeço também ao Prof. Dr. Miguel Basei que contribuiu muitíssimo para a construção do raciocínio geológico por trás da pesquisa.

E para finalizar, gostaria de agradecer meu marido, Dr. Tobias W. Höfig, pelo amor, companheirismo, apoio, sonhos, motivação e parceria durante todos os momentos. Eu não teria conseguido sem o teu apoio em todos os momentos e lugares. Você não mediu esforços por mim. *Vielen Dank, mein Schatz*!

RESUMO

O Cinturão Dom Feliciano é a principal unidade geotectônica do sudeste da America do Sul, sendo formado durante a aglutinação do Gondwana Ocidental no Neoproterozoico. Idades U-Pb em zircão do Neoproterozoico superior, encontradas em sequencias supracrustais da Antiforme Capané, desafiam a visão tradicional de um único evento de deposição para o Complexo Porongos durante o Neoproterozoico. As novas idades revelam três padrões diferentes de proveniência para a Antiforme Capané. Forte proveniência ediacarana tem sido identificada em sequências metavulcanossedimentares nos flancos, com picos mais jovens em 630–580 Ma. Por outro lado, unidades miloníticas axiais apresentam picos pronunciados de idade Paleoproterozoica, entre 2,2 e 2,0 Ga. Além disso, lentes de xisto de grau metamórfico médio, imbricadas na zona axial, mostram importantes picos tonianos, em 830 Ma, e uma significante contribuição mesoproterozoica, em 1,5–1,3 Ga. Os novos dados de proveniência combinados com os resultados geocronológicos previamente publicados, além de dados estratigráficos e tectônicos da area aflorante do Complexo Porongos, permitiu a identificação de três diferentes terrenos na Antiforme Capané. As rochas miloníticas da zona axial são interpretadas como Formação Santana, onde as lentes de xisto de médio grau metamórfico mostram proveniência similar à aquela encontrada regionalmente no Complexo Porongos. A sedimentação destas unidades seria constrita ao Toniano e aqui é sugerido o nome de sequência Porongos I para todo o grupo de rochas metavulcanossedimentares formadas neste período. Diferentemente, as unidades mais jovens, localizadas nos flancos, são interpretadas como pertencentes à uma bacia distinta ediacarana. É proposto que as sequencias mais jovens da Antiforme Capané, aqui cunhadas como sequencia Porongos II, estejam relacionadas à deposição sinorogênica desenvolvida ao longo do Ediacarano. Essas descobertas sugerem uma reconstrução tectônica e paleogeográfica, onde as unidades Capané mais jovens sejam interpretadas como depósitos sinorogênicos formados durante a deformação imposta pela justaposição do Batólito Pelotas. Esse complexo ígneo foi uma importante fonte para as unidades vulcanossedimentares mais jovens do Cinturão Porongos, desse modo provendo nova compreensão na dinâmica da aglutinação do Gondwana Ocidental.

Palavras-chave: Complexo Porongos, Antiforme Capané, Cinturão Dom Feliciano, Gondwana, Pan-Africano–Brasiliano

ABSTRACT

The Dom Feliciano Belt is the major geotectonic unit in southeastern South America, being formed during the Neoproterozoic amalgamation of southwestern Gondwana. Late Neoproterozoic U-Pb ages, found in supracrustal sequences at the Capané Antiform, challenges the traditional view of a single episode of deposition for the Porongos Complex during the Neoproterozoic. The new ages reveal three different provenance patterns for the Capané Antiform. A strong Ediacaran provenance has been identified in the metavolcano-sedimentary sequences from the limbs, with younger peak ages yielding 630–580 Ma. On the contrary, the axial mylonitic units have pronounced Paleoproterozoic peaks, between 2.2 and 2.0 Ga. Additionally, lenses of medium-grade schist imbricated to the axial zone show important Tonian peaks at 830 Ma and a significant Mesoproterozoic contribution, at 1.5–1.3 Ga. The new provenance data combined with previously published geochronological, stratigraphic and tectonic data from the outcropping Porongos Complex area enable to identify three different terranes within the Capané Antiform. The mylonitic rocks from the axial zone are interpreted as part of the Santana Formation. Whereas the medium-grade schist lenses show provenance similar to those found in the regionally exposed Porongos Complex. The sedimentation of these last units are constrained to the Tonian and here it is suggested the name Porongos I sequence to group all meta-volcanosedimentary rocks formed during this period. On the other hand, the younger units, located in the limbs, are interpreted as formed in a different basin during the Ediacaran. It is proposed that the younger sequences of the Capané Antiform, here coined as Porongos II sequence, are related to synorogenic deposition developed during the Ediacaran period. These findings suggest a tectonic and paleogeographic reconstruction, where the younger Capané units are interpreted as synorogenic deposits formed during the deformation imposed by the juxtaposition of the Pelotas Batholith. This igneous complex was an important source for the younger volcano-sedimentary units of the Porongos Belt, thereby giving new insights into the dynamics of the SW Gondwana assembly.

Keywords: Porongos Complex, Capané Antiform, Dom Feliciano Belt, Gondwana, Pan-African-Brasiliano

LISTA DE ILUSTRAÇÕES

SUMÁRIO

CAPÍTULO 1 – INTRODUÇÃO

1.1 Estrutura da dissertação

1.2 Apresentação

1.3 Objetivo

1.4 Localização e acesso

1.1 Estrutura da dissertação

Esta dissertação de mestrado está estruturada em torno de artigos publicados em periódicos ou publicações equivalentes. Consequentemente, sua organização compreende as seguintes partes principais:

a) *Capítulo 1 – Introdução*: discorre sobre o tema e descrição do objeto da pesquisa de mestrado, onde estão sumarizados os objetivos e a filosofia de pesquisa desenvolvida;

b) *Capítulo 2 – Estado da Arte*: apresenta o contexto geocronológico e geológico em que a área de estudo está inserida; o estado da arte sobre o tema de pesquisa;

c) *Capítulo 3 – Materiais e Métodos*: detalha as metodologia e ferramentas de interpretação utilizadas durante a execução da presente pesquisa, com breve revisão de conceitos fundamentais;

d) *Capítulo 4 – Artigos submetidoss*: anexa a carta de submissão e reproduz na íntegra o manuscrito submetido ao periódico *Precambrian Research* como produto do trabalho desenvolvido pelo autor durante o desenvolvimento de seu Mestrado;

e) *Capítulo 5 – Considerações finais:* sintetiza as principais conclusões acerca da presente pesquisa e lista as referencias bibliográficas utilizadas na dissertação de Mestrado;

c) *Anexos*: compreende os resumos publicados em eventos, relacionados ao tema central da dissertação.

1.2 Apresentação

A datação U-Pb de grãos detríticos de zircão para a análise de espectro de idades em sequencias metavulcanossedimentares fornece informações essenciais sobre o ambiente tectônico de deposição da bacia, além de apontar pistas sobre os mecanismos de evolução crustal terrestre (CAWOOD; HAWKESWORTH; DHUIME, 2012). Considerado como uma pequena cápsula do tempo, o zircão carrega informações ígneas e metamórficas de suas fontes, sendo uma importante ferramenta nos estudos da evolução geotectônica de qualquer ambiente geológico

(VERMEESCH, 2012). Portanto, o estudo de proveniência geocronológica é essencial para o entendimento de orogénos, os quais possuem relações estratigráficas obliteradas durante os sucessivos ciclos tectônicos.

O ciclo Neoproterozoico Pan-Africano-Brasiliano registrado ao longo da margem leste da América do Sul e oeste da África, gerou longas cadeias de montanhas, depositou bacias *foreland* com registro sinorogenico devido ao soerguimento continental, em resposta à acomodação do orogéno e ao seu consequente colapso (e.g., KRÖNER; STERN, 2005; SILVA *et al.*, 2005). O termo "Pan-Africano-Brasiliano" representa o intervalo de aproximadamente 800 a 550 Ma, no qual o fechamento do Oceano Adamastor gerou intensa colisão continental resultando no Supercontinente SW Gondwana, também denominando Gondwana Ocidental (WIT, DE; STANKIEWICZ; REEVES, 2008). "Brasiliano" refere-se aos cinturões sul-americanos formados nesse período e congrega as províncias Mantiqueira, Borborema e Tocantins (ALMEIDA *et al.*, 1981), tendo aproximadamente 6.000 km de largura e 3.000 em extensão (SILVA *et al.*, 2005). Por sua vez, "Pan-Africano", termo cunhado por Kennedy (1964), refere-se as unidades africanas representadas pelos cinturões Gariep, Kaoko, Damara, Saldanha, Moçambique, Zambezi, Congo-Oeste, Trans-Saara, África-central e Rokolide. O arranjo do Supercontinente Gondwana Oeste, após amalgamação, é mostrado na Figura 1.

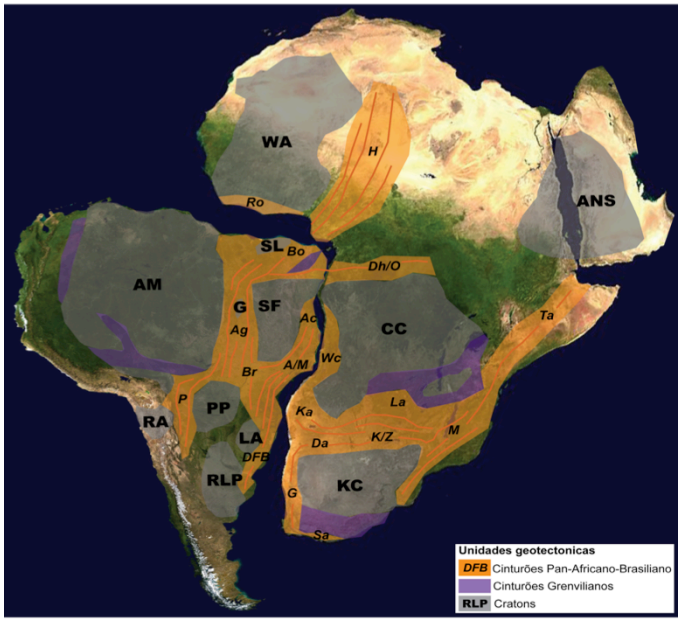

Legenda:

1) Unidades Cratôncias
Amazonas (*AM*), escudo Árabe-Nubio (*ANS*), Congo (*CC*), Bloco Goiás (*G*), Kalahari (*K*), Luís Alves (*LA*), Paranapanema (*PP*), Río Apa (*RA*), São Francisco (*SF*), São Luís (*SL*), África Ocidental (*WA*).

2) Cinturões Pan-Africano-Brasiliano
Araçuaí (*Ac*), Araguaia (*Ag*), Borborema (*Bo*), Brasília (*Br*), Damara (*Da*), Dom Feliciano (*DFB*), Dahomeides/Oubangides (*Dh/O*), Gariep (*G*), Hoggar (*H*), Kaoko (*Ka*), Katangan/Zambezi (*K/Z*), Arco Lufiliano (*La*), Moçambique (*M*), Ribeira/Manquieira (*R/M*), Rockelides (*Ro*), Tanzania (*Ta*), Tucavaca (*Tu*), Congo Ocidental (*Wc*).

Figura 1 – Reconstrução do Continente Gondwana Ocidental. Fonte: figura modificada de Vaughan e Pankhurst (2008) e Tohver et al. (2006).

Tal sistema orogênico se manifesta no extremo sul do Brasil e Uruguai como Cinturão Dom Feliciano (BABINSKI *et al.*, 1996; BASEI *et al.*, 2000; FRAGOSO-CESAR, 1980), Fig. 2. Sua subdivisão interna está baseada no agrupamento de segmentos (BASEI *et al.*, 2000): a oeste ocorre um sistema de bacias extensionais, originalmente denominadas *foreland*, englobando as bacias Itajaí, Camaquã e El Soldado; na parte central, uma faixa de rochas metavulcanossedimentares compreendendo os complexos Brusque, Porongos e Lavalleja; à leste aflora o cinturão granítico, representado pelos então chamados batólitos Florianópolis, Pelotas e Aiguá.

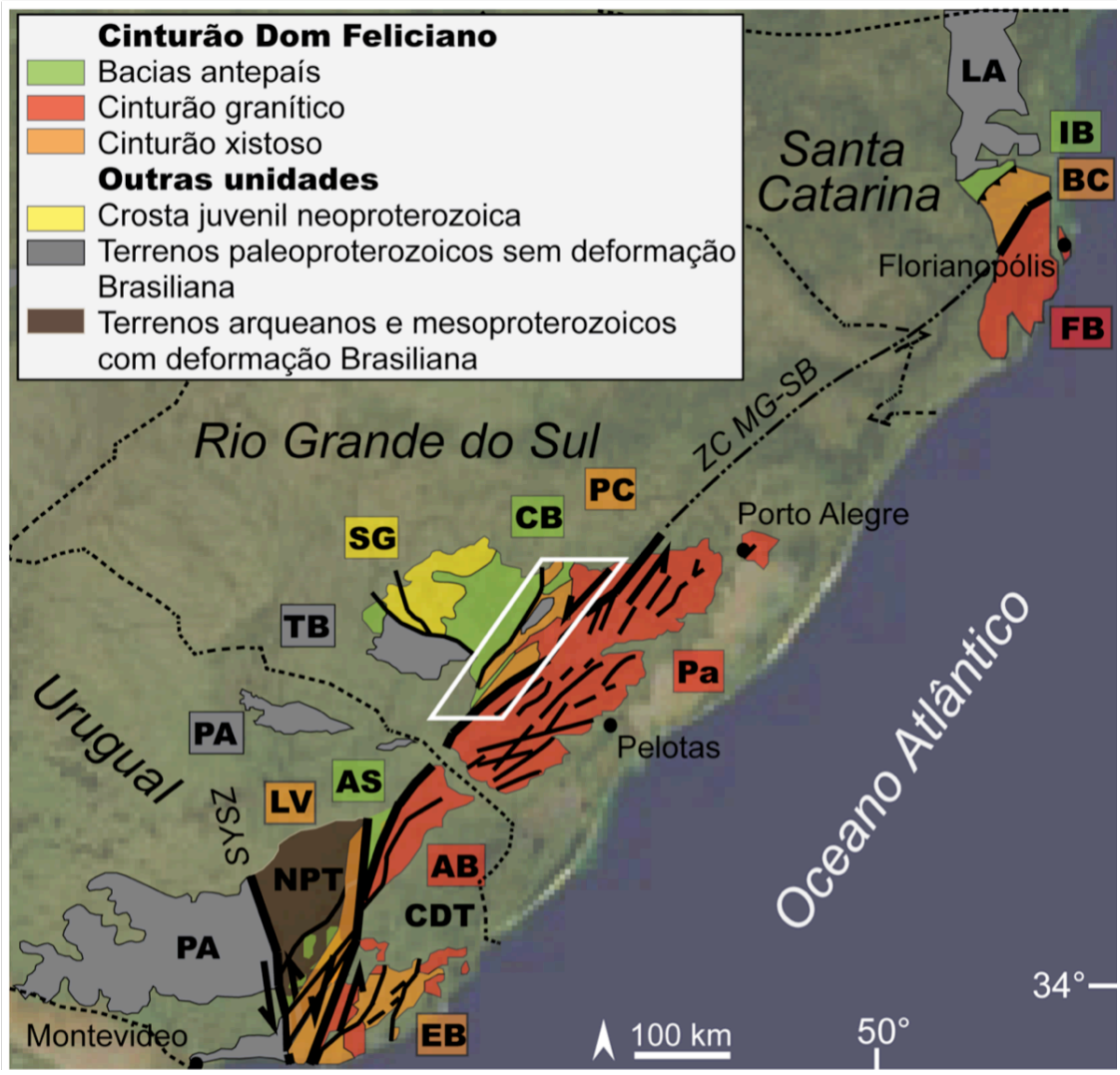

Figura 2 – Unidades geotectônicas do sul do Brasil e Uruguai. Fonte: figura baseada em Basei et al. (2000), Pecoits et al. (2016), Rapela et al. (2011) e Teixeira et al. (2013); modificada de Google Maps (2016).

Aflorando no Escudo Sul-Riograndense, o Complexo Porongos apresenta uma complexa história evolutiva dentro do Neoproterozoico. Esta sequencia supracrustal tem deposição tradicionalmente atribuída ao Toniano (PORCHER *et al.*, 1999; SAALMANN *et al.*, 2011) e mais recentemente reinterpretada como Ediacarana-Criogeniana (PERTILLE *et al.*, 2017). No entanto o intenso processo de deformação no qual esta unidade foi submetida obliterou as relações estratigráficas dentro e fora da sequência. Idades detríticas Ediacaranas reportadas no norte do Complexo Porongos (PERTILLE *et al.*, 2015, 2017), região definida como Antiforme Capané, contradizem o modelo deposicional vigente.

Apesar de mais de oito décadas de estudos, desde Carvalho (1932), o contexto tectônico para todo o Complexo Porongos ainda é especulativo. Nesta pesquisa propõe-se que as idades Ediacaranas encontradas na Antiforme Capané representam uma sequencia mais jovem que as sequencias da Bacia Porongos regional de idade Toniana, sendo chamadas de Porongos I e II, respectivamente. De maneira regional, este estudo contribui para o entendimento do contexto tectônico do Cinturão Dom Feliciano no extremo sul do Brasil durante a amalgamação do Gondwana Ocidental ao longo do Neoproterozoico.

1.3 Objetivo

O objetivo deste trabalho de dissertação é a análise de zircões detríticos pelo método U-Pb em amostras da sequencia supracrustal da Antiforme Capané, de maneira a interpretar coerentemente as idades antagônicas do Complexo Porongos. Desta maneira, foram assim estabelecidos os principais objetivos:

a) Compor uma base de dados geocronológicos sobre o Complexo Porongos e as unidades geotectônicas adjacentes; avaliando o método, localização das amostras e a qualidade dos dados obtidos da literatura.

b) Definir potenciais protólitos para as sequencias amostradas na Antiforme Capané através de petrografia e análise estatística dos dados geocronológicos obtidos via U-Pb em zircões detríticos.

c) Sugerir fontes e contextualização geológica para as idades encontradas nos grãos de zircão detríticos da Antiforme Capané.

d) Interpretar os dados obtidos à luz do contexto regional do Cinturão Dom Feliciano e sua configuração durante a amalgamação do Gondwana Ocidental ao longo do Neoproterozoico.

1.4 Localização e acesso

A Antiforme Capané está localizada no extremo norte do Complexo Porongos, parte central do estado do Rio Grande do Sul, como mostrado na Figura 3. O acesso, à cerca de 200 km à oeste de Porto Alegre, pode ser feito pela BR-290. Após a entrada da cidade de Cachoeira do Sul é necessário seguir pela estrada vicinal de sentido sul-sudoeste por aproximadamente 50km. Toda a região é cortada por vias secundárias e trilhas, as quais foram o principal meio utilizado para a coleta de amostras na região.

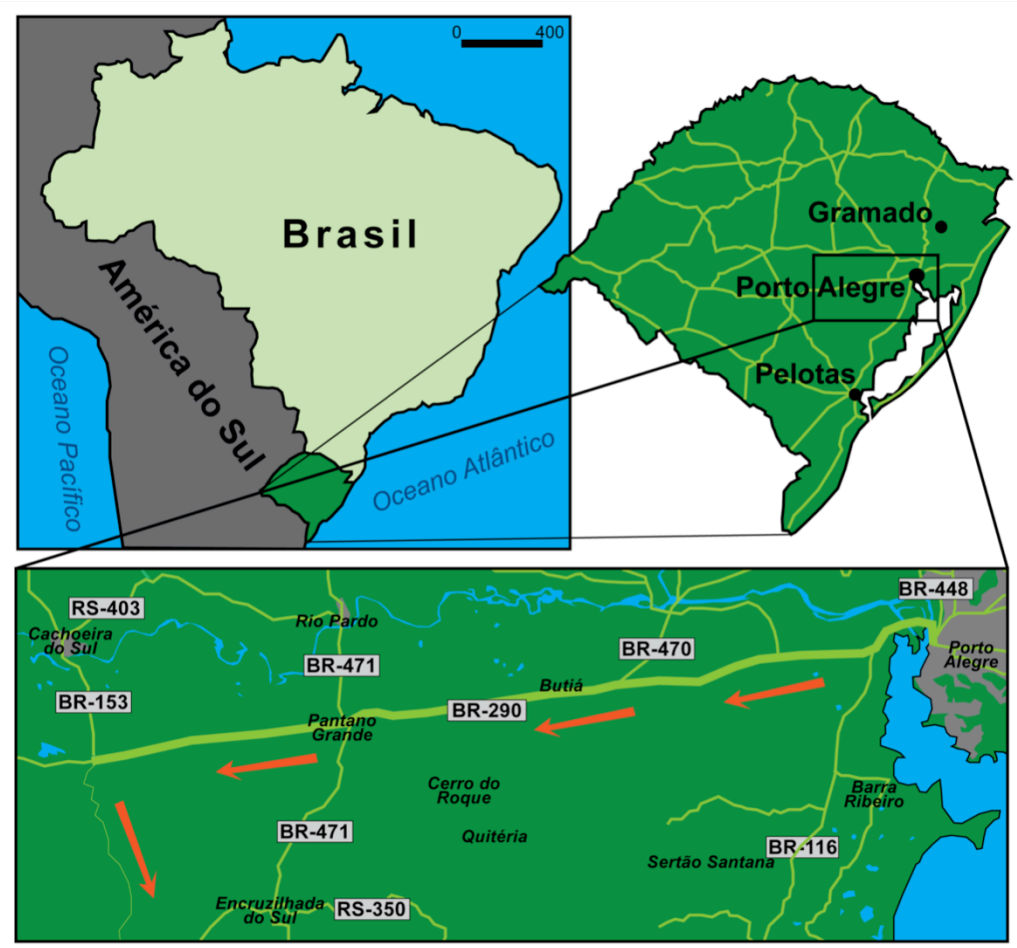

Figura 3 – Localização e acesso à área de estudo. Fonte: figura modificada de Google Maps (2016).

CAPÍTULO 2 – ESTADO DA ARTE

2.1 Arcabouço geocronológico do Gondwana Ocidental

2.2 Cinturão Dom Feliciano

2.3 Complexo Porongos

2.1 Arcabouço geocronológico do Gondwana Ocidental

A reconstrução dos principais eventos tectônicos do ciclo Pan-Africano-Brasiliano têm sido foco de inúmeros estudos desenvolvidos nas últimas décadas, impulsionados pelo advento de novas técnicas isotópicas e geocronológicas (e.g., BRITO NEVES; FUCK; PIMENTEL, 2014; FRAGOSO-CESAR, 1980; HARTMANN *et al.*, 2000; PORADA, 1979). De maneira a estabelecer um arcabouço geocronológico para os dados e interpretações apresentadas na presente pesquisa, faz-se necessária uma breve compilação das idades principais presentes no sistema orogênico do Gondwana Ocidental.

2.1.1 Arqueano e Paleoproterozoico

Na América do Sul, o principal evento formador de crosta continental é reconhecido como a orogenia paleoproterozoica Transamazônica, que durou de 2,2 a 2,0 Ga (SANTOS *et al.*, 2003). O cráton Rio de La Plata, cunhado por Almeida (1971), representa um mosaico heterogêneo com vestígios de idades Arqueanas e importante registro Paleoproterozoico (HARTMANN *et al.*, 2001), justapostos ao longo de zonas de cisalhamento (e.g., BOSSI; CAMPAL, 1992; PASSARELLI *et al.*, 2010). Apesar do debate acerca dos limites desta unidade, ainda não existe uma definição unânime na comunidade científica (e.g., CORDANI *et al.*, 2000; DALZIEL, 1997; RAMOS, 1988; RAPELA *et al.*, 2011; TROMPETTE, 1994; WEIL *et al.*, 1998).

No Uruguai, esta unidade é tradicionalmente relacionada aos terrenos Nico Perez e Piedra Alta (DALLA SALDA; BOSSI; CINGOLANI, 1988). No entanto, diferenças litológicas e geocronológicas apontas por estudos recentes consideram o Terreno Nico Perez como um bloco alóctone derivado do Bloco Angola (GAUCHER *et al.*,2011; OYHANTÇABAL *et al.*, 2009; PECOITS *et al.*, 2016; RAPELA *et al.*, 2011), o qual foi anexado ao cráton Rio de La Plata durante o Mesoproterozoico (GAUCHER *et al.*, 2011). Também aflorante no escudo Uruguaio, o Terreno Cuchilla Dionísio é um bloco alóctone derivado do cráton Kalahari (BASEI *et al.*, 2005, 2008; BOSSI; GAUCHER, 2004; GAUCHER *et al.*, 2008) e anexado ao craton Rio de La Plata durante o Cambriano (GAUCHER *et al.*, 2008).

Na Argentina, o paleoproterozoico Cinturão Tandilia (HARTMANN *et al.*, 2002) está relacionado ao craton Rio de La Plata e as idades arqueanas e paleoproterozoicas encontradas no Terreno Mar del Plata são consideradas como derivado do Bloco Angola (GAUCHER *et al.*, 2011). No extremo sul do Brasil, o craton Rio de La Plata é assinalado como Bloco Tamquarembó (e.g., CHEMALE, 2000; HARTMANN; CHEMALE; PHILIPP, 2007) e como o Gnaisse Encantadas, o qual é considerado um *inlier* dentro das sequencias neoproterozoicas (e.g., CHEMALE, 2000; HARTMANN *et al.*, 2000; OYHANTÇABAL *et al.*, 2009). Também relacionado ao Paleoproterozoico, remanescentes do início do desenvolvimento de arcos magmáticos são encontrados no Bloco São Gabriel (REMUS *et al.*, 1996), Complexo Arroio dos Ratos (GREGORY *et al.*, 2015, 2016; LEITE *et al.*, 2000) e Domo Vigia (CAMOZZATO; PHILIPP; CHEMALE, 2013).

Na margem Africana, o cráton Kalahari (CLIFFORD; 1970), mosaico heterogêneo com núcleo Arqueano, descendente dos crátons Zimbabwe e Kaapvaal (WIT, DE *et al.*, 1992), é cercado pela Subprovíncia Richtersveld de idade Paleoproterozoica (REID, 1997).

2.1.2 Mesoproterozoico

As similaridades encontradas em ambas margens do Oceano Adamastor mudam consideravelmente durante o Mesoproterozoico, sendo que na África reconhece-se intenso crescimento crustal e na América do Sul, os registros mais expressivos são encontrados no escudo uruguaio. Notavelmente, no norte do Brasil a orogenia mesoproterozoica Grenviliana é correlacionada ao Cinturão Sunsás (e.g., SANTOS *et al.*, 2000, 2003; TEIXEIRA *et al.*, 2010), no entanto para Gondwana Ocidental, apenas o Complexo Lavalleja aflorante no Uruguai foi eficientemente correlacionado com proveniencia Africana (BASEI *et al.*, 2005).

Neste cenário, os principais registros mesoproterozoicos são encontrados no Escudo Uruguaio, sendo reportados no Terreno Piedra Alta (BOSSI *et al.*, 1993; BOSSI; NAVARRO, 2001; HALLS *et al.*, 2001; IACUMIN *et al.*, 2001; TEIXEIRA *et al.*, 1999) e registrado em sucessões vulcano-sedimentares e corpos intrusivos no Terreno Nico Perez (BASEI *et al.*, 2008; BOSSI; CINGOLANI, 2009; CAMPAL;

SCHIPILOV, 1995; CHIGLINO *et al.*, 2010; GAUCHER *et al.*, 2008, 2011; OYHANTÇABAL *et al.*, 2005). No extremo sul do Brasil, idades estaterianas são reportadas no Anortosito Capivarita (CHEMALE *et al.*, 2011) e no Anfibolito Tupi Silveira (CAMOZZATO; PHILIPP; CHEMALE, 2013).

No sudoeste Africano, estas idades são relacionadas ao Cinturão Namaqua (REID, 1997), cujo voluminoso magmatismo está constrito entre 1,2 e 1,0 Ga (EGLINGTON, 2006).

2.1.3 Neoproterozoico

As sequencias neoproterozoicas encontradas no Gondwana Ocidental são intrínsecas ao desenvolvimento do Oceano Adamastor, o qual marca a quebra do Supercontinente Rodínia a sucessão de colisões oblíquas que geraram o continente Gondwana Ocidental (e.g., BRITO NEVES; CAMPOS NETO; FUCK, 1999).

A abertura dos Oceanos Adamastor e Khomas ocorreu principalmente entre c. 800 e 750 Ma, quando blocos de diversos tamanhos dissociaram-se dos cratons Rio de La Plata, Kalahari e Congo (FRIMMEL; HARTNADY; KOLLER, 1996; FRIMMEL; KLÖTZLI; SIEGFRIED, 1996; KUKLA; STANISTREET, 1991; PORADA, 1989). As complexas interações destes blocos geraram crosta juvenil, registrada no extremo sul do Brasil no Bloco São Gabriel e como xenólitos em meio à intrusões pós-colisionais (FERNANDES *et al.*, 1995; HARTMANN *et al.*, 2011; KOESTER *et al.*, 2016; LEITE *et al.*, 1998; LENA *et al.*, 2014; LENZ *et al.*, 2011; MARTIL *et al.*, 2017; PHILIPP, 1998; SAALMANN *et al.*, 2011). O Toniano é marcado pela deposição de bacias sedimentares periféricas ao Oceano Adamastor no extremo sul do Brasil e Uruguai (e.g., BASEI *et al.*, 2011; BOSSI *et al.*, 1993; PORCHER *et al.*, 1999; SAALMANN *et al.*, 2011). Idades ediacaranas-criogenianas são encontradas em corpos intrusivos nestas mesmas regiões e também em sequencias depositadas no Terreno Éden (BASEI *et al.*, 2011; OYHANTÇABAL *et al.*, 2005; PAZOS; SÁNCHEZ-BETTUCCI; TOFALO, 2003; PECOITS, 2003; PECOITS *et al.*, 2004, 2016)

Em última análise, a colisão destes blocos, cujos limites são assumidos como as pervasivas zonas de cisalhamento continentais, promoveu intensa

deformação e metamorfismo nestas sequencias vulcano-sedimentares e unidades associadas, obliterando importantes relações estratigráficas. A acomodação do orogéno promoveu a formação de zonas de cisalhamento transcorrentes magmatismo sin- e pós-colisional, e formação de bacias foreland (e.g., ALMEIDA *et al.*, 2012; FRAGOSO-CESAR, 1980; FRANTZ; BOTELHO, 2000; GERMS, 1983; OYHANTÇABAL *et al.*, 2009; PASSARELLI *et al.*, 2010). Em última análise, o continente Gondwana Ocidental, produto do ciclo Pan-Africano-Brasiliano durante o Neoproterozoico, aflora no Uruguai e na costa meridional Brasileira como Cinturão Dom Feliciano e no sudoeste da África como cinturões Kaoko, Damara e Gariep.

2.2 Cinturão Dom Feliciano

Desde o pioneiro trabalho de Hasui, Carneiro e Coimbra (1975), que estabelece faixas de dobramento, como Cinturão Tijucas, muito foi desenvolvido acerca do entendimento da evolução da costa meridional brasileira durante o Neoproterozoico. Porada (1979) define que estas faixas foram produto de subducção, na qual a placa oceânica mergulharia à oeste. Expandindo este modelo, Fragoso-Cesar (1980) detalha os segmentos que compõem estas faixas, definindo o conjunto como Cinturão Dom Feliciano: plútons graníticos à leste, bacias tipo-molassa à oeste e rochas supracrustais formadas em ambiente *back-arc* no meio da associação.

Durante as décadas de 90 e 80, diversos autores contribuíram para o detalhamento do Cinturão Dom Feliciano como um todo (e.g., BASEI, 1985; BOSSI; CAMPAL, 1992; FERNANDES *et al.*, 1995; LEITE *et al.*, 1998; SÁNCHEZ-BETTUCCI; RAMOS 1999; SILVA *et al.*, 1985; SILVA; DIAS, 1981; SOLIANI JR., 1986). A associação de unidades geotectônicas mais difundida, que define o Cinturão Dom Feliciano é a proposta por Basei *et al*. (2000), como mostrado na Fig. 2). No Escudo Sul-Riograndense, o Cinturão Dom Feliciano aflora como Batólito Pelotas, Bacia Camaquã e Complexo Porongos.

O então chamado Batólito Pelotas é subdivido em suítes remanescentes do magmatismo colisional à pós-colisional, predominantemente cálcio-alcalinas de alto potássio, cuja nomenclatura diverge consideravelmente na literatura (e.g., FRANTZ;

BOTELHO, 2000; FRANTZ; NARDI, 1992; PHILIPP, 1998; PHILIPP; MACHADO, 2005). Esta unidade é interpretada como produto de retrabalhamento crustal do embasamento gnáissico, sendo posicionada entre 800 e 550 Ma (BABINSKI *et al.*, 1997; FRANTZ; BOTELHO, 2000; HARTMANN *et al.*, 2000; SILVA *et al.*, 1999).

A Bacia Camaquã sobrepõem o Complexo Porongos à oeste e também ao longo de corredores estreitos de direção NNE-SWS, definidos como Sub-bacia do Camaquã Oriental ou Piquiri-Boici (ALMEIDA *et al.*, 2012; FAMBRINI; FRAGOSO-CESAR, 2006). Esta bacia é interpretada como desenvolvida em um nível estrutural rúptil a dúctil-rúptil (PAIM; CHEMALE; LOPES, 2000) e tem vulcanismo registrado em 540 Ma (JANIKIAN *et al.*, 2012).

O Complexo Porongos, Figura 4, tem orientação NW-SW, apresenta 150 km de comprimento e 50 km de largura, limitado à oeste pela Zona de Cisalhamento Dorçal do Canguçu, à leste pelo Batólito Pelotas e é parcialmente coberto pelas bacias do Camaquã e Paraná.

2.3 Complexo Porongos

O Complexo Porongos é uma sequencia de rochas metavulcanossedimentares de grau metamórfico variando de xisto-verde a anfibolito e apresentam duas foliações relativas a processos transversais e longitudinais, entendidos como de regime tangencial e transcorrente (FERNANDES *et al.*, 1995; FRANTZ; BOTELHO, 2000; LENZ, 2006; LENZ *et al.*, 2011; MARQUES, 1996; MARQUES *et al.*, 1998a, 1998b). Apesar de extensivamente mapeado e estudado desde Carvalho (1932), este complexo apresenta esparsas informações acerca de sua parte extremo sul, localizada na margem sul do Rio Camaquã.

Esta ambiguidade na densidade de informações disponíveis impossibilita o estabelecimento de um modelo geotectônico definitivo para a bacia precursora do Complexo Porongos. A intensa e heterogênea deformação superimposta ao Complexo Porongos permite a separação da sequencia em domínios estruturais, representados pelo Domo de Santana de Boa Vista, Serra dos Pedrosas e antiformes do Godinho e Capané (JOST; BITENCOURT, 1980; WILDNER *et al.*, 1996), como mostrado na Figura 4.

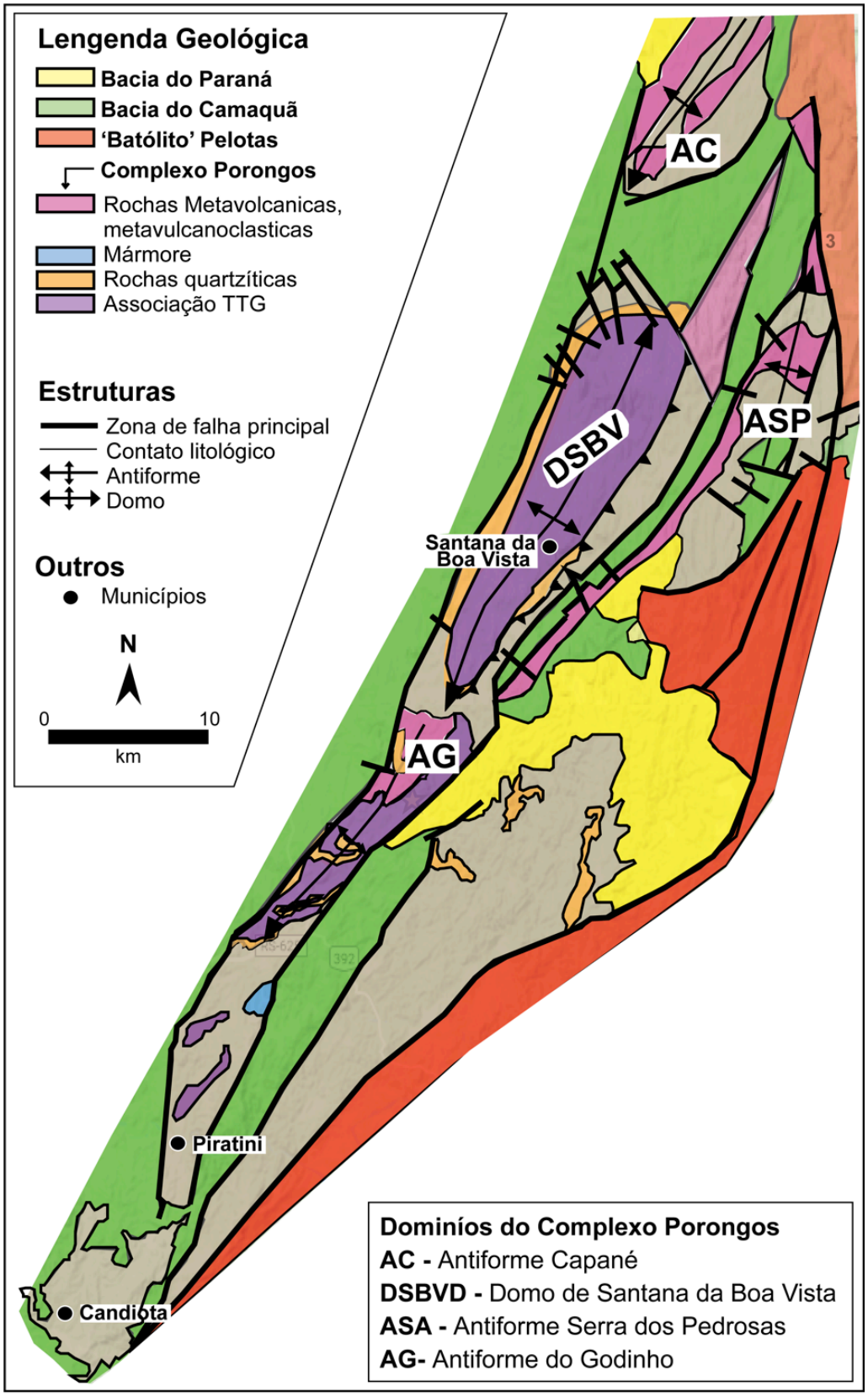

Figura 4 – Mapa geológico do Complexo Porongos. Fonte: mapa modificada de Almeida (2012), Chemale (2000), Google Maps (2016), Jost (1981) e Oliveira (2014).

2.3.1 Domo de Santana da Boa Vista

Este domínio está localizado na porção centro-oeste do Complexo Porongos, cuja sequencia supracrustal é definida como Grupo Cerro dos Madeiras. Esta sequencia é dividida nas formações Arroio dos Neves, Arroio Olaria e Irapuãzinho, composta por metarcósios, quartzitos e anfibolitos; quartzo ritmitos, formações ferríferas bandadas e xistos; mica xistos e mármore (JOST, 1981; JOST; BITENCOURT, 1980). O embasamento assumido para o Complexo Porongos, definido como Gnaisse Encantadas, aflora apenas neste domínio, o qual é representado por um domo contendo uma associação de gnaisses, granitoides milonitizados e anfibolitos, cuja cristalização é constrita em 2,0 Ga (CAMOZZATO; PHILIPP; CHEMALE, 2013; CHEMALE, 2000; HARTMANN *et al.*, 2003; LUSA; PHILIPP; NARDI, 2010; MACHADO; CÉSAR; FACCINI, 1987; PHILIPP; LUSA; NARDI, 2008; PORCHER; FERNANDES, L. A. D., 1990; SAALMANN *et al.*, 2011). O contato entre o embasamento e a sequencia supracrustal é tectônico, definido por uma zona de cisalhamento de baixo angulo (LUSA; PHILIPP; NARDI, 2010). Em uma abordagem recente, Pertille, Hartmann e Philipp (2015) definem a espessa camada quartzítica sobrepondo o Gnaisse Encantadas como Formação Santana, de idade Paleoproterozoica, a qual foi previamente interpretada como remanescente do intenso cisalhamento de granitoides milonitizados (FERNANDES *et al.*, 1992; FERNANDES; TOMMASI; PORCHER, 1992).

Trabalhos geocronológicos pioneiros neste domínio foram realizados usando isócrona de Rb-Sr rocha total para o Gnaisse Encantadas, obtendo-se 2,1 Ga para a cristalização e 544 ± 18 Ma para o metamorfismo em amostras de tonalito (CORDANI; HALPERN; BERENCHOLC, 1974; SOLIANI JR., 1986). Idades de U-Pb em cristais de zircão variam entre 2.263 ± 18 (HARTMANN *et al.*, 2003) e 2.078 ± 13 Ma (HARTMANN *et al.*, 2000) para a cristalização do tonalito associado ao Gnaisse Encantadas. Nesta mesma unidade, os picos metamórficos identificados são relacionados com o ciclo Transamazônico e Brasiliano (CHEMALE, 2000; HARTMANN *et al.*, 2000). Episódios de vulcanismo riolítico foram recentemente datados por Pertille et al. (2017), constritos em 801 ± 4.7 e 773 ± 3.1 Ma. A proveniência da sequencia supracrustal é obtida através de U-Pb em grãos detríticos de zircão, cujas idades se estendem do Mesoarqueano, 3.092 ± 19 Ma,

(HARTMANN *et al.*, 2004) ao Toniano, 1.041 ± 46 Ma, (GRUBER *et al.*, 2011) obtidas em amostras de quartzito via SHRIMP e clorita-muscovita xisto via LA-ICP-MS, respectivamente.

2.3.2 Antiforme da Serra dos Pedrosas

Aflorante na porção centro-leste do Complexo Porongos, a sequencia supracrustal deste domínio é definida como Complexo Cerro da Árvore, a qual é subdividida nos metapelítos Cerro do Facão, xistos Rincão do Maranhão, metandesitos Cerro Cambará, xistos Arroio Areião e metariolitos Cerro do Alemão (JOST, 1981; JOST; BITENCOURT, 1980). As condições registradas variam de fácies xisto verde à anfibolito de baixo grau metamórfico, em 425-590˚C e 1-6 kbar (JOST, 1981). As condições metamórficas progressivas em direção ao leste estão relacionadas à intrusão tardia da Suíte Encruzilhada do Sul (LENZ, 2006).

Idades LA-ICP-MS U-Pb em grãos detríticos de zircão variam do Neoarqueano (2.652 ± 32 Ma) a Esteniano (1.010 ± 17 Ma), obtidas em quartzo-muscovita xisto e clorita-muscovita xisto (GRUBER *et al.*, 2011), respectivamente. A idade deposicional máxima para a bacia precursora do Complexo Porongos, assumida na pesquisa como Bacia Porongos, é constrita ao Toniano tendo em as idades de 783 ± 6 Ma e 789 ± 7 Ma em amostras de metariolitos por Porcher et al. (1999) e Saalmann et al. (2011), respectivamente.

2.3.3 Antiforme do Godinho

Localizada no sul do Complexo Porongos, este domínio apresenta rochas metavulcânicas intercaladas com filitos, quartzitos, xistos, mármore e metagranitóides (WILDNER *et al.*, 1996). O primeiro estudo geocronológico deste domínio foi realizados em amostras de meta-andesito usando LA-ICP-MS U-Pb em cristais de zircão, o qual reportou idades de 1.356 ± 227 Ma para a cristalização e c. 700 Ma para o metamorfismo (WILDNER *et al.*, 1996). No entanto, estudos utilizando TIMS U-Pb em cristais de zircão mostram idade de 778 ± 8 Ma para a cristalização das mesmas rochas (CHEMALE, 2000). Metariolitos apresentam idade

de cristalização em 809 ± 4.1 Ma, via SHRIMP U-Pb em zircão (PERTILLE *et al.*, 2017). Estudos de proveniência usando LA-ICP-MS em grãos detríticos mostram idades variando do Mesoarqueano (2.906 ± 42 Ma) ao Estateriano (1.619 ± 39 Ma) em rochas quartzíticas (GRUBER *et al.*, 2011).

O extremo sul e sudeste do Complexo Porongos não são classificados em domínios e apresentam escarças informações geológicas e geocronológicas. Nos poucos estudos realizados no extremo sul, são descritas sequencias de xistos pelíticos, quartzitos, mármores, rochas metaultramáficas de fácies anfibolito de baixo grau e gnaisse alcalino (CAMOZZATO *et al.*, 1994; REMUS *et al.*, 1987; REMUS; HARTMANN; RIBEIRO, 1991). Idades SHRIMP U-Pb em grãos detríticos de zircão mostram contribuição Sideriana (2.452 ± 12 Ma) a Orosiana (1.998 ± 15 Ma) em amostras de quartzito desta região (HARTMANN *et al.*, 2004). Já no extremo sudeste, idades LA-ICP-MS U-Pb em grãos detríticos de zircão apontam idades variando do Mesoarqueano (2.863 ± 24 Ma) ao Esteniano (1.008 ± 12 Ma) em muscovita xistos (PERTILLE; HARTMANN; PHILIPP, 2015).

2.3.4 Antiforme Capané

Este domínio, objeto de estudo da presente pesquisa, aflora na região extremo norte do Complexo Porongos, sendo descrita em detalhe por Jost (1981), Marques (1996), Marques et al. (1998a, 1998b). Sua associação litológica é representada na Figura 5 e é dada por uma sequencia meta-vulcano-sedimentar cortada por metagranitos e milonitos, além de conter lentes de quartzito, estaurolita-granada xisto, mármore, gnaisse alcalino e rochas ultramáficas, diferindo consideravelmente dos outros setores do Complexo Porongos.

A antiforme regional tem linha de charneira mergulhando de 20˚ a 220˚, o flanco oeste 38˚NW e o leste 30˚SE, configurando um ângulo interflanco de cerca de 100˚ (MARQUES *et al.*, 1998a, 1998b) e plano axial mergulhando de 86˚SE (ZVIRTES, 2014). Zonas de cisalhamento NE-SW de baixo ângulo mergulho preservam texturas herdadas de maneira heterogênea (MARQUES *et al.*, 1998a, 1998b). Desta maneira, o flanco oeste contem sequencias metavulcânicas principais intercaladas com metapelíticas subordinadas, o flanco leste apresenta sequencias metapelíticas intercaladas com corpos metagraniticos e lentes de mármore, já na

zona axial afloram rochas intensamente deformadas, consideradas metapelíticas e lentes de estaurolita-granada xisto (MARQUES *et al.*, 1998a, 1998b). Todas as sequencias mostram quartzo milonitos a ultramilonitos, os quais são peculiarmente mais abundantes na região axial. Tanto o flanco oeste como a região axial mostram lascas de gnaisse alcalino e rochas metaultramáficas, sendo estas interpretadas como partes de um ofiólito desmembrado (MARQUES, 1996; MARQUES *et al.*, 1998a, 2003). As condições de metamorfismo variam de predominante fácies xisto verde a anfibolito de grau médio (MARQUES *et al.*, 1998a, 1998b).

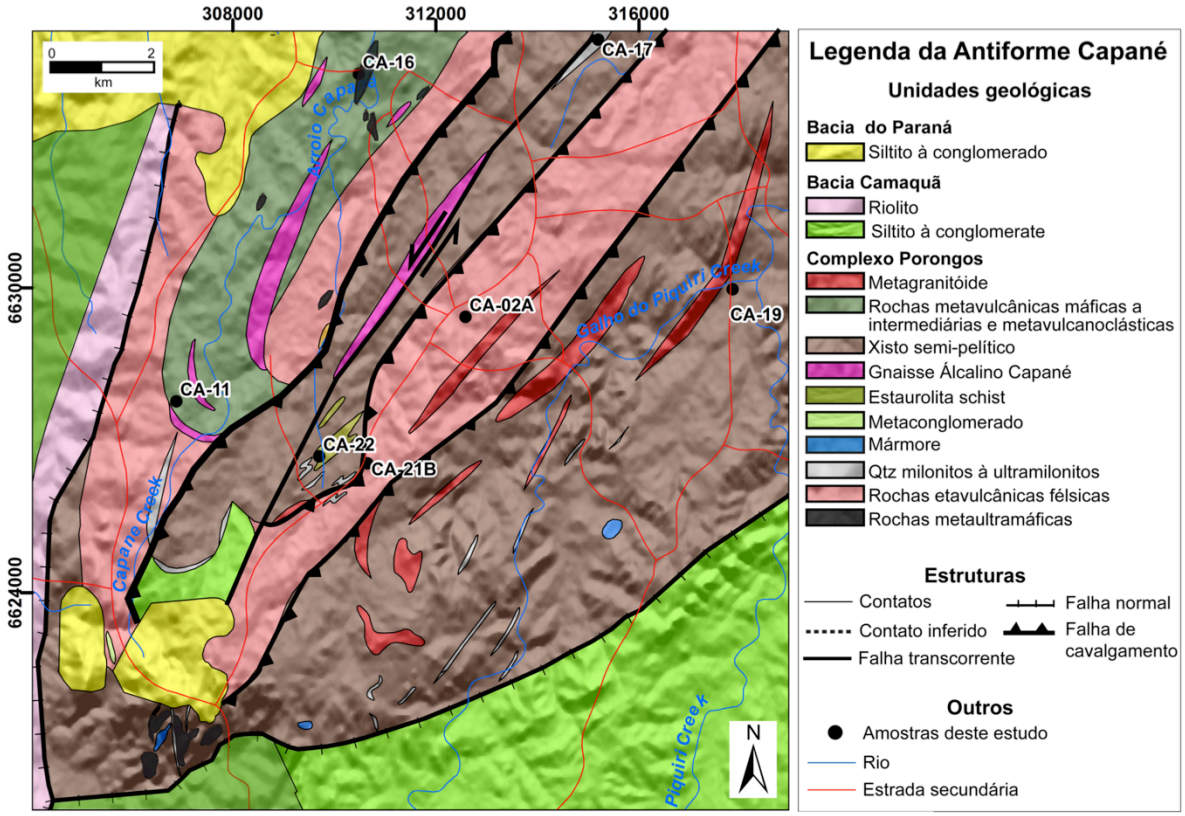

Figura 5 – Mapa geológico da Capané Antiforme, região extremo norte do Complexo Porongos. Fonte: mapa modificada de Jost e Bitencourt (1980), Marques (1996) e Marques et al (1998a, 1998b).

Em síntese, os estudos geocronológicos deste setor reportam idades de cristalização entre 600 a 530 Ma para o Gnaisse Alcalino Capané (CHEMALE, 2000; LAFON; HARTMANN; AZAMBUJA, 1990; ZVIRTES *et al.*, 2015), proveniência essencialmente Riaciana e Ediacarana para os xistos de ambos flancos (PERTILLE *et al.*, 2015, 2017) e metamorfismo em cerca de 540 Ma (CHEMALE, 2000; ZVIRTES *et al.*, 2015).

CAPÍTULO 3 – MATERIAIS E MÉTODOS

3.1 Revisão bibliográfica

3.2 Amostragem

3.3 Petrografia

3.4 Geocronologia U-Pb em zircão

3.1 Revisão Bibliográfica

A análise da literatura e compilação de dados consistiu na revisão de artigos publicados em periódicos científicos, trabalhos de conclusão de curso, dissertações, teses, livros, mapas, mídia digital e anais de eventos científicos, visando reunir um arcabouço geológico sobre o Complexo Porongos e consequentemente, sobre a Antiforme Capané.

O levantamento destas informações permitiu a construção de uma base de dados geocronológica, a qual foi utilizada no tratamento estático das idades dos grãos detríticos de zircão. As descrições de afloramento e petrografia, além de 151 laminas de delgadas do trabalhos de Marques (1996) e Marques et al. (1998a, 1998b) foram revistos em grande detalhe, de maneira a definir áreas chave para a abordagem geocronológica desta pesquisa.

3.2 Amostragem

A pauta do plano de amostram seguiu estações de campo previamente mapeadas e descritas por Marques (1996) para a Antiforme Capané, além de incluir novas áreas visando a reprodução das idades reportadas por Kohlraush (2013) e Pertille et al. (2015, 2017). No total, vinte e oito afloramentos foram visitados e amostrados (Figura 6), quinze novas laminas delgadas foram preparadas e sete amostras foram selecionadas para a datação dos grãos detríticos de zircão via LA-ICP-MS U-Pb.

Figura 6 – Exemplos de afloramentos amostrados durante a presente pesquisa. Foto da esquerda corresponde ao afloramento CA-17 e da direita ao afloramento CA-21B.

3.3 Petrografia

As amostras foram laminadas no Núcleo de Preparação de Amostras do Centro de Estudos em Petrologia e Geoquímica da Universidade Federal do Rio Grande do Sul. Dada a condição friável e pouco coesa das amostras, todas foram impregnadas com resina epóxi. Inicialmente, dezesseis amostras foram selecionadas para laminação, no entanto a amostra de filito CA-02 mesmo após impregnação não apresentou condições adequadas de laminação. Para as outras quinze amostras, a petrografia seguiu o sistema proposto pela *International Union of Geological Sciences Subcommission on the Systematics of Metamorphic Rocks*, cujo procedimento de nomenclatura segue Schmid et al. (2007) e Sibson (1977), sendo que a abreviação mineral segue Siivola & Schmid (2007).

3.4 Geocronologia U-Pb em zircão

3.4.1 Conceitos isotópicos

A concepção da geocronologia propiciou avanços notáveis quanto a noção de tempo geológico, o qual foi sistematizado de maneira pioneira por Henry S. Williams em 1983. A descoberta dos raios-X e da radioatividade natural do U no fim do século XIX, ampliou a potencial de utilização da radioatividade de maneira aplicada, a qual foi abordada para fins geológicos no trabalho de Holmes, em 1911, intitulado *"The Association of Lead with Uranium in Rock-Minerals and Its Application to the Measurement of Geological Time".*

O uso de espectrômetros de massa na para fins geocronológicos na década de 60 propiciou um crescimento exponencial deste tipo de abordagem, além de diminuir as limitações e aumentar a precisão da técnica (SCHOENE, 2014). A base do sistema isotópico U-Pb consiste no decaimento natural dos isótopos pai ^{238}U, ^{235}U e ^{232}Th nos isótopos filhos ^{206}Pb, ^{207}Pb e ^{208}Pb, através da emissão espontânea de partículas α, β ou γ (FAURE; MENSING, 2004), como mostrado na Figura 7.

A relação entre os isótopos de Pb radiogênicos e radioativos, desconsiderando o Pb não-radiogênico denominado também comum (^{204}Pb),

permite o cálculo de idade através da concordância do sistema ao longo de seu tempo de evolução, como mostrado nas equações 1 e 2 (FAURE; MENSING, 2004).

$$^{206}Pb/^{238}U = (e\lambda^{238}T-1) \qquad (1)$$

$$^{207}Pb/^{235}U = (e\lambda^{235}T-1) \qquad (2)$$

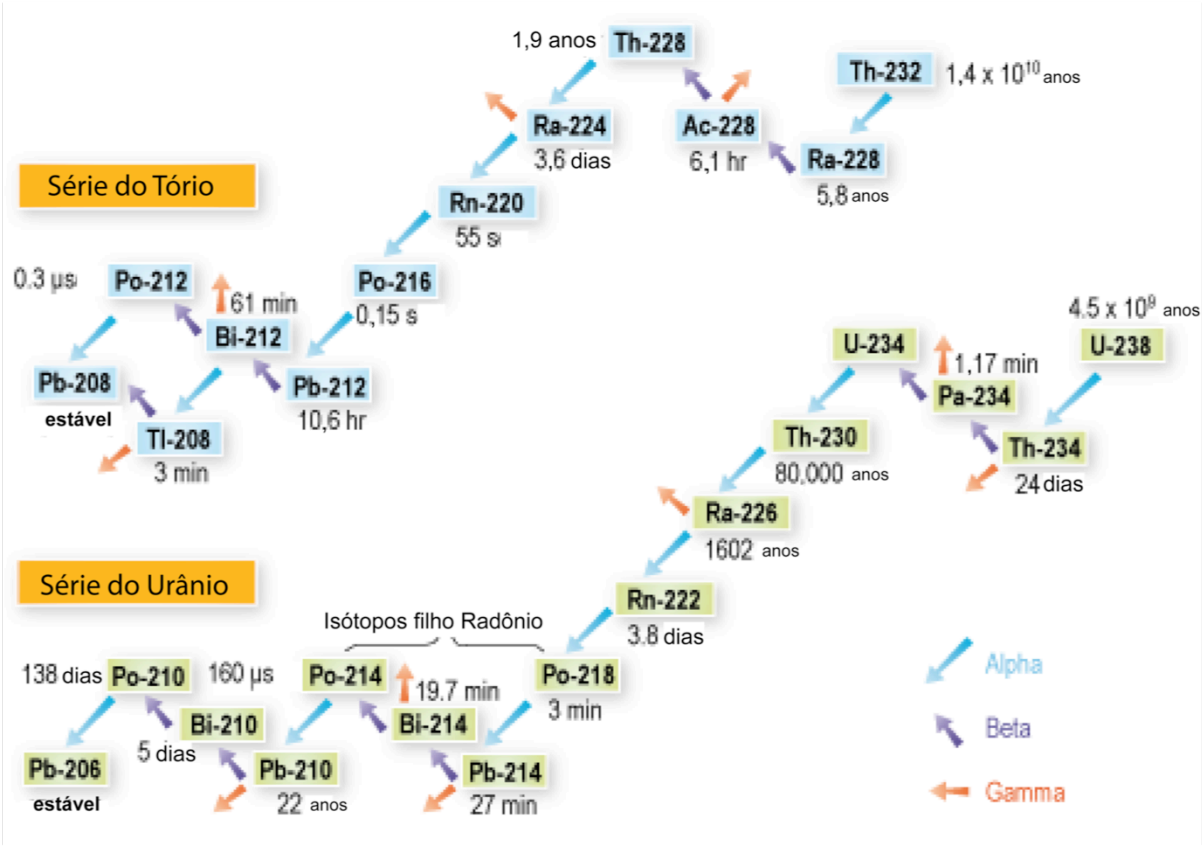

Figura 7 – Série de decaimento natural do Tório e Urânio. Fonte: figura modificada de World Nuclear Association (2016).

Desta maneira, diagramas de idade são construídos considerando-se as equações de decaimento dos isótopos pai em função do tempo, destituídos de ^{204}Pb inicial. Wetherill (1956) propôs uma curva evolutiva dentro do campo contrito pelas razoes $^{207}Pb/^{235}U$ versus $^{206}Pb/^{238}U$, definida pelos pontos onde as razões de mesma idade se encontram: Concordia. As aquisições ou perdas isotópicas ao longo do tempo são sinalizadas pela reta de discórdia, como mostrado na Figura 8.

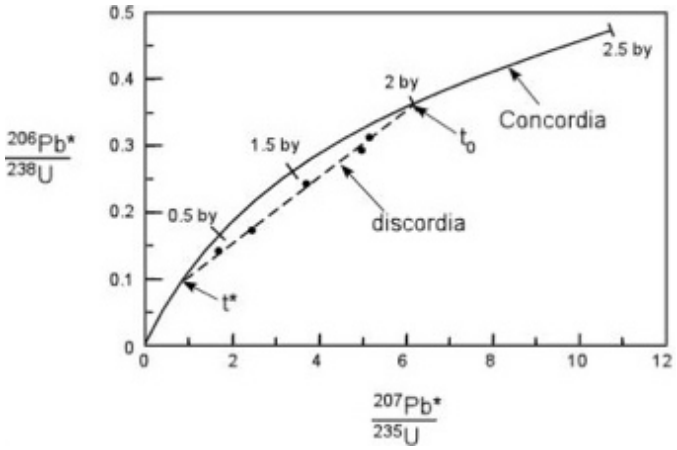

Figura 8 – Exemplo de Curva Concordia e reta Discórdia para um sistema U-Pb. Fonte: White (2015).

3.4.2 Zircão

O zircão é um mineral acessório, tetragonal, pertencente à família dos silicatos e apresenta formula $ZrSiO_4$, onde as cadeias de SiO_4-ZrO_8 são alternadas (HARLEY; KELLY, 2007). Sua estrutura não comporta espaços vacantes, os quais são ocupados por elementos traço e ultra-traço substituindo os cátions de Zr^{+4} (DEER; ZUSSMAN; HOWIE, 2013). Seu hábito é geralmente bipiramidal, cuja razão de elongação varia numa escala de 1 a 5, refletindo as condições de formação e/ou transporte deste cristal (CORFU, 2003). Apresenta cores que variam de amarelo, vermelho, marrom, verde até incolor. O zonação por crescimento é uma feição comum e representa a variação química dentro da estrutura do mineral, dada primariamente por Zr e Si e também na proporção dos elementos traço e ultra traço, refletindo o grau de polimerização do magma (BENISEK; FINGER, 1993; CORFU, 2003; HOSKIN, 2000). A presença de xenocristais ou núcleos herdados pode ocorrer pela absorção de um núcleo antigo que será circundado pelo novo cristal de zircão, havendo ou não distinção entre o núcleo e a borda (CORFU, 2003).

Bastante abundante e resistente a processos de desintegração geológica, torna-se um mineral ideal para a quantificação de idade de cristalização e também metamorfismo (DEER; ZUSSMAN; HOWIE, 2013). Holmes (1911) foi pioneiro no reconhecimento do zircão para fins geocronológicos, utilizando isótopos de U e Pb. Notavelmente, esta espécie mineral tem quantidades significativas e variadas de U, a qual tem sua proveniência balizada pela razão Th/U (RUBATTO, 2002). Sugere-se

que a perda de Th causando a diminuição da razão Th/U indicaria interação metamórfica e hidrotermal (HOSKIN; SCHALTEGGER, 2003; MÖLLER *et al.*, 2003; RUBATTO, 2002; WILLIAMS; CLAESSON, 1987).

3.4.3 Preparação

A separação de grãos de zircão foi executada no Núcleo de Preparação de Amostras do Centro de Estudos em Petrologia e Geoquímica da Universidade Federal do Rio Grande do Sul (PrepLab-CEPGq-UFRGS). Para tal objetivo os procedimentos padrões foram seguidos, exemplificados na Figura 9, os quais consistiram em limpeza e secagem em estufa de amostras para remoção de resíduos de solo e rochas; britagem de cerca de 3 a 5 kg destas amostras; moagem em moinho de disco; peneiramento em telas de 60 e 170 mesh; concentração dos grãos em bateia manual; separação isomagnética usando diferentes intensidades de corrente elétrica (0,4A, 0,8A, 1,2A e 1,8A) e por fim, separação utilizando líquidos pesados.

Figura 9 – Parte inicial de procedimentos para tratamento de amostras geocronológicas no PrepLab-CEPGq-UFRGS. *Esquerda*: Britador de amostras, tipo mandíbula, para moagem preliminar de rochas. *Centro*: Desagregação de nódulos das amostras em pistilo de madeira para posterior peneiramento manual. *Direita*: Cominuição do material maior que abertura da peneira em moinho de disco visando novo peneiramento.

Os grão de zircões concentrados, em média de cem grãos, são então agrupado em uma pastilha denominada *mount*, Figura 10. Ela é confeccionada com o auxilio de lupa binocular, onde os grãos aderidos a uma fita adesiva dupla face

disposta em uma lâmina de vidro. Uma cápsula circular de cerca de 5 mm é anexada à lâmina, utilizada como recipiente para o epóxi, o qual aprisionará os grãos de zircão.

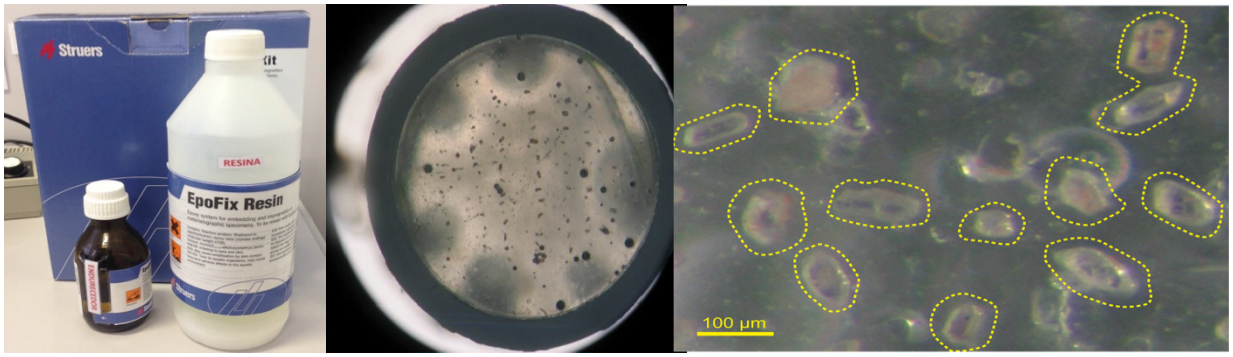

Figura 10 – *Esquerda*: Resina e endurecedor utilizados para confeccionar o epóxi da *mount*. *Centro*: Grãos de zircão distribuídos na *mount* de aproximadamente 5 mm. *Direita*: Detalhe da *mount* onde os grãos de zircão estão destacados em amarelo.

3.4.4 Morfologia

Os grãos de zircão foram primeiramente caracterizados com auxilio da petrografia de laminas delgadas, sempre quando identificados nas seções descritas. Na seguinte etapa, todas amostras tiveram seus grãos separados e analisados em lupa binocular, visando feições como cor, brilho, grau de transparência e morfologia externa. Após a confecção das *mounts*, os grãos foram mapeados para a delimitação das regiões com maior potencial de datação bem sucedida. As eletromicrografias de elétrons retroespalhados (*back-scattered*) foram obtidas através de microssonda eletrônica de varredura (MEV) tipo Jeol JSM 5800 no Centro de Microscopia Eletrônica da UFRGS. Este procedimento visa áreas livres de fraturas e inclusões, assim como indicado por Andersen (2005).

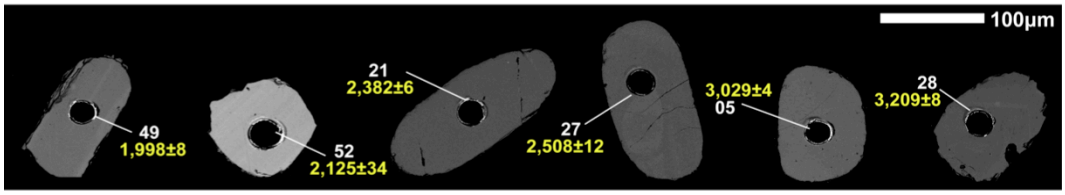

Figura 11 – Imagem MEV *back-scattered* de grãos de zircão representativos da amostra CA-02A. Números em branco representam o *spot* analisado e em amarelo a idade obtida.

Por fim, imagens de catodoluminescência foram adquiridas usando um microscópio eletrônico Quanta 250 FEG acoplado com um espectroscópio de

catodoluminescência Mono CL3+ do Centro de Pesquisas Geocronológicas da Universidade de São Paulo (CPGeo-USP). Estas imagens são utilizadas para distinção de núcleos herdados e sobrecrescimentos metamórficos, por exemplo.

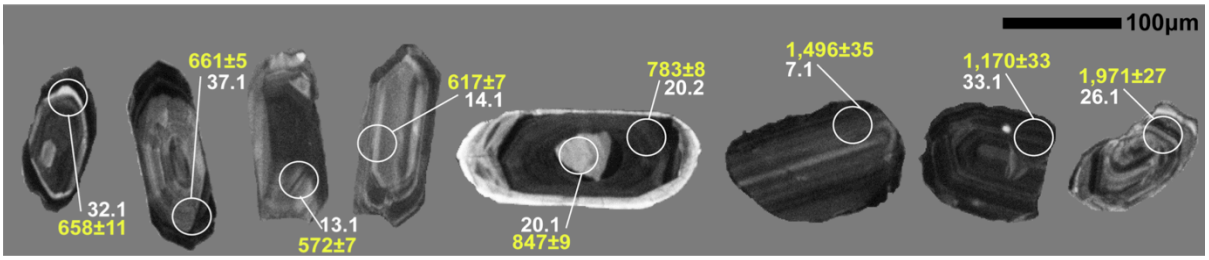

Figura 12 – Imagem de catodoluminescência de grãos de zircão representativos da amostra CA-19. Números em branco representam o *spot* analisado e em amarelo a idade obtida.

3.4.5 LA-ICP-MS

O espectrômetro de massa por plasma indutivamente acoplado com ablação à laser (LA-ICP-MS) é um equipamento que analisa a superfície de uma espécie mineral para determinação de elementos, em condições de vácuo, utilizando a relação de massa sobre carga elétrica durante ação de campo elétrico e magnético (SCHOENE, 2014), como mostrado esquematicamente na Figura 13.

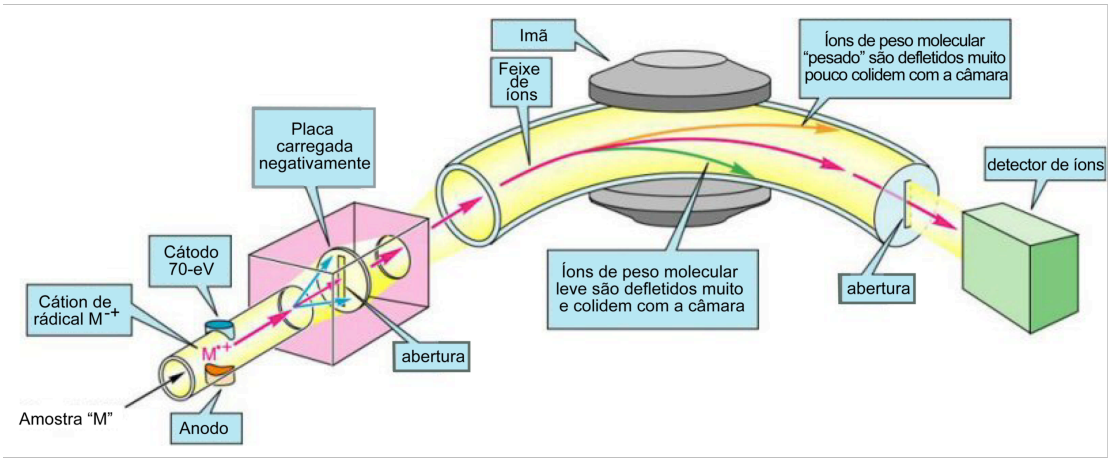

Figura 13 – Desenho esquemático do funcionamento de um espectrômetro de massa. Fonte: Figura modificada de The University of Maine (2017).

O sistema LA consiste em um laser de pequeno comprimento de onda (<266 nm), com taxas de emissão controladas, de maneira de analisar os elementos e diminuir a propensão a aquecimento ou fracionamento do material (GUILLONG;

HEINRICH, 2007; GÜNTHER; HEINRICH, 1999). A analise pontual consiste na varredura partículas pelo plasma, sendo incorporadas em um gás carreador (SCHOENE, 2014). Várias configurações do sistema ICP-MS são combinadas ao LA, a depender da capacidade dos coletores magnéticos. Erros inerentes do processo de datação são minimizados utilizando grãos padrão, cujos valores isotópicos são amplamente conhecidos e controlados (SCHOENE, 2014).

Para a presente pesquisa, as determinações de idade U-Pb realizadas no no CPGeo-USP e Laboratório de Geologia Isotópica da Universidade Federal do Rio Grande do Sul utilizaram um espectrômetro de massa acoplado a um sistema de abrasão a laser Excimer ArF Thermo-Fisher Neptune. Os procedimentos e condições de operação deste equipamento durante a análise são descritos por Sato et al. (2009, 2010) e também Sato e Kawashita (2002). As correções foram de massa foram realizadas pela análise do zircão padrão GJ-1, sendo $^{206}Pb/^{238}Pb$ age por IDTIMS = 608.5 ± 0.4 Ma (JACKSON *et al.*, 2004) e o chumbo comum foi corrigido com base no modelo de Stacey e Kramers (1975). O data obtido foi reduzido utilizando planilhas Excel desenvolvidas nos próprios laboratórios e as idades foram derivadas das razões $^{206}Pb/^{238}U$, $^{207}Pb/^{235}U$, $^{207}Pb/^{206}Pb$ e $^{232}Th/^{238}U$, as quais foram calculadas via ISOPLOT 3.6 (LUDWIG, 2008). Erros das razões isotópicas são apresentados a intervalo de confiança de ± 1 σ.

3.4.6 Plotagem de resultados

Os dados adquiridos foram filtrados antes da plotagem de maneira a removas análises acima de 10% de discordância ou com mais de 1% de chumbo comum. A interpretação da idade e plotagem seguiu as premissas de Gehrels (2014), onde idades $^{207}Pb/^{206}Pb$ foram utilizadas para grãos mais velhos que 1,2 Ga e $^{206}Pb/^{238}U$ para grãos mais jovens que 1,2 Ga. Os resultados finais foram plotados em diagramas de função da densidade de probabilidade e distribuição. Origens potenciais para as idades foram estabelecidas utilizando os valor de 0.02 para a razão Th/U, considerando-se os valores acima como magmático e os abaixo como metamórficos (RUBATTO, 2002).

CAPÍTULO 4 – ARTIGO SUBMETIDO

Successfully received: submission Polyphasic evolution of the Porongos Complex, Dom Feliciano Belt, southernmost Brazil: implications for the assembly of southwestern Gondwana for Precambrian Research

Precambrian Research <EviseSupport@elsevier.com> Tue, Mar 21, 2017 at 5:00 AM
Reply-To: precam-eo@elsevier.com
To: daianne.hofig@gmail.com

This message was sent automatically. Please do not reply.

Ref: PRECAM_2017_108
Title: Polyphasic evolution of the Porongos Complex, Dom Feliciano Belt, southernmost Brazil: implications for the assembly of southwestern Gondwana
Journal: Precambrian Research

Dear Mrs. Höfig,

Thank you for submitting your manuscript for consideration for publication in Precambrian Research. Your submission was received in good order.

To track the status of your manuscript, please log into EVISE® at: http://www.evise.com/evise/faces/pages/navigation/NavController.jspx?JRNL_ACR=PRECAM and locate your submission under the header 'My Submissions with Journal' on your 'My Author Tasks' view.

Thank you for submitting your work to this journal.

Kind regards,

Precambrian Research

Have questions or need assistance?
For further assistance, please visit our Customer Support site. Here you can search for solutions on a range of topics, find answers to frequently asked questions, and learn more about EVISE® via interactive tutorials. You can also talk 24/5 to our customer support team by phone and 24/7 by live chat and email.

Polyphasic evolution of the Porongos Complex, Dom Feliciano Belt, southernmost Brazil: implications for the assembly of southwestern Gondwana

Daianne Francis Höfig[1*], Juliana Charão Marques[2], Miguel Angelo Stipp Basei[3], Ronei Osório Giusti[4], Cassiano Kohlrausch[5], José Carlos Frantz[2]

[1]Programa de Pós-Graduação em Geociências, Universidade Federal do Rio Grande do Sul, Porto Alegre 91570900, Brazil

[2]Laboratório de Geologia Isotópica, Universidade Federal do Rio Grande do Sul, Porto Alegre 91570900, Brazil

[3]Centro de Pesquisas Geocronológicas, Universidade de São Paulo, São Paulo 05508080, Brazil

[4]Centro de Microscopia e Microanálises, Universidade Federal do Rio Grande do Sul, Porto Alegre 91591970, Brazil

[5]CIMCATARINA – Consórcio Intermunicipal Catarinense, Fraiburgo 89580000, Brazil

*Corresponding author e-mail: daianne.hofig@gmail.com (D.F. Höfig)

Abstract

New U-Pb detrital zircon ages for the Porongos Complex, Dom Feliciano Belt, south Brazil are presented. The Dom Feliciano Belt represents the major geotectonic unit in southeastern South America,

being formed during the Neoproterozoic amalgamation of southwestern Gondwana. A late Neoproterozoic (Ediacaran) zircon provenance found in the northernmost supracrustal sequences, at the Capané Antiform, challenges the traditional view of a single Neoproterozoic episode of deposition for the Porongos Complex. The new ages reveal three different provenance patterns for the Capané Antiform. A strong Ediacaran provenance has been identified in the metavolcano-sedimentary sequences from the limbs, with younger peak ages yielding 630–580 Ma. On the contrary, the axial mylonitic units have pronounced Paleoproterozoic peaks, constrained between 2.2 and 2.0 Ga. Additionally, lenses of medium-grade schist imbricated to the axial zone show important Tonian peaks at 830 Ma and a significant Mesoproterozoic contribution, being constrained at 1.5–1.3 Ga. The new provenance data combined with previously published geochronological, stratigraphic and tectonic data from the outcropping Porongos Complex area enable us to identify three different terranes within the Capané Antiform. The mylonitic rocks from the axial zone are interpreted as part of the Santana Formation. Whereas the medium-grade schist lenses show provenance similar to those found in the regionally exposed Porongos Metamorphic Complex. The sedimentation of these last units are constrained to the Tonian and here we suggest the name Porongos I sequence to group all meta-volcanosedimentary rocks formed during this period. On the other hand, the younger units, located in both limbs, are interpreted as formed in a different basin during the Ediacaran. We propose that the younger sequences of the Capané Antiform, here coined as Porongos II sequence, are

related to synorogenic deposition developed during the Ediacaran period. These findings suggest a tectonic and paleogeographic reconstruction, where the younger Capané units are interpreted as synorogenic deposits formed during the deformation imposed by the juxtaposition of the Pelotas Batholith. This igneous complex was an important source for the younger volcano-sedimentary units of the Porongos Belt, thereby giving new insights into the dynamics of the SW Gondwana assembly.

Keywords

Porongos Complex, Capané Antiform, Dom Feliciano Belt, Gondwana, U-Pb detrital zircon, Pan-African-Brasiliano

1. Introduction

The Neoproterozoic Pan-African–Brasiliano tectonic cycle represents a major period of intense crustal reworking of several nuclei generated during break-up of the Mesoproterozoic Rodinia supercontinent, leading to the assembly of the southwestern Gondwana supercontinent (e.g., Brito Neves et al., 1999, 2014; Cordani et al., 2003; Fuck et al., 2008; Li et al., 2008; Trompette, 1997, 2000; Fig. 1A). The resulting crustal mosaic crops out along the South Atlantic Ocean coastline as a branched system of orogens: in eastern South America as Mantiqueira Province (Almeida et al., 1981) and in southwestern Africa as Damara, Kaoko and Gariep belts (Basei et al., 2010; Porada, 1989; Schmitt et al., 2008; Stowe et al., 1984; Tohver et al., 2006; Torquato and Cordani, 1981; Trompette, 1994;).

Stretching over south Brazil and Uruguay along c. 1200 km, the

meridional segment of the Mantiqueira Province is referred to as Dom Feliciano Belt (*sensu* Basei et al., 2000 and Fragoso-Cesar, 1980; Fig. 1B). This association of overprinted granitic rocks and metavolcano-sedimentary successions is product of diachronic collisions, involving Rio de La Plata and Kalahari cratons as well as small drifting terranes, during the evolution of the Adamastor Ocean (e.g., Basei et al., 2000; Bento dos Santos et al., 2015; Frimmel et al., 1996a; Hartnady et al., 1985).

In this respect, the Neoproterozoic synorogenic sequences found in the Dom Feliciano Belt play a remarkable role in shedding light on the understanding of the southwestern Gondwana formation, as the geodynamic links between the Precambrian orogens on either side of the South Atlantic have remained poorly understood. Particularly in southernmost Brazil, the Porongos Complex (PC) has been a matter of debate, as its Tonian volcanic episodes, traditionally assumed as maximum depositional age (Porcher et al., 1999; Saalmann et al., 2011), contrast with Ediacaran detrital ages found in the northern area (Pertille et al., 2015b). In a recent approach, Pertille (2017) re-interpret the maximum depositional age for the whole PC as Ediacaran-Cryogenian, between 650 and 550 Ma, however, the Tonian volcanism remains unclear in such scenario.

The present study is aimed at constraining established tectonic phases in the central region of the Dom Feliciano Belt, southernmost Brazil, through both reviewing the published geochronological record and providing new U-Pb detrital zircon ages from the Capané Antiform of PC. These new age considerations combined with previously published geochronological, stratigraphic and tectonic data enable us to (1) identify different terrains within

the Capané Antiform; (2) propose that the younger sequences of the Capané Antiform are related to synorogenic deposition, developed during Cryogenian-Ediacaran times; and (3) discuss evolutionary models to conciliate the existence of two depositional basins in the Porongos Complex generated during the Pan-African–Brasiliano tectonic cycle, which has major implications for the interpretation of the formation of southwestern Gondwana.

2. Precambrian geochronological framework of SW Gondwana

2.1 Archean and Paleoproterozoic

In South America, the principal crustal-building event was recorded as the Paleoproterozoic Trans-Amazonian orogeny, lasting from 2.2 to 2.0 Ga (Santos et al., 2003). The Rio de La Plata Craton represents a heterogeneous mosaic of scarce Archean vestiges and dominant Paleoproterozoic record juxtaposed along major shear zones (Bossi and Campal, 1992; Hartmann et al., 2001). Several authors have attempted to define more accurate boundaries for the Rio de La Plata Craton, yet they are not precisely defined (e.g., Cordani et al., 2000; Dalziel, 1997; Rapela et al., 2011; Ramos, 1988; Trompette, 1994; Weil et al., 1998;). In Uruguay, the Rio de La Plata Craton is traditionally referred to as Nico Pérez and Piedra Alta terranes, however, recent studies have considered the former as an allochthonous block juxtaposed to the Rio de La Plata Craton (e.g., Gaucher et al., 2011; Oyhantçabal et al., 2011a, 2011b; Rapela et al., 2011) at c. 630 Ma (Oriolo et al., 2016). In Argentina, the Rio de La Plata Craton is associated with the Tandilia Belt basement

121 (Hartmann et al., 2002), while the so-called Taquarembó block forms the
122 most discernible part of this craton in southernmost Brazil (Chemale,
123 2000; Gaucher et al., 2011; Hartmann et al., 2007). Additionally, the
124 Paleoproterozoic Encantadas microcontinent is interpreted as basement
125 inlier along the Neoproterozoic Dom Feliciano Belt (Chemale, 2000;
126 Hartmann et al., 2000b). Other Paleoproterozoic remnants recorded in this
127 area are the Arroio dos Ratos Complex (Gregory et al., 2016; Leite et al.,
128 2000) and the Vigia Dome (Camozzato et al., 2013).

129 Along the African margin of the ancient Adamastor Ocean, the
130 present-day Kalahari Craton is made up of Archean nuclei surrounded by
131 younger Paleoproterozoic and Mesoproterozoic belts (e.g., Begg et al.,
132 2009; Frimmel et al., 2011; Hanson, 2003; Hartnady et al., 1985). The
133 Archean core, poorly exposed in the western margin, has been derived
134 from the Zimbabwe and Kaapvaal cratons (de Wit et al., 1992). Toward the
135 south, the assumed autochthonous Richtersveld subprovince represents
136 the Paleoproterozoic record (Reid, 1997).

137

138 *2.2 Mesoproterozoic*

139 Intense crustal growth marks the Mesoproterozoic in present-day
140 southwest Africa, whereas in southeast South America this era is partially
141 concealed.

142 Remarkably, Mesoproterozoic ages are found in the Uruguay shield
143 (e.g., Bossi et al., 1993; Bossi and Navarro, 2001; Teixeira et al., 1999;).
144 The allochthonous Cuchilla Dionisio Terrane, formerly Punta del Este

Terrane (Preciozzi et al., 1999), presents Mesoproterozoic basement, which was reworked during the Neoproterozoic (Basei et al., 2011a). This terrane was tangentially accreted to Rio de la Plata craton during the Cambrian (Gaucher et al., 2008). In the Nico Pérez Terrane, volcanic episodes, emplacements of plutons and provenance record have been identified as Mesoproterozoic (e.g., Basei et al., 2008; Bossi and Cingolani, 2009; Campal and Schipilov, 1995; Chiglino et al., 2010; Gaucher et al., 2008, 2011; Oyhantçabal et al., 2005). Particularly, the Lavalleja Group has been efficiently correlated with an African derivation (Basei et al., 2005, 2008). Its basal units present a singular U-Pb detrital zircon signature notably different from the upper units, being related to the Namaqua Belt (Basei et al., 2008). Additionally, interstratified igneous rocks crystallized at c. 1.4 Ga place part of this group into the Mesoproteroic (Gaucher et al., 2011; Oyhantçabal et al., 2005). For southeasternmost Uruguay, a recent study of Pecoits et al. (2016) has proposed the Éden Terrane, which comprises a Paleoproterozoic gneissic basement (c. 1.7 Ga) and Mesoproterozoic supracrustal rocks (c. 1.4 Ga).

In south Brazil, the period between 1.5 and 1.4 Ga is characterized by important dike magmatism mainly in the Apiaí Group (Siga Jr. et al., 2011) and in the Camboriú Complex (Basei et al., 2013), in Paraná and Santa Catarina states, respectively. Such ages have also been reported in Rio Grande do Sul State, represented by Capivarita anorthosite (Chemale et al., 2011) and Tupi Silveira amphibolite (Camozzato et al., 2013).

Stretching out in southwest Africa, the Namaqua Belt is result of successive collisions that deformed Paleoproterozoic units and produced

voluminous magmatism from 1.2–1.0 Ga (Eglington, 2006). However, in the context of SW Gondwana, this geochronological signature found in detrital zircon ages from Neoproterozoic supracrustal sequences is solely related to southwestern African sources. Other Mesoproterozoic sources may be underneath extensive sedimentary sequences of South America.

2.3 Neoproterozoic

The break-up of Rodinia and assembling of Western Gondwana orchestrated the major processes during the Neoproterozoic throughout the lifespan of the Adamastor Ocean (e.g., Brito Neves et al., 1999; Cordani et al., 2000). The resulting collision between the Rio de La Plata and Kalahari cratons in southeastern South America formed the Dom Feliciano Belt, as shown by Fragoso-Cesar (1980) and Basei et al. (2000). According to these authors, it consists of three geotectonic units. Its central part is made up of a schist segment, which represents the Tonian-Cryogenian metavolcano-sedimentary sequences established as Brusque, Porongos and Lavalleja complexes. The eastern part is a widespread granite belt, causing extensive magmatism during the Cryogenian-Ediacaran that gave rise to the Florianopolis, Pelotas and Aiguá batholiths. The western part exposes extensional foreland basins (Itajaí, Camaquã and Arroyo del Soldado) formed in response to further shortening of the orogen. After collision and crustal thickening, major sinistral strike-slip shear zones were developed, connecting all segments trough prominent lineaments termed Dorsal do Canguçu, Major Gercino and Sierra Ballena shear zones (e.g., Basei et al., 2000; Passarelli et al., 2010; Oyhantçabal

et al., 2010). Additionally, in Uruguay, Cryogenian-Ediacaran sequences are reported (Basei et al., 2005; Campal and Schipilov, 2005; Fambrini et al., 2005; Oyhantçabal et al., 2005; Pazos et al., 2003; Pecoits, 2003; Pecoits et al., 2004, 2008, 2011, 2016) and interpreted as deposited in small fault-bounded basins over the Nico Pérez, Cuchila Dionisio and Éden terranes during a tangential collisional event (Pecoits et al., 2016). In Argentina, Neoproterozoic deposition is exposed in the Tandilia Belt (Poiré and Spalletti, 2005) as well as in the Mar del Plata Terrane (Rapela et al., 2011).

On the contrary, southwestern African Neoproterozoic sequences document widespread extension and rifting of Tonian age (Jacobs et al., 2008). These fault systems had later been reactivated, generating continental rifting recorded by the Port Nolloth Zone and Marmora Terrane (Frimmel et al., 2001; Frimmel and Fölling, 2004).

3. Geological setting

The definition of the Dom Feliciano Belt (Fragoso-Cesar, 1980) has been changing greatly along the years (e.g., Basei et al. 2000, 2005, 2008, 2010; Chemale, 2000; Chemale et al., 1995a, 1995b; Fernandes et al., 1995; Frantz and Botellho, 2000; Hasui et al., 1975; Jost and Hartmann, 1984; Ribeiro and Fantinel, 1978; Soliani Jr., 1986). In southernmost Brazil, the three segments of the Dom Feliciano Belt (Fig. 1B) are grouped as foreland deposits (Camaquã Basin), schist belt (Porongos Complex) and granite belt (Pelotas Batholith).

219 The Camaquã Basin overlaps the schist belt to the west and along
220 several NNE-SSW corridors, related to transcurrent processes at brittle to
221 ductile-brittle structural levels and comprising the Eastern-Camaquã Sub-
222 Basin (Almeida et al., 2012; Fambrini et al., 2005; Paim et al., 2000).
223 Equally, the northwestern and southwestern regions of the Porongos
224 Complex (PC) as well as the Camaquã River beds are partially covered by
225 deposits of the Mesozoic Paraná Basin (Faccini, 1989, 2000; Faccini et al.,
226 1990; Milani et al., 1998).

227 The Pelotas Batholith, tectonically bounded to the PC by the Dorsal do
228 Canguçu Shear Zone, can be subdivided into several suites (e.g., Frantz
229 and Botelho, 2000; Frantz and Nardi, 1992; Philipp, 1998; Philipp and
230 Machado, 2005). The formation of this igneous unit is related to syn- and
231 post-collisional magmatism constrained at 650–550 Ma, showing mainly
232 high-K calc-alkaline, metaluminous and subordinate alkaline chemical
233 compositions (Babinski et al., 1997; Frantz et al., 1999, 2003; Philipp et al.,
234 2002, 2013; Philipp and Machado, 2005; Nardi et al., 2008; Silva et al.,
235 1999). Additionally, the Pelotas association has been interpreted as the
236 Neoproterozoic crustal reworking of the gneissic basement (Babinski et al.,
237 1997; Hartmann et al., 2000b; Silva et al., 1999).

238 The NE-SW striking PC is an 150 km long and 50 km wide
239 supracrustal sequence consisting of four major structural domains (Fig. 2),
240 which are referred to as Capané Antiform (CA), Santana da Boa Vista
241 Dome, Serra dos Pedrosas Antiform (Jost and Bitencourt, 1980) and
242 Godinho Antiform (Wildner et al., 1996). Common features among those
243 sectors include two low-dip foliations (S_1 and S_2), linked to transversal and

longitudinal deformation processes (Fernandes et al., 1992a); retrograde metamorphic conditions, from amphibolite to greenschist facies (Marques et al., 1998a); and NE-SW stretching sub-horizontal lineation and kinematic indicators pointing to NE displacement (Marques et al., 1998a).

Although the PC has been focus of intense research for eight decades (since Carvalho, 1932), a definitive geotectonic setting for the Porongos Basin has remained unresolved. Isotopic and geochronological approaches have been used to clarify the stratigraphic relations of PC (see the published compilation of ages from the PC in Tab. 1).

The CA, being the focus of this study, is located in the northernmost part of the PC (Fig. 3). It is a NE-SW oriented supracrustal sequence, approximately 20 km long and 12 km wide. A synthesis of the CA mappings and their lithological characteristics are presented in detail by Marques (1996) and Marques et al. (1998a, 1998b), who showed that the heterogeneous deformation locally preserved original features, allowing lithological differentiation within the limbs and axial zone. The western limb has major metavolcanic sequences intercalated with minor metapelitic sequences. The eastern limb contains metapelitic units, spatially associated with metagranitic bodies and lenses of marble. Both western limb and axial zone also expose sheets of the Capané Alkaline Gneiss and altered ultramafic rocks, the latter interpreted as a dismembered ophiolitic complex (Marques et al., 2003b, 1998b). The axial zone presents pervasively deformed rocks (unknown protoliths), metapelitic units and minor lenses of staurolite-garnet schist (Fig. 3). Additionally, all sequences contain synkinematic leucogranitic bodies as well as quartz mylonites to

ultramylonites, which are particularly dominant in the axial region (Fig. 3). The metamorphic conditions vary from predominant low greenschist to minor low-medium amphibolite facies, the latter restricted to the axial zone (Marques et al., 1998a, 1998b). Geochronological constraints are given by U-Pb detrital zircon ages, which have yielded provenance of sediments from Mesoarchean (3,156 ± 7 Ma), found in garnet-biotite-muscovite schist, to Ediacaran (550 ± 10 Ma), found in metapelite (SHRIMP; Pertille et al., 2015b). Crystallization ages for the Capané Alkaline Gneiss have been reported at 531 Ma (whole-rock Rb-Sr; Lafon et al., 1990) and at 603 ± 6 Ma by U-Pb ages (LA-ICP-MS; Zvirtes et al., 2015). For the same unit, peak metamorphism has been identified at 540 Ma using U-Pb (TIMS; Chemale, 2000). Sm-Nd analyses of metavolcanic whole-rock samples show model NdT_{DM} ages ranging from 2.59 to 0.90 Ga with negative ε_{Nd} values between -22.34 and -1.50 (Gollmann et al., 2008). In addition, Hf isotopes of detrital zircon from metasedimentary rocks show HfT_{DM} ages from 3.17 to 1.45 Ga and ε_{Hf} ranging from -18 to -4 (Pertille et al., 2015b). These data are in mutual agreement and suggest that Paleo- and Mesoproterozoic terranes are the site of origin for both the volcanic rocks and the detrital zircons of the sediments in the PC.

The Santana da Boa Vista Dome crops out in the central-western PC, where the Porongos Complex supracrustal sequence, represented by metapelites, quartzites and marbles, overlies a Paleoproterozoic basement dome, denominated as Encantadas Gneiss, a tonalite-trondhjemite-granodiorite sequence (Ribeiro et al., 1966) and Santana da Boa Vista Mylonitized Granitoids (Machado et al., 1987; Porcher and Fernades, 1990).

294 Recently, Pertille et al. (2015a) have considered the well selected, mature and
295 thick quartzite layer overlying the basement as the Paleoproterozoic Santana
296 Formation, which was previously interpreted as shear-related alteration of the
297 mylonitized granites (Fernandes et al., 1992a, 1992b; Porcher and Fernandes,
298 1990). The contact between the Encantadas Gneiss and the supracrustal
299 sequence is marked by a ductile low-angle shear zone (Lusa et al., 2010). U-
300 Pb crystallization ages obtained from tonalites range from 2,263 ± 18
301 (SHRIMP; Hartmann et al., 2003) to 2,078 ± 13 Ma (SHRIMP; Hartmann et
302 al., 2000a). Deformed rhyolitic volcanic rocks intercalated in
303 metasedimentary sequences have been reported in this sector in a recent
304 work from Pertille et al. (2017), showing two SHRIMP U-Pb zircon ages:
305 801 ± 4.7 and 773 ± 3.1 Ma. U-Pb zircon ages also record two major
306 metamorphic events: 2.0 Ga related to the Trans-Amazonian cycle (TIMS,
307 Chemale, 2000; SHRIMP, Hartmann et al., 2000a), and from 803 ± 14
308 (TIMS; Chemale, 2000) to 631 Ma (SHRIMP; Hartmann et al., 2000a)
309 attributed to the Brasiliano cycle. Provenance of the supracrustal sequence,
310 revealed by U-Pb detrital zircon ages, indicates Mesoarchean (3,092 ± 19 Ma,
311 SHRIMP; Hartmann et al., 2004) to Tonian (1,041 ± 46 Ma, LA-ICP-MS;
312 Gruber et al., 2011) sources, obtained from quartzite and chlorite-
313 muscovite schist, respectively.

314 The Serra dos Pedrosas Antiform is situated in the central-eastern PC,
315 where the supracrustal rocks are composed of metapelites, schists, meta-
316 andesites and meta-rhyolites (Jost, 1981; Jost and Bitencourt, 1980). The
317 low-pressure metamorphic conditions vary from greenschist to low
318 amphibolite facies (Jost, 1981). U-Pb detrital zircon ages yielded a

319 provenance interval from Neoarchean (2,652 ± 32 Ma), obtained from
320 quartz-muscovite schist, to Stenian (1,010 ± 17 Ma), found in chlorite-
321 muscovite schist (LA-ICP-MS; Gruber et al., 2011). The Tonian
322 depositional age for the Porongos Basin has been obtained from zircon
323 grains of a meta-rhyolite in this sector, which is reported at 783 ± 6 Ma
324 (SHRIMP; Porcher et al., 1999) to 789 ± 7 Ma (LA-ICP-MS; Saalmann et
325 al., 2011). Whole-rock Sm-Nd isotopic data obtained from metavolcanic
326 (from -6.87 to -21.72) and metasedimentary rocks (from -6.25 to -17.96) show
327 similar NdT_{DM} ages betwen c. 1.7 and 2.5 Ga (Saalmann et al., 2006).
328 These values suggest a Paleoproterozoic crust as a source for the
329 supracrustal sequence of PC (Saalmann et al., 2006).

330 The Godinho Antiform is the only defined domain south of Camaquã
331 River, although the PC extends farther south and east. This sector exposes
332 metavolcanic rocks, intercalated with phyllites, quartzites, schists, marble and
333 metagranitoids (Wildner et al., 1996). U-Pb crystallization ages for meta-
334 andesites diverge greatly, being reported at 1,356 ± 227 Ma (LA-ICP-MS;
335 Wildner et al., 1996) and 773 ± 8 Ma (TIMS; Chemale, 2000). Additionally, a
336 recent study of Pertille et al. (2017) on rhyolites of this sector has shown 809
337 ± 4.1 Ma as U-Pb crystallization age using SHRIMP. For quartzitic rocks,
338 LA-ICP-MS U-Pb ages of detrital zircon grains range from Mesoarchean
339 (2,906 ± 42 Ma) to Statherian (1,619 ± 39 Ma), according to Gruber et al.
340 (2011). Metamorphic episodes are recorded at c. 2.0 Ga for the quartzitic
341 rocks (LA-ICP-MS, Gruber et al., 2011; SHRIMP, Hartmann et al., 2004)
342 and at c. 700 Ma for the meta-andesite (LA-ICP-MS; Wildner et al., 1996).

343 A tectonic setting for the whole belt remains disputable due to lack of

344 systematic mapping and available data in the southernmost region of the PC,
345 i.e., south and east of the Godinho Antiform. Few studies were carried out in
346 this region (Camozzato et al., 1994; Remus et al., 1987, 1991), providing
347 evidence of similarity between this region and the western limb of the CA
348 (Camozzato et al., 1994; Marques et al., 2003a). Thrust zones have displaced
349 and imbricated the basement, comprising sequences of pelitic schists,
350 quartzites, marble, meta-ultramafic rocks, dacitic to rhyolitic metatuffs and
351 synkinematic metagranitoids metamorphosed under medium-pressure
352 conditions of low amphibolite facies (Remus et al., 1987, 1991). In addition,
353 the occurrence of alkaline gneiss similar to the Capané Gneiss has been
354 reported (Camozzato et al., 1994). U-Pb ages of detrital zircons obtained from
355 quartzite constrained the provenance in this region from Siderian (2,452 ±
356 12 Ma) to Ediacaran (605 ± 5 Ma) found in plagioclase-quartz-chlorite-
357 muscovite schist (SHRIMP; Hartmann et al., 2004). In the southeastern
358 part of the PC, the provenance age of muscovite schist ranges from
359 Mesoarchean (2,863 ± 24 Ma) to Stenian (1,008 ± 12 Ma), as revealed by
360 LA-ICP-MS (Pertille et al., 2015a).

361

362 **4. Samples and methods**

363 *4.1 Sample selection and preparation*

364 This study reviews the complete set of thin sections (151 samples)
365 of Marques, (1996) and Marques et al. (1998a, 1998b) obtained from
366 samples taken throughout the CA in order to establish a consistent
367 geological framework. Previously known key outcrops (described in detail

368 by Marques, 1996) and new areas were visited and selected for sampling.
369 From a total of 28 exposures surveyed, seven were chosen for sampling
370 and subsequent thin section preparation as well as LA-MC-ICP-MS U-Pb
371 zircon dating (see sample list in Tab. 2 and outcrop locations in Fig. 3).
372 Analyses were carried out in one sample from the eastern limb (CA-19),
373 two samples from the western limb (CA-16 and CA-11) and four samples
374 from the axial zone (CA-22, CA-17, CA-02A and CA-21B).

375 Fractions between 60 and 170 mesh of zircon grains were
376 separated following standard procedures: crushing 3–5 kg of cleaned and
377 dried samples, milling, sieving, panning and separating by a Frantz
378 isodynamic magnetic separator at different currents (0.4, 0.8, 1.2 and
379 1.8 A) and, additionally, by applying heavy liquid separation. The mount
380 montage was done with pastilles of Buehler epoxy, polished with emery
381 paper and diamond paste of 0.25–1 micron.

382

383 *4.2 Zircon imaging*

384 Imaging of zircon grains was performed by binocular microscopy,
385 where macroscopic properties such as color, degree of transparency and
386 external morphology were described. Back-scattered electron images
387 were obtained using the scanning electron microscope Jeol JSM 5800 at
388 the Electron Microscope Center of the Federal University of Rio Grande do
389 Sul for delimiting regions in zircon grains, which were free of fractures and
390 inclusions. This procedure enhanced adequate responses according the
391 optimized frequency of Andersen (2005). Cathodoluminescent images

were acquired using a Quanta 250 FEG electron microscope connected with Monto CL3+ cathodoluminescence spectroscope at the Geochronological Research Center at University of São Paulo (CPGeo-USP). Considering the large number of dated zircons, only the most representative images from zircon families are illustrated in order to support the interpretation.

4.3 U-Pb dating of zircon

U-Pb age determination took place at CPGeo-USP and at the Isotopic Geology Laboratory of Federal University of Rio Grande do Sul. All analyses were implemented on a Thermo-Fisher Neptune inductively coupled plasma-mass spectrometer (ICP-MS) coupled with an Excimer ArF laser ablation system (LA) of 193 nm. The mounts containing zircons were cleaned in a HNO_3 solution (3%) and in ultraclean water bath. The ablation was done with spot size of 32 μm, at frequency of 6 Hz, an intensity of 6 mJ and ablation time of 40 s. Corrections of mass bias was performed by the analysis of zircon standard GJ-1 ($^{206}Pb/^{238}Pb$ age by IDTIMS = 608.5 ± 0.4Ma; Jackson et al*.,* 2004) and common Pb based on Stacey and Kramers (1975) model. The obtained data was reduced through in-house Excel spreadsheets and ages were derived from $^{206}Pb/^{238}U$, $^{207}Pb/^{235}U$, $^{207}Pb/^{206}Pb$ and $^{232}Th/^{238}U$ ratios, calculated via ISOPLOT 3.6 (Ludwig, 2008). Errors for isotopic ratios are presented at ± 1σ confidence level.

The acquired data were filtered prior plotting in order to remove

analysis above 10% of discordance and with more than 1% of common lead. Also, the interpreted age and plotting followed recommendations by Gehrels (2014), where the $^{207}Pb/^{206}Pb$ age was selected for grains older than 1.2 Ga and $^{206}Pb/^{238}U$ for grains younger than 1.2 Ga. The final isotopic data results were evaluated by means of probability density plots and cumulative density plots using Microsoft Excel macros from the Arizona LaserChron Center (George Gehrels – https://www.laserchron.org). Potential origin of the ages was established using the threshold 0.02 for Th/U ratio, where values above are considered magmatic and below metamorphic (Rubatto, 2002). All zircon U-Pb isotopic data obtained for the present study are presented in the electronic appendix (Supplementary Data A).

5. Results

5.1 Petrographic sample characteristics

The petrographic descriptions follow the nomenclature and mineral abbreviation systems proposed by the International Union of Geological Sciences (Schmid et al., 2007; Siivola and Schmid, 2007). Exception is made for sample CA-02A, termed phyllonite, being very fine-grained and extremely friable, which was sampled for geochronological studies only. All units of the CA reveal a heterogeneous deformation character. Some studied samples show incipient deformation that support the original units proposed by (Marques et al., 1998a, 1998b). However, most of petrographic samples from Marques (1996) are affected by high strain that obliterate any original textures. In this case, the lithotypes can be grouped

440 from protomylonite to ultramylonite (according to the nomenclature of
441 Sibson, 1977) and present intensely deformed quartz associated with
442 strong mineral stretching lineation. Samples from the eastern limb (CA-19)
443 and western limb (CA-16 and CA-11) are less affected by the high strain,
444 while three samples from the axial zone (CA-17, CA-02A and CA-21B) are
445 strongly mylonitized and one sample from the axial area shows moderate
446 deformation (CA-22).

447 In the eastern limb, sample CA-19, a brown to light brown, fine- to
448 medium-grained (≤0.8 mm in diameter) quartz-muscovite schist shows a
449 lepidogranoblastic texture, where quartz grains are gathered as
450 asymmetric eye-shaped aggregates and the main foliation is defined by
451 muscovite lamellae (Fig. 4A). Quartz grains (55%) occur as ribbon, eye-
452 shaped aggregates, partially being dispersed in the matrix as new grains
453 and showing sutured boundaries, irregular shape and undulose extinction.
454 Anhedral muscovite lamellae (45%) surround the quartz aggregates as a
455 film and are partially crenulated.

456 In the western limb, a gray, fine- to medium-grained
457 metavolcaniclastic rock (sample CA-16) shows weak foliation and a
458 porphyroclastic texture (Fig. 4B). Its grain size varies from the
459 submillimeter (matrix) to 1 mm (porphyroclasts) level. The essential
460 constituent of this unit is given by quartz (35%), which occurs in the matrix
461 and as agglomerates of porphyroclasts, displaying undulose extinction.
462 Additionally, chlorite (35%) occurs both in matrix and reticular around
463 porphyroclastic quartz aggregates (Fig. 4B). Anhedral carbonate (30%)
464 has essentially been identified in the matrix, showing diffuse crystal

boundaries. Subordinate, few opaque minerals, apatite, zircon, epidote and mica also occur. Another gray, fine-grained (≤0.5 mm) metavolcaniclastic rock from the western limb (sample CA-11) displays an equigranular compositional banding, which defines the main foliation and incipient breccia texture (Fig. 4C). The main constituent of this rock is quartz (35%), showing undulose extinction. Rarely, it is also found as subgrains concentrated in parallel levels to the main foliation. The rest of the rock is composed of anhedral chlorite (30%) and carbonate (30%) crystals, both showing no clear crystal boundaries but haze appearance (Fig. 4C). Rare biotite (5%) is associated with chlorite and carbonate and has lamellae shape, hosting minute zircon grains.

At the boundary of the western limb and axial zone, defined by a tributary of Capané Creek, sample CA-22 was taken from lenses of staurolite-garnet-quartz-muscovite schist. This yellowish-gray to brownish-gray rock shows a porphyroblastic texture with coarse-grained, euhedral to subhedral grains of garnet (10%) in a fine-grained matrix (Fig. 4D). The porphyroblastic garnets contain poikilitic inclusions of quartz and partially reveal a snowball texture with an asymmetric pressure shadow. Minor staurolite occurs as porphyroblasts, generally being surrounded by thin chlorite halo. The matrix comprises strongly aligned muscovite lamellae (55%), defining the main anastomosed foliation, and stretched quartz grains (35%) with sutured grain boundaries arranged in segregated levels.

Collected in the northern part of the axial zone, sample CA-17 refers to a pink, fine-grained (up to 3 mm) muscovite-quartz mylonite with a granolepidoblastic texture. The subhorizontal main foliation is defined by

strong alignment of lamellar muscovite (30%), which configures submillimeter spacing and anastomosed levels. Anhedral quartz grains (70%) show sutured boundaries and manifest an oblique foliation defined by the mineral stretching (Fig. 4E). Chlorite rarely occurs as alteration product of muscovite and slightly stretched plagioclase grains, the latter being associated with the quartz-levels and presenting sutured boundaries as well as poorly developed polysynthetic twinning. Also obtained from the axial zone, sample CA-21B represents a pink to light pink, fine- to medium-grained chlorite-bearing quartz-muscovite ultramylonite with a lepidonematoblastic texture. The main foliation is revealed on a millimeter scale and defined by the strong mineral stretching of quartz aggregates (40%) and muscovite lamellae (60%; Fig. 4F).

All mylonitized samples from the axial zone (CA-17, CA-19 and CA-21B) present bimodal range of quartz grain size, which is grouped according fabric distinguishing larger subgrains with undulose extinction from new, small, uniform grains. The arrangement of both fabrics suggests two types of dynamic recrystallization: (1) quartz crystals vary from relic, elongate subgrains to new grains formed during the bulging recrystallization, and (2) the foliation is defined by the preferred orientation of polycrystalline quartz aggregates formed during subgrain rotation (Passchier and Trouw, 2005).

5.2 Detrital zircon morphology

The zircon grains from the eastern (CA-19, Fig. 5A) and western

514 (CA-16, Fig. 5B; CA-11, Fig. 5C) limbs and axial zone (CA-22, Fig. 5D;
515 CA-17, Fig. 5E; CA-02A, Fig. 5F; CA-21B, Fig. 5G) are generally
516 translucent and have length-to-width ratio of 2:1 when slightly rounded at
517 corners and 3:1 when (sub-)prismatic. Their morphology shows a mixture
518 of these patterns, with predominance of the latter at the limbs and the
519 former at the axial zone. Regarding size, zircon grains are 40–200 μm
520 long in samples of the eastern limb, 50–200 μm in the western limb and
521 75–275 μm in the axial zone. Under binocular microscope, they show light
522 yellow to light brown coloring in the eastern limb; predominant colorless to
523 light brown coloring in the western limb; and predominant light brown to
524 light yellow coloring and colorless in the axial zone. Cathodoluminescent
525 images have shown oscillatory zoning in all samples, overgrowths
526 evidenced by light gray color (Figs. 5A, 5D and 5E) and inherited (Figs. 5A,
527 5B and 5D) or homogenous nuclei (Figs. 5C and 5E). Back-scattered
528 images have evidenced variable degree of fracturing (Fig. 5F).

529

530 *5.3 U-Pb zircon ages*

531 In the eastern limb, the quartz-muscovite schist (CA-19) has
532 revealed Th/U ratios varying from 0.02 to 1.12, suggesting metamorphic
533 and magmatic ages for the zircon grains. A total of 46 spots were obtained
534 from 42 grains, yielding 27 concordant ages ranging from 572 ± 7 to 1,971
535 ± 27 Ma. The probability density plot displays a polymodal pattern with
536 main age peaks at 770 and 610 Ma, respectively, and minor peaks at
537 850 Ma, 1.0, 1.15, 1.4, 1.8 and 1.9 Ga (Fig. 6A). The contribution found is
538 mostly Neoproterozoic with subordinate Mesoproterozoic and

539 Paleoproterozoic ages (Fig. 6A).

540 In the western limb, both metavolcaniclastic rocks (samples CA-16
541 and CA-11) present Th/U ratios varying from 0.19 to 1.27 and from 0.28 to
542 1.52, respectively. The Th/U ratios allied to zircon textures suggest
543 magmatic origin for the zircon grains. Ages of 44 spots on 43 zircon grains
544 from the sample CA-16 yielded 23 concordant ages in an array of 619 ± 15
545 to 2,271 ± 25 Ma. The probability density plot displays bimodal pattern
546 with main age peak at 610 Ma that is assumed as the age of formation of
547 the rock and minor peaks at 2.0, 2.1 and 2.2 Ga (Fig. 6B). The dating of
548 sample CA-11 using 24 spots on 20 grains yielded 18 concordant ages in
549 an array of 607 ± 14 to 2,252 ± 34 Ma. The probability density plot
550 illustrates a polymodal pattern with main age peak at 600 Ma that is
551 assumed as the age of formation of the rock and minor peaks at 0.780 and
552 2.1 Ga (Fig. 6C). The data shows only Neoproterozoic and
553 Paleoproterozoic input for both samples, where the former is dominant for
554 CA-16 (Fig. 6B) and the latter for CA-11 (Fig. 6C).

555 In the axial zone, zircon textures suggest magmatic origin (allied to
556 Th/U ratios varying from 0.03 to 13.77). For samples CA-22, CA-17, CA-
557 02A and CA-21B, the data shows mostly Paleoproterozoic ages
558 (especially Rhyacian) and very restricted Neoproterozoic (only in CA-22),
559 Mesoproterozoic (both CA-22 and CA-17) and Archean contribution (CA-
560 17, CA-02A and CA-21B). In the staurolite-garnet-quartz-muscovite schist
561 (CA-22), a total of 91 spots were analyzed from 89 grains, which yielded
562 69 concordant ages in an array of 0.82 to 2.25 Ga. Probability density plot
563 displays polymodal pattern with main age peak at 2.12 Ga and minor

564 peaks at 0.83, 1.0, 1.13, 1.19 and 1.54 Ga (Fig. 6D). Dating 91 spots on
565 83 grains in the muscovite-quartz mylonite (CA-17) yielded 81 concordant
566 ages in an array of 1.3 to 2.8 Ga. Probability density plot displays
567 polymodal pattern with main age peak at 2.29 Ga and minor peaks at 1.36
568 and 2.86 Ga (Fig. 6E). In the phyllonite (CA-02A), a total of 55 concordant
569 ages yielded 1.89 to 3.26 Ga. Probability density plot displays polymodal
570 pattern with main age peak on Gaussian curve at 2.13 Ga and minor
571 peaks at 3.05 Ga (Fig. 6F). A total of 88 spots and grains from the quartz-
572 muscovite ultramylonite (CA-21B) yielded 49 concordant ages in an array
573 of 2.04 to 2.86 Ga. Probability density plot displays bimodal pattern with
574 main age peak on Gaussian curve at 2.17 Ga and minor peak at 2.85 Ga
575 (Fig. 6G).

576

577 **6. Discussion**

578 *6.1 Geochronological provenance signatures*

579 Based on the detrital zircon signatures of the supracrustal rocks of
580 the entire PC outcropping area, some geochronological patterns can be
581 identified (Fig. 7). Considering the zircon ages, three different sequences
582 can be pointed out: one with strong Rhyacian peaks and no
583 Neoproterozoic contribution; one with polymodal peaks but all younger
584 than Tonian; and, one with strong Ediacaran input. In the CA, all those
585 different geochronological signatures occur associated with distinct
586 lithological association.

587 Mylonitized rocks compose most of the area of the CA axial zone.

588 The quartz mylonites to ultramylonites (CA-02A, CA-17 and CA-21B) are
589 nearly unimodal, with a main peak at 2.2–2.1 Ga, with no Neoproterozoic
590 contribution. This provenance pattern is the same as for the quartzitic
591 rocks from Hartmann et al. (2004), Gruber et al. (2011) and Pertille et al.
592 (2015a, 2017) associated to the Santana Formation (*sensu* Pertille et al.,
593 2015a) that crops out in the Santana da Boa Vista Dome (Fig. 7). These
594 similarities support the interpretation that the mylonitic rocks from the CA
595 axial zone are part of the Santana Formation. The presence of rocks from
596 the Santana Formation in the CA axial zone is interpreted as basement
597 tectonic slices. Pertille (2015a) has suggested 1.7 Ga as the maximum
598 depositional age for the Santana Formation. However, given the
599 correlation proposed here, the presence of some Mesoproterozoic grains
600 in the mylonitic rocks from the Capané area place the maximum
601 depositional age of the Santana Formation at 1.3 Ga.

602 The geochronological pattern of the garnet-staurolite schist (CA-22)
603 is different from all other CA samples. The schist is polymodal with a
604 strong peak at the Rhyacian and many inputs from the Mesoproterozoic.
605 The younger grains are Tonian and mark the maximum depositional age
606 for this unit. Comparing its signature to other schists and metapelites from
607 the PC (Fig. 7), it is clear that the garnet-staurolite schist from the CA axial
608 zone can be better correlated to the Porongos Complex in special with the
609 units that occurs at the Serra dos Pedrosas Antiform (Porcher et al., 1999;
610 Saalmann et al., 2011) and the Santana da Boa Vista Dome (Pertille et al.,
611 2017). Consequently, the sedimentation of these units are constrained to
612 the Tonian and here we suggest the name Porongos I sequence to group

613 all meta-volcanosedimentary rocks formed during this period. The
614 Porongos I fragments found in the CA are considered as tectonic
615 imbrications.

616 The provenance patterns of the rocks that crop out in the limbs of
617 the CA show a significant Ediacaran-Cryogenian (c. 630–580 Ma)
618 contribution. The eastern limb, dominantly metapelitic (CA-19), presents
619 major Ediacaran-Cryogenian and Tonian zircon ages as well as minor
620 peaks from Stenian to Rhyacian. Similarly, the western limb, dominantly
621 metavolcaniclastic (CA-16 and CA-11), shows strong Ediacaran-
622 Cryogenian input and minor Rhyacian contribution. The sedimentation of
623 these units are constrained to the Ediacaran considering the volcaniclastic
624 nature of the rocks from the western limb (see Fig. 3 and Tab. 1 in the
625 Supplementary Material).

626 The strong Ediacaran detrital zircon ages observed in both limbs of
627 the CA (samples CA-11, CA-16, CA-19; see Tab. 1 for data from Pertile et al.,
628 2015b, 2017) represents a younger provenance signature than those found
629 in the Porongos I sequence. These supracrustal rocks are here considered
630 as remnants of younger basins, named Porongos II sequence. Considering
631 the geological similarities, already suggested by Marques et al. (2003a,
632 1998a) and Camozzato et al. (1994) between the CA rocks and the
633 supracrustal units that crop out in the southernmost areas of the PC (Remus
634 et al. 1991, 1987), it is proposed that both sequences belong to the Porongos
635 II sequence. This suggestion is also supported by sample 148 from Pertille
636 et al. (2017) (see Fig. 2, Tab. 1) that presents a strong Ediacaran input.

637

638 *6.2 Inferred sources for Porongos I and II sequences*

639 Regarding the possible source areas for the Porongos I sequence,
640 the few Archean ages may have come from the La China Complex and the
641 Las Tetas Complex, Uruguay (e.g., Hartmann et al., 2001). Another
642 possibility is that these crystals are derived from the reworking of the
643 Uruguayan Zanja del Tigre Formation, Lavalleja Group (correlated to
644 Porongos I?), which presents a large number of Archean zircon ages
645 (Basei et al., 2008). Early Paleoproterozoic sources for the Siderian
646 zircons may be related to Santa Maria Chico Granulite Complex
647 (Hartmann et al., 2008) or Neto Rodrigues Gneiss (Remus et al., 1996).
648 Dominant Rhyacian ages found throughout the PC (Gruber et al., 2011;
649 Pertille et al., 2015a, 2017) may be derived directly from the Encantadas
650 Gneiss, implying sedimentation from proximal reworked basement.
651 Orosian ages may correspond to sourcing from the Arroio dos Ratos
652 Complex (Leite et al., 2000). Mesoproterozoic provenances may be
653 related to Capivarita Anorthosite (Chemale et al., 2011), Tupi Silveira
654 Amphibolite (Camozzato et al., 2013) and alternatively to the Nico Pérez
655 or Piedra Alta terranes (Bossi et al., 1993; Bossi and Navarro, 2001;
656 Teixeira et al., 1999;). Remarkably, Stenian ages are labeled as typical
657 African geochronological signature (Basei et al., 2005). Nevertheless,
658 other sources of Mesoproterozoic age, not yet identified in this part of
659 South America, may be underneath extensive sedimentary covers. During
660 the Neoproterozoic, the Porongos I sequence recorded Tonian rhyolitic
661 volcanism, which is the marker of maximum depositional age for this
662 stratigraphic sector.

663 The Porongos II provenance pattern may include the observed
664 zircon signature shown by Porongos I meta-volcanosedimentary units, as
665 the latter is considered to be part of its basement. The predominant
666 Paleoproterozoic ages may have primarily derived from the Encantadas
667 Gneiss. The rare Mesoproterozoic zircon grains found in the Porongos II
668 may reflect the small amount of Mesoproterozoic zircons in the Porongos I
669 and the absence of areas with Mesoproterozoic rocks in the southern
670 Brazilian and Uruguayan regions. Late Neoproterozoic zircon ages are
671 abundant in the Porongos II sequence and represent its fingerprint. Tonian
672 ages may be derived from volcanic rocks found in the Porongos I, while
673 Cryogenian and Ediacaran peaks are proposed to be derived from the
674 Pelotas Batholith formed at 630–580 Ma.

675

676 *6.3 Configuration of SW Gondwana*

677 Combining the new U-Pb detrital zircon ages of this study with
678 those from the literature and taking into account previously published
679 tectonic (Fig. 9.1; Basei et al., 2008; Frimmel et al., 2011) and
680 paleogeographic (Johansson, 2014; Pecoits et al., 2016; Fig. 9.2) models,
681 it is suggested a modified tectonic model where the Porongos II sequence
682 evolved during the late stages of the Pan-African–Brasiliano orogeny in
683 southernmost Brazil. The tectonic phases were triggered by broad Tonian
684 rifting processes (Fig. 9.2A), which led to the diachronic break-up and
685 fission of the Rodinia supercontinent and ended up in the Ediacaran-
686 Cambrian assembling of SW Gondwana (Basei et al., 2005; Bossi and
687 Gaucher, 2004; Brito Neves et al., 1999). Several lithospheric segments,

688 representing cratons, blocks and terranes, drifted and interacted, forming
689 new oceans and basins. On a regional scale, the orogenic system related
690 to the Dom Feliciano Belt comprises the cyclic history of the Adamastor
691 Ocean, terminated by the collision process of Rio de La Plata and Kalahari
692 cratons (Basei et al., 2000; Figs. 9.1 and 9.2).

693 During the Tonian of present-day southernmost Brazil, the
694 deposition of Porongos I sequence may took place (Porcher et al., 1999;
695 Saalmann et al., 2011) in a marginal basin of the Encantadas Terrane
696 (Fig. 9.1A). Also, in the northern tip of Dom Feliciano Belt, the first
697 magmatic episode preceding the Brusque Basin has been constrained
698 between 930 and 840 Ma (Basei et al., 2011). Nearby, the Rio de La Plata
699 craton was subject to an active continental margin environment (Saalmann
700 et al., 2011), closing the São Gabriel Ocean and deforming the Porongos I
701 sequence (Saalmann et al., 2011; Figs. 9.1A-C).

702 On a regional scale, the approximation of eastern South American
703 blocks and the southwestern African units due to Adamastor Ocean
704 subduction may be recorded in xenoliths in the magmatic sector of Dom
705 Feliciano Belt (Gross et al., 2006; Koester et al., 2016; Lenz, 2010; Lenz
706 et al., 2011; Martil et al., 2017; Silva et al., 1999; Figs. 9.1A-C). Regarding
707 the subduction and the tectonic setting of the Dom Feliciano Belt formation,
708 several models have been put forward over the past decades (e.g.,
709 Fernandes et al., 1992b; Fragoso-Cesar, 1980; Sánchez-Bettucci and
710 Ramos, 1999). Basei et al. (2000) proposed eastward subduction in which
711 the magmatic arc was developed at the Kalahari cratonic margin and
712 tectonically imbricated at the South American margin during the Pan-

African–Brasiliano orogeny (Figs. 9.1B-D**).** This assumption is mostly corroborated by the genetic correlation of Rocha and Gariep basins, implying that the easternmost part of Uruguay has been derived from southwestern Africa (Basei et al., 2005).

Concomitantly, units in southwestern Africa registered widespread extension and rifting, whereas Neoproterozoic sequences were deposited over the Mesoproterozoic Namaqua Belt (Jacobs et al., 2008). Faulting may have triggered continental rifting that evolved to a narrow oceanic basin (Frimmel et al., 1996a, 1996b, 2002), represented by the Marmora Terrane that had later been juxtaposed to the continental Port Nolloth Zone through the Schakalsberg Thrust (Fig. 9.1C). Despite considerable ambiguity, few authors interpreted the Marmora Terrane as oceanic floor of the Adamastor Ocean (e.g., Frimmel and Fölling, 2004; Hartnady et al., 1985). However, small and short-living oceanic basins were common during the Pan-African–Brasiliano setting (Condie, 2002) and their premature closure took place synchronously with the Iapetus Ocean closure, producing compressive forces at both sides of the western Gondwana supercontinent (Grunow et al., 1996).

Conspicuous to the transition of the Cryogenian to the Ediacaran, the Rio de la Plata and Kalahari cratons obliquely collided due to NE-SW plate convergence (Figs. 9.1D and 9.2C), also accreting juvenile Neoproterozoic crust (Hartmann et al., 2011; Lena et al., 2014; Saalmann et al., 2005; Fig. 9.2B). Coevally, intense collisional to post-collisional magmatism lasted along the arc of the Dom Feliciano Belt (Babinski et al., 1997; Basei et al., 2000, 2008; Figs. 9.1D-E), which may have influenced

738 the metamorphic conditions of Porongos I sequence, reaching low-medium
739 amphibolite facies at Serra dos Pedrosas Antiform (Gruber et al., 2011; Lenz,
740 2006).

741 The global Marinoan and Gaskiers glaciations during the
742 Cryogenian and Ediacaran left important diamictite deposits in the African
743 side, such as the Numees Formation (Frimmel and Fölling, 2004; Fig.
744 9.1D). In spite of a well-documented isotopic and lithological record of
745 deposits from these glaciations around the world, the glaciogenic influence
746 on few deposits documented in Uruguay (e.g., Pazos et al., 2003; Pecoits
747 et al., 2008; Aubet et al., 2014 and references therein), Argentina (e.g.,
748 Pazos et al., 2008; Pazos and Rapalini, 2011) and southern Brazil (e.g.,
749 Eerola, 1994, 1995, 1997; Janikian et al., 2008) have largely been
750 disputed (e.g., Gaucher and Poiré, 2009; Masquelin and Pazos et al.
751 2010; Pecoits et al., 2010; Sánchez, 1993; Tohver et al., 2006;).

752 In southernmost Brazil, the Ediacaran compression may have
753 generated synorogenic deposits preserved in synforms, placed in front of
754 large nappes during the Dom Feliciano Belt deformation (Figs. 9.1D-E).
755 Synorogenic deposits refer to sedimentary units that were deposited in
756 active tectonic setting. Such sequences were deposited between
757 contracted orogenic belts and adjacent cratons, subsiding very quickly and
758 playing a fundamental role in determining the timing of tectonic inversion
759 (DeCelles and Giles, 1996). Alkaline magmatism dated at c. 600 Ma
760 (Chemale, 2000; Zvirtes et al., 2015), which is represented by the Capané
761 Alkaline Gneiss, heralds the accommodation of these sequences of
762 carbonate, metavolcaniclastic, metapelitic and metaquartzitic rocks during

763 the final stages of the Pan-African–Brasiliano tectonic cycle. This
764 synorogenic deposit has its maximum age deposition around 580 Ma and
765 is defined as Porongos II sequence.

766 Moreover, similar deposits are reported in the margins of Nico
767 Pérez and Cuchilla Dionisio terranes (Uruguay), described as a thin
768 interleaved association of conglomerates, sandstones, rhythmites as well
769 as volcanic and volcaniclastic rocks by Pecoits et al. (2016). According to
770 these authors, Playa Hermosa, Las Ventanas and Barriga Negra
771 formations were deposited up to 585 Ma. Therefore, even deposited in
772 very diverse tectonic context and being devoid of major deformation and
773 correlated to the Camaquã Basin, they can be interpreted as synorogenic
774 deposits as well. Considering the relative density plots of all these
775 synorogenic deposits (Fig. 10), both Brazilian and Uruguayan units show
776 significant contribution from the magmatic segment of Dom Feliciano Belt
777 (Fig. 9.1E). However, the contribution of Mesoproterozoic sediments is
778 more pronounced for the Uruguayan Ediacaran units, which is in
779 agreement with the African derivation of Punta del Este Terrane, as
780 proposed by Basei et al. (2000, 2008, 2011).

781 In the southernmost Brazilian São Gabriel Block, the transition from
782 compressional to extensional tectonics is reflected by the intrusion of the
783 Caçapava do Sul Granite Complex at c. 560 Ma (Frantz et al., 2000;Leite,
784 1997; Leite et al., 1995, 1998; Fig. 9.1D). The orogen collapse led to the
785 extensional setting, represented in SW Gondwana by the Camaquã and
786 Nama basins (Almeida et al., 2010; Blanco et al., 2011; Fragoso-Cesar,
787 1980; Germs, 1983; Janikian et al., 2008; Fig. 9.1E). Finally, the

788 metamorphism recorded at c. 540 Ma in the Capané Alkaline Gneiss
789 (Chemale, 2000; Zvirtes et al., 2015) possibly reflects the closing time of the
790 Porongos II sequence. During this phase, thrusting may have occurred
791 throughout the CA, leading to imbrication of sheets of several lithotypes,
792 such as alkaline gneisses, mylonites, which have been identified as part of
793 the Santana Formation, fragments of the Porongos I sequence (staurolite-
794 garnet schists) and meta-ultramafic rocks.

795

796 **7. Conclusions**

797 1) Different geochronological detrital zircon signatures observed in
798 different segments of the Porongos Complex allow us to propose the
799 existence of two basins of different ages called Porongos I and II.

800 2) The Porongos I sequence is considered Tonian based on the
801 rhyolitic intercalations that crop out in the Serra dos Pedrosas Antiform
802 and the Santana da Boa Vista Dome. The strong Ediacaran detrital zircon
803 contribution found in the limbs of Capané Antiform (CA) defines the
804 maximum age of deposition for the Porongos II sequence.

805 3) The axial zone of the CA represents a heterogeneous unit
806 tectonically imbricated in the supracrustal sequence of the CA, possibly as
807 part of the underlying basement, including the Porongos I unit and the
808 Santana Formation.

809 4) The CA staurolite-garnet schist has a provenance pattern similar to
810 the supracrustal sequence of the Serra dos Pedrosas Antiform. This medium-
811 grade metamorphic rock has documented a Mesoproterozoic input similar to

812 other sectors of the Porongos I sequence. The major Paleoproterozoic input
813 in the axial zone may represent sources from its own basement, i.e.,
814 Encantadas Gneiss.

815 5) Neoproterozoic Tonian detrital ages observed in the Porongos II
816 succession may have been derived from the Porongos I sequence, while
817 the Pelotas Batholith is proposed to be the source of the Ediacaran detrital
818 zircons of Porongos II.

819 6) The new data presented here allow us to refine previous tectonic
820 models proposed for the Pan-African–Brasilian orogeny in southern Brazil,
821 identifying the existence of syn-orogenic Ediacaran deposits, which
822 occurred during the final stages of the SW Gondwana assembly.

823

824 **Acknowledgments**

825 The first author was supported by a graduate scholarship (grant
826 132274/2015-9) from the National Council for Scientific and Technological
827 Development (CNPq), which is gratefully acknowledged. Luis Fernando de
828 Ros and Garibaldi Armelenti from the Instituto de Geociências at
829 Universidade Federal do Rio Grande do Sul are thanked for their support
830 for obtaining photomicrographs of the thin sections used in this work.
831 Tobias W. Höfig is thanked for his dedicated assistance in the final review
832 of the manuscript.

833 **Appendix**

834 Supplementary data related to this article can be found in the online
835 version.

References

Almeida, F.F.M., Hasui, Y., Brito Neves, B.B., Fuck, R.A., 1981. Brazilian structural provinces: An introduction. Earth-Science Rev. 17, 1–29. doi:10.1016/0012-8252(81)90003-9

Almeida, R.P., Janikian, L., Fragoso-Cesar, A.R.S., Fambrini, G.L., 2010. The Ediacaran to Cambrian Rift System of Southeastern South America: Tectonic Implications. J. Geol. 118, 145–161. doi:10.1086/649817

Almeida, R.P., Santos, M.G.M., Fragoso-Cesar, A.R.S., Janikian, L., Fambrini, G.L., 2012. Recurring extensional and strike-slip tectonics after the Neoproterozoic collisional events in the southern Mantiqueira province. An. Acad. Bras. Cienc. 84, 347–376. doi:10.1590/S0001-37652012005000034

Andersen, T., 2005. Detrital zircons as tracers of sedimentary provenance: limiting conditions from statistics and numerical simulation. Chem. Geol. 216, 249–270. doi:10.1016/j.chemgeo.2004.11.013

Aubet, N.R., Pecoits, E., Heaman, L.M., Veroslavsky, G., Gingras, M.K., Konhauser, K.O., 2014. Ediacaran in Uruguay: Facts and controversies, J. South Am. Earth Sci. 55, 43-57. doi: 10.1016/j.jsames.2014.06.007

Babinski, M., Chemale, F., Van Schmus, W.R., Hartmann, L.A., Silva, L.C., 1997. U-Pb and Sm-Nd geochronology of the neoproterozoic granitic-gneissic Dom Feliciano belt, Southern Brazil. J. South Am. Earth Sci. 10, 263–274. doi:10.1016/S0895-9811(97)00021-7

Basei, M.A.S., Brito Neves, B.B., Siga Jr., O., Babinski, M., Pimentel, M.M., Tassinari, C.C.G., Hollanda, M.H.B., Nutman, A.P., Cordani, U.G., 2010. Contribution of SHRIMP U–Pb zircon geochronology to unravelling the evolution of Brazilian Neoproterozoic fold belts. Precambrian Res. 183, 112–144. doi:10.1016/j.precamres.2010.07.015

Basei, M.A.S., Campos Neto, M.C., Castro, N.A., Nutman, A.P., Wemmer, K., Yamamoto, M.T., Hueck, M., Osako, L., Siga Jr., O., Passarelli, C.R., 2011b. Tectonic evolution of the Brusque Group, Dom Feliciano belt, Santa Catarina, Southern Brazil. J. South Am. Earth Sci. 32, 324–350. doi:10.1016/j.jsames.2011.03.016

Basei, M.A.S., Campos Neto, M.C., Lopes, A.P., Nutman, A.P., Liu, D., Sato, K., 2013. Polycyclic evolution of Camboriú Complex migmatites, Santa Catarina, Southern Brazil: integrated Hf isotopic and U-Pb age zircon evidence of episodic reworking of a Mesoarchean juvenile crust. Brazilian J. Geol. 43, 427–443. doi:10.5327/Z2317-48892013000300002

879 Basei, M.A.S., Frimmel, H.E., Nutman, A.P., Preciozzi, F., 2008. West Gondwana
880 amalgamation based on detrital zircon ages from Neoproterozoic Ribeira and Dom
881 Feliciano belts of South America and comparison with coeval sequences from SW Africa.
882 Geol. Soc. London, Spec. Publ. 294, 239–256. doi:10.1144/SP294.13

883

884 Basei, M.A.S., Frimmel, H.E., Nutman, A.P., Preciozzi, F., Jacob, J., 2005. A connection
885 between the Neoproterozoic Dom Feliciano (Brazil/Uruguay) and Gariep (Namibia/South
886 Africa) orogenic belts – evidence from a reconnaissance provenance study. Precambrian
887 Res. 139, 195–221. doi:10.1016/j.precamres.2005.06.005

888

889 Basei, M.A.S., Peel. E., Sánchez Bettucci, L., Preciozzi, F., Nutman, A.P., 2011a. The
890 basement of the Punta del Este Terrane (Uruguay): an African Mesoproterozoic
891 fragment at the eastern border of the South American Río de La Plata craton. Int. J.
892 Earth Sci. 100, 289–304. doi: 10.1007/s00531-010-0623-1

893

894 Basei, M.A.S., Siga Jr., O., Masquelin, H., Harara, O.M., Reis Neto, J.M., Preciozzi, F.,
895 2000. The Dom Feliciano Belt (Brazil-Uruguay) and its foreland domain, the Rio de la
896 Plata craton: framework, tectonic evolution and correlation with similar provinces of
897 Southwestern Africa, Tectonic Evolution of South America, in: Cordani, U.G., Milani, E.J.,
898 Thomaz Filho, A., Campos, D.A. (Eds.), Tectonic Evolution of South America. 31
899 International Geological Congress, Rio de Janeiro, Brazil, pp. 311–334.

900

901 Begg, G., Griffin, W., Natapov, L., O'Reilly, S., Grand, S., O'Neill, C., Hronsky, J.,
902 Poudjom Djomani, Y., Swain, C., Deen, T., Bowden, P., 2009. The lithospheric
903 architecture of Africa: seismic tomography, mantle petrology, and tectonic evolution.
904 Geosphere 5, 23–50. doi:10.1130/GES00179.1

905

906 Bento dos Santos, T.M., Tassinari, C.C.G., Fonseca, P.E., 2015. Diachronic collision,
907 slab break-off and long-term high thermal flux in the Brasiliano–Pan-African orogeny:
908 Implications for the geodynamic evolution of the Mantiqueira Province. Precambrian Res.
909 260, 1–22. doi:10.1016/j.precamres.2014.12.018

910

911 Blanco, G., Germs, G.J.B., Rajesh, H.M., Chemale, F., Dussin, I.A., Justino, D., 2011.
912 Provenance and paleogeography of the Nama Group (Ediacaran to early Palaeozoic,
913 Namibia): Petrography, geochemistry and U–Pb detrital zircon geochronology.
914 Precambrian Res. 187, 15–32. doi:10.1016/j.precamres.2011.02.002

915

916 Bossi, J., Campal, N., 1992. Magmatismo y tectónica transcurrente durante el
917 Paleozoico inferior del Uruguay, in: Paleozoico Inferior de Ibero-América. Universidad de
918 Extremadura, Alicante, pp. 343–356.

919

920 Bossi, J., Campal, N., Civetta, L., Demarchi, G., Girardi, V.A.V., Mazzucchelli, M.,
921 Negrini, L., Rivalenti, G., Fragoso-Cesar, A.R.S., Sinigoi, S., Teixeira, W., Piccirillo, E.M.,
922 Molesini, M., 1993. Early Proterozoic dike swarms from western Uruguay: geochemistry,
923 Sr-Nd isotopes and petrogenesis. Chem. Geol. 106, 263–277. doi:10.1016/0009-

924 2541(93)90031-D
925
926 Bossi, J., Cingolani, C.A., 2009. Extension and General Evolution of the Río de la Plata
927 Craton, in: Gaucher, C., Sial, A.N., Halverson, G.P., Frimmel, H.E. (Eds.),
928 Neoproterozoic-Cambrian Tectonics, Global Change and Evolution: A Focus on
929 Southwestern Gondwana. Elsevier, pp. 73–85. doi:10.1016/S0166-2635(09)01604-1
930
931 Bossi, J., Gaucher, C., 2004. The Cuchilla Dionisio Terrane, Uruguay: An Allochthonous
932 Block Accreted in the Cambrian to SW-Gondwana. Gondwana Res. 7, 661–674.
933 doi:10.1016/S1342-937X(05)71054-6
934
935 Bossi, J., Navarro, R., 2001. Grupo Carapé: su reivindicación. Rev. Soc. Uruguaya Geol.
936 8, 2–12.
937
938 Brito Neves, B.B., Campos Neto, M.C., Fuck, R.A., 1999. From Rodinia to western
939 Gondwana; an approach to the Brasiliano-Pan African cycle and orogenic collage.
940 Episodes 22, 155–166. doi:10.1016/j.precamres.2007.04.018
941
942 Brito Neves, B.B., Fuck, R.A., Pimentel, M.M., 2014. The Brasiliano collage in South
943 America: a review. Brazilian J. Geol. 44, 493–518. doi:10.5327/Z2317-
944 4889201400030010
945 Camozzato, E., Philipp, R.P., Chemale, F., 2013. Evolução Tectônica e Geocronologia
946 U-Pb em zircão da terminação sul do Terreno Tijucas (RS, Brasil), in: VII Congreso
947 Uruguayo de Geología. Montevideo, p. 7.
948
949 Camozzato, E., Sander, A., Ramgrab, G.E., Wildner, W., 1994. Milonitos alcalinos-
950 peralcalinos da região de Candiota, RS, in: 38th Brazilian Geological Congress.
951 Brazilian Geological Society, Camboriú, Brazil, pp. 88–89.
952
953 Campal, N., Schipilov, A., 1995. The Illescas bluish quartz rapakivi granite (Uruguay—
954 South America): some geological features, in: Symposium Rapakivi Granites and
955 Related Rocks. Belém, Brazil, p. 18.
956
957 Campal, N., Schipilov, A., 2005. La Formacion Cerros de Aguirre: evidencias de
958 magmatismo Vendiano en el Uruguay. Lat. Am. J. Sedimentol. Basin Anal. 12, 161–174.
959
960 Carvalho, P.F., 1932. Reconhecimento geológico do estado do Rio Grande do Sul, in:
961 Boletim Do Instituto Geólogico E Mineralógico Do Brasil, Vol. 66. Diretoria de estatística
962 da produção, Seccão de publicidade, Rio de Janeiro, Brazil, p. 72.
963
964 Chemale, F., 2000. Evolução geológica do Escudo Sul-Riograndense, in: Holz, M., De
965 Ros, L.F. (Eds.), Geologia Do Rio Grande Do Sul. Universidade Federal do Rio Grande
966 do Sul, Porto Alegre, pp. 13–52.

967

968 Chemale, F., Hartmann, L.A., Silva, L.C., 1995a. Stratigraphy and Tectonism of
969 Precambrian to Early Paleozoic units in Southern Brazil and Uruguay - Excursion
970 Guidebook. Acta Geol Leop 43, 4–115.

971

972 Chemale, F., Hartmann, L.A., Silva, L.C., 1995b. Stratigraphy and Tectonism of
973 Brasiliano Cycle in Southern Brazil. Communs. Geol. Survey of Namibia 10, 151–166.

974

975 Chemale, F., Philipp, R.P., Dussin, I.A., Formoso, M.L.L., Kawashita, K., Berttotti, A.L.,
976 2011. Lu–Hf and U–Pb age determination of Capivarita Anorthosite in the Dom Feliciano
977 Belt, Brazil. Precambrian Res. 186, 117–126. doi:10.1016/j.precamres.2011.01.005

978

979 Chiglino, L., Gaucher, C., Sial, A.N., Bossi, J., Ferreira, V.P., Pimentel, M.M., 2010.
980 Chemostratigraphy of Mesoproterozoic and Neoproterozoic carbonates of the Nico
981 Pérez Terrane, Río de la Plata Craton, Uruguay. Precambrian Res. 182, 313–336.
982 doi:10.1016/j.precamres.2010.06.002

983

984 Condie, K.C., 2002. Breakup of a Paleoproterozoic Supercontinent. Gondwana Res. 5,
985 41–43. doi:10.1016/S1342-937X(05)70886-8

986

987 Cordani, U.G., Brito Neves, B.B., D'Agrella-Filho, M.S., 2003. From Rodinia to
988 Gondwana: A Review of the Available Evidence from South America. Gondwana Res. 6,
989 275–283. doi:10.1016/S1342-937X(05)70976-X

990

991 Cordani, U.G., Sato, K., Teixeira, W., Tassinari, C.C.G., 2000. Crustal Evolution of the
992 South American Platform, in: Cordani, U.G., Milani, E.J., Thomaz Filho, A., Campos, D.A.
993 (eds.), Tectonic Evolution of South America. 31 International Geological Congress, Rio
994 de Janeiro, Brazil, pp. 19–40.

995

996 Dalziel, I.W.D., 1997. OVERVIEW: Neoproterozoic-Paleozoic geography and tectonics:
997 Review, hypothesis, environmental speculation. Geol. Soc. Am. Bull. 109, 16–42.
998 doi:10.1130/0016-7606(1997)109<0016:ONPGAT>2.3.CO;2

999

1000 de Wit, M.J., de Ronde, C.E.J., Tredoux, M., Roering, C., Hart, R.J., Armstrong, R.A.,
1001 Green, R.W.E., Peberdy, E., Hart, R.A., 1992. Formation of an Archaean continent.
1002 Nature 357, 553–562. doi:10.1038/357553a0

1003

1004 DeCelles, P.G., Giles, K.A., 1996. Foreland basin systems. Basin Res. 8, 105–123.
1005 doi:10.1046/j.1365-2117.1996.01491.x

1006

1007 Eglington, B.M., 2006. Evolution of the Namaqua-Natal Belt, southern Africa – A
1008 geochronological and isotope geochemical review. J. African Earth Sci. 46, 93–111.
1009 doi:10.1016/j.jafrearsci.2006.01.014

Eerola, T.T., 1994 The Proterozoic to Eopaleozoic supracrustal sequences of the Rio Grande do Sul Shield and the contemporaneous glaciogenic record of the SW Africa: possible tectonic, paleogeographic and paleoclimatic implications. in: 38th Brazilian Geological Congress. Brazilian Geological Society, Camboriú, pp. 624–625.

Eerola, T.T., 1995. From ophiolites to glaciers? Review on geology of the Neoproterozoic - Cambrian Lavras do Sul region, southern Brazil. in: Autio, S. (ed.) Special Paper 20: Current Research 1993-1994. Geological Survey of Finland, 5–16

Eerola, T.T., 1997. Neoproterozoic glaciation in southern Brazil?. J. South Am. Earth Sci. 10, VI, 1. doi: 10.1016/S0895-9811(97)90061-4

Faccini, U.F., 1989. O Permo-Triássico do Rio Grande do Sul. Uma análise sob o ponto de vista das seqüências deposicionais. Unpublished Master dissertation - Universidade Federal do Rio Grande do Sul, Porto Alegre. 121 p.

Faccini, U.F., 2000. Estratigrafia do Permo-Triássico do Rio Grande do Sul: estilos deposicionais versus espaço de acomodação. Unpublished PhD Thesis. Universidade Federal do Rio Grande do Sul, Porto Alegre. 121 p.

Faccini, U.F., Schultz, C.L., Figueiredo, C.E., Sangineto, L.R., Soares, S.C., 1990. Sobre a ocorrência de vertebrados fósseis triássicos na região de Santana da Boa Vista (RS). Ciência e Nat. 12, 103–104.

Fambrini, G.L., Fragoso-Cesar, A.R.S., Almeida, R.P., Riccomini, C., 2005. A Formação Barriga Negra (Ediacarano Do Uruguai): caracterização Estratigráfica e correlação com unidades do Estado Do Rio Grande Do Sul, Brasil. Rev. Bras. Geociências 35, 515–524.

Fernandes, L.A.D., Menegat, R., Costa, A.F.U., Koester, E., Porcher, C.C., Tommasi, A., Kramer, G., Ramgrab, G.E., Camozzato, E., 1995. Evolução Tectônica do Cinturão Dom Feliciano no Escudo Sul-rio-grandense: Parte II- Uma Contribuição a partir do registro geológico. Rev. Bras. Geociências 25, 351–374.

Fernandes, L.A.D., Tommasi, A., Porcher, C.C., 1992a. Deformation patterns in the southern Brazilian branch of the Dom Feliciano Belt: A reappraisal. J. South Am. Earth Sci. 5, 77–96. doi:10.1016/0895-9811(92)90061-3

Fernandes, L.A.D., Tommasi, A., Porcher, C.C., Koester, E., Kramer, G., Scherer, C.M.S., Menegat, R., 1992b. Granitóides brasilianos precoces do cinturão Dom Feliciano. Caracterização geoquímica e discussão estratigráfica. Pesqui. em Geociências 19, 195–215.

1053 Fragoso-Cesar, A.R.S., 1980. O Cráton do Rio de la Plata e o Cinturão Dom Feliciano
1054 no Escudo Uruguaio-Sul-Riograndense, in: 31th Brazilian Geological Congress. Brazilian
1055 Geological Society, Camboriú, pp. 2879–2892.

1056

1057 Frantz, J.C., Botelho, N.F., 2000a. Neoproterozoic Granitic Magmatism and Evolution of
1058 the Eastern Dom Feliciano Belt in Southernmost Brazil : A Tectonic Model. Gondwana
1059 Res. 3, 7–19. doi:http://dx.doi.org/10.1016/S1342-937X(05)70053-8

1060

1061 Frantz, J.C., Botelho, N.F., Pimentel, M.M., Potrel, A., Koester, E., Teixeira, R.S., 1999.
1062 Relações isotópicas Rb-Sr e Sm-Nd e idades do magmatismo granítico Brasiliano da
1063 região leste do Cinturão Dom Feliciano no Rio Grande do Sul: evidencias de
1064 retrabalhamento de crosta continental paleoproterozoica. Rev. Bras. Geociências 29,
1065 227–232.

1066

1067 Frantz, J.C., McNaughton, N.J., Marques, J.C., Hartmann, L.A., Botelho, N.F., Caravaca,
1068 G., 2003. SHRIMP U–Pb zircon ages of granitoids from southernmost Brazil: Constraints
1069 on the temporal evolution of the Dorsal de Canguc¸u transcurrent shear zone and the
1070 eastern Dom Feliciano Belt, in: IV South American Symposium on Isotope Geology. IRD-
1071 CBMM, Salvador, pp. 174–177.

1072

1073 Frantz, J.C., Nardi, L.V.S., 1992. Litoquímica e evolução de granitóides cálcio-alcalinos
1074 da região leste do escudo Sul-rio-grandense. Pesqui. em Geociências 19, 13–25.

1075

1076 Frantz, J.C., Remus, M.V.D., Hartmann, L.A., 2000b. Geological units, ages and tectonic
1077 evolution of the Neoproterozoic Dom Feliciano Belt, Southernmost Brazil - A review. Rev.
1078 Bras. Geociências 30, 055–057.

1079

1080 Frimmel, H.E., Basei, M.S., Gaucher, C., 2011. Neoproterozoic geodynamic evolution of
1081 SW- Gondwana: a southern African perspective. Int. J. of Earth Sci. 100, 323-354. doi:
1082 10.1007/s00531-010-0571-9

1083

1084 Frimmel, H.E., Fölling, P.G., Eriksson, P.G., 2002. Neoproterozoic tectonic and climatic
1085 evolution recorded in the Gariep Belt, Namibia and South Africa. Basin Res. 14, 55–67.
1086 doi:10.1046/j.1365-2117.2002.00166.x

1087

1088 Frimmel, H.E., Fölling, P.G., 2004. Late Vendian Closure of the Adamastor Ocean:
1089 Timing of Tectonic Inversion and Syn-orogenic Sedimentation in the Gariep Basin.
1090 Gondwana Res. 7, 685–699. doi:10.1016/S1342-937X(05)71056-X

1091

1092 Frimmel, H.E., Hartnady, C.J.H., Koller, F., 1996a. Geochemistry and tectonic setting of
1093 magmatic units in the Pan-African Gariep Belt, Namibia. Chem. Geol. 130, 101–121.
1094 doi:10.1016/0009-2541(95)00188-3

1095

1096 Frimmel, H.E., Klötzli, U.S., Siegfried, P.R., 1996b. New Pb-Pb Single Zircon Age
1097 Constraints on the Timing of Neoproterozoic Glaciation and Continental Break-up in
1098 Namibia. J. Geol. 104, 459–469. doi:10.1086/629839

1099

1100 Frimmel, H.E., Zartman, R.E., Späth, A., 2001. The Richtersveld Igneous Complex,
1101 South Africa: U-Pb Zircon and Geochemical Evidence for the Beginning of
1102 Neoproterozoic Continental Breakup. J. Geol. 109, 493–508. doi:10.1086/320795

1103

1104 Fuck, R.A., Brito Neves, B.B., Schobbenhaus, C., 2008. Rodinia descendants in South
1105 America. Precambrian Res. 160, 108–126. doi:10.1016/j.precamres.2007.04.018

1106

1107 Gaucher, C., Blanco, G., Chiglino, L., Poiré, D.G., Germs, G.J.B., 2008. Acritarchs of
1108 Las Ventanas Formation (Ediacaran, Uruguay): Implications for the timing of coeval
1109 rifting and glacial events in western Gondwana. Gondwana Res. 13, 488–501.
1110 doi:10.1016/j.gr.2007.05.008

1111

1112 Gaucher, C., Boggiani, P.C., Sprechmann, P., Sial, A.N., Fairchild, T.R., 2003.
1113 Integrated correlation of the Vendian to Cambrian Arroyo del Soldado and Corumbá
1114 Groups (Uruguay and Brazil): palaeogeographic, palaeoclimatic and palaeobiologic
1115 implications. Precambrian Res. 120, 241–278. doi:10.1016/S0301-9268(02)00140-7

1116

1117 Gaucher, C., Frei, R., Chemale, F., Frei, D., Bossi, J., Martínez, G., Chiglino, L.,
1118 Cernuschi, F., 2011. Mesoproterozoic evolution of the Río de la Plata Craton in Uruguay:
1119 at the heart of Rodinia? Int. J. Earth Sci. 100, 273–288. doi:10.1007/s00531-010-0562-x

1120

1121 Gaucher, C., Poiré, D.G., 2009. Palaeoclimatic events. Neoproterozoic–Cambrian
1122 evolution of the Río de la Plata Palaeocontinent. In: Gaucher, C., Sial, A.N., Halverson,
1123 G.P. and Frimmel, H.E. (eds) Neoproterozoic–Cambrian Tectonics, Global Change and
1124 Evolution. Elsevier, Amsterdam, Developments in Precambrian Geology, 16, 123–130.
1125 doi: 10.1016/S0166-2635(09)01633-8

1126

1127 Germs, G.J.B., 1983. Implications of sedimentary facies and depositional environmental
1128 analysis of the Nama Group in South West Africa/Namibia. Spec. Publ. - Geol. Soc.
1129 South Africa 11, 89–114.

1130

1131 Gollmann, K., Marques, J.C., Franz, J.C., Chemale, F., 2008. Geoquímica e Isotópos de
1132 Nd de Rochas Metavulcânicas da Antiforme Capané, Complexo Metamórfico Porongos,
1133 RS. Pesqui. em Geociências 35, 83–95.

Gregory, T.R., Bitencourt, M.F., Nardi, L.V.S., Florisbal, L.M., 2016. Petrogenesis of metamorphosed Paleoproterozoic, arc-related tonalites, granodiorites and coeval basic to intermediate rocks from southernmost Brazil, based on elemental and isotope geochemistry. Lithos. 'in press'. doi:10.1016/j.lithos.2016.08.007

Gross, A.O.M.S., Porcher, C.C., Fernandes, L.A.D., Koester, E,. 2006. Neoproterozoic low-pressure/high-temperature colisional metamorphic evolution in the Varzea do Capivarita Metamorphic Suite, SE Brazil: Thermobarometric and Sm/Nd evidence. Precambrian Res. 147, 41–64. doi: 10.1016/j.precamres.2006.02.001

Gruber, L., Porcher, C.C., Lenz, C., Fernandes, L.A.D., 2011. Proveniência de metassedimentos das sequências Arroio Areião, Cerro Cambará e Quartzo Milonitos no Complexo Metamórfico Porongos, Santana da Boa Vista, RS. Pesqui. em Geociências 38, 205–223.

Grunow, A., Hanson, R., Wilson, T., 1996. Were aspects of Pan-African deformation linked to Iapetus opening? Geology 24, 1063. doi:10.1130/0091-7613(1996)024<1063:WAOPAD>2.3.CO;2

Hanson, R.E., 2003. Proterozoic geochronology and tectonic evolution of southern Africa. Geol. Soc. London, Spec. Publ. 206, 427–463. doi: 10.1144/GSL.SP.2003.206.01.20

Hartmann, L.A., Campal, N., Santos, J.O.S., McNaughton, N.J., Bossi, J., Schipilov, A., Lafon, J.M., 2001. Archean crust in the Rio de la Plata Craton, Uruguay — SHRIMP U–Pb zircon reconnaissance geochronology. J. South Am. Earth Sci. 14, 557–570. doi:10.1016/S0895-9811(01)00055-4

Hartmann, L.A., Chemale, F., Philipp, R.P., 2007. Evolução geotectônica do Rio Grande do Sul no Pré- Cambriano, in: Iannuzzi, R., Frantz, J. (Eds.), 50 Anos de Geologia, Instituto de Geociências, Contribuições. Comunicação e Identidade, Porto Alegre, pp. 97–123.

Hartmann, L.A., Leite, J.A.D., Silva, L.C., Remus, M.V.D., McNaughton, N.J., Groves, D.I., Fletcher, I.R., Santos, J.O.S., Vasconcellos, M.A.Z., 2000a. Advances in SHRIMP geochronology and their impact on understanding the tectonic and metallogenic evolution of southern Brazil. Aust. J. Earth Sci. 47, 829–844. doi:10.1046/j.1440-0952.2000.00815.x

Hartmann, L.A., Liu, D., Wang, Y., Massonne, H.J., Santos, J.O.S., 2008. Protolith age of Santa Maria Chico granulites dated on zircons from an associated amphibolite-facies granodiorite in southernmost Brazil. An. Acad. Bras. Cienc. 80, 543–551. doi:10.1590/S0001-37652008000300014

1178 Hartmann, L.A., Philipp, R.P., Liu, D., Wan, Y., Wang, Y., Santos, J.O.S., Vasconcellos,
1179 M.A.Z., 2004. Paleoproterozoic Magmatic Provenance of Detrital Zircons, Porongos
1180 Complex Quartzites, Southern Brazilian Shield. Int. Geol. Rev. 46, 127–157.
1181 doi:10.2747/0020-6814.46.2.127

1182

1183 Hartmann, L.A., Philipp, R.P., Santos, J.O.S., McNaughton, N.J., 2011. Time frame of
1184 the 753–680 Ma juvenile accretion during the São Gabriel orogeny, Southern Brazilian
1185 shield. Gondwana Res. 19, 84–99. doi: 10.1016/j.gr.2010.05.001

1186

1187 Hartmann, L.A., Piñeyro, D., Bossi, J., Leite, J.A.D., McNaughton, N.J., 2000b. Zircon U-
1188 Pb SHRIMP dating of Palaeoproterozoic Isla Mala granitic magmatism in the Rio de la
1189 Plata Craton, Uruguay. J. South Am. Earth Sci. 13, 105–113. doi:10.1016/S0895-
1190 9811(00)00018-3

1191

1192 Hartmann, L.A., Santos, J.O.S., Cingolani, C.A., McNaughton, N.J., 2002. Two
1193 Paleoproterozoic Orogenies in the Evolution of the Tandilia Belt, Buenos Aires, as
1194 Evidenced by Zircon U-Pb SHRIMP Geochronology. Int. Geol. Rev. 44, 528–543.
1195 doi:10.2747/0020-6814.44.6.528

1196

1197 Hartmann, L.A., Santos, J.O.S., Leite, J.A.D., Porcher, C.C., McNaughton, N.J., 2003.
1198 Metamorphic evolution and U-Pb zircon SHRIMP geochronology of the Belizário
1199 ultramafic amphibolite, Encantadas Complex, southernmost Brazil. An. Acad. Bras.
1200 Cienc. 75. doi:10.1590/S0001-37652003000300010

1201

1202 Hartnady, C.J.H., Joubert, P., Stowe, C.W., 1985. Proterozoic crustal evolution in
1203 southwestern Africa. Episodes 8, 236–244.

1204

1205 Hasui, Y., Carneiro, A.W., Coimbra, C.D.R., 1975. The Ribeira folded belt. Rev. Bras.
1206 Geociências 5, 257–266.

1207

1208 Jacobs, J., Pisarevsky, S., Thomas, R.J., Becker, T., 2008. The Kalahari Craton during
1209 the assembly and dispersal of Rodinia. Precambrian Res. 160, 142–158.
1210 doi:10.1016/j.precamres.2007.04.022

1211

1212 Jackson, S.E., Pearson, N.J., Griffin, W.L., Belousova, E.A., 2004. The application of
1213 laser ablation-inductively coupled plasma-mass spectrometry to in situ U–Pb zircon
1214 geochronology. Chem. Geol. 211, 47–69. doi: 10.1016/j.chemgeo.2004.06.017

1215

1216 Janikian, L., Almeida, R.P., Trindade, R.I.F., Fragoso-Cesar, A.R.S., D'Agrella-Filho,
1217 M.S., Dantas, E.L., Tohver, E., 2008. The continental record of Ediacaran volcano-
1218 sedimentary successions in southern Brazil and their global implications. Terra Nov. 20,
1219 259–266. doi:10.1111/j.1365-3121.2008.00814.x

1220

Johansson, Å., 2014. From Rodinia to Gondwana with the “SAMBA” model—A distant view from Baltica towards Amazonia and beyond. Precambrian Res. 244, 226–235. doi:10.1016/j.precamres.2013.10.012

Jost, H., 1981. Geology and Metallogeny of the Santana da Boa Vista Region, Southern Brazil. Unpublished PhD Thesis. University of Georgia, Athens. 208 p.

Jost, H., Bitencourt, M.F., 1980. Estratigra a e tectônica de uma fração da Faixa de Dobramentos Tijucas no Rio Grande do Sul. Acta Geol Leop 11, 27–59.

Jost, H., Hartmann, L.A., 1984. Província Mantiqueira, Setor Meridional, in: Almeida, F.F., Hasui, Y. (Eds.), O Pré-Cambriano do Brasil, São Paulo: Edgard Blücher Ltda, Brazil, pp. 345–368.

Koester, E., Porcher, C.C., Pimentel, M.M., Fernandes, L.A.D., Vignol-Lelarge, M.L., Oliveira, L.D., Ramos, R.C., 2016. Further evidence of 777 Ma subduction-related continental arc magmatism in Eastern Dom Feliciano Belt, southern Brazil: The Chácara das Pedras Orthogneiss. J. South Am. Earth Sci. 68, 155–166. doi:10.1016/j.jsames.2015.12.006

Lafon, J.M., Hartmann, L.A., Azambuja, J.C., 1990. Datação Rb-Sr de gnaisses alcalinos do Arroio Capané, RS, in: 36th Brazilian Geological Congress. Brazilian Geological Society, Natal, p. 431.

Leite, J.A.D., 1997. A origem dos harzburgitos da Sequencia Cerro Mantiqueiras e implicacoes tectonicas para o desenvolvimento do Neoproterozoico no sul do Brasil. Unpublished PhD Thesis. Universidade Federal do Rio Grande do Sul, Porto Alegre. 224 p.

Leite, J.A.D., Hartmann, L.A., Fernandes, L.A.D., McNaughton, N.J., Soliani Jr., Ê., Koester, E., Santos, J.O.S., Vasconcellos, M.A.Z., 2000. Zircon U–Pb SHRIMP dating of gneissic basement of the Dom Feliciano Belt, southernmost Brazil. J. South Am. Earth Sci. 13, 739–750. doi:10.1016/S0895-9811(00)00058-4

Leite, J.A.D., Hartmann, L.A., McNaughton, N.J., Chemale, F., 1998. SHRIMP U/Pb Zircon Geochronology of Neoproterozoic Juvenile and Crustal-Reworked Terranes in Southernmost Brazil. Int. Geol. Rev. 40, 688–705. doi:10.1080/00206819809465232

Leite, J.A.D., McNaughton, N.J., Hartmann, L.A., Chemale, F., Remus, M.V.D., 1995. SHRIMP U/Pb zircon dating applied to the determination of tectonic events: the example of the Caçapava do Sul Batholith, Pedreira Inducal, Caçapava do Sul, Brazil, in: 5th National Symposium of Tectonic Studies. Brazilian Geological Society, Gramado, Brazil, pp. 387–388.

1265 Lena, L.O.F., Pimentel, M.M., Philipp, R.P., Armstrong, R.A., Sato, K., 2014. The
1266 evolution of the Neoproterozoic São Gabriel juvenile terrane, southern Brazil based on
1267 high spatial resolution U-Pb ages and δ18O data from detrital zircons. Precambrian Res.
1268 247, 126–138. doi:10.1016/j.precamres.2014.03.010

1269

1270 Lenz, C., 2006. Evolução metamórfica dos metapelitos da Antiforme Serra dos
1271 Pedrosas: condições e idades do metamorfismo. Unpublished Master dissertation.
1272 Universidade do Rio Grande do Sul, Porto Alegre. 111 p.

1273

1274 Lenz, C., 2010. Evolução tectônica Précambriana dos ortogneisses do Complexo Cerro
1275 Olivo - Domínio Leste do Cinturão Dom Feliciano no Uruguai. Unpublished PhD Thesis
1276 Universidade Federal do Rio Grande do Sul, Porto Alegre. 195 p.

1277

1278 Lenz, C., Fernandes, L.A.D., McNaughton, N.J., Porcher, C.C., Masquelin, H., 2011. U–
1279 Pb SHRIMP ages for the Cerro Bori Orthogneisses, Dom Feliciano Belt in Uruguay:
1280 Evidences of a ~800Ma magmatic and ~650Ma metamorphic event. Precambrian Res.
1281 185, 149–163. doi:10.1016/j.precamres.2011.01.007

1282

1283 Li, Z.X., Bogdanova, S.V., Collins, A.S., Davidson, A., De Waele, B., Ernst, R.E.,
1284 Fitzsimons, I.C.W., Fuck, R.A., Gladkochub, D.P., Jacobs, J., Karlstrom, K.E., Lu, S.,
1285 Natapov, L.M., Pease, V., Pisarevsky, S.A., Thrane, K., Vernikovsky, V., 2008. Assembly,
1286 configuration, and break-up history of Rodinia: A synthesis. Precambrian Res. 160, 179–
1287 210. doi:10.1016/j.precamres.2007.04.021

1288

1289 Ludwig, K.R., 2008. User's manual for Isoplot 3.6. A geochronological toolkit for
1290 Microsoft Excel. Berkeley Geochronologic Center, Special Publication No. 4, Berkeley,
1291 USA.

1292

1293 Lusa, M., Philipp, R.P., Nardi, L.V.S., 2010. Geoquímica e petrologia dos metagranitos
1294 do Complexo Encantadas, Santana da Boa Vista, (RS): a evolução de uma margem
1295 continental ativa no Paleoproterozóico. Rev. Bras. Geociências 40, 151–166.

1296

1297 Machado, R., César, A.R.S.F., Faccini, U.F., 1987. O Domo de Santana (RS): domo
1298 gnáissico manteado ou figura de interferência tipo domo e bacia?, in: 3th South-
1299 Brazilian Geological Symposium. Brazilian Geological Society, Curitiba, Brazil, pp. 167–
1300 182.

1301

1302 Marques, J.C., 1996. Petrologia e metalogênese da Seqüência Metaultramáfica da
1303 Antiforme Capané, Suíte Metamórfica Porongos, Cachoeira do Sul-RS. Unpublished
1304 Master dissertation. Universidade Federal do Rio Grande do Sul, Porto Alegre. 196 p.

1305

1306 Marques, J.C., Frantz, J.C., Jost, H., Roisenberg, A., 2003a. Stratigraphy of the
1307 Porongos Suíte: A remaining problem, in: I Encontro Sobre a Estratigrafia Do Rio
1308 Grande Do Sul: Escudos e Bacias. Porto Alegre, Brazil, pp. 77–82.

Marques, J.C., Jost, H., Roisenberg, A., Frantz, J.C., 1998a. Rochas metassedimentares, geologia estrutural e metamorfismo da suíte metamórfica Porongos na área da antiforme Capané, Cachoeira do Sul – RS. Rev. Bras. Geociências 28, 467–472.

Marques, J.C., Jost, H., Roisenberg, A., Frantz, J.C., 1998b. Eventos ígneos da Suíte Metamórfica Porongos na área da Antiforme Capané, Cachoeira do Sul - RS. Rev. Bras. Geociências 28, 419–430.

Marques, J.C., Roisenberg, A., Jost, H., Frantz, J.C., Teixeira, R.S., 2003b. Geologia e geoquímica das rochas metaultramáficas da antiforme Capané, suíte metamórfica Porongos, RS. Rev. Bras. Geociências 33, 83–94.

Martil, M.M.D., Bitencourt, M.F., Nardi, L.V.S., Koester, E., Pimentel, M.M., 2017. Pre-collisional, Tonian (ca. 790 Ma) continental arc magmatism in southern Mantiqueira Province, Brazil: Geochemical and isotopic constraints from the Várzea do Capivarita Complex. Lithos 274–275, 39–52. doi:10.1016/j.lithos.2016.11.011

Masquelin, H., Sánchez, L. 1993. Propuesta de evolución tectono-sedimentaria para la fosa tardi-brasiliana en la región de Piriápolis, Uruguay. Rev. Bras. Geociências 23, 313–322.

Milani, E.J., Faccini, U.F., Scherer, C.M.S., Araujo, L.M., Cupertino, J.A., 1998. Sequences and stratigraphic hierarchy of the Paraná Basin (Ordovician to Cretaceous), Southern Brazil. Bol. IG USP, Série Científica 29, 125–173.

Nardi, L.V.S., Plá-Cid, J., Bitencourt, M.F., Stabel, L.Z., 2008. Geochemistry and petrogenesis of post-collisional ultrapotassic syenites and granites from southernmost Brazil: the Piquiri Syenite Massif. An. Acad. Bras. Cienc. 80. doi:10.1590/S0001-37652008000200014

Oliveira, C.H.E., Chemale, F., Jelinek, A.R., Bicca, M.M., Philipp, R.P., 2014. U–Pb and Lu–Hf isotopes applied to the evolution of the late to post-orogenic transtensional basins of the Dom Feliciano Belt, Brazil. Precambrian Res. 246, 240–255. doi:10.1016/j.precamres.2014.03.008

Oriolo, S., Oyhantçabal, P., Basei, M.A.S., Wemmer, K., Siegesmund, S., 2016. The Nico Pérez Terrane (Uruguay): From Archean crustal growth and connections with the Congo Craton to late Neoproterozoic accretion to the Río de la Plata Craton. Precambrian Res. 280, 147–160. doi:10.1016/j.precamres.2016.04.014

Oyhantçabal, P., Sánchez-Bettucci, L., Pecoits, E., Aubet, N.R., Peel, E., Preciozzi, F., Basei, M.A.S., 2005. Nueva propuesta estratigrafica para las supracorticales del

1353 Cinturón Dom Feliciano (Proterozoico, Uruguay), in: XII Congreso Latinoamericano de
1354 Geología. Quito, Peru.
1355
1356 Oyhantçabal, P., Siegesmund, S., Wemmer, K., Layer, P., 2010. The Sierra Ballena
1357 Shear Zone in the southernmost Dom Feliciano Belt (Uruguay): evolution, kinematics,
1358 and deformation conditions. Int. J. Earth Sci. 99, 1227–1246. doi: 10.1007/s00531-009-
1359 0453-1
1360
1361 Oyhantçabal, P., Siegesmund, S., Wemmer, K., 2011a. The Río de la Plata Craton: a
1362 review of units, boundaries, ages and isotopic signature. Int. J. Earth Sci. 100, 201–220.
1363 doi:10.1007/s00531-010-0580-8
1364
1365 Oyhantçabal, P., Siegesmund, S., Wemmer, K., Passchier, C.W., 2011b. The
1366 transpressional connection between Dom Feliciano and Kaoko Belts at 580-550 Ma. Int.
1367 J. Earth Sci. 100, 379-390. doi: 10.1007/s00531-010-0577-3
1368
1369 Paim, P.S., Chemale, F., Lopes, R.C., 2000. A Bacia do Camaquã, in: Holtz, M., De Ros,
1370 L.F. (Eds.), Geologia Do Rio Grande Do Sul. Universidade Federal do Rio Grande do
1371 Sul, Porto Alegre, Brazil, pp. 231–274.
1372
1373 Passarelli, C.R., Basei, M.A.S., Siga Jr., O., Reath, I.M., Campos Neto, M.C., 2010.
1374 Deformation and geochronology of syntectonic granitoids emplaced in the Major Gercino
1375 Shear Zone, southeastern South America. Gondwana Res. 17, 688–703.
1376 doi:10.1016/j.gr.2009.09.013
1377
1378 Passchier, C.W., Trouw, R.A., 2005. Microtectonics. Springer-Verlag, Berlin/Heidelberg.
1379 doi:10.1007/3-540-29359-0
1380
1381 Pazos, P.J., Rapalini, A., 2011. Chapter 54 The controversial stratigraphy of the glacial
1382 deposits in the Tandilia System, Argentina. Geol. Soc. London, Mem. 36, 565–569. doi:
1383 10.1144/M36.54
1384
1385 Pazos, P.J., Sánchez-Bettucci, L., Tofalo, O.R., 2003. The Record of the Varanger
1386 Glaciation at the Río De La Plata Craton, Vendian-Cambrian of Uruguay. Gondwana Res.
1387 6, 65–77. doi:10.1016/S1342-937X(05)70644-4
1388
1389 Pazos, P.J., Sánchez-Bettucci, L., Loureiro, J., 2008. The Neoproterozoic glacial record
1390 in the Rio de la Plata Craton: a critical reappraisal. In: Pankhurst, M.J., Trouw, R.A.J.,
1391 Brito Neves, B.B., de Wit, M.J. (eds) West Gondwana: Pre-Cenozoic Correlations Across
1392 the South Atlantic Region. Geol. Soc. London Spec. Publ. 294, 343–364. doi:
1393 10.1144/SP294.18
1394
1395 Pazos, P.J., Sánchez-Bettucci, L., 2010. Reply to discussion 'The Neoproterozoic glacial

record in the Río de La Plata Craton: a critical reappraisal'. J. Geol. Soc. 167, 223. doi: 10.1144/0016-76492009-083

Pecoits, E., 2003. Sedimentología y consideraciones estratigráficas de la Formación Las Ventanas en su área tipo, departamento de Maldonado. Rev. Soc. Uruguaya Geol. 1, 124–140.

Pecoits, E., Aubet, N.R., Gingras, M.K., Konhauser, K.O. 2010. Discussion on 'The Neoproterozoic glacial record in the Río de La Plata Craton: a critical reappraisal'. J. Geol. Soc. 167, 221–222. doi: 10.1144/0016-76492009-045

Pecoits, E., Aubet, N.R., Heaman, L.M., Philippot, P., Rosière, C.A., Veroslavsky, G., Konhauser, K.O., 2016. UPb detrital zircon ages from some Neoproterozoic successions of Uruguay: Provenance, stratigraphy and tectonic evolution. J. South Am. Earth Sci. 71, 108–130. doi:10.1016/j.jsames.2016.07.003

Pecoits, E., Aubet, N.R., Oyhantçabal, P., Sánchez-Bettucci, L., 2004. Estratigrafía de sucesiones sedimentarias y volcanosedimentarias Neoproterozoicas del Uruguay. Rev. Soc. Uruguaya Geol. 11, 18–27.

Pecoits, E., Gingras, M.K., Aubet, N.R., Konhauser, K.O., 2008. Ediacaran in Uruguay: palaeoclimatic and palaeobiological implications. Sedimentology 55, 689–719. doi:10.1111/j.1365-3091.2007.00918.x

Pecoits, E., Gingras, M.K., Konhauser, K.O., 2011. Chapter 53 Las Ventanas and San Carlos formations, Maldonado Group, Uruguay. Geol. Soc. London, Mem. 36, 555–564. doi:10.1144/M36.53

Pertille, J., Hartmann, L.A., Philipp, R.P., 2015a. Zircon U–Pb age constraints on the Paleoproterozoic sedimentary basement of the Ediacaran Porongos Group, Sul-Riograndense Shield, southern Brazil. J. South Am. Earth Sci. 63, 334–345. doi:10.1016/j.jsames.2015.08.005

Pertille, J., Hartmann, L.A., Philipp, R.P., Petry, T.S., Lana, C.C., 2015b. Origin of the Ediacaran Porongos Group, Dom Feliciano Belt, southern Brazilian Shield, with emphasis on whole rock and detrital zircon geochemistry and U–Pb, Lu–Hf isotopes. J. South Am. Earth Sci. 64, 69–93. doi:10.1016/j.jsames.2015.09.001

Pertille, J., Hartmann, L.A., Santos, J.O.S., McNaughton, N.J., Armstrong, R., 2017. Reconstructing the Cryogenian–Ediacaran evolution of the Porongos fold and thrust belt, Southern Brasiliano Orogen, based on Zircon U–Pb–Hf–O isotopes. Int. Geol. Rev. 6814, 1–29. doi:10.1080/00206814.2017.1285257

1439 Philipp, R.P., 1998. A Evolução Geológica e Tectônica do Batólito Pelotas no Rio
1440 Grande do Sul. PhD Thesis. Universidade de São Paulo, São Paulo. 377 p.
1441 doi:10.11606/T.44.1998.tde-05112014-155445

1442

1443 Philipp, R.P., Machado, R., 2005. The Late Neoproterozoic granitoid magmatism of the
1444 Pelotas Batholith, southern Brazil. J. South Am. Earth Sci. 19, 461–478.
1445 doi:10.1016/j.jsames.2005.06.010

1446

1447 Philipp, R.P., Machado, R., Nardi, L.V.S., Lafon, J.M., 2002. O magmatismo granitico
1448 Neoproterozóico do Batólito Pelotas no sul do Brasil: novos dados e revisão da
1449 geocronologia regional. Rev. Bras. Geociências 32, 277–290.

1450

1451 Philipp, R.P., Massonne, H.J., Campos, R.S., 2013. Peraluminous leucogranites of the
1452 Cordilheira Suite: A record of Neoproterozoic collision and the generation of the Pelotas
1453 Batholith, Dom Feliciano Belt, Southern Brazil. J. South Am. Earth Sci. 43, 8–24.
1454 doi:10.1016/j.jsames.2012.10.006

1455

1456 Poiré, D.G., Spalletti, L., 2005. La cubierta sedimentaria Precámbrica - Paleozoica
1457 inferior del Sistema de Tandilia, in: Barrio, R.E., Etcheverry, R.O., Cabllé, M.F.,
1458 Llambías, E. (Eds.), Geología Y Recursos Minerales de La Provincia de Buenos Aires.
1459 16° Congreso Geológico Argentino, La Plata, pp. 51–68.

1460

1461 Porada, H., 1989. Pan-African rifting and orogenesis in southern to equatorial Africa and
1462 eastern Brazil. Precambrian Res. 44, 103–136. doi:10.1016/0301-9268(89)90078-8

1463

1464 Porcher, C.C., Fernandes, L.A.D., 1990. Relações Embasamento/"Cobertura" na Porção
1465 Ocidental do Cinturão Dom Feliciano: Um Esboço Estrutural. Pesqui. em Geociências 17,
1466 72–84.

1467

1468 Porcher, C.C., McNaughton, N.J., Leite, J.A.D., Hartmann, L.A., Fernandes, L.A.D.,
1469 1999. Idade SHRIMP em zircão: vulcanismo ácido do Complexo Metamórfico Porongos,
1470 in: I Simpósio de Vulcanism E Ambientes Associados. Brazilian Geological Society,
1471 Gramado, Brazil, p. 110.

1472

1473 Preciozzi, F., Masquelin, H., Basei, M.A.S., 1999. The Namaqua/Grenville terrane of
1474 eastern Uruguay:, in: II South American Symposium on Isotope Geology. Córdoba,
1475 Argentina, pp. 338–340.

1476

1477 Ramos, V.A., 1988. Late Proterozoic–early Paleozoic of South America – a collisional
1478 history. Episodes 11, 168–174.

1479

1480 Rapela, C.W., Fanning, C.M., Casquet, C., Pankhurst, R.J., Spalletti, L., Poiré, D.G.,
1481 Baldo, E.G., 2011. The Rio de la Plata craton and the adjoining Pan-African/brasiliano

terranes: Their origins and incorporation into south-west Gondwana. Gondwana Res. 20, 673–690. doi:10.1016/j.gr.2011.05.001

Rapela, C.W., Pankhurst, R.J., Casquet, C., Fanning, C.M., Baldo, E.G., González-Casado, J.M., Galindo, C., Dahlquist, J,. 2007. The Rio de la Plata craton and the assembly of SW Gondwana. Earth-Sci Rev. 83, 49–82. doi:10.1016/j.earscirev.2007.03.004

Reid, D.L., 1997. Sm-Nd age and REE geochemistry of Proterozoic arc-related igneous rocks in the Richtersveld subprovince, Namaqua Mobile Belt, Southern Africa. J. African Earth Sci. 24, 621–633. doi:10.1016/S0899-5362(97)00084-5

Remus, M.V.D., Tedesco, M.A., Philipp, R.P., Faccini, U.F., 1987. Evolução estrutural da unidade Porongos a sul do Rio Camaquã, RS, in: 3th South-Brazilian Geological Symposium. Brazilian Geological Society, Curitiba, Brazil, pp. 223–244.

Remus, M.V.D., Hartmann, L.A., Ribeiro, M., 1991. Nota sobre a geologia dos metamorfitos de pressão intermediária e granitóides associados da região de Pinheiro Machado/RS. Acta Geol. Leop. 34, 175–190.

Remus, M.V.D., McNaughton, N.J., Hartmann, L.A., Groves, D.I., 1996. SHRIMP U/Pb zircon dating at 2448 Ma of the oldest igneous rock in Southern Brazil: identification of the westernmost border of Dom Feliciano Belt, in: Symposium on Archean Terranes of the South American Plataform. Brasilia, Brazil, pp. 67–70.

Ribeiro, M., Bocchi, P., Figueiredo Filho, P.M., Tessari, R.I., 1966. Geologia da Quadrícula de Caçapava do Sul, Rio Grande do Sul. Boletim 27. Rio de Janeiro, Brazil.

Ribeiro, M.; Fantinel, L.M., 1978. Associações petrotectôncias do escudo Sul-rio-grandense: I Tabulação e descrição das associações petrotectônicas do Escudo do Rio Grande do Sul. Iheringia, Sér. Geol., 5, 19–54.

Rubatto, D., 2002. Zircon trace element geochemistry: partitioning with garnet and the link between U–Pb ages and metamorphism. Chem. Geol. 184, 123–138. doi:10.1016/S0009-2541(01)00355-2

Saalmann, K., Gerdes, A., Lahaye, Y., Hartmann, L.A., Remus, M.V.D., Läufer, A., 2011. Multiple accretion at the eastern margin of the Rio de la Plata craton: the prolonged Brasiliano orogeny in southernmost Brazil. Int. J. Earth Sci. 100, 355–378. doi:10.1007/s00531-010-0564-8

Saalmann, K., Hartmann, L.A., Remus, M.V.D., Koester, E., Conceição, R.V., 2005. Sm–Nd isotope geochemistry of metamorphic volcano-sedimentary successions in the São

Gabriel belt, southernmost Brazil: evidence for the existence of juvenile Neoproterozoic oceanic crust to the east of the La Plata Craton. Precambrian Res. 136, 159–175. doi: 10.1016/j.precamres.2004.10.006

Saalmann, K., Hartmann, L.A., Remus, M.V.D., 2007. The assembly of West Gondwana—The view from the Rio de la Plata craton, in: The Evolution of the Rheic Ocean: From Avalonian-Cadomian Active Margin to Alleghenian-Variscan Collision. Geol. Soc. Am. Spec. Pap. 423, pp. 1–26. doi:10.1130/2007.2423(01)

Saalmann, K., Remus, M.V.D., Hartmann, L.A., 2006. Structural evolution and tectonic setting of the Porongos belt, southern Brazil. Geol. Mag. 143, 59-88. doi: 10.1017/S0016756805001433

Sánchez-Bettucci, L., Ramos, V.A., 1999. Aspectos geológicos de las rocas metavolcánicas y metasedimentarias del Grupo Lavalleja, sudeste de Uruguay. Rev. Bras. Geociências 29, 557–570.

Santos, J.O.S., Hartmann, L.A., Bossi, J., Campal, N., Schipilov, A., Piñeyro, D., McNaughton, N.J., 2003. Duration of the Trans-Amazonian Cycle and Its Correlation within South America Based on U-Pb SHRIMP Geochronology of the La Plata Craton, Uruguay. Int. Geol. Rev. 45, 27–48. doi:10.2747/0020-6814.45.1.27

Schmid, R., Fettes, D., Harte, B., Davis, E., Desmons, J., 2007. How to name a metamorphic rock, in: Fettes, D., Desmons, J. (Eds.), Metamorphic Rocks: A Classification and Glossary of Terms. Cambridge University Press, Cambridge, UK, pp. 3–15.

Schmitt, R.S., Frimmel, H.E., Fairchild, T.R., 2008. Neoproterozoic–Early Paleozoic events in Southwest Gondwana: Introduction, Gondwana Res. 13, 435–436. doi: 10.1016/j.gr.2007.06.003.

Sibson, R.H., 1977. Fault rocks and fault mechanisms. J. Geol. Soc. London. 133, 191–213. doi:10.1144/gsjgs.133.3.0191

Siga Jr., O., Cury, L.F., McReath, I., Almeida Leite Ribeiro, L.M., Sato, K., Basei, M.A.S., Passarelli, C.R., 2011. Geology and geochronology of the Betara region in south-southeastern Brazil: Evidence for possible Statherian (1.80–1.75Ga) and Calymmian (1.50–1.45Ga) extension events. Gondwana Res. 19, 260–274. doi:10.1016/j.gr.2010.06.003

Siivola, J., Schmid, R., 2007. List of minerals abbreviations, in: Fettes, D., Desmons, J. (Eds.), Metamorphic Rocks: A Classification and Glossary of Terms. Cambridge University Press, Cambridge, UK, pp. 93–110.

1569 Silva, L.C., Hartmann, L.A., McNaughton, N.J., Fletcher, I.R., 1999. SHRIMP U/Pb
1570 Zircon Dating of Neoproterozoic Granitic Magmatism and Collision in the Pelotas
1571 Batholith, Southernmost Brazil. Int. Geol. Rev. 41, 531–551. doi:
1572 10.1080/00206819909465156

1573

1574 Soliani Jr., E., 1986. Os dados geocronológicos do Escudo Sul-Rio-Grandense e suas
1575 implicações de ordem geotectônica. Unpublished PhD Thesis - Universidade de São
1576 Paulo, São Paulo. 427 p. doi: 10.11606/T.44.1986.tde-15072015-153916

1577

1578 Stacey, J.S., Kramers, J.D., 1975. Approximation of terrestrial lead isotope evolution by
1579 a two-stage model. Earth Planet. Sci. Lett. 26, 207–221. doi:10.1016/0012-
1580 821X(75)90088-6

1581

1582 Stowe, C.W., Hartnady, C.J.H., Joubert, P., 1984. Proterozoic tectonic provinces of
1583 southern Africa. Precambrian Res. 25, 229–231. doi:10.1016/0301-9268(84)90034-2

1584

1585 Teixeira, W., D'Agrella-Filho, M.S., Hamilton, M.A., Ernst, R.E., Girardi, V.A.V.,
1586 Mazzucchelli, M., Bettencourt, J.S., 2013. U–Pb (ID-TIMS) baddeleyite ages and
1587 paleomagnetism of 1.79 and 1.59Ga tholeiitic dyke swarms, and position of the Rio de la
1588 Plata Craton within the Columbia supercontinent. Lithos 174, 157–174.
1589 doi:10.1016/j.lithos.2012.09.006

1590

1591 Teixeira, W., Renne, P.R., Bossi, J., Campal, N., D'Agrella-Filho, M.S., 1999. 40Ar–39Ar
1592 and Rb–Sr geochronology of the Uruguayan dike swarm, Rio de la Plata Craton and
1593 implications for Proterozoic intraplate activity in western Gondwana. Precambrian Res.
1594 93, 153–180. doi:10.1016/S0301-9268(98)00087-4

1595

1596 Tohver, E., D'Agrella-Filho, M.S., Trindade, R.I.F., 2006. Paleomagnetic record of Africa
1597 and South America for the 1200–500Ma interval, and evaluation of Rodinia and
1598 Gondwana assemblies. Precambrian Res. 147, 193–222.
1599 doi:10.1016/j.precamres.2006.01.015

1600

1601 Torquato, J.R., Cordani, U.G., 1981. Brazil-Africa geological links. Earth-Science Rev.
1602 17, 155–176. doi:10.1016/0012-8252(81)90010-6

1603

1604 Trompette, R., 1994. Geology of western Gondwana (2000 - 500Ma). Pan-African-
1605 Braziliano aggregation of South America and Africa. A.A. Balkema, Rotterdam,
1606 Netherlands. 350 pp.

1607

1608 Trompette, R., 1997. Neoproterozoic (~600 Ma) aggregation of Western Gondwana: a
1609 tentative scenario. Precambrian Res. 82, 101–112. doi:10.1016/S0301-9268(96)00045-9

1610

1611 Vaughan, A.P.M., Pankhurst, R.J., 2008. Tectonic overview of the West Gondwana

margin. Gondwana Res. 13, 150–162. doi:10.1016/j.gr.2007.07.004

Weil, A.B., Van der Voo, R., Mac Niocaill, C., Meert, J.G., 1998. The Proterozoic supercontinent Rodinia: paleomagnetically derived reconstructions for 1100 to 800 Ma. Earth Planet. Sci. Lett. 154, 13–24. doi:10.1016/S0012-821X(97)00127-1

Wildner, W., Camozzato, E., Orlandi Filho, V., Basei, M.A.S., 1996. Rochas vulcanogênicas do CinturãoMetamórfico Porongos na Antiforme do Godinho,região do Passo da Cuia-RS, in: 39th Brazilian Geological Congress. Brazilian Geological Society, Salvador, pp. 146–148.

Zvirtes, G., Philipp, R.P., Chemale, F., Camozzato, E., 2015. Evidências de rifteamento e metamorfismo orogênico nos estágios finais de evolução do Cinturão Dom Feliciano na Antiforme Capané, Cachoeira do Sul, RS, in: 9th South-Brazilian Geological Symposium. Brazilian Geological Society, pp. 141.

Figure captions

Figure 1: A) Neoproterozoic assemblage of the Western Gondwana supercontinent after Tohver et al. (2006) and Vaughan and Pankhurst (2008). Cratons are represented by gray color, Mesoproteorozoic belts are purple and Pan-African–Brasiliano belts are orange. The selected white area is detailed in Figure 2B. **B)** Simplified tectonic domains of southern Brazil and Uruguay (map modified from Basei et al., 2008; Pecoits et al., 2016; Rapela et al., 2011; Teixeira et al., 2013). The Dom Feliciano Belt segments refer to Itajaí (*IB)*, Camaquã (*CB*) and Arroyo del Soldado basins (*AS*); Florianopólis (*FB*), Pelotas (*Pa*) and Aiguá (*AB*) batholiths; Brusque (*BC*), Porongos (*PC*) and Lavalleja (*LV*) complexes and Éden Block (*EB*). The other units represent Luís Alves Craton (*LA*), São Gabriel (*SG*) and Taquarembó (*TB*) blocks; Piedra Alta (*PA*), Nico Pérez (*NPT)*, Cuchilla Dionisio (*CDT*), Tandilia (*TT*) and Mar del Plata (*MP*) terranes. The *SBSZ* and *SYSZ* stand for Sierra Ballena and Sarandí del Yí shear

zones, respectively. The area highlighted in white is subject of the present study, comprising the Porongos Complex, detailed in Figure 2. For interpretation of the references to color in both figures legend, the reader is referred to the web version of this article.

Figure 2: Geological map of the Porongos Complex displaying georeferenced samples from previous geochronological studies detailed in Table 2. Map modified from Almeida et al. (2012), Chemale (2000), Jost (1981) and Oliveira et al. (2014).

Figure 3: Geological map of the Capané Antiform showing the locations of the samples examined by this study (after Marques, 1996; Marques et al., 1998a, 1998b).

Figure 4: Selected photomicrographs of textures used for identification of protoliths for the key samples of Capané Antiform. **A)** Fine-grained muscovite lamellae, partially crenulated, surround quartz augen aggregates in the quartz-muscovite schist (crossed-polarized light [XPL], CA-19). **B)** Porphyroclastic aggregates of quartz and chlorite, which also occur in the fine-grained matrix of the metatuff (plane-polarized light [PPL], CA-16). **C)** Diffuse foliation is defined for the compositional banding of chlorite, carbonate and quartz in the metatuff (XPL, CA-11). **D)** Porphyroblastic texture of staurolite-garnet-quartz-muscovite schist (PPL, CA-22). **E)** Quartz aggregates present sutured boundaries and preserve foliation oblique to the main sub-horizontal foliation, defined for the muscovite lamellae (XPL, CA-17). **F)** Strong mineral stretching of quartz and muscovite aggregates in the quartz-muscovite ultramylonite (XPL, CA-21B). The mineral abbreviations *cb*, *chl*, *gr*, *ms* and *qtz* in the images

stand for carbonate, chlorite, garnet, muscovite and quartz, respectively.

Figure 5: Representative backscattered and cathodoluminescent images of the detrital zircon grains analyzed. The circles represent the LA-ICP-MS U-Pb analyzed spots. Yellow numbers refer to obtained age for each spot and white ones are the point position. For interpretation of the references to color in this figure legend, the reader is referred to the web version of this article

Figure 6: Isotopic analyses of detrital zircon crystals plotted on probability density plots, relative proportion of zircon ages and Concordia diagrams for the samples from the eastern limb (*A*: CA-19), western limb (*B*: CA-16, *C*: CA-11) and axial zone (*D*: CA-22, *E*: CA-17, *F*: CA-02A, *G*: CA-21B) of the Capané Antiform.

Figure 7: Probability density plot of U-Pb detrital zircon ages from the Porongos Complex, grouping the sectors according the geological features. Bold line stands for the maximum depositional age defined by volcanic event and dashed line represents speculative maximum depositional ages based on provenance of sediments. Sources of the samples plotted: 1 – Pertille et al. (2015b); 2 – Hartmann et al. (2004); 3 – Gruber et al. (2011); 4 – Basei et al. (2008); 5 – Pertille et al. (2015a); 6 – Saalmann (2011); 7 – Pertille et al. (2017). Samples from this study are indicated in the figure.

Figure 8: A) Lithological and geochronological sectors of the Capané Antiform (CA) and surrounding area. **B)** Simplified cross section of CA, showing three stages of evolution. First stage: deposition of Porongos I sequence (*P1*) over the Encantadas Gneiss (*EG?*). Second stage:

deposition of Porongos sequence II, represented by predominant metavolcano-sedimentary (P2mvs) and metasedimentary deposits (P2ms) in the front of large nappes. Third stage: thrusting of both sequences with imbrication of P1 and possibly EG. **C)** Simplified stratigraphy of Porongos Complex and Camaquã Basin (CB) in the CA area.

Figure 9: Simplified tectonic model (**1**; adapted from Basei et al., 2005; Frimmel and Fölling, 2004; Saalmann et al., 2011) and paleogeographic reconstruction (**2**; modified from Johansson, 2014; Pecoits et al., 2016) for southernmost Brazil during the amalgamation of SW Gondwana and accompanying closure of Adamastor Ocean. **1A)** *750–700 Ma*: Deposition of Porongos I sequence. Assembling of the São Gabriel block in the Rio de La Plata Craton, beginning of back-arc spreading at the African margin. **1B)** *700–650 Ma*: Closure of São Gabriel ocean and deformation of Porongos I sequence. At the African margin, onset of Gariep Basin deposition. **1C)** *650–600 Ma*: Intrusion of Capané Alkaline granite and metamorphism of Porongos I sequence. The compressional regime juxtaposes the Marmora Terrane and Port Nolloth Zone. **1D)** *600–550 Ma*: Closure of Adamastor Ocean; development of abundant collisional magmatism in the Pelotas arc and coeval synorogenic deposition of Porongos II sequence. Caçapava Granite intruded into the São Gabriel block and post-glacial deposits deposited in Africa. **1E)** *550–500 Ma*: Change to extensional regime, where the Camaquã and Nama basin successions are deposited. Pelotas arc records intense post-collisional magmatism. **2A)** ≥*750 Ma*: Rifting and plume-driven extension of Adamastor Ocean. **2B)** *750–650 Ma*: Development of Neoproterozoic

juvenile crust. **2C)** *650–550 Ma*: Amalgamation of Western Gondwana and full development of the Neoproterozoic fold belts.

Figure 10: Comparison of geochronological signatures of Neoproterozoic synorogenic basins in southernmost Brazil and Uruguay, for the Dom Feliciano Belt context. Syn- and post-collisional magmatism occurs between 600–550 Ma and refers to Pelotas and Aiguá batholiths. African signature refers to as sediments derived from Namaqua Complex with provenance constrained between 1.2 and 0.9 Ga. Transamazonian indicates the conspicuous crustal building events at 2.2–2.0 Ga. All of the samples present these three signatures in different ratios, according to their proximity to the arc and African cratons: closer to the former denotes more input of 600–550 Ma ages and closer to the latter more contribution of 1.2–0.9 Ga ages. Signatures of Porongos I and II sequences were obtained from the dataset presented in the Figure 7; Éden Block from Pecoits et al. (2016).

Table captions

Table 1: Summary of geochronological data of the Porongos Complex from previous works.

Table 2: Summary of samples from the Porongos Complex dated by LA-ICP-MS U-Pb detrital zircon grains presented in this study.

Figure 1

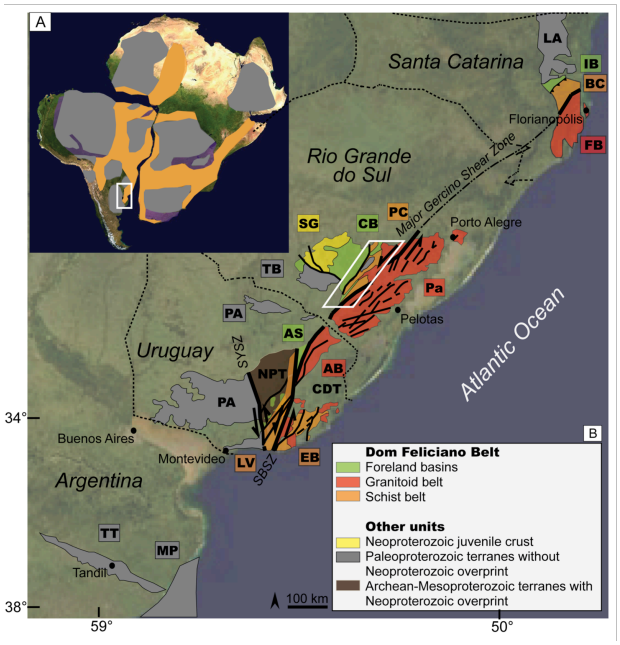
A
Santa Catarina
Rio Grande
do Sul
Florianópolis
Major Gercino Shear Zone
Porto Alegre
Pelotas
Atlantic Ocean
Uruguay
Argentina
Buenos Aires
Montevideo
Tandil
LA
IB
BC
FB
SG
CB
PC
Pa
TB
PA
AS
NPT
AB
CDT
EB
LV
TT
MP
SYSZ
SBSZ
34°
38°
59°
50°
100 km
B
Dom Feliciano Belt
Foreland basins
Granitoid belt
Schist belt
Other units
Neoproterozoic juvenile crust
Paleoproterozoic terranes without
Neoproterozoic overprint
Archean-Mesoproterozoic terranes with
Neoproterozoic overprint

Figure 2

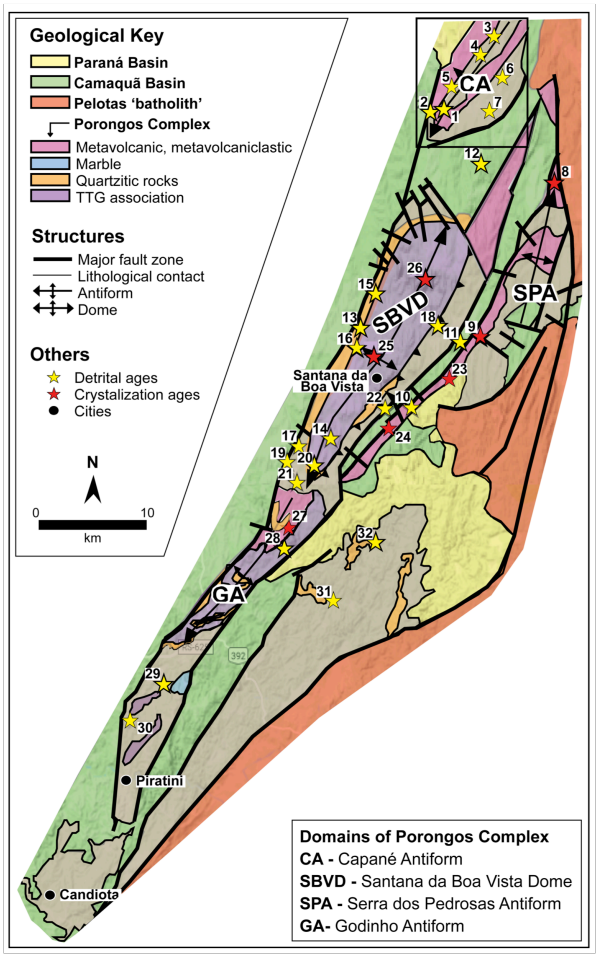
Geological Key
Paraná Basin
Camaquã Basin
Pelotas 'batholith'
Porongos Complex
Metavolcanic, metavolcaniclastic
Marble
Quartzitic rocks
TTG association
Structures
Major fault zone
Lithological contact
Antiform
Dome
Others
Detrital ages
Crystalization ages
Cities
N
0
10
km
CA
SBVD
SPA
GA
Santana da Boa Vista
Piratini
Candiota
Domains of Porongos Complex
CA - Capané Antiform
SBVD - Santana da Boa Vista Dome
SPA - Serra dos Pedrosas Antiform
GA- Godinho Antiform

Figure 3

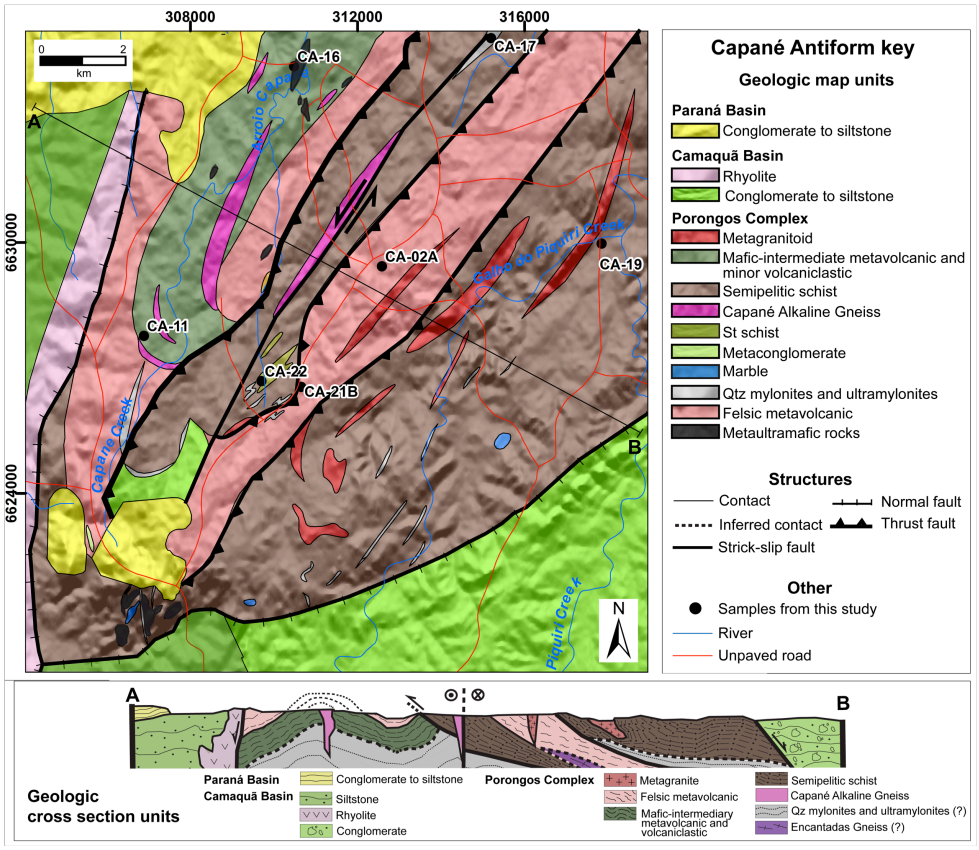
308000
312000
316000
6630000
6624000
0
2
km
CA-16
CA-17
CA-02A
CA-19
CA-11
CA-22
CA-21B
A
B
Capane Creek
Pigvirri Creek
N
Capané Antiform key
Geologic map units
Paraná Basin
Conglomerate to siltstone
Camaquã Basin
Rhyolite
Conglomerate to siltstone
Porongos Complex
Metagranitoid
Mafic-intermediate metavolcanic and minor volcaniclastic
Semipelitic schist
Capané Alkaline Gneiss
St schist
Metaconglomerate
Marble
Qtz mylonites and ultramylonites
Felsic metavolcanic
Metaultramafic rocks
Structures
Contact
Normal fault
Inferred contact
Thrust fault
Strick-slip fault
Other
Samples from this study
River
Unpaved road
Geologic cross section units
Paraná Basin
Camaquã Basin
Conglomerate to siltstone
Siltstone
Rhyolite
Conglomerate
Porongos Complex
Metagranite
Felsic metavolcanic
Mafic-intermediary metavolcanic and volcaniclastic
Semipelitic schist
Capané Alkaline Gneiss
Qz mylonites and ultramylonites (?)
Encantadas Gneiss (?)

Figure 4

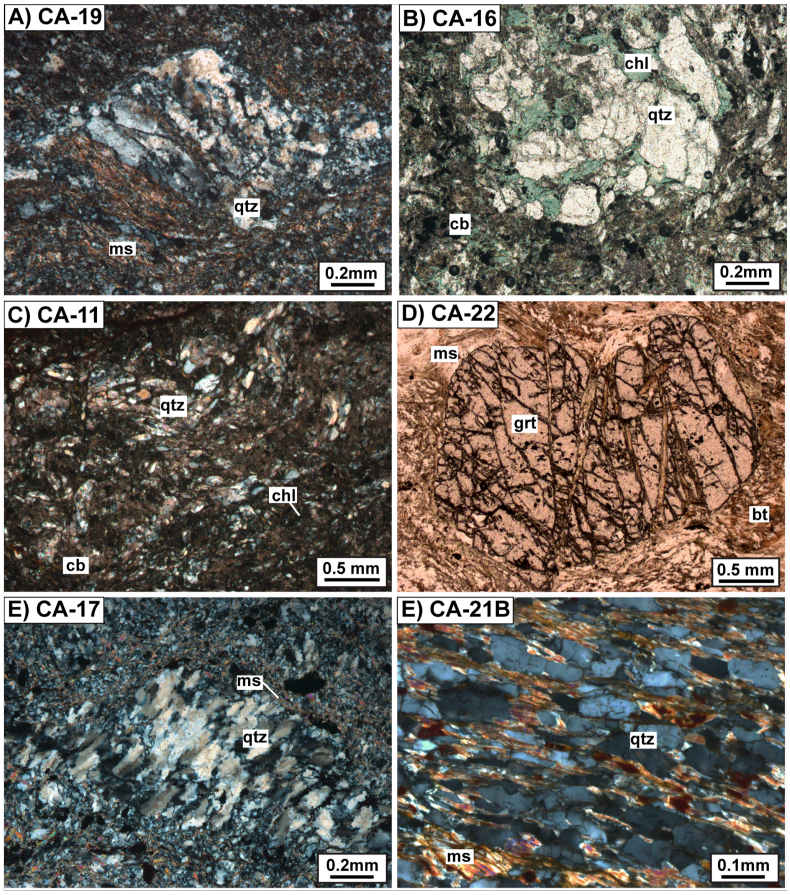
A) CA-19
qtz
ms
0.2mm
B) CA-16
chl
qtz
cb
0.2mm
C) CA-11
qtz
chl
cb
0.5 mm
D) CA-22
ms
grt
bt
0.5 mm
E) CA-17
ms
qtz
0.2mm
E) CA-21B
qtz
ms
0.1mm

Figure 5

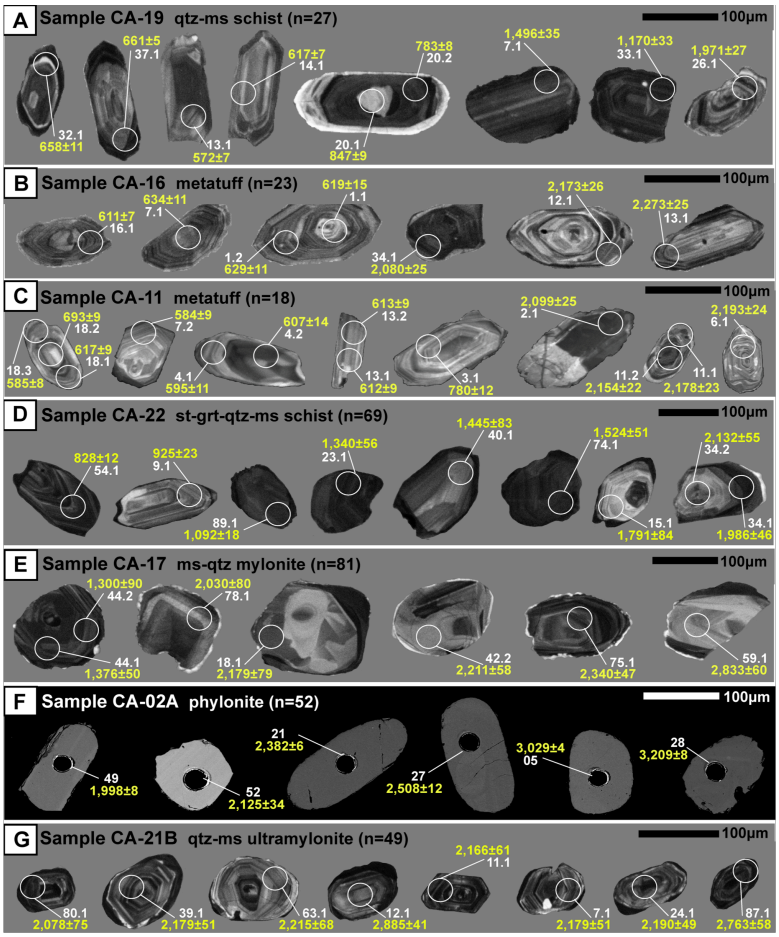
A Sample CA-19 qtz-ms schist (n=27)
100µm
661±5
37.1
617±7
14.1
783±8
20.2
1,496±35
7.1
1,170±33
33.1
1,971±27
26.1
32.1
658±11
13.1
572±7
20.1
847±9
B Sample CA-16 metatuff (n=23)
100µm
634±11
7.1
611±7
16.1
619±15
1.1
2,173±26
12.1
2,273±25
13.1
1.2
629±11
34.1
2,080±25
C Sample CA-11 metatuff (n=18)
100µm
693±9
18.2
584±9
7.2
607±14
4.2
613±9
13.2
2,099±25
2.1
2,193±24
6.1
617±9
18.1
18.3
585±8
4.1
595±11
13.1
612±9
3.1
780±12
11.2
2,154±22
11.1
2,178±23
D Sample CA-22 st-grt-qtz-ms schist (n=69)
100µm
828±12
54.1
925±23
9.1
1,340±56
23.1
1,445±83
40.1
1,524±51
74.1
2,132±55
34.2
89.1
1,092±18
15.1
1,791±84
34.1
1,986±46
E Sample CA-17 ms-qtz mylonite (n=81)
100µm
1,300±90
44.2
2,030±80
78.1
44.1
1,376±50
18.1
2,179±79
42.2
2,211±58
75.1
2,340±47
59.1
2,833±60
F Sample CA-02A phylonite (n=52)
100µm
21
2,382±6
3,029±4
05
28
3,209±8
49
1,998±8
52
2,125±34
27
2,508±12
G Sample CA-21B qtz-ms ultramylonite (n=49)
100µm
2,166±61
11.1
80.1
2,078±75
39.1
2,179±51
63.1
2,215±68
12.1
2,885±41
7.1
2,179±51
24.1
2,190±49
87.1
2,763±58

Figure 6

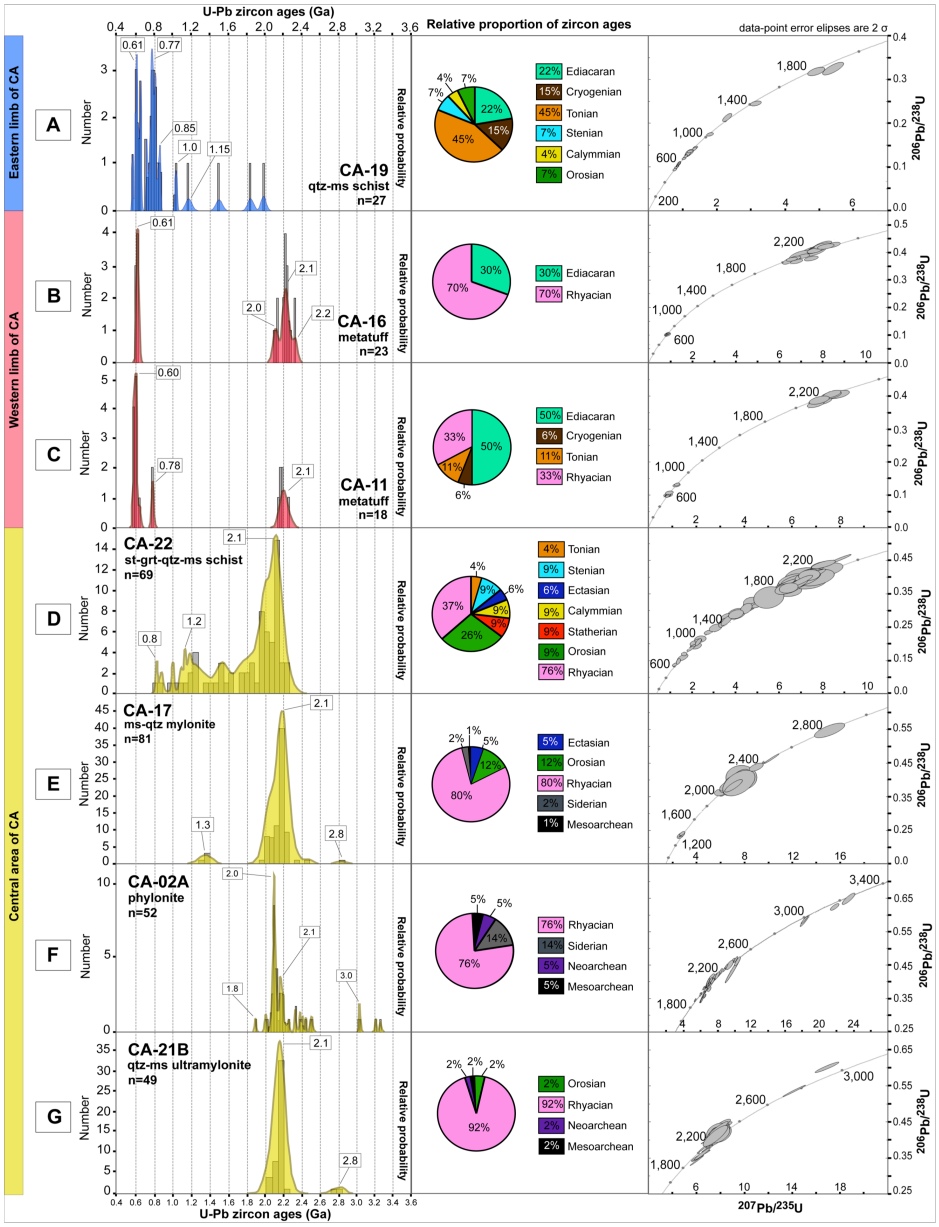
U-Pb zircon ages (Ga)
Relative proportion of zircon ages
data-point error elipses are 2 σ
Eastern limb of CA
Western limb of CA
Central area of CA
A
CA-19
qtz-ms schist
n=27
22% Ediacaran
15% Cryogenian
45% Tonian
7% Stenian
4% Calymmian
7% Orosian
B
CA-16
metatuff
n=23
30% Ediacaran
70% Rhyacian
C
CA-11
metatuff
n=18
50% Ediacaran
6% Cryogenian
11% Tonian
33% Rhyacian
D
CA-22
st-grt-qtz-ms schist
n=69
4% Tonian
9% Stenian
6% Ectasian
9% Calymmian
9% Statherian
9% Orosian
76% Rhyacian
E
CA-17
ms-qtz mylonite
n=81
5% Ectasian
12% Orosian
80% Rhyacian
2% Siderian
1% Mesoarchean
F
CA-02A
phylonite
n=52
76% Rhyacian
14% Siderian
5% Neoarchean
5% Mesoarchean
G
CA-21B
qtz-ms ultramylonite
n=49
2% Orosian
92% Rhyacian
2% Neoarchean
2% Mesoarchean
Number
Relative probability
206Pb/238U
207Pb/235U

Figure 7

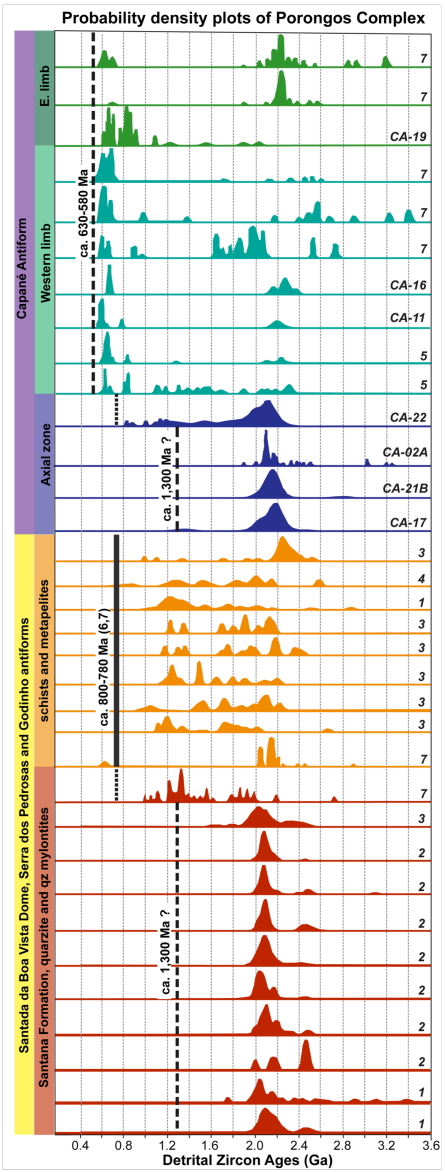
Probability density plots of Porongos Complex
Capané Antiform
E. limb
Western limb
Axial zone
Santada da Boa Vista Dome, Serra dos Pedrosas and Godinho antiforms
Santana Formation, quarzite and qz mylonites
schists and metapelites
ca. 630-580 Ma
ca. 1,300 Ma ?
ca. 800-780 Ma (6,7)
ca. 1,300 Ma ?
7
7
CA-19
7
7
7
CA-16
CA-11
5
5
CA-22
CA-02A
CA-21B
CA-17
3
4
1
3
3
3
3
3
7
7
3
2
2
2
2
2
2
2
2
1
1
0.4
0.8
1.2
1.6
2.0
2.4
2.8
3.2
3.6
Detrital Zircon Ages (Ga)

Figure 8

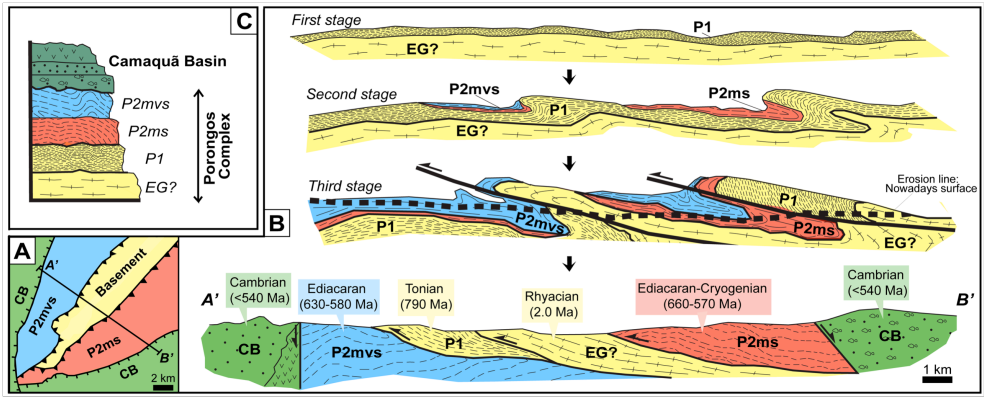
C
Camaquã Basin
P2mvs
P2ms
P1
EG?
Porongos Complex
B
First stage
P1
EG?
Second stage
P2mvs
P2ms
P1
EG?
Third stage
P1
P2mvs
P1
P2ms
EG?
Erosion line:
Nowadays surface
A
A'
CB
P2mvs
Basement
P2ms
B'
CB
2 km
A'
Cambrian
(<540 Ma)
Ediacaran
(630-580 Ma)
Tonian
(790 Ma)
Rhyacian
(2.0 Ma)
Ediacaran-Cryogenian
(660-570 Ma)
Cambrian
(<540 Ma)
B'
CB
P2mvs
P1
EG?
P2ms
CB
1 km

Figure 9

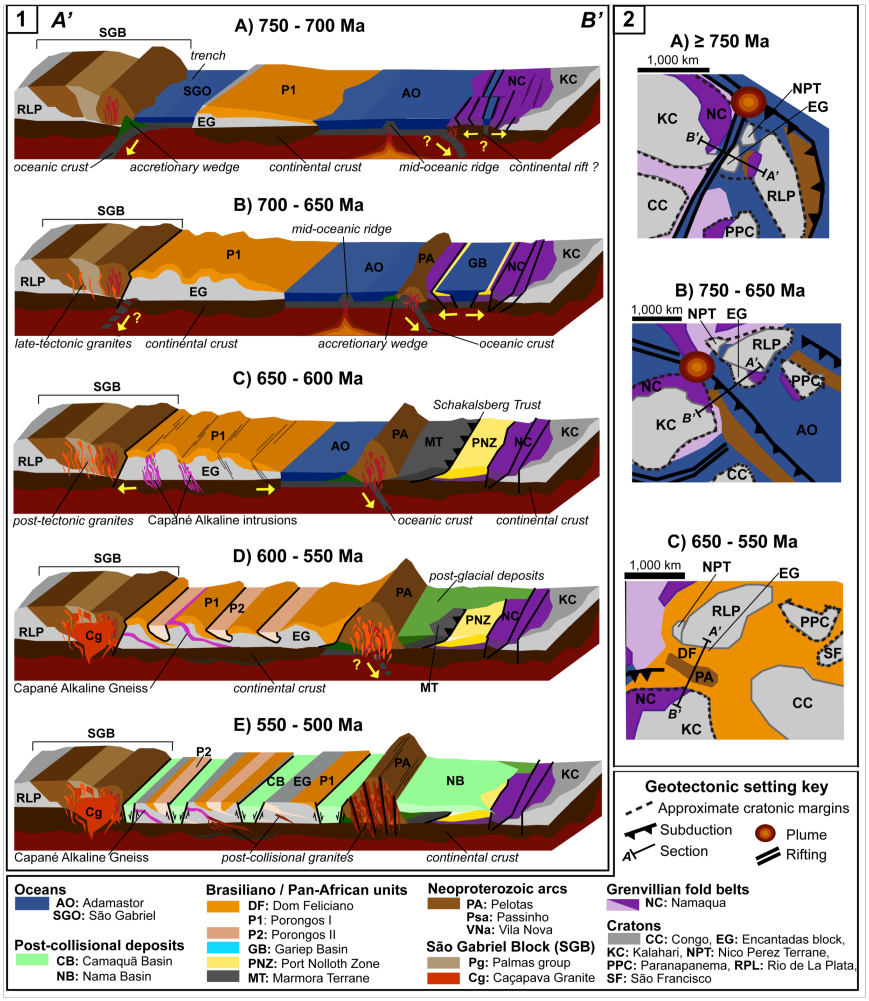
1
A'
B'
A) 750 - 700 Ma
SGB
trench
SGO
P1
AO
NC
KC
RLP
EG
oceanic crust
accretionary wedge
continental crust
mid-oceanic ridge
continental rift ?
B) 700 - 650 Ma
mid-oceanic ridge
PA
GB
late-tectonic granites
C) 650 - 600 Ma
Schakalsberg Trust
MT
PNZ
post-tectonic granites
Capané Alkaline intrusions
D) 600 - 550 Ma
post-glacial deposits
P2
Cg
Capané Alkaline Gneiss
E) 550 - 500 Ma
CB
NB
2
A) ≥ 750 Ma
1,000 km
NPT
B) 750 - 650 Ma
C) 650 - 550 Ma
CC
PPC
DF
SF
Geotectonic setting key
Approximate cratonic margins
Subduction
Section
Plume
Rifting
Oceans
AO: Adamastor
SGO: São Gabriel
Post-collisional deposits
CB: Camaquã Basin
NB: Nama Basin
Brasiliano / Pan-African units
DF: Dom Feliciano
P1: Porongos I
P2: Porongos II
GB: Gariep Basin
PNZ: Port Nolloth Zone
MT: Marmora Terrane
Neoproterozoic arcs
PA: Pelotas
Psa: Passinho
VNa: Vila Nova
São Gabriel Block (SGB)
Pg: Palmas group
Cg: Caçapava Granite
Grenvillian fold belts
NC: Namaqua
Cratons
CC: Congo, EG: Encantadas block,
KC: Kalahari, NPT: Nico Perez Terrane,
PPC: Paranapanema, RPL: Rio de La Plata,
SF: São Francisco

Figure 10

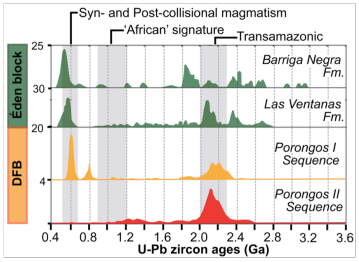
Syn- and Post-collisional magmatism
'African' signature
Transamazonic
Éden block
DFB
25
30
20
4
Barriga Negra Fm.
Las Ventanas Fm.
Porongos I Sequence
Porongos II Sequence
0.4
0.8
1.2
1.6
2.0
2.4
2.8
3.2
3.6
U-Pb zircon ages (Ga)

Table1. Summary of geochronological data of the Porongos Complex from previous works.

Domain		Fig.2 localization	Sample	Lithology	Dating method				Age (Ma)					Source	Position
					U-Pb zircon (number of analyses)			Rb-Sr whole rock	Crystallization	Provenance array		Main Peak	Metamorphism	Deformation		
					LA-ICP-MS	SHRIMP	TIMS									
Capané Antiform	Western limb	1	198	qtz-ms schist		30				2,267±14	579±20	585			Pertile et al. (2015b)	
		2	300	alb-chl schist		42				2,206±17	553±6	601				
		3	C-025	metapelite		29				2,811±12	550±10	585				
		4	C-275	metagreywake		33				2,231±16	569±8	606			Pertille et al. (2017)	
		5	C-175	qtz-ms schist		34				2,917±10	751±18	2196				
								x	531						Lafon (1990)	x
				alkaline gneiss	x				603±6				540		Zvirtes et al (2015)	x
							x		543±5				540		Chemale (2000)	x
	Eastern limb	6	C-041	gr-bt-ms schist		42				3,156±7	576±8	576			Pertille et al. (2017)	
		7	C-040	quartzite		36				2,481±30	618±15	2.105				
Serra dos Pedrosas Antiform		8		rhyolite		?			783±6					766 ± 13	Porcher et al. (1999)	
			CPM32, CPM34, CPM35, CPM6, CPM 4	muscovite				x					658±26		Lenz et al. (1999)	Gruber et al. (2011)
		9		metarhyolite	29				789.5±7.1						Saalmann et al. (2011)	
		10	RIP-04	chl-ms schist	39					2,520±51	1,010±17	2.254			Gruber et al. (2011)	
		11	POR-12	qtz-ms schist	22					2,652±32	1,149±26	1.217				
				intermediate volcanic rocks		x			789±39						Soliani Jr. (1986)	x
Santana da Boa Vista Dome	Supracrustal sequence	12	5 - Figueiras	quartzite		7				2,486±20	2,004±13	2.100			Hartmann et al. (2004)	
		13	3 - Godinho			31				2,488±12	1,990±15	2.079				
					98					3,384±24	1,766±40	2.082			Pertille et al. (2015a)	
		14	RIP-08	qtz mylonite	19					2,910±24	1,750±18	2.045			Gruber et al. (2011)	
		15	4 - Coxilha do Raio	quartzite		31				2,449±28	1,950±78	2.056			Hartmann et al. (2004)	
					96					2,506±38	1,980±34	2074			Pertille et al. (2015a)	
		16	1 - Alto Bonito			21				2,459±22	2,030±21	2.087			Hartmann et al. (2004)	
		17	2 - Aberto dos Cerros			34				3,092±19	2,015±15	2.078				
		18	POR-13A		13					2,195±31	1,113±42	1.488				
		19	RIP-03	chl-ms schist	13					2,414±31	1,164±21	2.100			Gruber et al. (2011)	
		20	RIP-05		11					2,169±15	1,153±22	2.100				
		21	RIP-06		15					2,220±28	1,041±46	2.100				
		22	BRAF34	sericitic phyllite		23				2,581±11	622±17	620			Basei et al. (2008)	
		23	R-088	rhyolite		11			773±3.1						Pertille et al. (2017)	
		24	R-015	rhyolite		17			801±4.7							
	Encantadas Gneiss	25	BR-140-1	ultramafic amphibolite		8			2,257±12				702±21		Hartmann et al. (2003)	
		26				x			2,263±18				2,045±10		Hartmann et al. (2000)	Hartmann et al. (2004)
				tonalite				x	2.1						Soliani Jr. (1986)	x
					31				2,234±28						Saalmann et al. (2011)	x
								x	2100				544±18		Cordani et al. (1974)	
				pegmatite	x				2,263±6				2,021±11		Chemale (2000), Hartmann et al. (2000)	x
				granodiorite	x				2,078±13				600-800		Hartmann et al. (2000)	x
					x								631			x
				gneiss			x		2,237±158				803±14		Chemale (2000)	x
Godinho Antiform				metandesite			x		773±8						Chemale (2000)	Gruber et al. (2011)
		27	R-001	rhyolite	19				809±4.1						Pertille et al. (2017)	
		28	RIP-11	qtz mylonite	48					2,906±42	1,619±39	2.039			Gruber et al. (2011)	
				metavolcanic	x				1,356±227				700		Wildner et al. (1996)	x
S-SW sectors		29	6 - Jaíba	quartzite		43				2,454±12	1,998±15	2.07			Hartmann et al. (2004)	
		30	T-148	plg-qtz-chl-ms schist		28				2,937±8	605±5	2.171			Pertille et al. (2017)	
		31	P-122	quartzite		36				2,705±17	994±5	1.306				
		32	PJP-06	ms schist	64					2,863±24	1,008±12	1.008			Pertille et al. (2015a)	

Mineral abreviation: *alb* - albite, *bt*- biotite, *chl* - chlorite, *gr*- garnet, *ms* - muscovite, *plg* - plagioclase, *qtz* - quartz. The symbol *x* stands for absent data.

Table 2. Summary of samples from the Porongos Complex dated by LA-ICP-MS U-Pb detrital zircon grains presented in this study.

Domain		Sample	Lithology	Coordinates UTM	
				W	S
Capané Antiform	Western limb	CA-11	metavolcaniclastic rock	306857	6627772
		CA-16	metavolcaniclastic rock	210450	6634224
	Eastern limb	CA-19	quartz-muscovite schist	317853	6629998
	Axial zone	CA-02A	phyllonite	312603	6629445
		CA-17	quartz mylonite	315834	6635619
		CA-21B	quartz-muscovite ultramylonite	310575	6626591
		CA-22	staurolite-garnet schist	309759	6626687

Table 1. LA-ICP-MS U-Pb in situ zircon analysis from CA-02A sample (phylonite). Italicized data were not used in age determinations and plotting, due high levels of discordance and common lead.

SAMPLE	SPOT	RATIOS								Th/U	Common Pb	AGES (Ma)						CONC. (%)
		207/235	1sigma	206/238	1 sigma	coef. corr	206/204	207/206	1 sigma		(%)	T206/208	1 sigma	T207/235	1 sigma	T207/206	1 sigma	
CA-02A	3	18.3106	1.2	0.58204	1.2	0.95	250007	0.22816	0.4	0.25	0.01	2957.1	27.9	3006.2	11.8	3039.2	5.8	97.30
CA-02A	4	6.6055	1.0	0.37268	1.0	0.95	15861	0.12855	0.3	0.42	0.10	2042.0	17.2	2060.1	9.0	2078.2	5.2	98.26
CA-02A	5	18.2929	0.8	0.58512	0.8	0.94	35045	0.22675	0.3	0.32	0.04	2969.6	18.5	3005.3	7.9	3029.2	4.2	98.03
CA-02A	6	6.6616	0.8	0.37173	0.7	0.89	45880	0.12997	0.4	0.28	0.03	2037.5	11.4	2067.5	6.8	2097.6	7.1	97.14
CA-02A	9	6.6463	0.8	0.36827	0.7	0.86	17491	0.13089	0.4	0.36	0.09	2021.3	12.3	2065.5	7.1	2110.0	6.8	95.80
CA-02A	10	7.1377	0.8	0.39756	0.7	0.87	19731	0.13021	0.4	0.76	0.08	2157.8	13.4	2128.8	7.3	2100.8	6.7	102.71
CA-02A	11	9.9368	0.8	0.46331	0.6	0.75	7813	0.15555	0.5	0.13	0.18	2454.1	12.8	2428.9	7.3	2407.9	8.1	101.92
CA-02A	12	6.4890	0.7	0.38008	0.6	0.81	19262	0.12382	0.5	0.32	0.08	2076.7	10.2	2044.4	6.5	2012.0	8.1	103.21
CA-02A	15	7.0712	0.9	0.39261	0.8	0.78	64022	0.13063	0.6	0.49	0.02	2134.9	13.9	2120.4	8.4	2106.4	9.8	101.35
CA-02A	16	6.5980	0.8	0.35572	0.6	0.80	10370	0.13453	0.4	0.36	0.15	1961.8	10.8	2059.1	6.7	2157.9	7.2	90.92
CA-02A	18	7.9212	1.1	0.41835	0.7	0.81	12942	0.13733	0.8	0.35	0.11	2253.0	13.9	2222.1	9.8	2193.8	14.0	102.70
CA-02A	21	9.4941	0.8	0.44936	0.7	0.84	85670	0.15323	0.4	0.72	0.02	2392.4	13.6	2387.0	7.2	2382.3	6.7	100.42
CA-02A	22	6.2599	1.7	0.34990	1.7	0.98	6456	0.12976	0.4	0.31	0.24	1934.1	28.4	2012.9	15.2	2094.7	6.6	92.34
CA-02A	24	8.9404	0.9	0.43693	0.7	0.85	34292	0.14840	0.6	0.50	0.04	2336.9	13.1	2331.9	8.2	2327.6	10.1	100.40
CA-02A	27	9.8507	3.6	0.43282	3.5	0.98	88601	0.16507	0.8	0.46	0.02	2318.4	67.6	2420.9	32.7	2508.3	12.7	92.43
CA-02A	28	21.8382	0.9	0.62380	0.7	0.77	611764	0.25391	0.5	0.39	0.00	3125.0	17.2	3176.6	8.3	3209.3	8.0	97.37
CA-02A	30	6.9464	1.7	0.38775	1.0	0.77	153649	0.12993	1.4	0.46	0.01	2112.4	17.5	2104.6	15.1	2097.0	24.6	100.73
CA-02A	35	7.6522	0.9	0.40387	0.8	0.89	78624	0.13742	0.4	0.29	0.02	2186.8	15.2	2191.0	8.1	2194.9	6.8	99.63
CA-02A	36	8.3872	1.3	0.42688	1.2	0.91	60179	0.14250	0.5	0.84	0.02	2291.6	23.1	2273.8	11.9	2257.8	9.2	101.50
CA-02A	37	6.9068	0.8	0.38908	0.7	0.87	61053	0.12875	0.4	0.51	0.02	2118.6	12.8	2099.5	7.1	2080.9	6.4	101.81
CA-02A	38	7.0524	1.4	0.39497	1.2	0.95	38606	0.12950	0.6	0.74	0.04	2145.8	22.0	2118.1	12.2	2091.2	11.4	102.61
CA-02A	41	7.0276	0.9	0.39234	0.8	0.83	85995	0.12991	0.5	0.59	0.02	2133.7	14.5	2114.9	8.4	2096.7	8.8	101.76
CA-02A	42	6.8154	1.2	0.37811	1.0	0.83	27840	0.13073	0.7	0.95	0.05	2067.4	17.8	2087.7	10.7	2107.8	11.5	98.09
CA-02A	43	7.1319	1.2	0.37686	0.8	0.63	5869	0.13725	0.9	13.77	0.26	2061.6	14.5	2128.0	11.1	2192.8	16.3	94.02
CA-02A	44	7.4825	1.2	0.40172	0.8	0.85	80934	0.13509	0.8	0.77	0.02	2176.9	15.3	2170.9	10.4	2165.2	14.2	100.54
CA-02A	47	10.4422	1.4	0.46044	1.2	0.83	38009	0.16448	0.8	0.36	0.04	2441.5	23.8	2474.8	13.0	2502.3	12.8	97.57
CA-02A	48	7.2702	0.7	0.39048	0.6	0.84	56914	0.13503	0.3	0.69	0.03	2125.1	11.1	2145.2	6.3	2164.4	6.0	98.18
CA-02A	49	6.1172	0.8	0.36106	0.7	0.79	44561	0.12288	0.5	0.72	0.03	1987.2	11.7	1992.7	7.3	1998.4	8.5	99.44
CA-02A	50	6.8456	1.1	0.38591	0.8	0.87	24504	0.12865	0.7	0.38	0.06	2103.8	15.1	2091.6	9.9	2079.7	12.8	101.16
CA-02A	52	7.2950	3.0	0.40059	2.3	0.75	19590	0.13208	2.0	0.88	0.08	2171.7	42.3	2148.2	27.1	2125.8	34.8	102.16
CA-02A	53	6.2712	1.3	0.34553	1.2	0.92	11427	0.13163	0.5	0.55	0.13	1913.2	19.4	2014.4	11.1	2119.9	8.6	90.25
CA-02A	54	7.1585	1.2	0.39305	1.0	0.86	57538	0.13209	0.6	0.84	0.03	2137.0	19.0	2131.3	10.7	2125.9	10.6	100.52
CA-02A	55	7.6132	1.6	0.40601	1.1	0.87	8453	0.13600	1.1	0.37	0.17	2196.6	21.2	2186.4	14.5	2176.9	19.9	100.91
CA-02A	60	6.9946	1.3	0.39777	1.1	0.82	5463	0.12754	0.7	0.33	0.27	2158.8	20.3	2110.7	11.9	2064.3	13.2	104.58
CA-02A	61	7.1418	0.9	0.39760	0.7	0.77	41826	0.13028	0.5	0.31	0.04	2158.0	13.1	2129.3	7.9	2101.7	9.4	102.68
CA-02A	62	7.7953	1.1	0.41547	0.7	0.78	130676	0.13608	0.8	0.68	0.01	2239.9	13.3	2207.7	9.6	2177.9	14.0	102.85
CA-02A	65	23.4493	1.3	0.64845	1.1	0.86	126706	0.26227	0.6	0.33	0.01	3222.2	27.6	3245.8	12.2	3260.4	9.8	98.83
CA-02A	66	5.4842	0.7	0.34363	0.6	0.81	292352	0.11575	0.4	0.11	0.01	1904.1	10.3	1898.1	6.3	1891.6	7.1	100.66
CA-02A	67	8.0793	1.4	0.41784	1.1	0.79	27115	0.14024	0.9	0.71	0.05	2250.7	21.7	2239.9	12.9	2230.1	15.0	100.92
CA-02A	68	6.5548	1.0	0.35606	0.7	0.85	36013	0.13352	0.7	0.38	0.04	1963.5	12.4	2053.3	8.7	2144.7	11.5	91.55
CA-02A	71	9.5221	1.8	0.44914	1.3	0.74	220151	0.15376	1.2	0.97	0.01	2391.4	26.7	2389.7	16.4	2388.2	20.1	100.14
CA-02A	72	7.5200	0.8	0.40090	0.7	0.82	188479	0.13604	0.4	0.54	0.01	2173.2	13.1	2175.4	7.5	2177.4	7.8	99.81
CA-02A	73	6.5853	0.7	0.36763	0.7	0.88	126069	0.12992	0.3	0.64	0.01	2018.2	11.6	2057.4	6.5	2096.8	5.6	96.25
CA-02A	74	9.1297	0.8	0.44538	0.7	0.88	169691	0.14867	0.5	0.19	0.01	2374.7	13.4	2351.1	7.5	2330.7	7.9	101.89
CA-02A	77	6.7702	1.0	0.37782	0.9	0.86	68064	0.12996	0.5	0.20	0.02	2066.1	15.2	2081.8	8.6	2097.4	8.2	98.51
CA-02A	78	6.8280	0.9	0.38089	0.8	0.89	98342	0.13001	0.4	0.22	0.02	2080.4	13.9	2089.4	7.6	2098.2	6.4	99.16
CA-02A	79	6.9427	0.8	0.38811	0.8	0.90	235387	0.12974	0.3	0.60	0.01	2114.1	13.9	2104.1	7.5	2094.5	6.1	100.94
CA-02A	80	6.6936	1.2	0.37567	0.7	0.76	86882	0.12923	0.9	0.38	0.02	2056.0	12.4	2071.8	10.3	2087.5	16.2	98.49
CA-02A	83	10.2068	0.9	0.46590	0.8	0.86	456308	0.15889	0.4	0.38	0.00	2465.6	16.4	2453.7	8.4	2443.9	7.4	100.89
CA-02A	84	7.5127	1.1	0.40109	0.9	0.80	127193	0.13585	0.7	0.68	0.01	2174.1	17.2	2174.5	10.2	2174.9	11.5	99.96
CA-02A	85	7.3361	1.0	0.40450	0.8	0.75	121596	0.13154	0.6	0.72	0.01	2189.7	14.3	2153.2	8.9	2118.6	10.9	103.36
CA-02A	86	7.1301	0.8	0.39302	0.6	0.85	270375	0.13158	0.5	0.23	0.01	2136.8	11.4	2127.8	7.3	2119.1	9.4	100.84
CA-02A	*17*	*5.6990*	*1.9*	*0.31047*	*1.9*	*0.97*	*6371*	*0.13313*	*0.5*	*0.74*	*0.25*	*1743.0*	*28.3*	*1931.2*	*16.6*	*2139.7*	*8.7*	*81.46*
CA-02A	*23*	*0.9321*	*1.6*	*0.05510*	*1.0*	*0.60*	*381*	*0.12268*	*1.3*	*0.24*	*4.77*	*345.8*	*3.4*	*668.7*	*7.9*	*1995.6*	*22.5*	*17.33*
CA-02A	*29*	*4.7487*	*3.0*	*0.25048*	*3.0*	*0.99*	*1214*	*0.13750*	*0.5*	*0.70*	*1.34*	*1441.0*	*38.7*	*1775.9*	*25.5*	*2195.9*	*9.0*	*65.62*
CA-02A	*59*	*4.1373*	*2.3*	*0.23404*	*2.2*	*0.98*	*2560*	*0.12821*	*0.4*	*0.38*	*0.64*	*1355.7*	*27.1*	*1661.7*	*18.5*	*2073.6*	*7.7*	*65.38*

Table 2. LA-ICP-MS U-Pb in situ zircon analysis from CA-11 sample (metatuff). Italicized data were not used in age determinations and plotting, due high levels of discordance and common lead. Data marked with (*) represent inherited nucleis.

SAMPLE	SPOT	RATIOS											Commom Pb	Pb rad	Th	U	Th/U	AGES (Ga)				CONC. (%)
		207/235	1sigma	206/238	1 sigma	coef. corr	238/206	1 sigma	207/206	1 sigma	208/206	1 sigma	(%)	ppm	ppm	ppm		T206/208	1 sigma	T207/206	1 sigma	
CA-11	4.1	0.8264	0.0666	0.0988	0.0023	0.18	10.1228	0.2402	0.0607	0.0054	0.3052	0.0168	0.50	23.9	176.6	170.1	1.038	0.607	0.014	0.628	0.193	96
CA-11	4.2	0.8073	0.0462	0.0966	0.0018	0.52	10.3499	0.1963	0.0606	0.0037	0.3174	0.0161	0.86	31.8	253.1	229.4	1.103	0.595	0.011	0.625	0.133	95
CA-11	7.2	0.7878	0.0362	0.0949	0.0016	0.45	10.5424	0.1725	0.0602	0.0029	0.1497	0.0143	0.52	42.2	194.2	347.6	0.559	0.584	0.009	0.612	0.104	95
CA-11	12.1	0.8062	0.0283	0.0969	0.0013	0.58	10.3244	0.1393	0.0604	0.0020	0.1636	0.0160	0.26	86.5	436.8	691.4	0.632	0.596	0.008	0.617	0.072	96
CA-11	13.1	0.8433	0.0371	0.0997	0.0015	0.54	10.0257	0.1505	0.0613	0.0026	0.3653	0.0693	0.27	80.1	808.7	504.6	1.603	0.613	0.009	0.650	0.089	94
CA-11	13.2	0.8433	0.0330	0.0996	0.0014	0.70	10.0406	0.1428	0.0614	0.0024	0.3628	0.0684	0.16	74.4	736.7	485.2	1.518	0.612	0.008	0.654	0.089	93
CA-11	18.1	0.8303	0.0385	0.1004	0.0015	0.83	9.9615	0.1493	0.0600	0.0028	0.2644	0.0891	3.33	65.5	779.2	509.3	1.530	0.617	0.009	0.603	0.100	102
CA-11	18.2	0.8317	0.0377	0.0981	0.0015	0.64	10.1933	0.1519	0.0615	0.0027	0.4317	0.0653	0.48	33.7	256.9	233.5	1.100	0.603	0.009	0.656	0.096	91
CA-11	18.3	0.7963	0.0299	0.0949	0.0013	0.97	10.5327	0.1444	0.0608	0.0022	0.1056	0.0147	0.43	45.1	150.2	385.8	0.389	0.585	0.008	0.633	0.079	92
CA-11	1.1*	0.8748	0.0606	0.1056	0.0023	0.01	9.4665	0.2033	0.0601	0.0044	0.1867	0.0455	0.54	17.1	104.6	118.4	0.8840	0.647	0.013	0.606	0.159	106
CA-11	2.1*	7.1744	0.1766	0.3850	0.0053	0.99	2.5976	0.0358	0.1352	0.0032	0.1285	0.0287	0.66	112.0	181.3	214.6	0.845	2.099	0.025	2.166	0.041	96
CA-11	3.1*	1.1801	0.0535	0.1285	0.0022	0.42	7.7793	0.1312	0.0666	0.0032	0.1730	0.0153	0.52	35.8	110.0	223.6	0.492	0.780	0.012	0.825	0.097	94
CA-11	5.1*	1.2064	0.0432	0.1304	0.0019	0.25	7.6670	0.1142	0.0671	0.0024	0.2138	0.0086	0.17	74.0	340.3	415.1	0.820	0.790	0.011	0.840	0.076	94
CA-11	6.1*	7.9351	0.1761	0.4051	0.0052	0.96	2.4684	0.0315	0.1421	0.0028	0.2521	0.0102	0.08	181.4	314.8	310.6	1.013	2.193	0.024	2.252	0.034	97
CA-11	9.1*	6.9879	0.1394	0.3750	0.0043	0.97	2.6665	0.0308	0.1351	0.0023	0.0977	0.0134	0.09	363.3	339.0	752.6	0.450	2.053	0.020	2.166	0.030	94
CA-11	11.1*	7.6273	0.1648	0.4020	0.0050	0.84	2.4878	0.0310	0.1376	0.0026	0.1087	0.0026	0.09	198.7	166.2	388.1	0.428	2.178	0.023	2.198	0.033	99
CA-11	11.2*	7.6704	0.1535	0.4053	0.0048	1.00	2.4671	0.0293	0.1372	0.0022	0.1775	0.0121	0.00	242.9	199.4	400.7	0.4970	2.194	0.022	2.193	0.029	100
CA-11	15.1*	7.1337	0.1643	0.3874	0.0050	0.31	2.5810	0.0336	0.1335	0.0027	0.0792	0.0321	0.40	112.0	82.2	220.6	0.373	2.111	0.023	2.145	0.035	98
CA-11	*7.1*	*0.7680*	*0.0500*	*0.0978*	*0.0020*	*0.26*	*10.2199*	*0.2039*	*0.0569*	*0.0039*	*0.1491*	*0.0253*	*0.75*	*32.1*	*143.9*	*253.1*	*0.569*	*0.602*	*0.011*	*0.489*	*0.151*	*123*
CA-11	*8.1*	*0.8102*	*0.0332*	*0.0981*	*0.0015*	*0.82*	*10.1975*	*0.1555*	*0.0599*	*0.0026*	*0.4202*	*0.0186*	*5.94*	*75.4*	*987.0*	*536.0*	*1.841*	*0.603*	*0.009*	*0.601*	*0.091*	*100*
CA-11	*10.1*	*0.8190*	*0.0225*	*0.0970*	*0.0012*	*0.85*	*10.3092*	*0.1292*	*0.0612*	*0.0016*	*0.0293*	*0.0035*	*1.34*	*117.1*	*127.4*	*1082.7*	*0.118*	*0.597*	*0.007*	*0.648*	*0.055*	*92*
CA-11	*14.1*	*0.8211*	*0.0330*	*0.0993*	*0.0014*	*0.89*	*10.0691*	*0.1418*	*0.0600*	*0.0025*	*0.6933*	*0.1135*	*30.69*	*82.5*	*1205.4*	*428.5*	*2.813*	*0.610*	*0.008*	*0.602*	*0.088*	*101*
CA-11	*16.1*	*0.6914*	*0.0184*	*0.0829*	*0.0010*	*0.99*	*12.0639*	*0.1411*	*0.0605*	*0.0016*	*0.0642*	*0.0112*	*2.35*	*131.5*	*361.8*	*1309.4*	*0.276*	*0.513*	*0.006*	*0.621*	*0.054*	*82*
CA-11	*17.1**	*1.1250*	*0.0316*	*0.1243*	*0.0016*	*0.96*	*8.0483*	*0.1026*	*0.0657*	*0.0017*	*0.0941*	*0.0031*	*3.17*	*120.9*	*361.8*	*908.7*	*0.398*	*0.755*	*0.009*	*0.796*	*0.053*	*94*

Table 3. LA-ICP-MS U-Pb in situ zircon analysis from CA-16 sample (metatuff). Italicized data were not used in age determinations and plotting, due high levels of discordance and common lead.

SAMPLE	SPOT	RATIOS												Commom Pb	Pb rad	Th	U	Th/U	AGES (Ga)						CONC. (%)	
		207/235	1sigma	206/238	1 sigma	coef. corr	238/206	1 sigma	207/206	1 sigma	208/206	1 sigma		(%)	ppm	ppm	ppm		T206/208	1 sigma	T207/235	1 sigma	T207/206	1 sigma	206/238 207/235	206/238 207/206
CA-16	1.1	0.8654	0.0513	0.1008	0.0026	0.82	9.9164	0.2517	0.0622	0.0038	0.2845	0.0210		0.49	13	69	80	0.87	0.619	0.015	0.633	0.027	0.682	0.131	97	90
CA-16	1.2	0.8592	0.0290	0.1024	0.0019	0.91	9.7649	0.1806	0.0608	0.0020	0.1866	0.0116		0.25	23	102	160	0.64	0.629	0.011	0.630	0.016	0.634	0.072	99	99
CA-16	2.1	6.4751	0.1178	0.3705	0.0056	0.92	2.6994	0.0408	0.1268	0.0018	0.2774	0.0102		0.21	108	156	173	0.91	2.032	0.026	2.043	0.016	2.054	0.025	99	98
CA-16	5.1	7.5561	0.1939	0.4037	0.0080	0.96	2.4772	0.0489	0.1358	0.0034	0.3707	0.0699		0.61	20	36	29	1.27	2.186	0.037	2.180	0.024	2.174	0.044	100	100
CA-16	6.1	7.9675	0.1577	0.4240	0.0069	0.83	2.3585	0.0382	0.1363	0.0022	0.1447	0.0025		0.02	56	42	91	0.45	2.279	0.031	2.227	0.018	2.181	0.028	102	104
CA-16	7.1	0.8582	0.0301	0.1034	0.0020	0.76	9.6758	0.1828	0.0602	0.0021	0.1588	0.0168		0.98	21	80	148	0.54	0.634	0.011	0.629	0.017	0.612	0.076	100	103
CA-16	8.1	6.9128	0.1602	0.3891	0.0070	0.76	2.5700	0.0464	0.1288	0.0026	0.2108	0.0144		0.10	48	50	82	0.60	2.119	0.033	2.100	0.020	2.082	0.036	100	101
CA-16	9.1	7.6990	0.1373	0.4133	0.0062	0.99	2.4194	0.0362	0.1351	0.0020	0.1823	0.0064		0.22	77	68	122	0.56	2.230	0.028	2.196	0.016	2.165	0.025	101	102
CA-16	12.1	7.6926	0.1462	0.4111	0.0065	0.92	2.4324	0.0384	0.1357	0.0021	0.1899	0.0078		0.24	77	86	122	0.70	2.220	0.030	2.196	0.017	2.173	0.026	101	102
CA-16	13.1	8.4582	0.1381	0.4268	0.0040	0.94	2.3431	0.0221	0.1437	0.0020	0.2148	0.0061		0.09	104	126	153	0.82	2.291	0.018	2.281	0.015	2.273	0.025	100	100
CA-16	14.1	0.8664	0.0332	0.1026	0.0014	0.43	9.7453	0.1358	0.0612	0.0025	0.1285	0.0225		0.72	17	51	118	0.43	0.630	0.008	0.634	0.018	0.648	0.091	99	97
CA-16	16.1	0.8157	0.0240	0.0995	0.0012	0.86	10.0544	0.1180	0.0595	0.0017	0.2218	0.0129		0.72	24	100	159	0.63	0.611	0.007	0.606	0.013	0.585	0.063	100	104
CA-16	18.1	7.7213	0.1440	0.4101	0.0044	0.87	2.4382	0.0260	0.1365	0.0023	0.1801	0.0043		0.60	61	60	95	0.63	2.216	0.020	2.199	0.017	2.184	0.029	100	101
CA-16	19.1	0.8310	0.0246	0.1000	0.0012	0.52	9.9952	0.1168	0.0602	0.0018	0.1948	0.0072		0.42	24	98	155	0.63	0.615	0.007	0.614	0.014	0.612	0.061	100	100
CA-16	22.1	7.6230	0.1336	0.4068	0.0041	0.87	2.4583	0.0245	0.1359	0.0021	0.1955	0.0060		0.08	67	65	107	0.61	2.200	0.019	2.188	0.016	2.176	0.027	100	101
CA-16	24.1	7.9772	0.1489	0.4233	0.0045	0.91	2.3621	0.0251	0.1367	0.0023	0.0887	0.0228		0.18	57	39	92	0.43	2.276	0.020	2.228	0.017	2.185	0.029	102	104
CA-16	27.1	7.1135	0.1020	0.3860	0.0034	0.97	2.5909	0.0226	0.1337	0.0018	0.0771	0.0450		0.15	105	100	187	0.53	2.104	0.016	2.126	0.013	2.147	0.024	98	98
CA-16	29.1	8.1334	0.1443	0.4213	0.0043	0.97	2.3738	0.0240	0.1400	0.0023	0.2169	0.0118		0.45	42	37	66	0.57	2.266	0.019	2.246	0.016	2.228	0.028	100	101
CA-16	30.1	7.4700	0.1263	0.3772	0.0037	0.96	2.6509	0.0259	0.1436	0.0021	0.1532	0.0623		0.43	97	151	145	1.04	2.063	0.017	2.169	0.014	2.271	0.025	95	90
CA-16	33.1	6.7984	0.1095	0.3675	0.0035	0.93	2.7214	0.0260	0.1342	0.0019	0.1387	0.0246		0.41	101	116	164	0.71	2.017	0.016	2.086	0.014	2.153	0.025	96	93
CA-16	34.1	6.7159	0.1038	0.3786	0.0035	0.70	2.6416	0.0244	0.1287	0.0018	0.1018	0.0018		0.26	101	77	191	0.40	2.070	0.016	2.075	0.014	2.080	0.025	99	99
CA-16	38.1	0.8478	0.0155	0.1011	0.0008	0.67	9.8906	0.0804	0.0608	0.0011	0.1837	0.0121		0.75	57	241	414	0.58	0.621	0.005	0.623	0.009	0.633	0.039	99	98
CA-16	40.1	6.5711	0.0961	0.3744	0.0028	0.99	2.6706	0.0203	0.1273	0.0018	0.0504	0.0043		0.17	97	39	203	0.19	2.05	0.013	2.055	0.013	2.061	0.025	99	99
CA-16	*3.1*	*0.7804*	*0.0183*	*0.0927*	*0.0015*	*0.89*	*10.7882*	*0.1717*	*0.0611*	*0.0012*	*0.0639*	*0.0027*		*2.38*	*51*	*85*	*423*	*0.20*	*0.571*	*0.009*	*0.586*	*0.010*	*0.641*	*0.043*	*97*	*89*
CA-16	*4.1*	*7.0581*	*0.1564*	*0.3988*	*0.0069*	*0.43*	*2.5076*	*0.0434*	*0.1284*	*0.0024*	*0.1961*	*0.0089*		*1.62*	*41*	*39*	*67*	*0.59*	*2.163*	*0.032*	*2.119*	*0.020*	*2.076*	*0.033*	*102*	*104*
CA-16	*10.1*	*4.1297*	*0.0677*	*0.2458*	*0.0034*	*0.98*	*4.0691*	*0.0564*	*0.1219*	*0.0016*	*0.0385*	*0.0164*		*3.38*	*134*	*28*	*370*	*0.07*	*1.417*	*0.018*	*1.660*	*0.014*	*1.984*	*0.024*	*85*	*71*
CA-16	*15.1*	*0.8362*	*0.0268*	*0.1005*	*0.0013*	*0.20*	*9.9465*	*0.1241*	*0.0603*	*0.0019*	*0.2947*	*0.0550*		*2.93*	*29*	*203*	*173*	*1.17*	*0.618*	*0.007*	*0.617*	*0.015*	*0.615*	*0.070*	*100*	*100*
CA-16	*17.1*	*0.8602*	*0.0357*	*0.1022*	*0.0015*	*0.92*	*9.7800*	*0.1427*	*0.0610*	*0.0027*	*0.1629*	*0.0145*		*4.44*	*12*	*50*	*71*	*0.71*	*0.628*	*0.009*	*0.630*	*0.020*	*0.640*	*0.095*	*99*	*98*
CA-16	*20.1*	*0.8187*	*0.0185*	*0.0977*	*0.0010*	*0.43*	*10.2326*	*0.1055*	*0.0608*	*0.0013*	*0.3320*	*0.0142*		*1.00*	*46*	*294*	*285*	*1.03*	*0.601*	*0.006*	*0.607*	*0.010*	*0.631*	*0.047*	*98*	*95*
CA-16	*21.1*	*0.8455*	*0.0213*	*0.1007*	*0.0011*	*0.55*	*9.9327*	*0.1074*	*0.0609*	*0.0015*	*0.1507*	*0.0066*		*1.07*	*31*	*104*	*220*	*0.47*	*0.618*	*0.006*	*0.622*	*0.012*	*0.636*	*0.053*	*99*	*97*
CA-16	*23.1*	*0.4241*	*0.0273*	*0.0510*	*0.0010*	*0.98*	*19.6061*	*0.3966*	*0.0603*	*0.0032*	*0.2744*	*0.0217*		*6.89*	*11*	*85*	*83*	*1.03*	*0.321*	*0.006*	*0.359*	*0.018*	*0.615*	*0.118*	*89*	*52*
CA-16	*25.1*	*3.7598*	*0.0795*	*0.2397*	*0.0027*	*1.00*	*4.1727*	*0.0473*	*0.1138*	*0.0022*	*0.0983*	*0.0057*		*0.61*	*39*	*29*	*86*	*0.34*	*1.385*	*0.014*	*1.584*	*0.016*	*1.861*	*0.035*	*87*	*74*
CA-16	*26.1*	*4.1108*	*0.1069*	*0.2634*	*0.0034*	*1.00*	*3.7969*	*0.0486*	*0.1132*	*0.0019*	*0.1050*	*0.0234*		*0.78*	*92*	*109*	*171*	*0.64*	*1.507*	*0.016*	*1.656*	*0.014*	*1.851*	*0.024*	*90*	*81*
CA-16	*27.1*	*5.5442*	*0.0876*	*0.3206*	*0.0030*	*1.00*	*3.1189*	*0.0288*	*0.1254*	*0.0019*	*0.0264*	*0.0099*		*1.86*	*45*	*114*	*111*	*1.03*	*1.793*	*0.014*	*1.907*	*0.014*	*2.035*	*0.026*	*93*	*88*
CA-16	*28.1*	*5.3107*	*0.0707*	*0.2985*	*0.0024*	*0.98*	*3.3499*	*0.0272*	*0.1290*	*0.0017*	*0.0575*	*0.0026*		*3.28*	*173*	*106*	*423*	*0.25*	*1.684*	*0.012*	*1.871*	*0.012*	*2.085*	*0.023*	*90*	*80*
CA-16	*31.1*	*0.7239*	*0.0147*	*0.0890*	*0.0008*	*0.01*	*11.2415*	*0.1018*	*0.0590*	*0.0012*	*0.3136*	*0.0387*		*2.32*	*63*	*662*	*464*	*1.43*	*0.549*	*0.005*	*0.553*	*0.009*	*0.568*	*0.043*	*99*	*96*
CA-16	*32.1*	*0.8591*	*0.0258*	*0.1023*	*0.0011*	*0.80*	*9.7737*	*0.1097*	*0.0609*	*0.0018*	*0.2009*	*0.0233*		*1.85*	*37*	*186*	*252*	*0.74*	*0.628*	*0.007*	*0.630*	*0.014*	*0.636*	*0.062*	*99*	*98*
CA-16	*35.1*	*0.8065*	*0.0158*	*0.0974*	*0.0009*	*0.81*	*10.2690*	*0.0960*	*0.0601*	*0.0011*	*0.3087*	*0.0280*		*4.57*	*79*	*612*	*533*	*1.15*	*0.599*	*0.005*	*0.600*	*0.009*	*0.606*	*0.041*	*99*	*98*
CA-16	*36.1*	*0.8662*	*0.0242*	*0.1032*	*0.0011*	*0.15*	*9.6886*	*0.1039*	*0.0609*	*0.0017*	*0.1983*	*0.0438*		*1.34*	*19*	*89*	*131*	*0.68*	*0.633*	*0.006*	*0.634*	*0.013*	*0.635*	*0.064*	*99*	*99*
CA-16	*37.1*	*0.8978*	*0.0184*	*0.1043*	*0.0010*	*0.97*	*9.5834*	*0.0904*	*0.0624*	*0.0012*	*0.0484*	*0.0037*		*4.43*	*50*	*78*	*342*	*0.23*	*0.640*	*0.006*	*0.651*	*0.010*	*0.688*	*0.043*	*98*	*93*
CA-16	*39.1*	*0.6720*	*0.0115*	*0.0779*	*0.0006*	*0.82*	*12.8444*	*0.0999*	*0.0626*	*0.0011*	*0.0574*	*0.0201*		*4.83*	*65*	*210*	*633*	*0.33*	*0.483*	*0.004*	*0.522*	*0.007*	*0.695*	*0.038*	*92*	*69*
CA-16	*41.1*	*5.9599*	*0.0855*	*0.3251*	*0.0024*	*0.93*	*3.0760*	*0.0230*	*0.1330*	*0.0018*	*0.0485*	*0.0173*		*0.00*	*20*	*14*	*39*	*0.36*	*1.815*	*0.012*	*1.97*	*0.013*	*2.137*	*0.024*	*92*	*84*
CA-16	*42.1*	*0.8178*	*0.0147*	*0.0968*	*0.0008*	*0.95*	*10.3338*	*0.0825*	*0.0613*	*0.0011*	*0.0904*	*0.0160*		*1.64*	*58*	*204*	*474*	*0.43*	*0.595*	*0.005*	*0.607*	*0.008*	*0.649*	*0.039*	*98*	*91*
CA-16	*43.1*	*0.8473*	*0.0443*	*0.1009*	*0.0014*	*0.01*	*9.9103*	*0.1409*	*0.0609*	*0.0035*	*0.3325*	*0.0137*		*1.04*	*8*	*52*	*53*	*0.97*	*0.62*	*0.008*	*0.623*	*0.024*	*0.636*	*0.119*	*99*	*97*

Table 4. LA-ICP-MS U-Pb in situ zircon analysis from CA-17 sample (ms-qtz mylonite). Italicized data were not used in age determinations and plotting, due high levels of discordance and common lead.

SAMPLE	SPOT	RATIOS											Commom Pb
		207/235	1sigma	206/238	1 sigma	coef. corr	238/206	1 sigma	207/206	1 sigma	208/206	1 sigma	(%)
CA-17	1.1	7.7318	0.2282	0.4038	0.0062	0.0100	2.4767	0.0380	0.1389	0.0045	0.1638	0.0090	0.38
CA-17	1.2	7.6639	0.1854	0.4019	0.0047	0.6500	2.4882	0.0291	0.1383	0.0035	0.1454	0.0042	0.30
CA-17	2.1	7.5461	0.2283	0.3951	0.0062	0.0100	2.5311	0.0395	0.1385	0.0047	0.4336	0.0137	0.27
CA-17	3.1	7.6479	0.2300	0.3983	0.0062	0.6200	2.5106	0.0391	0.1393	0.0046	0.3189	0.0129	0.19
CA-17	4.1	7.8325	0.2573	0.4086	0.0072	0.6300	2.4473	0.0430	0.1390	0.0052	0.3776	0.0142	0.36
CA-17	5.1	6.9489	0.2672	0.3851	0.0080	0.9000	2.5969	0.0539	0.1309	0.0059	0.3138	0.0152	0.15
CA-17	5.2	6.5073	0.1611	0.3773	0.0044	0.6500	2.6505	0.0309	0.1251	0.0032	0.0190	0.0052	0.42
CA-17	6.1	7.5163	0.2430	0.3945	0.0068	0.6100	2.5351	0.0438	0.1382	0.0051	0.2468	0.0158	0.68
CA-17	8.1	6.5147	0.1513	0.3719	0.0040	0.4800	2.6886	0.0289	0.1270	0.0030	0.1660	0.0259	0.42
CA-17	10.1	7.2396	0.2381	0.3872	0.0069	0.1300	2.5824	0.0461	0.1356	0.0050	0.4729	0.0150	0.18
CA-17	11.1	10.3167	0.2520	0.4624	0.0059	0.9800	2.1627	0.0276	0.1618	0.0043	0.2248	0.0212	0.33
CA-17	12.1	7.2434	0.2268	0.3932	0.0051	0.4400	2.5432	0.0330	0.1336	0.0045	0.2054	0.0044	0.10
CA-17	12.2	7.6099	0.2135	0.4043	0.0045	0.5800	2.4736	0.0273	0.1365	0.0039	0.1905	0.0031	0.12
CA-17	15.1	6.9695	0.3191	0.3834	0.0081	0.3700	2.6080	0.0550	0.1318	0.0067	0.3355	0.0169	0.75
CA-17	16.1	6.3818	0.2020	0.3699	0.0047	0.8700	2.7037	0.0347	0.1251	0.0041	0.0436	0.0040	0.30
CA-17	17.1	7.6331	0.2798	0.4117	0.0064	0.6700	2.4288	0.0378	0.1345	0.0052	0.4383	0.0300	0.12
CA-17	18.1	7.3937	0.3121	0.3939	0.0073	0.1800	2.5387	0.0473	0.1361	0.0064	1.2211	0.2130	0.44
CA-17	18.2	6.3325	0.1179	0.3672	0.0035	0.5000	2.7231	0.0257	0.1251	0.0021	0.1373	0.0027	0.29
CA-17	19.1	7.1331	0.2590	0.3890	0.0061	0.3100	2.5706	0.0401	0.1330	0.0052	0.2372	0.0095	0.37
CA-17	20.1	7.7831	0.3309	0.3969	0.0079	0.0100	2.5197	0.0499	0.1422	0.0067	0.3466	0.0170	0.27
CA-17	21.1	7.7582	0.3095	0.3997	0.0073	0.4100	2.5022	0.0457	0.1408	0.0060	0.1579	0.0093	0.31
CA-17	22.1	7.5184	0.2880	0.3952	0.0067	0.0100	2.5307	0.0427	0.1380	0.0057	0.1863	0.0116	0.31
CA-17	23.1	7.3315	0.2909	0.3948	0.0069	0.1200	2.5331	0.0444	0.1347	0.0058	0.3784	0.0129	0.60
CA-17	24.1	6.6549	0.1880	0.3752	0.0051	0.8100	2.6651	0.0363	0.1286	0.0034	0.2818	0.0256	0.20
CA-17	25.1	7.5402	0.2516	0.3956	0.0065	0.5300	2.5278	0.0415	0.1382	0.0044	0.5068	0.0324	0.66
CA-17	26.1	6.2359	0.1708	0.3653	0.0047	0.2800	2.7375	0.0356	0.1238	0.0032	0.3181	0.0105	0.44
CA-17	27.1	7.4471	0.2103	0.3994	0.0056	0.2600	2.5037	0.0348	0.1352	0.0037	0.2673	0.0107	0.05
CA-17	28.1	7.5762	0.1752	0.4018	0.0047	0.6800	2.4886	0.0291	0.1367	0.0029	0.3467	0.0058	0.31
CA-17	29.1	6.2937	0.1462	0.3685	0.0042	0.0100	2.7137	0.0310	0.1239	0.0027	0.0124	0.0065	0.30
CA-17	30.1	6.8293	0.1909	0.3825	0.0052	0.2400	2.6146	0.0355	0.1295	0.0034	0.3561	0.0084	0.42
CA-17	30.2	6.2656	0.1287	0.3602	0.0037	0.5600	2.7765	0.0286	0.1262	0.0024	0.0846	0.0044	0.29
CA-17	31.1	7.6101	0.2993	0.4028	0.0078	0.6900	2.4827	0.0478	0.1370	0.0054	0.4757	0.0269	0.29
CA-17	32.1	7.6018	0.1972	0.4059	0.0053	0.2400	2.4636	0.0319	0.1358	0.0033	0.1944	0.0232	0.24
CA-17	33.1	7.7975	0.1465	0.4109	0.0040	0.5900	2.4337	0.0236	0.1376	0.0023	0.1982	0.0030	0.25
CA-17	34.1	7.5407	0.1730	0.4023	0.0046	0.7100	2.4854	0.0287	0.1359	0.0030	0.1506	0.0076	0.91
CA-17	35.1	7.0286	0.2139	0.3883	0.0052	0.8800	2.5755	0.0343	0.1313	0.0043	0.2542	0.0171	0.26
CA-17	38.1	7.4253	0.2548	0.3908	0.0063	0.4900	2.5587	0.0411	0.1378	0.0053	0.4527	0.0250	0.24
CA-17	39.1	7.5378	0.2747	0.3957	0.0068	0.4200	2.5274	0.0432	0.1382	0.0055	0.4489	0.0346	0.48
CA-17	40.1	7.6471	0.2403	0.4016	0.0057	0.7400	2.4903	0.0356	0.1381	0.0047	0.1705	0.0077	0.25
CA-17	41.1	7.7626	0.1966	0.4042	0.0043	0.0600	2.4742	0.0266	0.1393	0.0036	0.5137	0.0551	0.14
CA-17	42.1	7.6288	0.2330	0.3988	0.0056	0.4500	2.5074	0.0350	0.1387	0.0045	0.0507	0.0064	0.47
CA-17	43.1	7.3856	0.2497	0.3975	0.0061	0.6300	2.5157	0.0384	0.1348	0.0051	0.4303	0.0186	0.68
CA-17	44.1	2.7069	0.1123	0.2328	0.0035	0.5400	4.2960	0.0639	0.0843	0.0039	0.1817	0.0124	0.03
CA-17	44.2	2.8581	0.0721	0.2364	0.0022	0.5300	4.2302	0.0394	0.0877	0.0023	0.1086	0.0094	0.21

CA-17	45.1	7.5355	0.2251	0.3966	0.0053	0.7100	2.5211	0.0337	0.1378	0.0044	0.1497	0.0070	0.36
CA-17	46.1	6.2339	0.1731	0.3653	0.0039	0.6600	2.7376	0.0295	0.1238	0.0036	0.1814	0.0138	0.07
CA-17	47.1	7.5784	0.2581	0.3985	0.0058	0.7400	2.5092	0.0368	0.1379	0.0051	0.3438	0.0370	0.33
CA-17	48.1	8.0242	0.2269	0.4242	0.0049	0.5400	2.3575	0.0270	0.1372	0.0040	0.1833	0.0031	0.23
CA-17	50.1	7.5441	0.2229	0.4038	0.0048	0.5400	2.4764	0.0296	0.1355	0.0043	0.4064	0.0093	0.37
CA-17	51.1	7.2817	0.2682	0.3934	0.0064	0.4600	2.5418	0.0412	0.1342	0.0056	0.3276	0.0125	0.58
CA-17	52.1	7.6826	0.2103	0.4073	0.0044	0.5900	2.4550	0.0264	0.1368	0.0039	0.2733	0.0051	0.17
CA-17	53.1	7.7107	0.2780	0.4045	0.0065	0.0100	2.4721	0.0397	0.1382	0.0058	0.2321	0.0127	0.38
CA-17	54.1	7.7762	0.1943	0.4117	0.0038	0.7300	2.4291	0.0226	0.1370	0.0035	0.1806	0.0024	0.17
CA-17	55.1	7.6417	0.2296	0.4040	0.0051	0.0100	2.4752	0.0310	0.1372	0.0044	0.4019	0.0091	0.17
CA-17	57.1	7.6128	0.2765	0.4024	0.0064	0.3800	2.4849	0.0398	0.1372	0.0055	0.4099	0.0089	0.48
CA-17	58.1	7.7924	0.5292	0.4065	0.0147	0.0100	2.4599	0.0889	0.1390	0.0122	0.3473	0.0627	0.89
CA-17	59.1	15.1457	0.5120	0.5468	0.0089	0.7200	1.8288	0.0298	0.2009	0.0073	0.2027	0.0306	0.28
CA-17	60.1	5.9957	0.1915	0.3617	0.0042	0.2200	2.7645	0.0319	0.1202	0.0042	0.1520	0.0069	0.70
CA-17	61.1	6.4461	0.1647	0.3762	0.0034	0.3500	2.6581	0.0243	0.1243	0.0033	0.4023	0.0062	0.06
CA-17	62.1	6.5833	0.2377	0.3745	0.0053	0.0100	2.6701	0.0378	0.1275	0.0050	0.3091	0.0191	0.26
CA-17	63.1	6.6396	0.2702	0.3757	0.0060	0.4100	2.6616	0.0425	0.1282	0.0058	0.1880	0.0113	0.83
CA-17	64.1	7.1556	0.2063	0.3929	0.0043	0.4500	2.5452	0.0276	0.1321	0.0041	0.1778	0.0064	0.22
CA-17	65.1	7.3232	0.1813	0.3963	0.0036	0.8900	2.5236	0.0228	0.1340	0.0035	0.2600	0.0066	0.09
CA-17	66.1	7.1956	0.3098	0.3907	0.0069	0.4600	2.5592	0.0449	0.1336	0.0063	0.2813	0.0169	0.43
CA-17	68.1	7.5583	0.2134	0.3963	0.0043	0.0100	2.5234	0.0275	0.1383	0.0042	0.1901	0.0059	0.14
CA-17	67.1	2.7992	0.0992	0.2352	0.0027	0.9900	4.2524	0.0488	0.0863	0.0034	0.1292	0.0406	0.20
CA-17	67.2	2.8339	0.0944	0.2394	0.0025	0.6500	4.1773	0.0445	0.0859	0.0031	0.1019	0.0095	0.16
CA-17	70.1	7.2865	0.2268	0.3939	0.0048	0.4700	2.5385	0.0307	0.1341	0.0045	0.3993	0.0089	0.28
CA-17	71.1	7.6418	0.2711	0.4029	0.0067	0.7100	2.4822	0.0412	0.1376	0.0054	0.1841	0.0118	0.53
CA-17	72.1	7.4196	0.2407	0.3972	0.0058	0.1500	2.5178	0.0368	0.1355	0.0048	0.2694	0.0188	0.41
CA-17	73.1	7.2198	0.3478	0.3908	0.0091	0.2600	2.5587	0.0594	0.1340	0.0075	0.1874	0.0178	0.52
CA-17	74.1	7.1417	0.3586	0.3759	0.0094	0.4900	2.6606	0.0667	0.1378	0.0081	0.4033	0.0197	0.72
CA-17	75.1	9.0154	0.2367	0.4375	0.0050	0.5900	2.2857	0.0259	0.1495	0.0042	0.1315	0.0079	0.17
CA-17	76.1	7.5493	0.2719	0.3996	0.0067	0.4700	2.5028	0.0417	0.1370	0.0055	0.3440	0.0136	0.38
CA-17	77.1	7.7610	0.2638	0.4155	0.0065	0.5800	2.4066	0.0375	0.1355	0.0051	0.3199	0.0138	0.42
CA-17	78.1	6.5790	0.2539	0.3816	0.0066	0.6000	2.6209	0.0457	0.1251	0.0055	0.3143	0.0118	0.27
CA-17	79.1	7.5144	0.3127	0.3963	0.0079	0.3700	2.5234	0.0502	0.1375	0.0066	0.1550	0.0147	0.93
CA-17	80.1	7.5416	0.2465	0.4017	0.0060	0.6700	2.4891	0.0372	0.1361	0.0050	0.1663	0.0086	0.21
CA-17	81.1	7.3159	0.3064	0.3943	0.0078	0.2400	2.5359	0.0504	0.1346	0.0064	0.1673	0.0158	0.28
CA-17	82.1	7.5747	0.5532	0.3899	0.0154	0.4800	2.5648	0.1012	0.1409	0.0124	0.3402	0.0312	0.81
CA-17	83.1	7.1326	0.3006	0.3819	0.0077	0.8500	2.6184	0.0531	0.1354	0.0066	0.2114	0.0168	0.71
CA-17	*7.1*	*7.5737*	*0.2727*	*0.4003*	*0.0077*	*0.2200*	*2.4982*	*0.0479*	*0.1372*	*0.0058*	*0.4058*	*0.0140*	*1.75*
CA-17	*9.1*	*7.2138*	*0.4224*	*0.3934*	*0.0131*	*0.4600*	*2.5421*	*0.0849*	*0.1330*	*0.0096*	*0.3045*	*0.0264*	*1.09*
CA-17	*13.1*	*8.3696*	*0.4291*	*0.4041*	*0.0104*	*0.5800*	*2.4745*	*0.0634*	*0.1502*	*0.0091*	*0.3022*	*0.0233*	*1.46*
CA-17	*14.1*	*7.2282*	*0.7734*	*0.3695*	*0.0213*	*0.4200*	*2.7060*	*0.1563*	*0.1419*	*0.0184*	*0.3627*	*0.0996*	*2.25*
CA-17	*36.1*	*7.6577*	*0.4134*	*0.4076*	*0.0110*	*0.5700*	*2.4536*	*0.0660*	*0.1363*	*0.0090*	*0.5349*	*0.0592*	*1.16*
CA-17	*37.1*	*6.6006*	*0.1623*	*0.3723*	*0.0038*	*0.9700*	*2.6863*	*0.0275*	*0.1286*	*0.0034*	*0.0821*	*0.0124*	*14.08*
CA-17	*40.2*	*7.4648*	*0.4195*	*0.3978*	*0.0112*	*0.3100*	*2.5141*	*0.0708*	*0.1361*	*0.0091*	*0.3661*	*0.0233*	*2.46*
CA-17	*49.1*	*7.6242*	*0.3335*	*0.3993*	*0.0086*	*0.9200*	*2.5041*	*0.0539*	*0.1385*	*0.0072*	*0.3029*	*0.0572*	*1.16*
CA-17	*56.1*	*7.7465*	*0.7153*	*0.3892*	*0.0206*	*0.2000*	*2.5694*	*0.1361*	*0.1444*	*0.0167*	*0.3362*	*0.0631*	*1.83*
CA-17	*69.1*	*6.2363*	*0.3178*	*0.3662*	*0.0074*	*0.0100*	*2.7309*	*0.0552*	*0.1235*	*0.0073*	*0.3675*	*0.0230*	*1.14*

Pb rad	Th	U	Th/U	AGES (Ga)						CONC. (%)
ppm	ppm	ppm		T206/208	1 sigma	T207/235	1 sigma	T207/206	1 sigma	
23.00	18.00	39.00	0.46	2.186	0.028	2.200	0.027	2.213	0.057	98
49.00	33.00	84.00	0.40	2.178	0.022	2.192	0.022	2.206	0.044	98
28.00	51.00	41.00	1.25	2.146	0.028	2.178	0.027	2.209	0.058	97
27.00	35.00	41.00	0.86	2.161	0.028	2.191	0.027	2.218	0.057	97
22.00	34.00	32.00	1.04	2.209	0.033	2.212	0.029	2.215	0.064	99
19.00	25.00	29.00	0.87	2.100	0.037	2.105	0.034	2.110	0.079	99
46.00	6.00	92.00	0.06	2.064	0.021	2.047	0.022	2.030	0.046	101
16.00	18.00	26.00	0.69	2.144	0.032	2.175	0.029	2.205	0.065	97
60.00	52.00	112.00	0.47	2.039	0.019	2.048	0.020	2.057	0.042	99
20.00	40.00	29.00	1.37	2.110	0.032	2.141	0.030	2.172	0.067	97
39.00	39.00	62.00	0.63	2.450	0.026	2.464	0.024	2.475	0.046	98
58.00	55.00	101.00	0.55	2.138	0.024	2.142	0.028	2.146	0.057	99
154.00	138.00	263.00	0.52	2.189	0.020	2.186	0.025	2.184	0.050	100
19.00	27.00	31.00	0.86	2.092	0.038	2.108	0.041	2.122	0.090	98
78.00	26.00	156.00	0.17	2.029	0.022	2.030	0.028	2.031	0.058	99
55.00	94.00	77.00	1.21	2.223	0.029	2.189	0.032	2.157	0.067	103
35.00	108.00	34.00	3.18	2.141	0.034	2.160	0.037	2.179	0.079	98
83.00	100.00	156.00	0.64	2.016	0.016	2.023	0.016	2.030	0.029	99
34.00	35.00	59.00	0.59	2.118	0.028	2.128	0.032	2.138	0.068	99
27.00	39.00	41.00	0.96	2.155	0.036	2.206	0.038	2.255	0.081	95
28.00	20.00	48.00	0.41	2.167	0.034	2.203	0.036	2.237	0.076	96
31.00	35.00	55.00	0.63	2.147	0.031	2.175	0.034	2.202	0.071	97
31.00	47.00	47.00	1.00	2.145	0.032	2.153	0.035	2.160	0.075	99
26.00	35.00	42.00	0.83	2.054	0.024	2.067	0.024	2.079	0.045	98
17.00	31.00	23.00	1.37	2.149	0.030	2.178	0.029	2.205	0.054	97
24.00	37.00	39.00	0.95	2.007	0.022	2.009	0.024	2.012	0.046	99
21.00	27.00	33.00	0.81	2.166	0.026	2.167	0.026	2.167	0.047	99
33.00	47.00	48.00	0.97	2.177	0.022	2.182	0.021	2.186	0.037	99
34.00	2.00	71.00	0.03	2.022	0.020	2.018	0.020	2.013	0.038	100
21.00	32.00	32.00	1.00	2.088	0.024	2.090	0.025	2.091	0.047	99
42.00	22.00	84.00	0.26	1.983	0.018	2.014	0.018	2.045	0.033	96
13.00	23.00	17.00	1.32	2.182	0.036	2.186	0.036	2.190	0.069	99
26.00	20.00	43.00	0.45	2.196	0.024	2.185	0.023	2.175	0.042	100
75.00	77.00	120.00	0.64	2.219	0.018	2.208	0.017	2.198	0.029	100
32.00	30.00	54.00	0.55	2.180	0.021	2.178	0.021	2.176	0.038	100
32.00	38.00	52.00	0.73	2.115	0.024	2.115	0.027	2.115	0.057	99
26.00	46.00	37.00	1.25	2.127	0.029	2.164	0.031	2.200	0.068	96
19.00	35.00	27.00	1.33	2.149	0.031	2.177	0.032	2.204	0.070	97
28.00	25.00	47.00	0.52	2.176	0.026	2.190	0.028	2.204	0.060	98
56.00	95.00	80.00	1.18	2.188	0.020	2.204	0.023	2.218	0.045	98
24.00	6.00	46.00	0.14	2.164	0.026	2.188	0.028	2.211	0.058	97
22.00	37.00	32.00	1.13	2.158	0.028	2.159	0.030	2.161	0.065	99
25.00	39.00	73.00	0.53	1.349	0.018	1.330	0.031	1.300	0.090	103
96.00	85.00	300.00	0.28	1.368	0.012	1.371	0.019	1.376	0.050	99

30.00	21.00	52.00	0.41	2.154	0.025	2.177	0.027	2.200	0.057	97
52.00	52.00	98.00	0.53	2.007	0.019	2.009	0.025	2.011	0.052	99
32.00	55.00	47.00	1.16	2.162	0.027	2.182	0.030	2.201	0.064	98
56.00	49.00	92.00	0.53	2.279	0.022	2.234	0.025	2.192	0.052	103
51.00	89.00	74.00	1.21	2.187	0.022	2.178	0.026	2.170	0.054	100
23.00	34.00	35.00	0.96	2.139	0.029	2.147	0.033	2.154	0.072	99
59.00	75.00	91.00	0.82	2.203	0.020	2.195	0.025	2.187	0.050	100
22.00	24.00	35.00	0.67	2.190	0.030	2.198	0.033	2.205	0.071	99
99.00	89.00	160.00	0.55	2.223	0.017	2.205	0.023	2.190	0.044	101
54.00	81.00	69.00	1.17	2.188	0.023	2.190	0.027	2.192	0.056	99
31.00	72.00	44.00	1.62	2.180	0.029	2.186	0.032	2.192	0.069	99
10.00	13.00	16.00	0.83	2.199	0.067	2.207	0.063	2.215	0.150	99
28.00	23.00	32.00	0.73	2.812	0.037	2.824	0.032	2.833	0.060	99
41.00	34.00	78.00	0.44	1.990	0.020	1.975	0.027	1.959	0.060	101
88.00	158.00	137.00	1.15	2.059	0.016	2.039	0.022	2.018	0.048	101
30.00	42.00	49.00	0.87	2.051	0.025	2.057	0.032	2.064	0.072	99
21.00	18.00	39.00	0.47	2.056	0.028	2.065	0.036	2.073	0.080	99
41.00	36.00	71.00	0.51	2.136	0.020	2.131	0.026	2.126	0.055	100
79.00	94.00	129.00	0.73	2.152	0.017	2.152	0.022	2.152	0.046	100
16.00	19.00	26.00	0.74	2.126	0.031	2.136	0.038	2.145	0.084	99
42.00	37.00	71.00	0.53	2.152	0.020	2.180	0.026	2.206	0.053	97
47.00	48.00	124.00	0.39	1.362	0.014	1.355	0.025	1.346	0.070	101
46.00	48.00	146.00	0.33	1.384	0.013	1.365	0.025	1.335	0.071	103
39.00	67.00	59.00	1.13	2.141	0.022	2.147	0.028	2.153	0.058	99
28.00	24.00	47.00	0.51	2.182	0.031	2.190	0.032	2.197	0.069	99
43.00	48.00	71.00	0.68	2.156	0.027	2.163	0.029	2.170	0.062	99
15.00	14.00	26.00	0.51	2.127	0.042	2.139	0.043	2.151	0.097	98
15.00	27.00	24.00	1.15	2.057	0.044	2.129	0.045	2.200	0.105	93
65.00	36.00	104.00	0.35	2.339	0.022	2.340	0.024	2.340	0.047	99
32.00	49.00	49.00	1.01	2.167	0.031	2.179	0.032	2.190	0.071	98
34.00	45.00	51.00	0.88	2.240	0.029	2.204	0.031	2.170	0.067	103
35.00	52.00	59.00	0.89	2.084	0.031	2.057	0.035	2.030	0.080	102
18.00	15.00	32.00	0.48	2.152	0.036	2.175	0.037	2.196	0.082	97
34.00	29.00	58.00	0.50	2.177	0.028	2.178	0.030	2.179	0.065	99
23.00	18.00	40.00	0.46	2.143	0.036	2.151	0.037	2.158	0.082	99
10.00	13.00	15.00	0.88	2.122	0.072	2.182	0.067	2.238	0.159	94
21.00	24.00	36.00	0.66	2.085	0.036	2.128	0.038	2.170	0.085	96
18.00	*31.00*	*26.00*	*1.21*	*2.170*	*0.036*	*2.182*	*0.032*	*2.192*	*0.072*	*98*
7.00	*10.00*	*11.00*	*0.88*	*2.138*	*0.061*	*2.138*	*0.049*	*2.138*	*0.122*	*100*
12.00	*15.00*	*21.00*	*0.74*	*2.188*	*0.048*	*2.272*	*0.047*	*2.348*	*0.102*	*93*
5.00	*6.00*	*8.00*	*0.75*	*2.027*	*0.099*	*2.140*	*0.092*	*2.250*	*0.221*	*90*
9.00	*15.00*	*12.00*	*1.18*	*2.204*	*0.051*	*2.192*	*0.050*	*2.180*	*0.113*	*101*
58.00	*49.00*	*111.00*	*0.44*	*2.040*	*0.018*	*2.059*	*0.022*	*2.079*	*0.046*	*98*
10.00	*17.00*	*15.00*	*1.17*	*2.159*	*0.052*	*2.169*	*0.051*	*2.178*	*0.116*	*99*
9.00	*14.00*	*11.00*	*1.25*	*2.166*	*0.040*	*2.188*	*0.041*	*2.208*	*0.094*	*98*
5.00	*7.00*	*8.00*	*0.95*	*2.119*	*0.097*	*2.202*	*0.089*	*2.280*	*0.221*	*92*
16.00	*31.00*	*28.00*	*1.10*	*2.011*	*0.035*	*2.010*	*0.045*	*2.008*	*0.105*	*100*

Table 5. LA-ICP-MS U-Pb in situ zircon analysis from CA-19 sample (qtz-ms schist). Italicized data were not used in age determinations and plotting, due high levels of discordance and common lead.

SAMPLE	SPOT	RATIOS											Commom Pb	Pb rad	Th	U	Th/U	AGES (Ga)						CONC. (%)	
		207/235	1sigma	206/238	1 sigma	coef. corr	238/206	1 sigma	207/206	1 sigma	208/206	1 sigma	(%)	ppm	ppm	ppm		T206/208	1 sigma	T207/235	1 sigma	T207/206	1 sigma	206/238 207/235	206/238 207/206
CA-19	1.1	1.1878	0.0348	0.1317	0.0015	0.82	7.5914	0.0856	0.0654	0.0019	0.3350	0.0128	0.55	38	184	171	1.08	0.798	0.008	0.795	0.016	0.787	0.062	100	101
CA-19	3.1	1.3732	0.0256	0.1434	0.0013	0.78	6.9756	0.0640	0.0695	0.0013	0.0374	0.0058	0.14	167	108	840	0.13	0.864	0.007	0.878	0.011	0.913	0.039	98	94
CA-19	3.2	0.8518	0.0155	0.1032	0.0009	0.49	9.6922	0.0889	0.0599	0.0011	0.0042	0.0015	0.11	172	25	1334	0.02	0.633	0.006	0.626	0.008	0.599	0.039	101	105
CA-19	4.2	1.2211	0.0258	0.1351	0.0013	0.98	7.4029	0.0707	0.0656	0.0014	0.0173	0.0030	0.49	57	17	331	0.05	0.817	0.007	0.81	0.012	0.792	0.046	100	103
CA-19	6.1	1.8029	0.0393	0.1738	0.0018	0.91	5.7548	0.0581	0.0753	0.0016	0.0508	0.0120	0.84	68	88	274	0.32	1.033	0.01	1.047	0.014	1.075	0.043	98	96
CA-19	7.1	3.1448	0.0613	0.2442	0.0023	0.74	4.0955	0.0391	0.0934	0.0018	0.0945	0.0094	0.49	136	152	340	0.45	1.408	0.012	1.444	0.014	1.496	0.035	97	94
CA-19	9.1	1.1456	0.0282	0.1270	0.0013	0.95	7.8733	0.0806	0.0654	0.0017	0.0655	0.0080	0.37	36	47	200	0.24	0.771	0.007	0.775	0.013	0.788	0.054	99	97
CA-19	10.1	1.1746	0.0241	0.1289	0.0016	0.99	7.7607	0.0961	0.0661	0.0014	0.0385	0.0304	0.00	15	24	75	0.32	0.781	0.009	0.789	0.011	0.81	0.043	99	96
CA-19	13.1	0.7667	0.0191	0.0928	0.0012	0.66	10.7752	0.1434	0.0599	0.0015	0.1951	0.0055	0.38	20	95	140	0.68	0.572	0.007	0.578	0.011	0.6	0.055	99	95
CA-19	14.1	0.8468	0.0166	0.1005	0.0012	0.38	9.9515	0.1208	0.0611	0.0012	0.2264	0.0160	0.26	29	122	183	0.67	0.617	0.007	0.623	0.009	0.643	0.043	99	95
CA-19	15.1	1.1350	0.0229	0.1254	0.0015	0.96	7.9768	0.0960	0.0657	0.0014	0.0838	0.0215	0.69	32	50	176	0.28	0.761	0.009	0.77	0.012	0.796	0.047	98	95
CA-19	16.1	4.9126	0.0864	0.3181	0.0040	0.99	3.1438	0.0392	0.1120	0.0019	0.2384	0.0823	0.49	32	62	56	1.12	1.78	0.019	1.804	0.015	1.832	0.032	98	97
CA-19	17.1	0.8400	0.0139	0.1001	0.0011	0.67	9.9929	0.1129	0.0609	0.0010	0.0690	0.0040	0.39	83	158	595	0.27	0.615	0.007	0.619	0.008	0.635	0.034	99	96
CA-19	20.1	1.3363	0.0218	0.1403	0.0016	0.99	7.1256	0.0822	0.0691	0.0011	0.0630	0.0148	0.00	52	42	221	0.19	0.847	0.009	0.862	0.009	0.901	0.031	98	94
CA-19	20.2	1.1707	0.0187	0.1292	0.0014	0.99	7.7417	0.0861	0.0657	0.0010	0.0682	0.0066	0.48	61	71	349	0.20	0.783	0.008	0.787	0.009	0.798	0.033	99	98
CA-19	23.1	1.1964	0.0411	0.1326	0.0029	0.67	7.5407	0.1623	0.0654	0.0022	0.1202	0.0163	0.75	28	44	155	0.29	0.803	0.016	0.799	0.02	0.788	0.074	100	101
CA-19	24.1	1.1579	0.0280	0.1291	0.0024	0.90	7.7452	0.1423	0.0650	0.0013	0.0975	0.0210	0.07	54	82	302	0.27	0.783	0.014	0.781	0.013	0.776	0.043	100	100
CA-19	26.1	5.4110	0.1094	0.3243	0.0059	0.97	3.0836	0.0566	0.1210	0.0018	0.1958	0.0363	0.63	71	94	128	0.74	1.811	0.029	1.887	0.017	1.971	0.027	95	91
CA-19	28.1	1.0762	0.0212	0.1221	0.0020	0.99	8.1908	0.1365	0.0639	0.0010	0.0988	0.0428	0.65	104	301	589	0.51	0.743	0.012	0.742	0.01	0.739	0.033	100	100
CA-19	29.1	0.8409	0.0143	0.0997	0.0016	0.99	10.0254	0.1580	0.0611	0.0008	0.0094	0.0063	0.40	343	61	2625	0.02	0.613	0.009	0.62	0.008	0.644	0.028	98	95
CA-19	32.1	0.8990	0.0193	0.1075	0.0018	0.86	9.3043	0.1574	0.0607	0.0011	0.0204	0.0061	0.74	75	129	567	0.23	0.658	0.011	0.651	0.01	0.627	0.039	101	104
CA-19	33.1	2.3122	0.0488	0.2125	0.0038	0.95	4.7063	0.0833	0.0789	0.0013	0.1808	0.0297	0.14	76	93	253	0.37	1.242	0.02	1.216	0.015	1.17	0.033	102	106
CA-19	34.1	1.0399	0.0213	0.1182	0.0010	0.97	8.4597	0.0734	0.0638	0.0013	0.0987	0.0194	0.16	47	126	269	0.47	0.72	0.006	0.724	0.01	0.735	0.044	99	97
CA-19	35.1	1.2126	0.0316	0.1345	0.0013	0.99	7.4364	0.0720	0.0654	0.0017	0.0758	0.0191	0.99	19	35	115	0.31	0.813	0.007	0.806	0.014	0.787	0.055	100	103
CA-19	36.1	0.8068	0.0204	0.0972	0.0009	0.45	10.2931	0.0971	0.0602	0.0016	0.4195	0.0116	0.41	29	244	185	1.32	0.598	0.005	0.601	0.012	0.612	0.057	99	97
CA-19	37.1	0.9032	0.0143	0.1080	0.0008	0.91	9.2552	0.0719	0.0606	0.0009	0.0337	0.0145	0.00	96	95	738	0.13	0.661	0.005	0.653	0.008	0.626	0.033	101	105
CA-19	*2.1*	*1.4250*	*0.0336*	*0.1496*	*0.0015*	*0.94*	*6.6848*	*0.0688*	*0.0691*	*0.0016*	*0.1577*	*0.0368*	*1.17*	*58*	*150*	*275*	*0.55*	*0.899*	*0.009*	*0.899*	*0.014*	*0.901*	*0.049*	*99*	*99*
CA-19	*2.2*	*0.7332*	*0.0142*	*0.0877*	*0.0008*	*0.95*	*11.4019*	*0.1087*	*0.0606*	*0.0011*	*0.0263*	*0.0037*	*0.32*	*262*	*191*	*2072*	*0.09*	*0.542*	*0.005*	*0.558*	*0.008*	*0.626*	*0.04*	*97*	*86*
CA-19	*4.1*	*3.0720*	*0.0641*	*0.2127*	*0.0021*	*0.99*	*4.7008*	*0.0470*	*0.1047*	*0.0021*	*0.0811*	*0.0323*	*0.50*	*98*	*79*	*218*	*0.37*	*1.243*	*0.011*	*1.426*	*0.015*	*1.71*	*0.035*	*87*	*72*
CA-19	*5.1*	*0.8017*	*0.0399*	*0.0980*	*0.0014*	*0.38*	*10.2000*	*0.1431*	*0.0593*	*0.0031*	*0.3089*	*0.0338*	*1.59*	*13*	*68*	*87*	*0.79*	*0.603*	*0.008*	*0.598*	*0.023*	*0.578*	*0.118*	*100*	*104*
CA-19	*8.1*	*0.8291*	*0.0194*	*0.0984*	*0.0010*	*0.95*	*10.1631*	*0.1014*	*0.0611*	*0.0015*	*0.1176*	*0.0316*	*4.09*	*67*	*404*	*476*	*0.85*	*0.605*	*0.006*	*0.613*	*0.011*	*0.643*	*0.053*	*98*	*94*
CA-19	*8.2*	*0.7949*	*0.0167*	*0.0949*	*0.0009*	*0.88*	*10.5353*	*0.0994*	*0.0607*	*0.0013*	*0.1322*	*0.0552*	*2.22*	*82*	*492*	*563*	*0.87*	*0.585*	*0.005*	*0.594*	*0.009*	*0.63*	*0.048*	*98*	*92*
CA-19	*11.1*	*0.7911*	*0.0335*	*0.0989*	*0.0015*	*0.01*	*10.1119*	*0.1550*	*0.0580*	*0.0029*	*0.1195*	*0.1545*	*0.25*	*38*	*120*	*190*	*0.63*	*0.608*	*0.009*	*0.592*	*0.02*	*0.53*	*0.097*	*102*	*114*
CA-19	*12.1*	*0.8013*	*0.0210*	*0.0907*	*0.0014*	*0.97*	*11.0246*	*0.1645*	*0.0641*	*0.0013*	*0.1300*	*0.0486*	*1.22*	*37*	*126*	*181*	*0.70*	*0.56*	*0.008*	*0.598*	*0.01*	*0.744*	*0.042*	*93*	*75*
CA-19	*18.1*	*4.5141*	*0.0631*	*0.2840*	*0.0031*	*0.99*	*3.5207*	*0.0387*	*0.1153*	*0.0016*	*0.1814*	*0.0216*	*0.31*	*65*	*81*	*137*	*0.59*	*1.612*	*0.016*	*1.734*	*0.012*	*1.884*	*0.026*	*92*	*85*
CA-19	*19.2*	*0.6436*	*0.0094*	*0.0763*	*0.0008*	*0.99*	*13.1069*	*0.1460*	*0.0612*	*0.0008*	*0.0407*	*0.0016*	*1.19*	*178*	*383*	*2046*	*0.19*	*0.474*	*0.005*	*0.505*	*0.006*	*0.646*	*0.028*	*93*	*73*
CA-19	*20.3*	*0.9629*	*0.0186*	*0.1077*	*0.0009*	*0.85*	*9.2867*	*0.0767*	*0.0649*	*0.0013*	*0.0532*	*0.0122*	*2.10*	*51*	*89*	*348*	*0.26*	*0.659*	*0.005*	*0.685*	*0.01*	*0.77*	*0.041*	*96*	*85*
CA-19	*21.1*	*0.9566*	*0.0287*	*0.1118*	*0.0023*	*0.86*	*8.9483*	*0.1814*	*0.0621*	*0.0016*	*0.0930*	*0.0512*	*1.83*	*25*	*84*	*125*	*0.67*	*0.683*	*0.013*	*0.682*	*0.014*	*0.677*	*0.053*	*100*	*100*
CA-19	*22.1*	*3.8697*	*0.0868*	*0.2644*	*0.0050*	*0.99*	*3.7827*	*0.0721*	*0.1062*	*0.0019*	*0.3016*	*0.1625*	*0.44*	*65*	*159*	*112*	*1.43*	*1.512*	*0.026*	*1.607*	*0.018*	*1.735*	*0.033*	*94*	*87*
CA-19	*25.1*	*0.9797*	*0.0331*	*0.1083*	*0.0024*	*0.96*	*9.2328*	*0.2048*	*0.0656*	*0.0020*	*0.1152*	*0.0146*	*0.81*	*30*	*79*	*164*	*0.48*	*0.663*	*0.014*	*0.693*	*0.016*	*0.794*	*0.065*	*95*	*83*
CA-19	*27.1*	*1.1666*	*0.0313*	*0.1296*	*0.0024*	*0.98*	*7.7165*	*0.1457*	*0.0653*	*0.0016*	*0.0442*	*0.0067*	*1.36*	*27*	*33*	*160*	*0.21*	*0.786*	*0.014*	*0.785*	*0.015*	*0.784*	*0.051*	*100*	*100*
CA-19	*30.1*	*1.2534*	*0.0308*	*0.1356*	*0.0025*	*0.99*	*7.3753*	*0.1383*	*0.0670*	*0.0014*	*0.0567*	*0.0302*	*2.40*	*22*	*32*	*58*	*0.55*	*0.82*	*0.014*	*0.825*	*0.014*	*0.839*	*0.043*	*99*	*97*
CA-19	*31.1*	*0.8118*	*0.0423*	*0.0970*	*0.0025*	*0.89*	*10.3056*	*0.2702*	*0.0607*	*0.0033*	*0.1722*	*0.0551*	*1.22*	*14*	*89*	*99*	*0.90*	*0.597*	*0.015*	*0.603*	*0.024*	*0.628*	*0.118*	*98*	*95*
CA-19	*38.1*	*0.8930*	*0.0169*	*0.1073*	*0.0009*	*0.90*	*9.3209*	*0.0764*	*0.0604*	*0.0011*	*0.2605*	*0.1719*	*7.67*	*13*	*-55*	*89*	*-0.62*	*0.657*	*0.005*	*0.648*	*0.009*	*0.617*	*0.04*	*101*	*106*
CA-19	*39.1*	*0.7746*	*0.0139*	*0.0923*	*0.0007*	*0.75*	*10.8301*	*0.0876*	*0.0608*	*0.0010*	*0.1977*	*0.0425*	*1.53*	*88*	*596*	*654*	*0.91*	*0.569*	*0.004*	*0.582*	*0.008*	*0.634*	*0.037*	*97*	*89*

Table 6. LA-ICP-MS U-Pb in situ zircon analysis from CA-21B sample (qtz-ms ultramylonite). Italicized data were not used in age determinations and plotting, due high levels of discordance and commor

SAMPLE	SPOT	RATIOS									
		207/235	1sigma	206/238	1 sigma	coef. corr	238/206	1 sigma	207/206	1 sigma	208/206	1 sigma
CA-21B	1.1	7.8759	0.2730	0.4090	0.0053	0.0100	2.4449	0.0318	0.1397	0.0051	0.2705	0.0118
CA-21B	3.1	8.2603	0.2624	0.4446	0.0053	0.8100	2.2492	0.0270	0.1347	0.0044	0.2844	0.0446
CA-21B	4.1	7.5242	0.2132	0.3997	0.0043	0.9800	2.5016	0.0268	0.1365	0.0042	0.4104	0.0177
CA-21B	7.1	7.8402	0.2247	0.4176	0.0045	0.9000	2.3947	0.0257	0.1362	0.0041	0.3120	0.0062
CA-21B	8.1	7.9503	0.2048	0.4245	0.0042	0.7700	2.3557	0.0232	0.1358	0.0035	0.3673	0.0135
CA-21B	9.1	7.3030	0.2021	0.3862	0.0041	0.9400	2.5896	0.0272	0.1372	0.0038	0.3837	0.0106
CA-21B	10.1	7.4965	0.2137	0.3997	0.0043	0.9800	2.5018	0.0271	0.1360	0.0042	0.4514	0.0310
CA-21B	11.1	7.4643	0.2483	0.4006	0.0050	0.9800	2.4962	0.0312	0.1351	0.0047	0.4943	0.0279
CA-21B	12.1	16.9608	0.4108	0.6008	0.0060	0.9500	1.6646	0.0167	0.2048	0.0051	0.1682	0.0095
CA-21B	13.1	6.0704	0.1896	0.3498	0.0040	0.9100	2.8588	0.0327	0.1259	0.0040	0.2013	0.0185
CA-21B	14.1	6.1676	0.1960	0.3489	0.0036	0.9700	2.8665	0.0294	0.1282	0.0042	0.3731	0.1021
CA-21B	15.1	7.9296	0.2503	0.4179	0.0044	0.8500	2.3930	0.0254	0.1376	0.0044	0.2631	0.0082
CA-21B	17.1	7.4358	0.2487	0.4162	0.0046	0.9300	2.4027	0.0266	0.1296	0.0045	0.1027	0.0179
CA-21B	18.1	8.1260	0.2373	0.4298	0.0042	0.9600	2.3266	0.0227	0.1371	0.0043	0.3292	0.0267
CA-21B	19.1	6.6942	0.2003	0.3626	0.0036	0.9600	2.7581	0.0272	0.1339	0.0038	0.4798	0.0145
CA-21B	20.1	7.7997	0.2496	0.4261	0.0045	0.9400	2.3467	0.0247	0.1327	0.0043	0.3495	0.0285
CA-21B	21.1	7.2773	0.2299	0.3910	0.0040	0.9900	2.5572	0.0264	0.1350	0.0049	0.2711	0.0297
CA-21B	22.1	8.2765	0.2966	0.4371	0.0053	0.8800	2.2880	0.0279	0.1373	0.0053	0.3615	0.0157
CA-21B	24.1	7.6657	0.2043	0.4057	0.0035	0.9900	2.4648	0.0214	0.1370	0.0038	0.2467	0.0467
CA-21B	25.1	7.9438	0.2831	0.4161	0.0051	0.6200	2.4031	0.0293	0.1384	0.0052	0.3543	0.0165
CA-21B	26.1	6.8982	0.1988	0.3978	0.0037	0.9900	2.5139	0.0233	0.1258	0.0038	0.0975	0.0460
CA-21B	27.1	7.7994	0.2481	0.4209	0.0040	0.9000	2.3760	0.0227	0.1344	0.0043	0.3469	0.0195
CA-21B	30.1	7.5824	0.2553	0.4015	0.0043	0.9500	2.4906	0.0266	0.1370	0.0047	0.3341	0.0256
CA-21B	31.1	7.9927	0.2528	0.4266	0.0041	0.8500	2.3441	0.0227	0.1359	0.0042	0.3537	0.0105
CA-21B	32.1	8.0065	0.2513	0.4270	0.0041	0.5200	2.3421	0.0223	0.1360	0.0042	0.3051	0.0491
CA-21B	33.1	7.7801	0.2222	0.4125	0.0034	0.6700	2.4240	0.0202	0.1368	0.0037	0.4392	0.0485
CA-21B	45.1	8.1216	0.2600	0.4321	0.0054	0.8600	2.3144	0.0288	0.1363	0.0045	0.4274	0.0130
CA-21B	48.1	7.9730	0.2622	0.4288	0.0055	0.8600	2.3321	0.0301	0.1349	0.0048	0.3155	0.0349
CA-21B	49.1	7.9191	0.3541	0.4224	0.0080	0.9500	2.3677	0.0450	0.1360	0.0068	0.3194	0.0256
CA-21B	50.1	7.7324	0.2756	0.4121	0.0058	0.8800	2.4266	0.0341	0.1361	0.0051	0.3481	0.0157
CA-21B	51.1	7.8371	0.2413	0.4217	0.0050	0.9700	2.3712	0.0279	0.1348	0.0044	0.3956	0.0082
CA-21B	54.1	7.8259	0.2443	0.4200	0.0062	0.8300	2.3809	0.0353	0.1351	0.0048	0.2574	0.1222
CA-21B	55.1	6.9083	0.2394	0.3726	0.0061	0.9800	2.6835	0.0442	0.1345	0.0054	0.5353	0.0247
CA-21B	56.1	7.9317	0.4247	0.4191	0.0111	0.2300	2.3859	0.0632	0.1373	0.0089	0.3091	0.0238
CA-21B	62.1	7.9636	0.2089	0.4319	0.0053	0.9900	2.3152	0.0283	0.1337	0.0046	0.3899	0.0365
CA-21B	63.1	8.1043	0.2858	0.4227	0.0072	0.4600	2.3655	0.0404	0.1390	0.0054	0.2639	0.0094
CA-21B	65.1	7.6470	0.2254	0.4076	0.0056	0.4800	2.4536	0.0338	0.1361	0.0044	0.5388	0.0204
CA-21B	70.1	6.5222	0.2712	0.3608	0.0069	0.9600	2.7716	0.0530	0.1311	0.0061	0.5673	0.0392
CA-21B	71.1	7.5102	0.3081	0.4025	0.0079	0.5100	2.4847	0.0491	0.1353	0.0063	0.3284	0.0168
CA-21B	72.1	7.8867	0.2643	0.4194	0.0065	0.0100	2.3846	0.0368	0.1364	0.0050	0.2872	0.0160
CA-21B	73.1	6.9354	0.1858	0.3763	0.0044	0.9900	2.6577	0.0313	0.1337	0.0039	0.2495	0.0439
CA-21B	74.1	7.7264	0.2167	0.4107	0.0050	0.6200	2.4346	0.0298	0.1364	0.0040	0.4541	0.0881

CA-21B	78.1	7.8724	0.3822	0.4148	0.0102	0.4500	2.4106	0.0590	0.1376	0.0076	0.2829	0.0217
CA-21B	80.1	6.0509	0.2225	0.3414	0.0055	0.9900	2.9294	0.0472	0.1286	0.0054	0.0392	0.0136
CA-21B	81.1	7.8818	0.3295	0.4313	0.0081	0.9300	2.3186	0.0438	0.1325	0.0063	0.3537	0.0255
CA-21B	82.1	6.9611	0.2989	0.3855	0.0080	0.9900	2.5942	0.0542	0.1310	0.0071	0.2994	0.0241
CA-21B	84.1	7.6178	0.4221	0.4102	0.0119	0.8400	2.4376	0.0709	0.1347	0.0095	0.2869	0.0208
CA-21B	87.1	14.2089	0.3838	0.5355	0.0065	0.9900	1.8676	0.0226	0.1925	0.0066	0.0967	0.0182
CA-21B	*2.1*	*5.9853*	*0.1941*	*0.3237*	*0.0039*	*0.9900*	*3.0889*	*0.0374*	*0.1341*	*0.0044*	*0.1010*	*0.0071*
CA-21B	*5.1*	*5.8285*	*0.1899*	*0.3226*	*0.0038*	*0.9700*	*3.0996*	*0.0367*	*0.1310*	*0.0042*	*0.3549*	*0.0166*
CA-21B	*6.1*	*6.6784*	*0.1863*	*0.3824*	*0.0039*	*0.9600*	*2.6148*	*0.0265*	*0.1267*	*0.0040*	*0.3153*	*0.0340*
CA-21B	*16.1*	*4.1341*	*0.1574*	*0.2584*	*0.0030*	*0.9900*	*3.8705*	*0.0449*	*0.1160*	*0.0037*	*0.0324*	*0.0072*
CA-21B	*23.1*	*8.2719*	*0.3698*	*0.4314*	*0.0066*	*0.1400*	*2.3179*	*0.0354*	*0.1391*	*0.0066*	*0.2995*	*0.0262*
CA-21B	*28.1*	*2.9585*	*0.1418*	*0.1765*	*0.0024*	*0.9900*	*5.6663*	*0.0776*	*0.1216*	*0.0042*	*0.3506*	*0.0163*
CA-21B	*29.1*	*5.2649*	*0.1841*	*0.2985*	*0.0032*	*0.9800*	*3.3497*	*0.0356*	*0.1279*	*0.0040*	*0.4498*	*0.0133*
CA-21B	*34.1*	*8.3239*	*0.2228*	*0.4516*	*0.0036*	*0.9800*	*2.2145*	*0.0176*	*0.1337*	*0.0038*	*0.3936*	*0.0298*
CA-21B	*35.1*	*4.2665*	*0.2091*	*0.2255*	*0.0035*	*0.9700*	*4.4352*	*0.0694*	*0.1372*	*0.0060*	*0.3226*	*0.0190*
CA-21B	*36.1*	*7.0142*	*0.2695*	*0.3756*	*0.0048*	*0.9300*	*2.6621*	*0.0341*	*0.1354*	*0.0056*	*0.3197*	*0.0323*
CA-21B	*37.1*	*8.0317*	*0.2944*	*0.4218*	*0.0051*	*0.5800*	*2.3710*	*0.0289*	*0.1381*	*0.0051*	*0.3282*	*0.0142*
CA-21B	*38.1*	*5.3257*	*0.1865*	*0.3122*	*0.0031*	*0.9700*	*3.2027*	*0.0321*	*0.1237*	*0.0038*	*0.3293*	*0.0342*
CA-21B	*39.1*	*8.1993*	*0.2479*	*0.4368*	*0.0040*	*0.6300*	*2.2896*	*0.0210*	*0.1362*	*0.0040*	*0.4153*	*0.0164*
CA-21B	*40.1*	*5.5795*	*0.2364*	*0.3054*	*0.0051*	*0.9900*	*3.2748*	*0.0543*	*0.1325*	*0.0059*	*0.4606*	*0.0232*
CA-21B	*41.1*	*7.1478*	*0.2606*	*0.4178*	*0.0058*	*0.9700*	*2.3936*	*0.0334*	*0.1241*	*0.0054*	*0.1963*	*0.0347*
CA-21B	*42.1*	*3.9992*	*0.1974*	*0.2254*	*0.0045*	*0.9600*	*4.4369*	*0.0892*	*0.1287*	*0.0059*	*0.2782*	*0.0321*
CA-21B	*43.1*	*8.2807*	*0.2750*	*0.4506*	*0.0057*	*0.7700*	*2.2193*	*0.0282*	*0.1333*	*0.0045*	*0.4739*	*0.0301*
CA-21B	*44.1*	*4.9070*	*0.1838*	*0.2762*	*0.0040*	*0.9900*	*3.6202*	*0.0524*	*0.1288*	*0.0048*	*0.4081*	*0.0233*
CA-21B	*46.1*	*8.6307*	*0.3471*	*0.4611*	*0.0076*	*0.8200*	*2.1686*	*0.0356*	*0.1357*	*0.0056*	*0.3551*	*0.0182*
CA-21B	*47.1*	*5.8275*	*0.1432*	*0.3230*	*0.0030*	*0.9900*	*3.0960*	*0.0289*	*0.1309*	*0.0040*	*0.3906*	*0.0413*
CA-21B	*52.1*	*6.7745*	*0.3124*	*0.3599*	*0.0072*	*0.5600*	*2.7788*	*0.0554*	*0.1365*	*0.0074*	*0.2935*	*0.0153*
CA-21B	*53.1*	*8.0400*	*0.3166*	*0.4534*	*0.0086*	*0.9300*	*2.2057*	*0.0416*	*0.1286*	*0.0056*	*0.2737*	*0.0297*
CA-21B	*57.1*	*3.5207*	*0.1678*	*0.2197*	*0.0045*	*0.9600*	*4.5524*	*0.0940*	*0.1162*	*0.0069*	*0.1393*	*0.0310*
CA-21B	*58.1*	*3.7460*	*0.1592*	*0.2348*	*0.0043*	*0.9700*	*4.2584*	*0.0771*	*0.1157*	*0.0052*	*0.4144*	*0.0321*
CA-21B	*59.1*	*6.0034*	*0.2633*	*0.3295*	*0.0070*	*0.8300*	*3.0345*	*0.0649*	*0.1321*	*0.0062*	*0.3640*	*0.0132*
CA-21B	*60.1*	*7.7758*	*0.2205*	*0.4234*	*0.0055*	*0.9600*	*2.3616*	*0.0308*	*0.1332*	*0.0045*	*0.3544*	*0.0242*
CA-21B	*61.1*	*4.2727*	*0.1612*	*0.2433*	*0.0042*	*0.9800*	*4.1107*	*0.0702*	*0.1274*	*0.0047*	*0.3090*	*0.0263*
CA-21B	*64.1*	*4.5390*	*0.2010*	*0.2819*	*0.0055*	*0.9900*	*3.5479*	*0.0695*	*0.1168*	*0.0060*	*0.1372*	*0.0304*
CA-21B	*66.1*	*8.2311*	*0.2997*	*0.4289*	*0.0075*	*0.7400*	*2.3314*	*0.0405*	*0.1392*	*0.0054*	*0.3608*	*0.0280*
CA-21B	*67.1*	*8.7773*	*0.2510*	*0.4721*	*0.0063*	*0.9800*	*2.1184*	*0.0283*	*0.1349*	*0.0044*	*0.2705*	*0.1062*
CA-21B	*68.1*	*5.2088*	*0.2823*	*0.3335*	*0.0081*	*0.9400*	*2.9986*	*0.0730*	*0.1133*	*0.0074*	*0.0926*	*0.0501*
CA-21B	*69.1*	*4.1737*	*0.2785*	*0.2454*	*0.0076*	*0.9800*	*4.0745*	*0.1269*	*0.1233*	*0.0097*	*0.3809*	*0.0298*
CA-21B	*75.1*	*6.8763*	*0.2780*	*0.3710*	*0.0073*	*0.9500*	*2.6951*	*0.0533*	*0.1344*	*0.0065*	*0.2082*	*0.0794*
CA-21B	*76.1*	*5.0530*	*0.1791*	*0.2941*	*0.0046*	*0.9900*	*3.4004*	*0.0535*	*0.1246*	*0.0054*	*0.2720*	*0.0269*
CA-21B	*77.1*	*7.6329*	*0.3495*	*0.4120*	*0.0093*	*0.5000*	*2.4272*	*0.0546*	*0.1344*	*0.0069*	*0.3703*	*0.0225*
CA-21B	*79.1*	*6.0476*	*0.2924*	*0.3732*	*0.0083*	*0.9000*	*2.6792*	*0.0597*	*0.1175*	*0.0070*	*0.1084*	*0.0404*
CA-21B	*83.1*	*4.6873*	*0.2859*	*0.2957*	*0.0087*	*0.9600*	*3.3820*	*0.0994*	*0.1150*	*0.0078*	*0.0831*	*0.0589*
CA-21B	*85.1*	*8.6840*	*0.3492*	*0.4616*	*0.0093*	*0.9900*	*2.1666*	*0.0435*	*0.1365*	*0.0071*	*0.4204*	*0.0542*
CA-21B	*86.1*	*7.8293*	*0.3525*	*0.4090*	*0.0092*	*0.6200*	*2.4449*	*0.0548*	*0.1388*	*0.0075*	*0.3581*	*0.0138*
CA-21B	*88.1*	*5.5655*	*0.3001*	*0.2914*	*0.0073*	*0.9800*	*3.4318*	*0.0863*	*0.1385*	*0.0076*	*0.1388*	*0.0683*

ı lead.

Commom Pb	Pb rad	Th	U	Th/U	AGES (Ga)						CONC. (%)
(%)	ppm	ppm	ppm		T206/208	1 sigma	T207/235	1 sigma	T207/206	1 sigma	
0.77	26.60	35.10	44.10	1/0/00	2.210	0.024	2.217	0.032	2.223	0.065	99
0.80	42.70	76.50	63.90	1/1/00	2.371	0.024	2.260	0.029	2.161	0.058	109
0.27	51.40	90.70	78.20	1/1/00	2.168	0.020	2.176	0.027	2.183	0.054	99
0.41	62.10	85.50	97.60	1/0/00	2.250	0.021	2.213	0.026	2.179	0.051	103
0.05	100.60	155.80	151.60	1/1/00	2.281	0.019	2.225	0.023	2.175	0.044	104
0.42	55.70	92.60	91.60	1/1/00	2.105	0.019	2.149	0.025	2.192	0.049	96
0.37	78.70	144.10	126.70	1/1/00	2.168	0.020	2.173	0.027	2.177	0.054	99
0.66	95.30	270.30	127.20	1/2/00	2.172	0.023	2.169	0.030	2.166	0.061	100
0.40	68.40	38.70	80.80	1/0/00	3.033	0.025	2.933	0.024	2.865	0.041	105
0.53	66.30	90.60	127.60	1/0/00	1.934	0.019	1.986	0.027	2.041	0.056	94
0.62	62.40	32.80	114.60	1/0/00	1.929	0.017	2.000	0.028	2.074	0.057	93
0.45	43.40	65.50	70.40	1/0/00	2.251	0.020	2.223	0.029	2.198	0.057	102
0.38	42.10	48.90	76.50	1/0/00	2.243	0.021	2.165	0.031	2.092	0.062	107
0.95	51.90	82.50	79.30	1/1/00	2.305	0.019	2.245	0.028	2.191	0.054	105
0.34	70.10	211.10	100.60	1/2/00	1.994	0.017	2.072	0.025	2.150	0.049	92
0.61	57.20	158.20	95.50	1/1/00	2.288	0.020	2.208	0.028	2.135	0.055	107
0.52	34.90	37.50	61.60	1/0/00	2.128	0.019	2.146	0.031	2.164	0.062	98
0.72	27.60	37.80	40.20	1/0/00	2.337	0.024	2.262	0.034	2.194	0.069	106
0.95	69.30	141.40	114.10	1/1/00	2.195	0.016	2.193	0.025	2.190	0.049	100
0.66	38.90	77.20	60.90	1/1/00	2.243	0.023	2.225	0.033	2.208	0.066	101
0.68	47.60	60.40	84.50	1/0/00	2.159	0.017	2.098	0.026	2.040	0.052	105
0.28	49.30	79.70	72.30	1/1/00	2.264	0.018	2.208	0.029	2.156	0.054	105
0.35	32.00	48.40	50.80	1/0/00	2.176	0.020	2.183	0.031	2.189	0.060	99
0.23	51.70	70.00	74.30	1/0/00	2.290	0.019	2.230	0.029	2.175	0.054	105
0.28	57.60	132.90	82.90	1/1/00	2.292	0.018	2.232	0.028	2.177	0.053	105
0.07	85.80	155.60	114.00	1/1/00	2.227	0.016	2.206	0.025	2.187	0.047	101
0.61	59.50	151.50	87.10	1/1/00	2.315	0.024	2.245	0.029	2.181	0.058	106
0.15	47.90	78.50	73.10	1/1/00	2.300	0.025	2.228	0.031	2.162	0.063	106
0.38	25.00	29.40	38.10	1/0/00	2.271	0.036	2.222	0.040	2.177	0.087	104
0.25	48.10	65.40	69.80	1/0/00	2.225	0.026	2.200	0.032	2.178	0.065	102
0.14	59.20	101.60	85.90	1/1/00	2.268	0.023	2.212	0.029	2.161	0.057	104
0.22	43.70	70.70	63.40	1/1/00	2.261	0.029	2.211	0.029	2.166	0.064	104
0.04	68.00	141.40	81.60	1/1/00	2.042	0.029	2.100	0.032	2.157	0.071	94
0.55	18.80	21.10	28.60	1/0/00	2.257	0.050	2.223	0.047	2.193	0.106	102
0.42	91.40	124.30	128.50	1/0/00	2.314	0.025	2.227	0.027	2.147	0.059	107
0.44	37.80	64.00	58.90	1/1/00	2.273	0.033	2.243	0.031	2.215	0.068	102
0.35	95.20	179.60	127.20	1/1/00	2.204	0.026	2.190	0.026	2.178	0.057	101
0.24	43.90	76.60	55.10	1/1/00	1.986	0.033	2.049	0.036	2.113	0.080	93
0.79	31.80	44.50	50.40	1/0/00	2.180	0.037	2.174	0.037	2.168	0.081	100
0.01	43.30	56.70	65.40	1/0/00	2.258	0.029	2.218	0.030	2.182	0.064	103
0.13	62.60	86.40	101.00	1/0/00	2.059	0.021	2.103	0.025	2.147	0.053	95
0.43	87.80	148.20	119.40	1/1/00	2.218	0.023	2.200	0.025	2.182	0.052	101

0.56	19.80	22.20	29.50	1/0/00	2.237	0.046	2.217	0.044	2.198	0.097	101
0.69	72.60	21.50	125.00	1/0/00	1.893	0.026	1.983	0.032	2.078	0.075	91
0.22	61.30	125.20	74.60	1/1/00	2.312	0.036	2.218	0.035	2.132	0.080	108
0.49	50.30	65.50	72.60	1/0/00	2.102	0.039	2.106	0.040	2.111	0.094	99
0.37	20.70	25.90	28.60	1/0/00	2.216	0.055	2.187	0.050	2.160	0.121	102
0.42	122.50	63.60	145.70	1/0/00	2.764	0.027	2.764	0.029	2.763	0.058	100
1.31	*71.10*	*34.30*	*133.40*	*1/0/00*	*1.808*	*0.019*	*1.974*	*0.028*	*2.152*	*0.057*	*84*
2.33	*56.20*	*108.60*	*97.50*	*1/1/00*	*1.803*	*0.018*	*1.951*	*0.027*	*2.112*	*0.057*	*85*
1.71	*81.00*	*110.70*	*154.00*	*1/0/00*	*2.088*	*0.019*	*2.070*	*0.027*	*2.052*	*0.055*	*101*
1.38	*59.00*	*13.70*	*122.90*	*1/0/00*	*1.481*	*0.015*	*1.661*	*0.027*	*1.896*	*0.060*	*78*
1.09	*17.30*	*33.80*	*27.30*	*1/1/00*	*2.312*	*0.030*	*2.261*	*0.041*	*2.216*	*0.081*	*104*
4.11	*57.90*	*124.60*	*108.20*	*1/1/00*	*1.048*	*0.013*	*1.397*	*0.027*	*1.980*	*0.059*	*52*
1.70	*97.50*	*186.50*	*133.70*	*1/1/00*	*1.684*	*0.015*	*1.863*	*0.027*	*2.069*	*0.055*	*81*
0.29	*55.40*	*93.20*	*83.70*	*1/1/00*	*2.402*	*0.016*	*2.267*	*0.026*	*2.147*	*0.050*	*111*
1.40	*29.50*	*44.30*	*50.50*	*1/0/00*	*1.311*	*0.018*	*1.687*	*0.035*	*2.193*	*0.078*	*59*
2.63	*28.60*	*53.30*	*49.30*	*1/1/00*	*2.056*	*0.023*	*2.113*	*0.036*	*2.169*	*0.073*	*94*
1.02	*25.50*	*34.80*	*39.30*	*1/0/00*	*2.268*	*0.023*	*2.235*	*0.034*	*2.204*	*0.065*	*102*
1.22	*64.60*	*99.60*	*96.00*	*1/1/00*	*1.752*	*0.015*	*1.873*	*0.027*	*2.010*	*0.055*	*87*
0.11	*66.20*	*99.10*	*93.80*	*1/1/00*	*2.336*	*0.018*	*2.253*	*0.027*	*2.179*	*0.051*	*107*
1.77	*56.20*	*92.00*	*75.30*	*1/1/00*	*1.718*	*0.025*	*1.913*	*0.035*	*2.132*	*0.077*	*80*
2.19	*42.60*	*77.80*	*64.60*	*1/1/00*	*2.250*	*0.028*	*2.130*	*0.035*	*2.016*	*0.076*	*111*
2.18	*44.50*	*59.90*	*75.80*	*1/0/00*	*1.310*	*0.023*	*1.634*	*0.036*	*2.080*	*0.084*	*62*
0.25	*68.40*	*122.50*	*89.30*	*1/1/00*	*2.398*	*0.025*	*2.262*	*0.030*	*2.142*	*0.058*	*111*
1.85	*87.10*	*164.70*	*140.60*	*1/1/00*	*1.572*	*0.019*	*1.803*	*0.030*	*2.082*	*0.067*	*75*
1.64	*39.90*	*93.80*	*57.50*	*1/1/00*	*2.445*	*0.033*	*2.300*	*0.035*	*2.174*	*0.072*	*112*
3.32	*67.00*	*175.80*	*108.50*	*1/1/00*	*1.804*	*0.015*	*1.951*	*0.026*	*2.109*	*0.055*	*85*
2.19	*19.60*	*29.00*	*36.50*	*1/0/00*	*1.982*	*0.034*	*2.082*	*0.042*	*2.184*	*0.094*	*90*
1.01	*39.30*	*90.00*	*60.50*	*1/1/00*	*2.410*	*0.038*	*2.236*	*0.036*	*2.079*	*0.079*	*115*
2.12	*50.30*	*86.90*	*102.60*	*1/0/00*	*1.280*	*0.024*	*1.532*	*0.039*	*1.899*	*0.109*	*67*
3.12	*49.60*	*160.90*	*88.40*	*1/1/00*	*1.360*	*0.022*	*1.581*	*0.032*	*1.891*	*0.083*	*71*
0.95	*48.30*	*154.00*	*82.30*	*1/1/00*	*1.836*	*0.034*	*1.976*	*0.037*	*2.126*	*0.087*	*86*
1.67	*87.30*	*195.40*	*131.00*	*1/1/00*	*2.276*	*0.025*	*2.205*	*0.027*	*2.140*	*0.058*	*106*
0.00	*71.00*	*156.60*	*101.70*	*1/1/00*	*1.404*	*0.021*	*1.688*	*0.028*	*2.062*	*0.067*	*68*
2.33	*27.90*	*41.20*	*50.20*	*1/0/00*	*1.601*	*0.028*	*1.738*	*0.037*	*1.908*	*0.093*	*83*
1.55	*38.70*	*46.50*	*58.90*	*1/0/00*	*2.301*	*0.033*	*2.257*	*0.033*	*2.217*	*0.068*	*103*
0.33	*81.70*	*179.80*	*104.00*	*1/1/00*	*2.493*	*0.028*	*2.315*	*0.028*	*2.162*	*0.058*	*115*
6.62	*41.80*	*71.30*	*85.20*	*1/0/00*	*1.855*	*0.040*	*1.854*	*0.048*	*1.853*	*0.117*	*100*
4.30	*28.10*	*56.30*	*40.90*	*1/1/00*	*1.415*	*0.038*	*1.669*	*0.054*	*2.005*	*0.141*	*70*
1.23	*25.20*	*31.90*	*44.50*	*1/0/00*	*2.034*	*0.035*	*2.096*	*0.040*	*2.156*	*0.091*	*94*
8.49	*36.30*	*71.60*	*71.70*	*1/0/00*	*1.662*	*0.023*	*1.828*	*0.033*	*2.023*	*0.080*	*82*
7.90	*22.10*	*55.30*	*35.50*	*1/1/00*	*2.224*	*0.042*	*2.189*	*0.041*	*2.156*	*0.090*	*103*
1.34	*49.20*	*80.60*	*86.20*	*1/0/00*	*2.045*	*0.040*	*1.983*	*0.043*	*1.919*	*0.106*	*106*
1.11	*23.60*	*44.60*	*40.10*	*1/1/00*	*1.670*	*0.042*	*1.765*	*0.048*	*1.879*	*0.131*	*88*
1.03	*49.30*	*111.70*	*61.80*	*1/1/00*	*2.446*	*0.041*	*2.305*	*0.039*	*2.183*	*0.089*	*112*
1.04	*25.80*	*40.30*	*39.50*	*1/1/00*	*2.210*	*0.042*	*2.212*	*0.040*	*2.213*	*0.093*	*99*
0.00	*35.40*	*26.10*	*47.70*	*1/0/00*	*1.648*	*0.033*	*1.911*	*0.040*	*2.209*	*0.103*	*74*

Table 7. LA-ICP-MS U-Pb in situ zircon analysis from CA-22 sample (st-grt-qtz-ms schist). Italicized data were not used in age determinations and plotting, due high levels of discordance and common lead.

SAMPLE	SPOT	RATIOS											Commom Pb
		207/235	1sigma	206/238	1 sigma	coef. corr	238/206	1 sigma	207/206	1 sigma	208/206	1 sigma	(%)
CA-22	1.1	2.1939	0.1055	0.1930	0.0039	0.2700	5.1823	0.1051	0.0825	0.0047	0.1188	0.0120	0.39
CA-22	2.2	7.1995	0.1612	0.3934	0.0041	0.9600	2.5419	0.0262	0.1327	0.0030	0.1515	0.0070	0.19
CA-22	3.1	6.0300	0.1464	0.3599	0.0041	0.8400	2.7785	0.0320	0.1215	0.0031	0.3031	0.0055	0.17
CA-22	4.1	6.4149	0.2589	0.3607	0.0080	0.0100	2.7723	0.0619	0.1290	0.0062	0.2207	0.0233	0.60
CA-22	6.1	7.0411	0.1492	0.3880	0.0037	0.9000	2.5772	0.0243	0.1316	0.0028	0.1135	0.0014	0.13
CA-22	7.1	6.9057	0.1820	0.3982	0.0052	0.6100	2.5116	0.0325	0.1258	0.0035	0.1401	0.0065	0.16
CA-22	9.1	1.5885	0.1022	0.1579	0.0041	0.6400	6.3312	0.1632	0.0729	0.0059	0.8869	0.0737	0.03
CA-22	11.1	7.2645	0.4040	0.3955	0.0130	0.0900	2.5284	0.0831	0.1332	0.0092	0.2441	0.0302	0.94
CA-22	12.1	7.5050	0.2089	0.4031	0.0056	0.5600	2.4807	0.0345	0.1350	0.0040	0.1098	0.0065	0.63
CA-22	13.1	8.2917	0.2742	0.4228	0.0077	0.4400	2.3653	0.0433	0.1422	0.0052	0.1825	0.0157	0.29
CA-22	14.1	6.2272	0.1329	0.3681	0.0037	0.7800	2.7164	0.0271	0.1227	0.0026	0.2517	0.0068	0.18
CA-22	15.1	4.8453	0.1930	0.3210	0.0064	0.5100	3.1157	0.0617	0.1095	0.0050	0.2951	0.0140	0.40
CA-22	17.1	7.8947	0.1691	0.4369	0.0042	0.7500	2.2888	0.0220	0.1310	0.0028	0.1239	0.0264	0.20
CA-22	18.1	5.2513	0.1224	0.3318	0.0036	0.8300	3.0136	0.0327	0.1148	0.0027	0.1814	0.0049	0.83
CA-22	19.1	6.4496	0.2117	0.3799	0.0062	0.3900	2.6321	0.0432	0.1231	0.0045	0.3612	0.0130	0.26
CA-22	20.1	2.9106	0.1180	0.2374	0.0041	0.9200	4.2118	0.0735	0.0889	0.0038	0.1453	0.0084	0.73
CA-22	21.1	4.6049	0.1076	0.2985	0.0033	0.9600	3.3497	0.0365	0.1119	0.0027	0.1644	0.0159	0.33
CA-22	22.1	2.1611	0.0952	0.2010	0.0036	0.3700	4.9759	0.0896	0.0780	0.0040	0.0977	0.0115	0.60
CA-22	23.1	2.7757	0.0789	0.2339	0.0028	0.4800	4.2762	0.0516	0.0861	0.0026	0.0875	0.0053	0.19
CA-22	24.1	6.0371	0.1414	0.3582	0.0040	0.7700	2.7919	0.0313	0.1222	0.0030	0.4028	0.0081	0.17
CA-22	25.1	7.3420	0.1715	0.4078	0.0047	0.4300	2.4520	0.0280	0.1306	0.0031	0.1553	0.0047	0.21
CA-22	26.1	4.0534	0.1666	0.2895	0.0066	0.3500	3.4548	0.0785	0.1016	0.0046	0.2881	0.0137	0.68
CA-22	27.1	1.6543	0.0522	0.1685	0.0023	0.0100	5.9348	0.0824	0.0712	0.0022	0.1010	0.0064	0.25
CA-22	28.1	7.4702	0.2351	0.4148	0.0070	0.8000	2.4109	0.0405	0.1306	0.0040	0.1411	0.0076	0.10
CA-22	29.1	6.5150	0.2148	0.3924	0.0071	0.6400	2.5482	0.0459	0.1204	0.0041	0.1451	0.0105	0.17
CA-22	30.1	8.7739	0.2339	0.4523	0.0061	0.9700	2.2111	0.0298	0.1407	0.0037	0.2321	0.0248	0.63
CA-22	32.1	6.1487	0.1626	0.3661	0.0048	0.9800	2.7316	0.0356	0.1218	0.0032	0.2731	0.0149	0.11
CA-22	33.1	5.9727	0.1642	0.3584	0.0048	0.8600	2.7905	0.0376	0.1209	0.0031	0.1716	0.0524	0.07
CA-22	34.1	7.3460	0.2303	0.4019	0.0069	0.5300	2.4884	0.0429	0.1326	0.0042	0.1586	0.0085	0.20
CA-22	34.2	6.6022	0.1869	0.3924	0.0055	0.8100	2.5482	0.0355	0.1220	0.0032	0.0521	0.0060	0.33
CA-22	35.1	5.2486	0.1449	0.3338	0.0045	0.7000	2.9954	0.0400	0.1140	0.0030	0.2831	0.0087	0.11
CA-22	37.1	3.6616	0.1147	0.2797	0.0043	0.2700	3.5759	0.0544	0.0950	0.0029	0.1089	0.0118	0.65
CA-22	38.1	2.3463	0.0634	0.2073	0.0023	0.7000	4.8228	0.0535	0.0821	0.0023	0.0761	0.0088	0.09
CA-22	40.1	3.0946	0.1191	0.2469	0.0048	0.3800	4.0508	0.0780	0.0909	0.0040	0.1165	0.0128	0.38
CA-22	41.1	7.5676	0.2297	0.4101	0.0062	0.2800	2.4383	0.0370	0.1338	0.0043	0.1520	0.0106	0.23
CA-22	45.1	6.2252	0.2043	0.3712	0.0065	0.7400	2.6939	0.0470	0.1216	0.0045	0.2320	0.0112	0.24
CA-22	47.1	4.8324	0.1794	0.3229	0.0066	0.0400	3.0971	0.0633	0.1085	0.0046	0.2673	0.0179	0.31
CA-22	48.1	2.0873	0.0577	0.1924	0.0022	0.6600	5.1977	0.0602	0.0787	0.0023	0.0224	0.0148	0.08
CA-22	51.1	4.6436	0.1329	0.3140	0.0038	0.9300	3.1851	0.0381	0.1073	0.0031	0.1522	0.0078	0.23
CA-22	52.1	8.0553	0.2252	0.4375	0.0052	0.7300	2.2859	0.0271	0.1335	0.0036	0.1210	0.0036	0.07
CA-22	54.1	1.2330	0.0501	0.1371	0.0021	0.5300	7.2926	0.1135	0.0652	0.0028	0.1180	0.0114	0.26
CA-22	55.1	2.4039	0.1040	0.2138	0.0040	0.1700	4.6777	0.0868	0.0816	0.0039	0.0836	0.0116	0.35
CA-22	56.1	7.5735	0.2473	0.4024	0.0064	0.0100	2.4853	0.0394	0.1365	0.0046	0.4291	0.0102	0.15
CA-22	57.1	5.4893	0.1952	0.3336	0.0060	0.9600	2.9977	0.0538	0.1193	0.0047	0.7714	0.0504	0.30

CA-22	59.1	6.7792	0.2245	0.3802	0.0061	0.4100	2.6304	0.0422	0.1293	0.0045	0.2555	0.0145	0.78
CA-22	60.1	3.5457	0.1073	0.2683	0.0033	0.6600	3.7267	0.0462	0.0958	0.0029	0.1259	0.0037	0.27
CA-22	61.1	2.3078	0.0650	0.2086	0.0022	0.2800	4.7934	0.0512	0.0802	0.0022	0.0951	0.0035	0.06
CA-22	62.1	6.5018	0.1698	0.3782	0.0038	0.5600	2.6443	0.0267	0.1247	0.0030	0.1424	0.0034	0.23
CA-22	63.1	6.4502	0.2802	0.3741	0.0089	0.7700	2.6728	0.0634	0.1250	0.0060	0.3032	0.0178	0.28
CA-22	64.1	2.3064	0.0596	0.2044	0.0045	0.7200	4.8933	0.1069	0.0819	0.0023	0.0972	0.0081	0.17
CA-22	66.1	1.3913	0.0426	0.1463	0.0034	0.4600	6.8352	0.1575	0.0690	0.0024	0.1729	0.0047	0.35
CA-22	68.1	4.5014	0.1102	0.3048	0.0065	0.4200	3.2812	0.0705	0.1071	0.0029	0.1080	0.0024	0.11
CA-22	70.1	6.8490	0.1857	0.3733	0.0089	0.8500	2.6785	0.0639	0.1330	0.0041	0.1241	0.0046	0.34
CA-22	71.1	6.4510	0.1520	0.3658	0.0078	0.9100	2.7339	0.0580	0.1279	0.0033	0.0802	0.0025	0.10
CA-22	72.1	5.5489	0.2855	0.3386	0.0134	0.1600	2.9534	0.1173	0.1189	0.0077	0.5161	0.0556	0.80
CA-22	74.1	3.4318	0.0821	0.2626	0.0055	0.5900	3.8079	0.0797	0.0948	0.0026	0.0893	0.0035	0.02
CA-22	75.1	3.6080	0.1032	0.2688	0.0063	0.7300	3.7208	0.0877	0.0974	0.0032	0.1552	0.0139	0.38
CA-22	77.1	7.7279	0.3391	0.3980	0.0102	0.4100	2.5127	0.0644	0.1408	0.0065	0.2134	0.0127	0.44
CA-22	78.1	7.2823	0.2640	0.3936	0.0084	0.6900	2.5405	0.0543	0.1342	0.0048	0.1207	0.0079	0.33
CA-22	80.1	7.2762	0.2371	0.3929	0.0076	0.6200	2.5451	0.0493	0.1343	0.0043	0.1728	0.0058	0.22
CA-22	81.1	6.3145	0.2013	0.3643	0.0069	0.4100	2.7450	0.0521	0.1257	0.0038	0.1970	0.0065	0.29
CA-22	82.1	6.8121	0.2152	0.3766	0.0072	0.7500	2.6555	0.0508	0.1312	0.0040	0.1262	0.0045	0.25
CA-22	83.1	7.6540	0.2077	0.4072	0.0070	0.9100	2.4558	0.0422	0.1363	0.0033	0.2472	0.0159	0.17
CA-22	84.1	7.2471	0.2018	0.4063	0.0070	0.7600	2.4614	0.0423	0.1294	0.0033	0.1070	0.0048	0.05
CA-22	85.1	4.0427	0.1423	0.2877	0.0056	0.3500	3.4762	0.0676	0.1019	0.0035	0.1192	0.0053	0.24
CA-22	86.1	7.4062	0.2009	0.4057	0.0068	0.2000	2.4646	0.0413	0.1324	0.0032	0.1535	0.0149	0.16
CA-22	87.1	7.0657	0.2016	0.3891	0.0068	0.8700	2.5704	0.0450	0.1317	0.0035	0.1611	0.0039	0.15
CA-22	88.1	6.4645	0.1774	0.3669	0.0062	0.2800	2.7253	0.0458	0.1278	0.0032	0.1140	0.0042	0.13
CA-22	89.1	1.9476	0.0698	0.1847	0.0034	0.8100	5.4155	0.0992	0.0765	0.0027	0.1066	0.0050	0.13
CA-22	*2.1*	*7.6294*	*7.6294*	*0.1793*	*0.4106*	*0.0045*	*0.8700*	*2.4354*	*0.0270*	*0.1348*	*0.0032*	*0.2650*	*2.48*
CA-22	*5.1*	*3.1747*	*3.1747*	*0.2576*	*0.2416*	*0.0093*	*0.7500*	*4.1397*	*0.1597*	*0.0953*	*0.0097*	*0.1743*	*11.84*
CA-22	*8.1*	*2.0558*	*0.1116*	*0.1890*	*0.0043*	*0.3800*	*5.2901*	*0.1197*	*0.0789*	*0.0052*	*0.5530*	*0.0180*	*1.49*
CA-22	*10.1*	*6.6515*	*0.2177*	*0.3714*	*0.0065*	*0.0900*	*2.6927*	*0.0472*	*0.1299*	*0.0049*	*0.1589*	*0.0100*	*1.62*
CA-22	*16.1*	*8.5976*	*0.1753*	*0.4685*	*0.0045*	*0.6900*	*2.1346*	*0.0206*	*0.1331*	*0.0028*	*0.1710*	*0.0055*	*0.13*
CA-22	*31.1*	*2.9173*	*0.3472*	*0.2460*	*0.0167*	*0.2600*	*4.0650*	*0.2755*	*0.0860*	*0.0137*	*0.1621*	*0.0737*	*3.58*
CA-22	*36.1*	*1.3720*	*0.0914*	*0.1526*	*0.0045*	*0.2500*	*6.5515*	*0.1936*	*0.0652*	*0.0051*	*0.2252*	*0.0227*	*1.43*
CA-22	*39.1*	*3.0478*	*0.0829*	*0.2463*	*0.0028*	*0.8700*	*4.0597*	*0.0461*	*0.0897*	*0.0026*	*0.0904*	*0.0049*	*1.23*
CA-22	*42.1*	*2.4949*	*0.1001*	*0.2169*	*0.0042*	*0.7200*	*4.6096*	*0.0902*	*0.0834*	*0.0040*	*0.1110*	*0.0174*	*1.01*
CA-22	*43.1*	*3.1659*	*0.1599*	*0.2508*	*0.0069*	*0.5500*	*3.9867*	*0.1102*	*0.0915*	*0.0056*	*0.1204*	*0.0139*	*1.40*
CA-22	*44.1*	*5.2265*	*0.1546*	*0.3002*	*0.0042*	*0.9900*	*3.3307*	*0.0461*	*0.1263*	*0.0038*	*0.1348*	*0.0139*	*0.86*
CA-22	*46.1*	*2.4616*	*0.1245*	*0.2154*	*0.0058*	*0.3400*	*4.6426*	*0.1240*	*0.0829*	*0.0053*	*0.1400*	*0.0309*	*1.51*
CA-22	*49.1*	*1.6195*	*0.0805*	*0.1701*	*0.0039*	*0.1400*	*5.8777*	*0.1345*	*0.0690*	*0.0041*	*0.0973*	*0.0223*	*0.61*
CA-22	*50.1*	*5.8960*	*0.1592*	*0.3601*	*0.0045*	*0.9800*	*2.7771*	*0.0348*	*0.1188*	*0.0040*	*0.1396*	*0.0137*	*3.21*
CA-22	*53.1*	*2.2429*	*0.0707*	*0.2049*	*0.0024*	*0.4800*	*4.8808*	*0.0584*	*0.0794*	*0.0026*	*0.2076*	*0.0381*	*14.56*
CA-22	*58.1*	*7.0076*	*0.2182*	*0.4162*	*0.0060*	*0.9200*	*2.4026*	*0.0344*	*0.1221*	*0.0038*	*0.1580*	*0.0102*	*0.08*
CA-22	*65.1*	*0.7679*	*0.0494*	*0.0942*	*0.0031*	*0.0700*	*10.6134*	*0.3524*	*0.0591*	*0.0046*	*0.3104*	*0.0151*	*1.14*
CA-22	*67.1*	*4.8602*	*0.1124*	*0.2947*	*0.0061*	*0.9800*	*3.3937*	*0.0705*	*0.1196*	*0.0032*	*0.0384*	*0.0186*	*4.82*
CA-22	*69.1*	*2.6418*	*0.1497*	*0.2236*	*0.0081*	*0.2700*	*4.4730*	*0.1616*	*0.0857*	*0.0060*	*0.3611*	*0.0227*	*1.01*
CA-22	*73.1*	*5.4432*	*0.1362*	*0.3355*	*0.0074*	*0.9600*	*2.9806*	*0.0655*	*0.1177*	*0.0032*	*0.0700*	*0.0311*	*1.08*
CA-22	*76.1*	*4.1599*	*0.1098*	*0.2576*	*0.0060*	*0.9700*	*3.8821*	*0.0912*	*0.1171*	*0.0032*	*0.1568*	*0.0033*	*0.73*
CA-22	*79.1*	*3.6919*	*0.1622*	*0.2824*	*0.0063*	*0.8100*	*3.5408*	*0.0784*	*0.0948*	*0.0044*	*0.1081*	*0.0209*	*1.55*

Pb rad	Th	U	Th/U	AGES (Ga)						CONC. (%)
ppm	ppm	ppm		T206/208	1 sigma	T207/235	1 sigma	T207/206	1 sigma	
17.10	23.70	63.90	2.19	1.137	0.021	1.179	0.033	1.256	0.111	90
88.50	83.70	154.90	7.20	2.139	0.019	2.136	0.020	2.134	0.039	100
76.20	115.80	129.60	6.03	1.982	0.020	1.980	0.021	1.979	0.046	100
17.40	20.20	31.00	6.41	1.986	0.038	2.034	0.036	2.084	0.086	95
134.40	83.50	237.30	7.04	2.114	0.017	2.117	0.019	2.120	0.036	99
53.70	39.70	96.80	6.91	2.161	0.024	2.099	0.023	2.040	0.050	105
17.80	142.20	47.50	1.59	0.945	0.023	0.966	0.044	1.012	0.173	93
10.60	13.10	16.20	7.26	2.148	0.060	2.144	0.049	2.141	0.119	100
37.70	21.70	66.40	7.51	2.183	0.026	2.174	0.024	2.164	0.051	100
23.40	21.10	35.40	8.29	2.273	0.035	2.263	0.030	2.255	0.062	100
110.40	143.50	190.30	6.23	2.021	0.017	2.008	0.019	1.996	0.038	101
16.60	25.70	31.50	4.85	1.794	0.031	1.793	0.034	1.791	0.084	100
143.30	97.90	218.10	7.89	2.337	0.019	2.219	0.019	2.112	0.037	110
71.70	78.00	143.70	5.25	1.847	0.017	1.861	0.020	1.876	0.043	98
35.90	54.70	55.60	6.45	2.076	0.029	2.039	0.028	2.002	0.063	103
21.00	27.80	55.40	2.91	1.373	0.021	1.385	0.028	1.402	0.079	97
80.70	66.50	179.30	4.60	1.684	0.016	1.750	0.020	1.830	0.044	92
15.90	15.20	58.70	2.16	1.181	0.020	1.169	0.031	1.147	0.100	102
42.50	45.00	132.60	2.78	1.355	0.015	1.349	0.021	1.340	0.056	101
72.90	182.70	116.80	6.04	1.974	0.019	1.981	0.021	1.989	0.044	99
72.90	52.50	120.00	7.34	2.205	0.021	2.154	0.021	2.106	0.043	104
18.10	30.60	40.50	4.05	1.639	0.033	1.645	0.034	1.653	0.084	99
55.80	65.10	255.50	1.65	1.004	0.013	0.991	0.020	0.963	0.062	104
51.70	36.10	92.60	7.47	2.237	0.032	2.169	0.028	2.106	0.053	106
40.60	29.50	78.40	6.52	2.134	0.033	2.048	0.029	1.962	0.060	108
85.30	60.50	130.60	8.77	2.405	0.027	2.315	0.025	2.236	0.046	107
104.10	117.40	198.50	6.15	2.011	0.023	1.997	0.024	1.983	0.047	101
135.20	80.40	285.00	5.97	1.974	0.023	1.972	0.024	1.969	0.045	100
36.60	31.90	62.30	7.35	2.178	0.032	2.154	0.028	2.132	0.055	102
82.10	38.00	163.30	6.60	2.134	0.025	2.060	0.025	1.986	0.046	107
88.00	121.20	170.30	5.25	1.857	0.022	1.861	0.024	1.865	0.047	99
62.20	51.90	160.20	3.66	1.590	0.021	1.563	0.025	1.527	0.057	104
78.70	86.80	299.80	2.35	1.215	0.012	1.226	0.019	1.247	0.055	97
20.50	18.50	63.50	3.09	1.422	0.025	1.431	0.029	1.445	0.083	98
44.90	58.50	79.20	7.57	2.215	0.028	2.181	0.027	2.149	0.056	103
29.00	34.20	53.70	6.23	2.035	0.030	2.008	0.029	1.980	0.066	102
18.90	26.20	38.70	4.83	1.804	0.032	1.791	0.031	1.775	0.078	101
58.60	17.90	258.70	2.09	1.134	0.012	1.145	0.019	1.164	0.059	97
73.40	65.60	180.90	4.64	1.760	0.018	1.757	0.024	1.754	0.053	100
78.10	44.10	141.80	8.06	2.339	0.023	2.237	0.025	2.145	0.047	109
34.20	59.30	199.10	1.23	0.828	0.012	0.816	0.023	0.781	0.092	106
21.70	18.00	84.90	2.40	1.249	0.021	1.244	0.031	1.235	0.097	101
41.90	69.20	64.30	7.57	2.180	0.029	2.182	0.029	2.183	0.058	99
38.20	80.40	52.60	5.49	1.856	0.029	1.899	0.032	1.946	0.074	95

31.90	36.10	57.50	6.78	2.077	0.028	2.083	0.029	2.089	0.060	99
51.90	52.90	144.60	3.55	1.532	0.017	1.537	0.024	1.545	0.057	99
100.90	96.60	386.50	2.31	1.221	0.012	1.215	0.020	1.203	0.053	101
182.80	135.60	355.80	6.50	2.068	0.018	2.046	0.023	2.024	0.043	102
19.30	30.20	32.90	6.45	2.049	0.041	2.039	0.038	2.029	0.084	100
67.50	87.40	251.20	2.31	1.199	0.024	1.214	0.018	1.242	0.056	96
27.70	69.20	141.90	1.39	0.880	0.019	0.885	0.018	0.898	0.072	98
68.30	50.10	169.80	4.50	1.715	0.032	1.731	0.020	1.751	0.049	97
31.20	23.30	60.40	6.85	2.045	0.042	2.092	0.024	2.139	0.054	95
76.80	38.00	164.90	6.45	2.009	0.037	2.039	0.021	2.069	0.046	97
10.30	43.50	17.30	5.55	1.880	0.065	1.908	0.045	1.939	0.119	96
68.20	49.40	208.00	3.43	1.503	0.028	1.512	0.019	1.524	0.051	98
33.40	39.50	94.20	3.61	1.535	0.032	1.551	0.023	1.574	0.063	97
15.60	16.90	27.40	7.73	2.160	0.047	2.200	0.040	2.237	0.080	96
26.30	16.80	50.90	7.28	2.140	0.039	2.147	0.032	2.153	0.062	99
34.30	32.00	64.20	7.28	2.136	0.035	2.146	0.029	2.155	0.055	99
42.30	51.30	84.60	6.31	2.003	0.033	2.020	0.028	2.039	0.054	98
38.60	39.50	78.30	6.81	2.060	0.034	2.087	0.028	2.114	0.053	97
90.70	109.60	140.90	7.65	2.202	0.031	2.191	0.024	2.181	0.042	100
108.00	63.10	213.40	7.25	2.198	0.032	2.142	0.025	2.089	0.045	105
30.60	25.00	82.90	4.04	1.630	0.028	1.643	0.029	1.659	0.064	98
100.10	75.30	188.50	7.41	2.195	0.031	2.162	0.024	2.130	0.042	103
61.90	50.90	117.30	7.07	2.118	0.032	2.120	0.025	2.121	0.046	99
73.30	50.40	154.50	6.46	2.015	0.029	2.041	0.024	2.068	0.044	97
45.90	56.30	199.90	1.95	1.092	0.018	1.098	0.024	1.108	0.070	98
69.80	*76.80*	*107.90*	*0.71*	*2.218*	*0.021*	*2.188*	*0.020*	*2.161*	*0.041*	*102*
7.90	*16.20*	*22.90*	*0.71*	*1.395*	*0.048*	*1.451*	*0.062*	*1.534*	*0.189*	*90*
16.80	*76.00*	*49.20*	*2.06*	*1.116*	*0.023*	*1.134*	*0.038*	*1.169*	*0.133*	*95*
23.20	*20.60*	*41.70*	*6.65*	*2.036*	*0.031*	*2.066*	*0.029*	*2.097*	*0.067*	*97*
131.30	*100.60*	*216.80*	*8.60*	*2.477*	*0.020*	*2.296*	*0.019*	*2.139*	*0.036*	*115*
3.50	*4.90*	*9.70*	*2.92*	*1.418*	*0.086*	*1.386*	*0.091*	*1.338*	*0.292*	*105*
8.30	*22.10*	*39.80*	*1.37*	*0.916*	*0.025*	*0.877*	*0.039*	*0.781*	*0.166*	*117*
59.30	*80.60*	*183.90*	*3.05*	*1.419*	*0.014*	*1.420*	*0.021*	*1.420*	*0.056*	*99*
19.30	*23.40*	*71.40*	*2.49*	*1.266*	*0.023*	*1.271*	*0.030*	*1.279*	*0.096*	*98*
12.20	*11.40*	*36.90*	*3.17*	*1.443*	*0.036*	*1.449*	*0.037*	*1.458*	*0.110*	*98*
108.00	*79.50*	*209.10*	*5.23*	*1.692*	*0.020*	*1.857*	*0.024*	*2.046*	*0.053*	*82*
11.40	*12.40*	*41.20*	*2.46*	*1.258*	*0.031*	*1.261*	*0.038*	*1.266*	*0.127*	*99*
11.90	*15.40*	*54.90*	*1.62*	*1.013*	*0.021*	*0.978*	*0.031*	*0.900*	*0.122*	*112*
55.10	*39.60*	*110.40*	*5.90*	*1.983*	*0.023*	*1.961*	*0.026*	*1.938*	*0.059*	*102*
70.70	*219.80*	*253.20*	*2.24*	*1.202*	*0.013*	*1.195*	*0.022*	*1.182*	*0.062*	*101*
63.70	*72.40*	*118.40*	*7.01*	*2.243*	*0.027*	*2.112*	*0.028*	*1.987*	*0.056*	*112*
8.40	*54.80*	*60.20*	*0.77*	*0.580*	*0.018*	*0.579*	*0.028*	*0.571*	*0.164*	*101*
72.70	*20.70*	*196.10*	*4.86*	*1.665*	*0.031*	*1.795*	*0.020*	*1.951*	*0.046*	*85*
7.20	*22.70*	*21.40*	*2.64*	*1.301*	*0.043*	*1.312*	*0.041*	*1.332*	*0.131*	*97*
77.20	*61.20*	*179.50*	*5.44*	*1.865*	*0.035*	*1.892*	*0.021*	*1.921*	*0.049*	*97*
81.90	*97.90*	*198.50*	*4.16*	*1.478*	*0.031*	*1.666*	*0.020*	*1.913*	*0.051*	*77*
23.40	*30.00*	*68.70*	*3.69*	*1.604*	*0.032*	*1.570*	*0.036*	*1.524*	*0.088*	*105*

CAPÍTULO 5 – CONSIDERAÇÕES FINAIS

5.1 Conclusões

5.1 Conclusões

As diferentes assinaturas litológicas e geocronológicas encontradas dentro da Antiforme Capané, sugerem que o contexto evolutivo do Complexo Porongos não está contido no clássico modelo de uma única bacia regional de idade Toniana.

Os flancos da Antiforme Capané mostram forte contribuição Ediacarana-Criogeniana, estando associados as unidades metavolcanoclásticas a oeste e metapelíticas a leste. Diferentemente, a zona axial mostra assinatura polimodal, cuja idade mais jovem é Toniana nas lentes de granada-estaurolita xisto e com picos principais acentuados no Riaciano para as rochas quartzíticas milonitizadas. Isto sugere que a zona axial é composta por terrenos exóticos aos flancos, de origem ainda especulativa, sendo imbricados tectonicamente durante o Ciclo Pan-Africano-Brasiliano. A zona axial é definida como sequencia Porongos I e os flancos como sequencia Porongos II, sendo que ambas sequencias representam partes de bacias de diferentes idades e contexto tectônico.

Na base da estratigrafia de todo o complexo estão ocorreriam os milonitos quartzíticos associados à Formação Santana e ao Gnaisse Encantadas da região do Domo de Santana da Boa Vista. A sequencia Porongos I seria depositada sobre estes, sendo representada pelas as lentes de granada-estaurolita xisto, as quais mostram grande afinidade com a sequencia supracrustal da Antiforme Serra dos Pedrosas. Estas unidades compartilham o mais alto grau metamórfico de todo o complexo, definido como fácies anfibolito inferior em contraste com o predominante fácies xisto verde para quase todo o complexo. Tanto na região de do Domo de Santana de Boa Vista e Antiforme Serra dos Pedrosas, aflora um dos únicos marcadores estratigráficos do Complexo Porongos, e também da sequencia Porongos I: vulcanismo riolítico datado em c. 780 a 800 Ma.

A sequencia Porongos II representa uma bacia de deposição sinorogênica, depositada na região frontal de grandes nappes em resposta aos processos colisionais durante o Ciclo Pan-Africano-Brasiliano. Seu inicio é sugerido congruente ao magmatismo que originou o Gnaisse Alcalino Capané (c. 600 Ma) e fechamento relacionado a um episódio metamórfico registrado na mesma unidade (c. 540 Ma).

Em relação as áreas fontes, especula-se que as poucas idades Arqueanas e predomino de contribuição Paleoproterozoica refletem erosão do próprio

embasamento representado como o Gnaisse Encantadas. Idades mesoproterozoicas constritas são Esteniano são interpretadas como provenientes do Cinturão Namaqua, refletindo uma assinatura africana. As idades neoproterozoicas representam contribuição do vulcanismo riolítico, magmatismo colisional e pós-colisional no arco Pelotas além do próprio episódio vulcanoclástico registrado no flanco oeste da Antiforme Capané. Nesse contexto o arco Pelotas serviu como uma barreira física aos sedimentos provenientes do continente Africano, impedindo uma contribuição melhor definida como no caso das unidades análogas pertencentes ao Bloco Éden no Uruguai.

REFERENCIAS

ALMEIDA, F. F. M. Geochronological division of the Precambrian of South America. revista brasileira de geociência. **Rev. Bras. Geo.**, 1971. v. 1, p. 13–21.

ALMEIDA, F. F. M.; HASUI, Y.; BRITO NEVES, B.B.; FUCK, R.A. Brazilian Structural Provinces: an introduction. **Earth-Sci. Rev.**, abr. 1981. v. 17, n. 1–2, p. 1–29. Disponível em: <http://linkinghub.elsevier.com/retrieve/pii/0012825281900039>.

ALMEIDA, R. P; SANTOS, M.G.M; FRAGOSO-CESAR, A.R.S; JANIKIAN, L.; FAMBRINI, L.G. Recurring extensional and strike-slip tectonics after the Neoproterozoic collisional events in the Southern Mantiqueira Province. **An. Acad. Bras. Ciênc.**, jun. 2012. v. 84, n. 2, p. 347–376. Disponível em: <http://www.scielo.br/scielo.php?script=sci_arttext&pid=S0001-37652012000200009&lng=en&nrm=iso&tlng=en>.

ANDERSEN, T. Detrital zircons as tracers of Sedimentary Provenance: limiting conditions from statistics and numerical simulation. **Chem. Geol.** mar. 2005. v. 216, n. 3–4, p. 249–270. Disponível em: <http://linkinghub.elsevier.com/retrieve/pii/S0009254104004796>.

ASSOCIATION, W. N. Radioactive Decay in Thorium and Uranium Series. **Naturally-ocurring radioactive materials (NORM)**, [S.l.], 2016. Disponível em: <http://www.world-nuclear.org/information-library/safety-and-security/radiation-and-health/naturally-occurring-radioactive-materials-norm.aspx>.

BABINSKI, M.; CHEMALE, F.; HARTMANN, L.A.; VAN SCHMUS, W.R.; SILVA, L.C. Juvenile accretion at 750–700 Ma in Southern Brazil. **Geology**, 1996. v. 24, n. 5, p. 439. Disponível em: <http://geology.gsapubs.org/cgi/doi/10.1130/0091-7613(1996)024%3C0439:JAAMIS%3E2.3.CO;2>.

_____ CHEMALE, F.; VAN SCHMUS, W.R.; HARTMANN, L.A.; SILVA, L.C. U-Pb and Sm-Nd Geochronology of the Neoproterozoic Granitic-Gneissic Dom Feliciano Belt, Southern Brazil. **J. South Am. Earth Sci.**, maio. 1997. v. 10, n. 3–4, p. 263–274. Disponível em: <http://linkinghub.elsevier.com/retrieve/pii/S0895981197000217>.

BARBEAU, D. L.; DAVIS, J.; MURRAY, K.; VALENCIA, V.; GEHRELS, G.; ZAHID, K.M.; GOMBOSI, D.J. Detrital-zircon Geochronology of the Metasedimentary rocks of north-western Graham Land. **Antarct. Sci.**, 10 fev. 2010. v. 22, n. 1, p. 65. Disponível em: <http://www.journals.cambridge.org/abstract_S095410200999054X>.

BASEI, M. A. S. **O Cinturão Dom Feliciano em Santa Catarina**. São Paulo: Universidade de São Paulo, 1985. Disponível em: <http://www.teses.usp.br/teses/disponiveis/44/44131/tde-27102015-160910/>.

_____ SIGA JR., O.; MASQUELIN, H.; HARARA, O.M.; REIS NETO, J.M.; PRECIOZZI, F. The Dom Feliciano Belt (Brazil-Uruguay) and its Foreland Domain, the Rio de la Plata Craton: framework, tectonic evolution and correlation with similar provinces of Southwestern Africa, tectonic evolution of South America. *In*: CORDANI,

U.G.; MILANI, E.J.; THOMAZ FILHO, A; CAMPOS, D.A.(Org.). **Tectonic evolution of South America**. Rio de Janeiro, Brazil: 31 International Geological Congress, 2000, p. 311–334.

_____ FRIMMEL, H.E.; NUTMAN, A.P.; PRECIOZZI, F.; JACOB, J. A connection between the Neoproterozoic Dom Feliciano (Brazil/Uruguay) and Gariep (Namibia/South Africa) Orogenic Belts – evidence from a reconnaissance provenance study. **Precambrian Res.**, 9 set. 2005. v. 139, n. 3–4, p. 195–221. Disponível em: <http://linkinghub.elsevier.com/retrieve/pii/S0301926805000914>.

_____ FRIMMEL, H.E.; NUTMAN, A.P.; PRECIOZZI, F. West Gondwana amalgamation based on Detrital zircon ages from Neoproterozoic Ribeira and Dom Feliciano Belts of South America and comparation with coeval sequencies from SW Africa. **J. Geol. Soc., London, Special Publications**, 2008. v. 294, n. 1, p. 239–256. Disponível em: <http://sp.lyellcollection.org/lookup/doi/10.1144/SP294.13>.

_____ CAMPOS NETO, M.C.; CASTRO, N.A.; NUTMAN, A.P.; WEMMER, K.; YAMAMOTO, M.T.; HUECK, M.; OSAKO, L.; SIGA JR., O.; PASSARELLI, C.R. Tectonic evolution of the Brusque Group, Dom Feliciano Belt, Santa Catarina, Southern Brazil. **J. South Am. Earth Sci.**,, dez. 2011. v. 32, n. 4, p. 324–350. Disponível em: <http://linkinghub.elsevier.com/retrieve/pii/S089598111100040X>.

BENISEK, A.; FINGER, F. Factors controlling the development of prism faces in granite zircons: a microprobe study. **Contrib. Mineral. Petrol.**, set. 1993. v. 114, n. 4, p. 441–451. Disponível em: <http://link.springer.com/10.1007/BF00321749>.

BERRY, R.; JENNER, G.A; MEFFRE, S; TUBRETT, M.N. A North American provenance for Neoproterozoic to Cambrian sandstones in Tasmania? **Earth Planet. Sci. Lett**, out. 2001. v. 192, n. 2, p. 207–222. Disponível em: <http://linkinghub.elsevier.com/retrieve/pii/S0012821X01004368>.

BOSSI, J.; CAMPAL, N.; CIVETTA, L.; DEMARCHI, G.; GIRARDI, V.A.V.; MAZZUCCHELLI, M.; NEGRINI, L.; RIVALENTI, G.; FRAGOSO-CESAR, A.R.S.; SINIGOI, S.; TEIXEIRA, W.; PICCIRILLO, E.M.; MOLESINI, M.. Early proterozoic dike swarms from western Uruguay: geochemistry, Sr-Nd isotopes and petrogenesis. **Chem. Geol.**, jun. 1993. v. 106, n. 3–4, p. 263–277. Disponível em: <http://linkinghub.elsevier.com/retrieve/pii/000925419390031D>.

_____; CAMPAL, N. Magmatismo y tectónica transcurrente durante el Paleozoico Inferior del Uruguay. **Paleozoico Inferior de Ibero-América**. Alicante: Universidad de Extremadura, 1992, p. 343–356.

_____; CINGOLANI, C. A. Extension and general evolution of the Rio de la Plata Craton. *In*: GAUCHER, C.; SIAL, A.N.; HALVERSON, G.P.; FRIMMEL, H.E. (Org.). **Neoproterozoic-Cambrian tectonics, global change and evolution: a focus on Southwestern Gondwana**. ed. Elsevier, 2009, p. 73–85.

_____; GAUCHER, C. The Cuchilla Dionisio Terrane, Uruguay: an allochthonous block accreted in the Cambrian to SW-Gondwana. **Gondwana Res.**, jul. 2004. v. 7, n.

3, p. 661–674. Disponível em: <http://linkinghub.elsevier.com/retrieve/pii/S1342937X05710546>.

_____; NAVARRO, R. Grupo Carapé: su reivindicación. **Revista Sociedad Uruguaya Geología**, 2001. v. 8, p. 2–12.

BRITO NEVES, B. B.; CAMPOS NETO, M. C.; FUCK, R. A. From Rodinia to Western Gondwana; an approach to the Brasiliano-Pan African Cycle and orogenic collage. **Episodes**, 1999. v. 22, p. 155–166.

_____; FUCK, R. A.; PIMENTEL, M. M. The Brasiliano Collage In South America: a review. **Braz. J. Geol.**, 1 nov. 2014. v. 44, n. 3, p. 493–518. Disponível em: <http://www.scielo.br/scielo.php?script=sci_arttext&pid=S2317-48892014000200493&lng=en&nrm=iso&tlng=en>.

CAMOZZATO, E.; SANDER, A.; RAMGRAB, G.E.; WILDNER, W. (1994). Milonitos alcalinos- peralcalinos da região de Candiota, RS. *In:* Congresso Brasileiro de Geologia, 38, 1994, Camboriú, **Anais...** Camboriú, Sociedade Brasileira de Geologia, p. 88–89.

_____; PHILIPP, R. P.; CHEMALE, F. (2013). Evolução tectônica e geocronologia U-Pb em zircão da terminação sul do Terreno Tijucas (RS, Brasil). *In:* Congreso Uruguayo de Geología, VII, 2013, Montevideo, p. 7.

CAMPAL, N.; SCHIPILOV, A. (1995). The Illescas bluish quartz rapakivi granite (Uruguay—South America): some geological features. *In:* Symposium Rapakivi Granites and Related Rocks, Belém, 1995. p. 18.

CARVALHO, P. F. Reconhecimento Geológico do Estado do Rio Grande do Sul. **Boletim do Instituto Geólogico e Mineralógico Do Brasil, vol. 66**. Rio de Janeiro, Brazil: Diretoria de estatística da produção, Seccão de publicidade, 1932, p. 72.

CAWOOD, P. A.; HAWKESWORTH, C. J.; DHUIME, B. Detrital zircon record and tectonic setting. **Geology**, 1 out. 2012. v. 40, n. 10, p. 875–878. Disponível em: <http://geology.gsapubs.org/cgi/doi/10.1130/G32945.1>.

CHEMALE, F. Evolução geológica do Escudo Sul-Riograndense. *In*: HOLZ, M.; ROS, L. F. DE (Org.). **Geologia do Rio Grande do Sul**. Porto Alegre: Universidade Federal do Rio Grande do Sul, 2000, p. 13–52.

_____ PHILIPP, R.P.; DUSSIN, I.A.; FORMOSO, M.L.L.; KAWASHITA, K.; BERTTOTTI, A.L. Lu–Hf and U–Pb age determination of Capivarita Anorthosite in the Dom Feliciano Belt, Brazil. **Precambrian Res.**, abr. 2011. v. 186, n. 1–4, p. 117–126. Disponível em: <http://linkinghub.elsevier.com/retrieve/pii/S0301926811000064>.

CHIGLINO, L.; GAUCHER, C.; SIAL, A.N.; BOSSI, J.; FERREIRA, V.P.; PIMENTEL, M.M. Chemostratigraphy of Mesoproterozoic and Neoproterozoic carbonates of the Nico Pérez Terrane, Río de la Plata Craton, Uruguay. **Precambrian Res.**, out. 2010.

v. 182, n. 4, p. 313–336. Disponível em: <http://linkinghub.elsevier.com/retrieve/pii/S030192681000135X>.

CLIFFORD, T. N. The structural framework of Africa. *In*: CLIFFORD, T. N.; GASS, I. G. (Org.). **African Magmatism and Tectonics**. Edinburgh: Oliver and Boyd, 1970, p. 1–26.

CORDANI, U. G.; SATO, K.; TEIXEIRA, W.; TASSINARI, C.C.G.. Crustal evolution of the South American Platform. *In*: CORDANI, U. G.; MILANI, E.J.; THOMAZ FILHO, A.; CAMPOS, D.A.. (Org.). **Tectonic evolution of South America**. Rio de Janeiro, Brazil: 31 International Geological Congress, 2000, p. 19–40.

_____; HALPERN, M.; BERENCHOLC, M. Comentários sobre as determinações geocronológicas da Folha de Porto Alegre. **Carta geológica do Brasil ao milionésimo**. Brasília: DNPM, 1974.

CORFU, F. Atlas of zircon textures. **Rev. Mineral. Geochem.**, 1 jan. 2003. v. 53, n. 1, p. 469–500. Disponível em: <http://rimg.geoscienceworld.org/cgi/doi/10.2113/0530469>.

DALLA SALDA, L.; BOSSI, J.; CINGOLANI, C. A. The Río De La Plata Cratonic region of Southwestern Gondwanaland. **Episodes**, 1988. v. 11, p. 263–269.

DALZIEL, I. W. D. Overview: Neoproterozoic-Paleozoic geography and tectonics: review, hypothesis, environmental speculation. **Geol. Soc. Am. Bull.**, jan. 1997. v. 109, n. 1, p. 16–42. Disponível em: <http://gsabulletin.gsapubs.org/cgi/doi/10.1130/0016-7606(1997)109%3C0016:ONPGAT%3E2.3.CO;2>.

DEER, R. A.; ZUSSMAN, J.; HOWIE, W. A. **An introduction to the rock-forming minerals**. Mineralogical Society of Great Britain and Ireland, 2013.

DEGRAAFF-SURPLESS, K.; GRAHAM, S.A.; WOODEN, J.L.; MCWILLIAMS, M.O. Detrital zircon provenance analysis of the Great Valley Group, California: evolution of an arc-forearc system. **Geol. Soc. Am. Bull.**, maio. 2003. v. 115, p. 639–639. Disponível em: <http://gsabulletin.gsapubs.org/cgi/doi/10.1130/0016-7606(2003)115%3C0639:DZPAOT%3E2.0.CO;2>.

EGLINGTON, B. M. Evolution of the Namaqua-Natal Belt, Southern Africa – a geochronological and isotope geochemical review. **J. Afr. Earth Sci.**, set. 2006. v. 46, n. 1–2, p. 93–111. Disponível em: <http://linkinghub.elsevier.com/retrieve/pii/S1464343X06001348>.

FAMBRINI, G. L.; FRAGOSO-CESAR, A. R. S. Análise estratigráfica do Grupo Santa Barbára (Ediacarano) na sub-bacia Camaquã Oriental, RS. **Rev. Bras. Geo.**, 2006. v. 36, n. 4, p. 663–678. Disponível em: <http://sbg.sitepessoal.com/bjg/2006/n.4/9.pdf>.

FAURE, G.; MENSING, T. M. **Isotopes: principles and applications**. 3. ed. Wiley, 2004.

FERNANDES, L. A. D.; TOMMASI, A.; PORCHER, C.C.; KOESTER, E.; KRAMER, G.; SCHERER, C.M.S.; MENEGAT, R. Granitóides brasilianos precoces do Cinturão Dom Feliciano. caracterização geoquímica e discussão estratigráfica. 1992b: **Pesquisas em Geociências**, 1992. v. 19, n. 2, p. 195–215.

_____ Menegat, R.; Costa, A.F.U.; Koester, E.; Porcher, C.C.; Tommasi, A.; Kramer, G.; Ramgrab, G.E.; Camozzato, E. Evolução tectônica do Cinturão Dom Feliciano no Escudo Sul-Rio-Grandense: parte II- uma contribuição a partir do registro geofísico. **Rev. Bras. Geo.**, 1995. v. 25, p. 351–374.

_____; TOMMASI, A.; PORCHER, C. C. Deformation patterns in the Southern Brazilian branch of the Dom Feliciano Belt: a reappraisal. 1992A: **J. South Am. Earth Sci.**, jan. 1992. v. 5, n. 1, p. 77–96. Disponível em: <http://linkinghub.elsevier.com/retrieve/pii/0895981192900613>.

FERNÁNDEZ-SUÁREZ, J.; GUTIÉRREZ-ALONSO, G.; PASTOR-GALÁN, D.; HOFMANN, M.; MURPHY, J. B.; LINNEMANN, U. The Ediacaran–Early Cambrian detrital zircon record of NW Iberia: possible sources and paleogeographic constraints. **Int. J. Earth Sci.**, 16 jul. 2014. v. 103, n. 5, p. 1335–1357. Disponível em: <http://link.springer.com/10.1007/s00531-013-0923-3>.

FRAGOSO-CESAR, A. R. S. (1980) O cráton do Rio De La Plata e o Cinturão Dom Feliciano no escudo Uruguaio-Sul-Riograndense. *In*: Congresso Brasileiro de Geologia, 31, Camboriú, **Anais...** Camboriú: SBG, 1980. p. 2879–2892.

FRANTZ, J. C.; BOTELHO, N. F. Neoproterozoic granitic magmatism and evolution of the Eastern Dom Feliciano Belt in Southernmost Brazil : a tectonic model. **Gondwana Res.**, 2000. v. 3, n. I, p. 7–19.

_____; NARDI, L. V. S. Litoquímica e evolução de granitóides cálcio-alcalinos da região leste do Escudo Sul-Rio-Grandense. **Pesquisas em Geociências**, 1992. v. 19, n. 1, p. 13–25.

FRIMMEL, H. E.; BASEI, M.A.S.; CORREA, V.X.; MBANGULA, N. A new lithostratigraphic subdivision and geodynamic model for the Pan-African Western Saldania Belt, South Africa. **Precambrian Res.**, jul. 2013. v. 231, p. 218–235. Disponível em: <http://linkinghub.elsevier.com/retrieve/pii/S0301926813001009>.

_____; HARTNADY, C. J. H.; KOLLER, F. Geochemistry and tectonic setting of magmatic units in the Pan-African Gariep Belt, Namibia. **Chem. Geol.**, ago. 1996. v. 130, n. 1–2, p. 101–121. Disponível em: <http://linkinghub.elsevier.com/retrieve/pii/0009254195001883>.

_____; KLÖTZLI, U. S.; SIEGFRIED, P. R. New Pb-Pb single zircon age constraints on the timing of Neoproterozoic glaciation and continental break-up in Namibia. **J. Geol.**, jul. 1996. v. 104, n. 4, p. 459–469. Disponível em: <http://www.journals.uchicago.edu/doi/10.1086/629839>.

GAUCHER, C.; BLANCO, G.; CHIGLINO, L.; POIRÉ, D.G.; GERMS, G.J.B. Acritarchs of Las Ventanas Formation (Ediacaran, Uruguay): implications for the

timing of coeval rifting and glacial events in Western Gondwana. **Gondwana Res.**, jul. 2008. v. 13, n. 4, p. 488–501. Disponível em: <http://linkinghub.elsevier.com/retrieve/pii/S1342937X07000925>.

_____ Frei, R.; Chemale, F.; Frei, D.; Bossi, J.; Martínez, G.; Chiglino, L.; Cernuschi, F. Mesoproterozoic evolution of the Río De La Plata Craton in Uruguay: at the heart of Rodinia? **Int. J. Earth Sci.**, 11 abr. 2011. v. 100, n. 2–3, p. 273–288. Disponível em: <http://link.springer.com/10.1007/s00531-010-0562-x>.

GEHRELS, G. E. Detrital zircon U-Pb geochronology applied to tectonics. **Annu. Rev. Earth Planet. Sci.**, 30 maio. 2014. v. 42, n. 1, p. 127–149. Disponível em: <http://www.annualreviews.org/doi/10.1146/annurev-earth-050212-124012>.

GERMS, G. J. B. Implications of sedimentary facies and depositional environmental analysis of the Nama Group in South West Africa/Namibia. **Special Publication – Geol. Soc. S. Africa**, 1983. v. 11, p. 89–114.

GOOGLE MAPS. [Região sul do Brasil e Uruguai]. **Google Maps**, 2016. Disponível em: <https://www.google.com/maps>.

GREGORY, T. R.; BITENCOURT, M.F.; NARDI, L.V.S.; FLORISBAL, L.M.; CHEMALE, F. Geochronological data from TTG-type rock associations of the Arroio dos Ratos Complex and implications for crustal evolution of Southernmost Brazil in Paleoproterozoic times. **J. South Am. Earth Sci.**, jan. 2015. v. 57, p. 49–60. Disponível em: <http://linkinghub.elsevier.com/retrieve/pii/S0895981114001631>.

_____ BITENCOURT, M.F.; NARDI, L.V.S.; FLORISBAL, L.M.. Petrogenesis of metamorphosed paleoproterozoic, arc-related tonalites, granodiorites and coeval basic to intermediate rocks from southernmost Brazil, based on elemental and isotope geochemistry. **Lithos**, Agosto. 2016. Disponível em: <http://linkinghub.elsevier.com/retrieve/pii/S0024493716302237>.

GRUBER, L.; PORCHER, C.C.; LENZ, C.; FERNANDES, L.A.D. Proveniência de metassedimentos das sequências Arroio Areião, Cerro Cambará e quartzo milonitos no Complexo Metamórfico Porongos, Santana da Boa Vista, RS. **Pesquisas em geociências**, 2011. v. 38, n. 3, p. 205–223. Disponível em: <http://www.ufrgs.br/igeo/pesquisas/3803/1-3803.pdf>.

GUILLONG, M.; HEINRICH, C. A. Sensitivity enhancement in laser ablation ICP-MS using small amounts of hydrogen in the carrier gas. **J. Anal. At. Spectrom.**, 2007. v. 22, n. 12, p. 1488. Disponível em: <http://xlink.rsc.org/?DOI=b709489b>.

GÜNTHER, D.; HEINRICH, C. A. Comparison of the ablation behaviour of 266 nm Nd:Yag and 193 nm ArF excimer lasers for LA-ICP-MS analysis. **J. anal. at. Spectrom.**, 1999. v. 14, n. 9, p. 1369–1374. Disponível em: <http://xlink.rsc.org/?DOI=A901649J>.

HALLS, H. C.; CAMPAL, N.; DAVIS, D.W.; BOSSI, J.. Magnetic studies and U–Pb Geochronology of the Uruguayan dyke swarm, Rio de la Plata Craton, Uruguay:

paleomagnetic and economic implications. **J. South Am. Earth Sci.**, set. 2001. v. 14, n. 4, p. 349–361. Disponível em: <http://linkinghub.elsevier.com/retrieve/pii/S0895981101000311>.

HARLEY, S. L.; KELLY, N. M. Zircon tiny but timely. **Elements**, 1 fev. 2007. v. 3, n. 1, p. 13–18. Disponível em: <http://elements.geoscienceworld.org/cgi/doi/10.2113/gselements.3.1.13>.

HARTMANN, L. A.; LEITE, J.A.D.; SILVA, L.C.; REMUS, M.V.D.; MCNAUGHTON, N.J.; GROVES, D.I.; FLETCHER, I.R.; SANTOS, J.O.S.; VASCONCELLOS, M.A.Z.. Advances in SHRIMP Geochronology and their impact on understanding the tectonic and metallogenic evolution of Southern Brazil. 2000A: **Austral. J. Earth Sci.**, 8 out. 2000. v. 47, n. 5, p. 829–844. Disponível em: <http://www.tandfonline.com/doi/abs/10.1046/j.1440-0952.2000.00815.x>.

_____ CAMPAL, N.; SANTOS, J.O.S.; MCNAUGHTON, N.J.; BOSSI, J.; SCHIPILOV, A.; LAFON, J.M.. Archean crust in the Rio de la Plata Craton, Uruguay — SHRIMP U–Pb zircon reconnaissance Geochronology. **J. South Am. Earth Sci.**, nov. 2001. v. 14, n. 6, p. 557–570. Disponível em: <http://linkinghub.elsevier.com/retrieve/pii/S0895981101000554>.

_____ SANTOS, J.O.S.; CINGOLANI, C.; MCNAUGHTON, N.J. Two Paleoproterozoic orogenies in the evolution of the Tandilia Belt, Buenos Aires, as evidenced by zircon U-Pb SHRIMP Geochronology. **Int. Geol. Rev.**, jun. 2002. v. 44, n. 6, p. 528–543. Disponível em: <http://www.tandfonline.com/doi/abs/10.2747/0020-6814.44.6.528>.

_____ SANTOS, J.O.S.; LEITE, J.A.D.; PORCHER, C.C.; MCNAUGHTON, N.J. Metamorphic evolution and U-Pb zircon SHRIMP geochronology of the Belizário Ultramafic Amphibolite, Encantadas Complex, Southernmost Brazil. **An. Acad. Bras. Ciênc.**, set. 2003. v. 75, n. 3. Disponível em: <http://www.scielo.br/scielo.php?script=sci_arttext&pid=S0001-37652003000300010&lng=en&nrm=iso&tlng=en>.

_____ PHILIPP, R.P.; LIU, D.; WAN, Y; WANG, Y.; SANTOS, J.O.S.; VASCONCELLOS, M.A.Z.. Paleoproterozoic magmatic provenance of detrital zircons, Porongos Complex quartzites, Southern Brazilian Shield. **Int. Geol. Rev.**, fev. 2004. v. 46, n. 2, p. 127–157. Disponível em: <http://www.tandfonline.com/doi/abs/10.2747/0020-6814.46.2.127>.

_____ PHILIPP, R.P.; SANTOS, J.O.S.; MCNAUGHTON, N.J. Time frame of 753–680 Ma juvenile accretion during the São Gabriel Orogeny, Southern Brazilian Shield. **Gondwana Res.**, jan. 2011. v. 19, n. 1, p. 84–99. Disponível em: <http://linkinghub.elsevier.com/retrieve/pii/S1342937X10000900>.

_____; CHEMALE, F.; PHILIPP, R. P. Evolução geotectônica do Rio Grande do Sul no Pré-Cambriano. *In*: IANNUZZI, R.; FRANTZ, J. (Org.). **50 anos de Geologia, Instituto De Geociências, Contribuições**. Porto Alegre: Comunicação e Identidade, 2007, p. 97–123.

HASUI, Y.; CARNEIRO, A. W.; COIMBRA, C. D. R. The Ribeira Folded Belt. **Rev. Bras. Geo.**, 1975. v. 5, p. 257–266.

HOLMES, A. The association of Lead with Uranium in rock-minerals, and its application to the measurement of Geological Time. **Proceedings of the Royal Society A: Mathematical, Physical And Engineering Sciences**, 9 jun. 1911. v. 85, n. 578, p. 248–256. Disponível em: <http://rspa.royalsocietypublishing.org/cgi/doi/10.1098/rspa.1911.0036>.

HOSKIN, P. W. O. Patterns of chaos: fractal statistics and the oscillatory chemistry of zircon. **Geochim. Cosmochim. Acta**, jun. 2000. v. 64, n. 11, p. 1905–1923. Disponível em: <http://linkinghub.elsevier.com/retrieve/pii/S0016703700003306>.

_____; SCHALTEGGER, U. The composition of zircon and igneous and metamorphic petrogenesis. **Rev. Mineral. Geochem.**, 1 jan. 2003. v. 53, n. 1, p. 27–62. Disponível em: <http://rimg.geoscienceworld.org/cgi/doi/10.2113/0530027>.

IACUMIN, M.; PICCIRILLO, E.M.; GIRARDI, V.A.V.; TEIXEIRA, W.; BELLIENI, G.; ECHEVESTE, H.; FERNANDES, R.; PINESE, J.P.P.; RIBOT, A. Early proterozoic calc-alkaline and middle Proterozoic tholeiitic dyke swarms from central-eastern Argentina: petrology, geochemistry, Sr-Nd isotopes and tectonic implications. **J. Petrol.**, 1 nov. 2001. v. 42, n. 11, p. 2109–2143. Disponível em: <http://petrology.oxfordjournals.org/cgi/doi/10.1093/petrology/42.11.2109>.

JACKSON, S. E.; PEARSON, N.J.; GRIFFIN, W.L.; BELOUSOVA, E.A.. The application of laser ablation-inductively coupled plasma-mass spectrometry to in situ U–Pb zircon Geochronology. **Chem. Geol.**, nov. 2004. v. 211, n. 1–2, p. 47–69. Disponível em: <http://linkinghub.elsevier.com/retrieve/pii/S0009254104002074>.

JANIKIAN, L.; ALMEIDA, R.P.; FRAGOSO-CESAR, A.R.S.; MARTINS, V.T.S.; DANTAS, E.L.; TOHVER, E.; MCREATH, I.; D'AGRELLA-FILHO, M.S. Ages (U–Pb SHRIMP and La-ICP-MS) and stratigraphic evolution of the Neoproterozoic volcano-sedimentary successions from the extensional Camaquã Basin, Southern Brazil. **Gondwana Res.**, mar. 2012. v. 21, n. 2–3, p. 466–482. Disponível em: <http://linkinghub.elsevier.com/retrieve/pii/S1342937X11001304>.

JOST, H. (1981). **Geology and metallogeny of the Santana Da Boa Vista region, Southern Brazil**. 193f. Tese de Doutorado, University of Georgia.

_____; BITENCOURT, M. F. Estratigrafia a e tectônica de uma fração da faixa de dobramentos tijucas no rio grande do sul. **Acta Geol. Leop.**, 1980. v. 11, n. 7, p. 27–59.

KENNEDY, W. Q. **The structural differentiation of Africa in the Pan African (± 500 Ma) tectonic episode**. Anual Report of the Institute of African Geology. [S.l.], 1964.

KOESTER, E., PORCHER, C.C.; PIMENTEL, M.M.; FERNANDES, L.A.D.; VIGNOL-LELARGE, M.L.; OLIVEIRA, L.D.; RAMOS, R.C. Further evidence of 777 Ma subduction-related continental arc magmatism in Eastern Dom Feliciano Belt,

Southern Brazil: The Chácara Das Pedras Orthogneiss. **J. South Am. Earth Sci.**, jul. 2016. v. 68, p. 155–166. Disponível em: <http://linkinghub.elsevier.com/retrieve/pii/S0895981115301012>.

KOHLRAUSCH, C. B. (2013). **Determinação de idades U-Pb em zircão por LA-ICP-MS nas rochas metavulcânicas da Antiforme Capané, Complexo Metamórfico Porongos**. Porto Alegre, 61f. Trabalho de Conclusão de Curso, Instituto de Geociências, Universidade Federal do Rio Grande do Sul.

KRÖNER, A.; STERN, R. J. Africa | Pan-African Orogeny. *In*: SELLEY, R. C.; COCKS, R.; PLIMER, I. (Org.). **Encyclopedia of Geology**. 1st Edition ed. Elsevier, 2005, p. 1–12.

KUKLA, P. A.; STANISTREET, I. G. Record of the Damaran Khomas Hochland accretionary prism in Central Namibia: refutation of an “ensialic” origin of a Late Proterozoic Orogenic Belt. **Geology**, 1991. v. 19, n. 5, p. 473. Disponível em: <http://geology.gsapubs.org/cgi/doi/10.1130/0091-7613(1991)019%3C0473:ROTDKH%3E2.3.CO;2>.

LAFON, J. M.; HARTMANN, L. A.; AZAMBUJA, J. C. Datação Rb-Sr de Gnaisses Alcalinos Do Arroio Capané, RS. Natal: SBG, 1990. p. 431.

LEITE, J. A. D.; HARTMANN, L.A.; MCNAUGHTON, N.J.; CHEMALE, F.. SHRIMP U/Pb zircon geochronology of Neoproterozoic juvenile and crustal-reworked terranes in Southernmost Brazil. **Int. Geol. Rev.**, 6 ago. 1998. v. 40, n. 8, p. 688–705. Disponível em: <http://www.tandfonline.com/doi/abs/10.1080/00206819809465232>.

_____ HARTMANN, L.A.; FERNANDES, L.A.D.; MCNAUGHTON, N.J.; SOLIANI JR., E.; KOESTER, E.; SANTOS, J.O.S. VASCONCELLOS, M.A.Z. Zircon U–Pb SHRIMP dating of gneissic basement of the Dom Feliciano Belt, Southernmost Brazil. **J. South Am. Earth Sci.**, dez. 2000. v. 13, n. 8, p. 739–750. Disponível em: <http://linkinghub.elsevier.com/retrieve/pii/S0895981100000584>.

LENA, L. O. F.; PIMENTEL, M.M.; PHILIPP, R.P.; ARMSTRONG, R.A.; SATO, K. The evolution of the Neoproterozoic São Gabriel Juvenile Terrane, Southern Brazil based on high spatial resolution U-Pb ages and δ18o data from detrital zircons. **Precambrian Res.**, jul. 2014. v. 247, p. 126–138. Disponível em: <http://linkinghub.elsevier.com/retrieve/pii/S0301926814000849>.

LENZ, C. (2010) **Evolução metamórfica dos metapelítos da antiforme serra dos pedrosas: condições e idades do metamorfismo**. Porto Alegre, 150f. Tese de Doutorado. Programa de Pós-Graduação em Geociências, Universidade do Rio Grande do Sul.

_____ FERNANDES, L.A.D.; MCNAUGHTON, N.J.; PORCHER, C.C.; MASQUELIN, H. U–Pb SHRIMP ages for the Cerro Bori Orthogneisses, Dom Feliciano Belt in Uruguay: evidences of a ~800 Ma magmatic and ~650 Ma metamorphic event. **Precambrian Res.**, mar. 2011. v. 185, n. 3–4, p. 149–163. Disponível em: <http://linkinghub.elsevier.com/retrieve/pii/S0301926811000088>.

LUDWIG, K. R. **Isoplot 3.6**. Berkeley Geochronology Center. Disponível em: <http://www.bgc.org/isoplot_etc/isoplot.html>.

LUSA, M.; PHILIPP, R. P.; NARDI, L. V. S. Geoquímica e petrologia dos metagranitos do Complexo Encantadas, Santana Da Boa Vista, (RS): a evolução de uma margem continental ativa no Paleoproterozoico. **Rev. Bras. Geo.**, 2010. v. 40, n. 2, p. 151–166.

MACHADO, R.; CÉSAR, A. R. S. F.; FACCINI, U. F. (1987) O Domo De Santana (RS): domo gnáissico manteado ou figura de interferência tipo domo e bacia? *In:* Simpóio Sul-Brasileiro de Geologia, 3, 1987, Curitiba, **Anais...** Curitiba, SBG, p. 167–182.

MARQUES, J. C. (1996) **Petrologia e metalogênese da seqüência metaultramáfica da Antiforme Capané, Suíte Metamórfica Porongos, Cachoeira Do Sul-RS**. Porto Alegre, 196f. Dissertação de mestrado, Programa de Pós-Graduação em Geociências, Universidade Federal do Rio Grande do Sul, 1996.

_____ JOST, H.; ROISENBERG, A.; FRANTZ, J.C. Rochas metassedimentares, geologia estrutural e metamorfismo da Suíte Metamórfica Porongos na área da Antiforme Capané, Cachoeira do Sul – RS. 1998B: **Rev. Bras. Geo.**, 1998a. v. 28, n. 4, p. 467–472. Disponível em: <http://sbg.sitepessoal.com/bjg/1998/n.4/7.pdf>.

_____ JOST, H.; ROISENBERG, A.; FRANTZ, J.C. Eventos ígneos da suíte metamórfica Porongos na área da Antiforme Capané, Cachoeira Do Sul - RS. 1998A: **Rev. Bras. Geo.**, 1998b. v. 28, n. 4, p. 419–430. Disponível em: <http://sbg.sitepessoal.com/bjg/1998/n.4/2.pdf>.

_____ JOST, H.; ROISENBERG, A.; FRANTZ, J.C; TEIXEIRA, R.S. Geologia e geoquímica das rochas metaultramáficas da Antiforme Capané, Suíte Metamórfica Porongos, RS. 2003A: **Rev. Bras. Geo.**, 2003. v. 33, n. 1, p. 83–94. Disponível em: <http://sbg.sitepessoal.com/bjg/2003/1Suppl1/9.pdf>.

MARTIL, M. M. D.; BITENCOURT, M.F.; NARDI, L.V.S.; KOESTER, E.; PIMENTEL, M.M.. Pre-collisional, Tonian (ca. 790 Ma) continental arc magmatism in Southern Mantiqueira Province, Brazil: geochemical and isotopic constraints from the Várzea do Capivarita Complex. **Lithos**, mar. 2017. v. 274–275, p. 39–52. Disponível em: <http://linkinghub.elsevier.com/retrieve/pii/S0024493716304078>.

MÖLLER, A.; O'BRIEN, P.J.; KENNEDY, A.; KRÖNER, A. (2013) The use and abuse of Th-U ratios in the interpretation of zircon. *In:* EGS-AGU-EUG Joint Assembly, 2013, Nice, France, 2003. p. 12113.

OLIVEIRA, C. H. E.; CHEMALE, F.; JELINEK, A.R.; BICCA, M.M.; PHILIPP, R.P.. U–Pb and Lu–Hf isotopes applied to the evolution of the late to post-orogenic transtensional basins of the Dom Feliciano Belt, Brazil. **Precambrian Res.**, jun. 2014. v. 246, p. 240–255. Disponível em: <http://linkinghub.elsevier.com/retrieve/pii/S0301926814000825>.

OYHANTÇABAL, P.; SÁNCHEZ-BETTUCCI, L.; PECOITS, E.; AUBET, N.R.; PEEL, E.; PRECIOZZI, F.; BASEI, M.A.S. (2005). Nueva propuesta estratigrafica para las supracorticales del Cinturón Dom Feliciano (Proterozoico, Uruguay). *In:* Congreso Latinoamericano de Geología, XII, Quito, Peru, 2005.

_____ SIEGESMUND, S.; WEMMER, K.; PRESNYAKOV, S.; LAYER, P. Geochronological constraints on the evolution of the southern Dom Feliciano Belt (Uruguay). **J. Geol. Soc.,** 1 dez. 2009. v. 166, n. 6, p. 1075–1084. Disponível em: <http://jgs.lyellcollection.org/cgi/doi/10.1144/0016-76492008-122>.

PAIM, P. S. .; CHEMALE, F.; LOPES, R. C. A bacia do Camaquã. *In*: HOLTZ, M.; ROS, L. F. DE (Org.). **Geologia do Rio Grande do Sul**. Porto Alegre, Brazil: Universidade Federal do Rio Grande do Sul, 2000, p. 231–274.

PASSARELLI, C. R.; BASEI, M.A.S.; SIGA JR., O.; REATH, I.M.; CAMPOS NETO, M.C. Deformation and geochronology of syntectonic granitoids emplaced in the Major Gercino Shear Zone, southeastern South America. **Gondwana Res.**, maio. 2010. v. 17, n. 4, p. 688–703. Disponível em: <http://linkinghub.elsevier.com/retrieve/pii/S1342937X09001944>.

PAZOS, P. J.; SÁNCHEZ-BETTUCCI, L.; TOFALO, O. R. The record of the Varanger Glaciation at the Río de la Plata Craton, Vendian-Cambrian of Uruguay. **Gondwana Res.**, jan. 2003. v. 6, n. 1, p. 65–77. Disponível em: <http://linkinghub.elsevier.com/retrieve/pii/S1342937X05706444>.

PECOITS, E. Sedimentología y consideraciones estratigraficas de la formacion las ventanas en su area tipo, Departamento de Maldonado. **Revista Sociedad Uruguaya Geología**, 2003. v. 1, n. Special Issue, p. 124–140.

_____ AUBET, N.R.; OYHANTÇABAL, P.; SÁNCHEZ-BETTUCCI, L. Estratigrafía de sucesiones sedimentarias y volcanosedimentarias neoproterozoicas del Uruguay. **Revista Sociedad Uruguaya Geología**, 2004. v. 11, p. 18–27.

_____ AUBET, N.R.; HEAMAN, L.M.; PHILIPPOT, P.; ROSIÈRE, C.A.; VEROSLAVSKY, G.; KONHAUSER, K.O. U-Pb detrital zircon ages from some Neoproterozoic successions of Uruguay: provenance, stratigraphy and tectonic evolution. **J. South Am. Earth Sci.**, nov. 2016. v. 71, p. 108–130. Disponível em: <http://linkinghub.elsevier.com/retrieve/pii/S0895981116301067>.

PERTILLE, J.; HARTMANN, L.A.; PHILIPP, R.P.; PETRY, T.S.; LANA, C.C.. Origin of the Ediacaran Porongos Group, Dom Feliciano Belt, southern Brazilian Shield, with emphasis on whole rock and detrital zircon geochemistry and U–Pb, Lu–Hf isotopes. 2015b: **J. South Am. Earth Sci.**, dez. 2015. v. 64, p. 69–93. Disponível em: <http://linkinghub.elsevier.com/retrieve/pii/S0895981115300535>.

_____ HARTMANN, L.A.; SANTOS, J. O. S.; MCNAUGHTON, N. J.; ARMSTRONG, R.. Reconstructing the Cryogenian–Ediacaran evolution of the Porongos Fold and thrust belt, Southern Brasiliano Orogen, based on zircon U–Pb–Hf–O isotopes. **Int. Geol. Rev.**, 2017. v. 6814, n. February, p. 1–29. Disponível em: <https://www.tandfonline.com/doi/full/10.1080/00206814.2017.1285257>.

_____; HARTMANN, L. A.; PHILIPP, R. P. Zircon u–Pb age constraints on the paleoproterozoic sedimentary basement of the Ediacaran Porongos Group, Sul-Riograndense Shield, southern Brazil. 2015a: **J. South Am. Earth Sci.**, nov. 2015. v. 63, p. 334–345. Disponível em: <http://linkinghub.elsevier.com/retrieve/pii/S0895981115300420>.

PHILIPP, R. P. (1998). **A evolução geológica e tectônica do batólito pelotas no rio grande do sul**. São Paulo, 255f. Tese de Doutorado, Universidade de São Paulo. Disponível em: <http://www.teses.usp.br/teses/disponiveis/44/44134/tde-05112014-155445/>.

_____; LUSA, M.; NARDI, L. V. S. Petrology of dioritic, tonalitic and trondhjemitic gneisses from Encantadas Complex, Santana da Boa Vista, Southernmost Brazil: paleoproterozoic continental-arc magmatism. **An. Acad. Bras. Ciênc.**, dez. 2008. v. 80, n. 4, p. 735–748. Disponível em: <http://www.scielo.br/scielo.php?script=sci_arttext&pid=S0001-37652008000400013&lng=en&nrm=iso&tlng=en>.

_____; MACHADO, R. The late Neoproterozoic granitoid magmatism of the Pelotas Batholith, southern Brazil. **J. South Am. Earth Sci.**, set. 2005. v. 19, n. 4, p. 461–478. Disponível em: <http://linkinghub.elsevier.com/retrieve/pii/S0895981105001069>.

PORADA, H. The Damara-Ribeira Orogen of the Pan-African-Brasiliano cycle in Namibia (Southwest Africa) and Brazil as interpreted in terms of continental collision. **Tectonophysics**, ago. 1979. v. 57, n. 2–4, p. 237–265. Disponível em: <http://linkinghub.elsevier.com/retrieve/pii/0040195179901501>.

_____. Pan-African rifting and orogenesis in southern to equatorial Africa and eastern Brazil. **Precambrian Res.**, ago. 1989. v. 44, n. 2, p. 103–136. Disponível em: <http://linkinghub.elsevier.com/retrieve/pii/0301926889900788>.

PORCHER, C. C.; MCNAUGHTON, N.J.; LEITE, J.A.D.; HARTMANN, L.A.; FERNANDES, L.A.D. (1999). Idade SHRIMP em zircão: vulcanismo ácido do complexo metamórfico Porongos. *In:* Simpósio de Vulcânismo e Ambientes Associados, I, 1999, Gramado, **Anais...**, Gramado: SBG, p. 110.

_____; FERNANDES, L. A. D. Relações embasamento-cobertura na porção Ocidental do Cinturão Dom Feliciano: um esboço estrutural. **Pesquisas em Geociências**, 1990. v. 17, p. 72–84.

RAMOS, V. A. Late Proterozoic–early Paleozoic of South America – a collisional history. **Episodes**, 1988. v. 11, p. 168–174.

RAPELA, C. W., FANNING, C.M.; CASQUET, C.; PANKHURST, R.J.; SPALLETTI, L.; POIRÉ, D.G.; BALDO, E.G.. The Rio de la Plata Craton and the adjoining Pan-African/Brasiliano terranes: their origins and incorporation into south-west Gondwana. **Gondwana Res.**, nov. 2011. v. 20, n. 4, p. 673–690. Disponível em: <http://linkinghub.elsevier.com/retrieve/pii/S1342937X11001407>.

REID, D. L. Sm-Nd age and REE geochemistry of Proterozoic arc-related igneous rocks in the Richtersveld Subprovince, Namaqua Mobile Belt, Southern Africa. **J. Afr. Earth Sci.**, maio. 1997. v. 24, n. 4, p. 621–633. Disponível em: <http://linkinghub.elsevier.com/retrieve/pii/S0899536297000845>.

REMUS, M. V. D., TEDESCO, M.A.; PHILIPP, R.P.; FACCINI, U.F. (1987) Evolução estrutural da unidade Porongos a sul do Rio Camaquã, RS. *In*: Simpósio Sul-Brasileiro de Geologia, 1987, Curitiba, **Anais...**, Curitiba: SBG, p. 223–244.

_____ MCNAUGHTON, N.J.; HARTMANN, L.A.; GROVES, D.I. (1996). SHRIMP U/Pb zircon dating at 2448 Ma of the oldest igneous rock in southern Brazil: identification of the westernmost border of Dom Feliciano Belt. *In*: Simpósio dos Terrenos Arqueanos da Plataforma da América do Sul, 1996, Brasília, **Anais...,** Brasília, p. 67–70.

_____; HARTMANN, L. A.; RIBEIRO, M. Nota sobre a geologia dos metamorfitos de pressão intermediária e granitóides associados da região de pinheiro machado/RS. **Acta Geol. Leop.**, 1991. v. 34, p. 175–190.

RUBATTO, D. Zircon trace element geochemistry: partitioning with garnet and the link between U–Pb ages and metamorphism. **Chem. Geol.**, mar. 2002. v. 184, n. 1–2, p. 123–138. Disponível em: <http://linkinghub.elsevier.com/retrieve/pii/S0009254101003552>.

SAALMANN, K.; GERDES, A.; LAHAYE, Y.; HARTMANN, L.A.; REMUS, M.V.D.; LÄUFER, A. Multiple accretion at the eastern margin of the Rio de la Plata Craton: the prolonged Brasiliano orogeny in southernmost Brazil. **Int. J. Earth Sci.**, 17 abr. 2011. v. 100, n. 2–3, p. 355–378. Disponível em: <http://link.springer.com/10.1007/s00531-010-0564-8>.

_____; HARTMANN, L. A.; REMUS, M. V. D. The assembly of west Gondwana—the view from the Rio de la Plata Craton. **Special Paper 423: the evolution of the Rheic Ocean: from Avalonian-Cadomian Active Margin To Alleghenian-Variscan Collision**. Geol. Soc. Am., 2007, p. 1–26.

SÁNCHEZ-BETTUCCI, L.; RAMOS, V. A. Aspectos geológicos de las rocas metavolcánicas y metasedimentarias del Grupo Lavalleja, sudeste de Uruguay. **Rev. Bras. Geo.**, 1999. v. 29, n. 4, p. 557–570. Disponível em: <http://sbg.sitepessoal.com/bjg/1999/n.4/14.pdf>.

SANTOS, J. O. S.; HARTMANN, L.A.; GAUDETTE, H.E.; GROVES, D.I.; MCNAUGHTON, N.J.; FLETCHER, I.R. A new understanding of the provinces of the Amazon Craton based on integration of field mapping and U-Pb and Sm-Nd geochronology. **Gondwana Res.**, out. 2000. v. 3, n. 4, p. 453–488. Disponível em: <http://linkinghub.elsevier.com/retrieve/pii/S1342937X05707553>.

_____ HARTMANN, L.A.; BOSSI, J.; CAMPAL, N.; SCHIPILOV, A.; PIÑEYRO, D.; MCNAUGHTON, N.J.. Duration of the Trans-Amazonian Cycle and its correlation within South America based on U-Pb SHRIMP geochronology of the La Plata Craton,

Uruguay. **Int. Geol. Rev.**, jan. 2003. v. 45, n. 1, p. 27–48. Disponível em: <http://www.tandfonline.com/doi/abs/10.2747/0020-6814.45.1.27>.

SATO, K.; BASEI, M.A.S.; SIGA JR., O.; SPROESSER, W.M.; ONOE, A.T. (2009). Excimer laser (193 nm) acoplado ao ICP-MS Neptune : primeiros resultados de análises isotópicas “in situ” de U, Pb, Lu e Hf em zircão, monazita e xenotima no CPGEO-IGC-USP. *In*: 45 Anos de Geocronologia no Brasil, São Paulo, 2009. p. 131–133.

_____ BASEI, M.A.S.; FERREIRA, C.M.; VLACH, S.R.F.; IVANUCH, W.; SIGA JR., O.; ONOI, A.T. (2010). In situ U–Th–Pb isotopic analyses by excimer laser ablation/ICP-MS on Brazilian xenotime megacrystal: first results of U-Pb isotopes at CPGEO-IG-USP. *In*: South American Symposium on Isotope Geology, VII, Brasília: CD Room, 2010.

_____; KAWASHITA, K. Espectrometria de massas em geologia isotópica. **Geol. USP. Sér. Cient.**, 1 dez. 2002. v. 2, n. 1, p. 57–77. Disponível em: <http://www.revistas.usp.br/guspsc/article/view/27372>.

SCHMID, R.; FETTES, D.; HARTE, B.; DAVIS, E.; DESMONS, J.. How to name a metamorphic rock. *In*: FETTES, D.; DESMONS, J. (Org.). **Metamorphic rocks: a classification and glossary of terms**. Cambridge, UK: Cambridge University Press, 2007, p. 3–15.

SCHOENE, B. U–Th–Pb geochronology. **Treatise on geochemistry**. Elsevier, 2014, p. 341–378.

SIBSON, R. H. Fault rocks and fault mechanisms. **J. Geol. Soc.**, 1 mar. 1977. v. 133, n. 3, p. 191–213. Disponível em: <http://jgs.lyellcollection.org/cgi/doi/10.1144/gsjgs.133.3.0191>.

SIIVOLA, J.; SCHMID, R. List of minerals abbreviations. *In*: FETTES, D.; DESMONS, J. (Org.). **Metamorphic rocks: a classification and glossary of terms**. Cambridge, UK: Cambridge University Press, 2007, p. 93–110.

SILVA, L. C.; OLIVEIRA, J.M.P; AUMOND, J.J.; LOPES, R.M.M.; EIPPER, J.; FERRO, G. (1985). Caracterização petrográfica da sequência (meta) vulcano-sedimentar Rio do Oliveira (Cinturão do Itajaí Mirim, SC). *In*: Simpósio Sul-Brasileiro de Geologia, II, 1985, Florianopolis, **Anais...** Florianópolis: SBG, p. 11–23.

_____ HARTMANN, L.A.; MCNAUGHTON, N.J.; FLETCHER, I.R.. SHRIMP U/Pb zircon dating of Neoproterozoic granitic magmatism and collision in the Pelotas Batholith, Southernmost Brazil. **Int. Geol. Rev.**, jun. 1999. v. 41, n. 6, p. 531–551. Disponível em: <http://www.tandfonline.com/doi/abs/10.1080/00206819909465156>.

_____ MCNAUGHTON, N.J.; ARMSTRONG, R.; HARTMANN, L.A.; FLETCHER, I.R. The Neoproterozoic Mantiqueira Province and its African connections: a zircon-based U–Pb geochronologic subdivision for the Brasiliano/Pan-African systems of orogens. **Precambrian Res.**, fev. 2005. v. 136, n. 3–4, p. 203–240. Disponível em: <http://linkinghub.elsevier.com/retrieve/pii/S0301926804002608>.

_____; DIAS, A. A. **Projeto Timbó-Barra Velha, Brasil**. Porto Alegre, 1981.

SOLIANI JR., E. **Os dados geocronológicos do Escudo Sul-Rio-Grandense e suas implicações de ordem geotectônica**. São Paulo: Universidade de São Paulo, 1986. Disponível em: <http://www.teses.usp.br/teses/disponiveis/44/44131/tde-15072015-153916/>.

STACEY, J. S.; KRAMERS, J. D. Approximation of terrestrial lead isotope evolution by a two-stage model. **Earth Planet. Sci. Lett.**, jun. 1975. v. 26, n. 2, p. 207–221. Disponível em: <http://linkinghub.elsevier.com/retrieve/pii/0012821X75900886>.

TEIXEIRA, W.; RENNE, P.R.; BOSSI, J.; CAMPAL, N.; D'AGRELLA-FILHO, M.S. 40Ar–39Ar and Rb–Sr geochronology of the Uruguayan dike swarm, Rio de la Plata Craton and implications for proterozoic intraplate activity in western Gondwana. **Precambrian Res.**, jan. 1999. v. 93, n. 2–3, p. 153–180. Disponível em: <http://linkinghub.elsevier.com/retrieve/pii/S0301926898000874>.

_____ GERALDES, M.C.; MATOS, R.; RUIZ, A.S.; SAES, G.; VARGAS-MATTOS, G. A review of the tectonic evolution of the Sunsás Belt, SW Amazonian craton. **J. South Am. Earth Sci.**, jan. 2010. v. 29, n. 1, p. 47–60. Disponível em: <http://linkinghub.elsevier.com/retrieve/pii/S0895981109001497>.

_____ D'AGRELLA-FILHO, M.S.; HAMILTON, M.A.; ERNST, R.E.; GIRARDI, V.A.V.; MAZZUCCHELLI, M.; BETTENCOURT, J.S. U–Pb (ID-TIMS) baddeleyite ages and paleomagnetism of 1.79 and 1.59 Ga tholeiitic dyke swarms, and position of the Rio de la Plata Craton within the Columbia Supercontinent. **Lithos**, ago. 2013. v. 174, p. 157–174. Disponível em: <http://linkinghub.elsevier.com/retrieve/pii/S0024493712003702>.

THE UNIVERSITY OF MAINE. Department of chemistry. [S.l.], 2017. Disponível em: <http://chemistry.umeche.maine.edu/CHY251/Ch13-Overhead4.html>. Acesso em: 25 nov. 2016.

TOHVER, E.; D'AGRELLA-FILHO, M. S.; TRINDADE, R. I. F. Paleomagnetic record of Africa and South America for the 1200–500 Ma interval, and evaluation of Rodinia and Gondwana assemblies. **Precambrian Res.**, jul. 2006. v. 147, n. 3–4, p. 193–222. Disponível em: <http://linkinghub.elsevier.com/retrieve/pii/S0301926806000398>.

TROMPETTE, R. **Geology of western Gondwana (2000 - 500ma). Pan-African-Braziliano aggregation of South America and Africa**. Rotterdam, Netherlands: A.A. Balkema, 1994.

VAUGHAN, A. P. M.; PANKHURST, R. J. Tectonic overview of the west Gondwana margin. **Gondwana Res.**, mar. 2008. v. 13, n. 2, p. 150–162. Disponível em: <http://linkinghub.elsevier.com/retrieve/pii/S1342937X0700161X>.

VERMEESCH, P. On the visualisation of detrital age distributions. **Chem. Geol.**, jun. 2012. v. 312–313, p. 190–194. Disponível em: <http://linkinghub.elsevier.com/retrieve/pii/S0009254112001878>.

WEIL, A. B.; VAN DER VOO, R.; MAC NIOCAILL, C.; MEERT, J.G. The Proterozoic Supercontinent Rodinia: Paleomagnetically derived reconstructions for 1100 to 800 Ma. **Earth Planet. Sci. Lett**, jan. 1998. v. 154, n. 1–4, p. 13–24. Disponível em: <http://linkinghub.elsevier.com/retrieve/pii/S0012821X97001271>.

WETHERILL, G. W. Discordant Uranium-Lead Ages, I. **Transactions, AGU**, 1956. v. 37, n. 3, p. 320. Disponível em: <http://www.agu.org/pubs/crossref/1956/TR037i003p00320.shtml>.

WHITE, W. M. EAS 6560 Lecture Notes - Isotopic Geochemistry. **Cornel University**, [S.l.], 2015. Disponível em: <http://www.geo.cornell.edu/geology/classes/Geo656/656home.html>.

WILDNER, W.; CAMOZZATO, E.; ORLANDI FILHO, V.; BASEI, M.A.S. (1996). Rochas vulcanogênicas do Cinturão Metamórfico Porongos na Antiforme Do Godinho, região do Passo da Cuia-RS. *In*: Congresso Brasileiro de Geologia, 39, 1996, Salvador, **Anais...** , Salvador: SBG, p. 146–148.

WILLIAMS, I. S.; CLAESSON, S. Isotopic evidence for the Precambrian Provenance and Caledonian metamorphism of high grade paragneisses from the Seve Nappes, Scandinavian Caledonides. **Contrib. Mineral. Petrol.**, out. 1987. v. 97, n. 2, p. 205–217. Disponível em: <http://link.springer.com/10.1007/BF00371240>.

WIT, M. J. DE *et al.* Formation of an Archaean Continent. **Nature**, 18 jun. 1992. v. 357, n. 6379, p. 553–562. Disponível em: <http://www.nature.com/doifinder/10.1038/357553a0>.

WIT, M. J. DE; STANKIEWICZ, J.; REEVES, C. Restoring Pan-African-Brasiliano connections: more Gondwana control, less Trans-Atlantic corruption. **J. Geol. Soc., London, Special Publications**, 2008. v. 294, n. 1, p. 399–412. Disponível em: <http://sp.lyellcollection.org/lookup/doi/10.1144/SP294.20>.

ZVIRTES, G. (2014). **Análise estrutural do Metagranito Capané no Complexo Porongos, Cachoeira Do Sul, RS**. Porto Alegre, Dissertação de Mestrado, Programa de Pós-Graduação em Geociências, Universidade Federal do Rio Grande do Sul.

_____ PHILIPP, R.P.; CHEMALE, F.; CAMOZZATO, E. (2015). Evidências de rifteamento e metamorfismo orogênico nos estágios finais de evolução do Cinturão Dom Feliciano na Antiforme Capané, Cachoeira do Sul, RS. *In*: Simpósio Sul Brasileiro de Geologia, 9, 2015, Florianópolis, **Anais...,** Florianópolis: SBG, p. 141.

ANEXOS

Trabalhos apresentados em eventos científicos

- *10th South American Symposium on Isotope Geology, 2016*

Paleoproterozoic basement in the Capané Antiform, Porongos Complex, Brazil: evidences from zircon U-Pb ages

Silveira, D.F.S.[1], Marques, J.C.[2], Basei, M.A.S.[3], Frantz, J.C.[4] and Giusti, R.O.[5]

1 Universidade Federal do Rio Grande do Sul, Porto Alegre, Brazil, silveiradfs@gmail.com
2 Universidade Federal do Rio Grande do Sul, Porto Alegre, Brazil, juliana.marques@ufrgs.br
3 Universidade de São Paulo, São Paulo, Brazil, baseimas@usp.br
4 Universidade Federal do Rio Grande do Sul, Porto Alegre, Brazil, jose.frantz@ufrgs.br
5 Universidade Federal do Rio Grande do Sul, Porto Alegre, Brazil, roneigiusti@gmail.com

On the large scale scenario, the Western Gondwana Supercontinent was product of Ediacaran-Ordovician amalgamation of several nucleis generated during the fission of Rodinia Supercontinent ca 1000 Ma (i.g. Fuck *et al*., 2008). In the Brazilian shield, the Dom Feliciano Belt is the meridional part of this complex orogenic branching system. This study addresses the evolution of the northern part of Porongos Complex which crops out in the central region of the Rio Grande do Sul shield. Although this geological sector, Capané Antiform, has been focus of intense research effort over the last decades, the tectonic models proposed remains speculative due to obliterated stratigraphic relationship caused by pervasive metamorphism and deformation process. Here, new (LA-IPC-MS and SHRIMP) U-Pb zircon ages from the Capané Antiform are presented together with data from previous works in an attempt to establish a temporal relationship between the sequences of the Porongos belt in this area. The Capané Antiform is grouped in three sectors defined as western and eastern limbs which surround a central area correlated with the axial area. The western limb is dominated by metavolcanic sequences intercalated with metapelites with minor staurolite-garnet schists lenses. The western limb and the hinge zone have also sheets of alkaline gneiss, quartzite and metaultramafic bodies, the later interpreted as a dismembered ophiolite (Marques *et al.,* 1998). The eastern limb is composed mainly by metapelites, intercalated with granitic bodies, lenses of quartz mylonites and marble. The axial area presents ultramylonites (some of them possibly igneous-derived), muscovite schists and quartz mylonites. Zircon ages from the metasedimentary sequences from the western limb revealed Paleoproterozoic, Mesoproterozoic and a significant Neoproterozoic provenance and suggested Edicarian for the maximum deposition age of the basin, in agreement to previous data from Pertille *et al*. (2015). However, our data from the mylonites from of the whole axial area show homogeneous peaks constrained in the Paleoproterozoic. The notorious difference among the geological features, such as distinct lithological sequences and the geochronological results, suggest that the central part of the Capané Antiform represents a different terrain. The axial area of the Capane Antifom can be considered either an exposed older basement rocks, such as the Santana da Boa Vista Dome in the central area of Porongos Complex, or a possible basement fragment imbricated during the tangential deformation phase. Further work is ongoing to better understand the origin of the mylonites.

- *35th International Geological Congress*, *2016*

Tectonic setting and provenance of the Capané Antiform, Porongos Complex, Dom Feliciano Belt, Brazil: Evidence from U-Pb ages

Silveira, D.F.S.[1], Marques, J.C.[2], Basei, M.A.S.[3], Frantz, J.C.[4] and Giusti, R.O.[5]

1 Universidade Federal do Rio Grande do Sul, Porto Alegre, Brazil, silveiradfs@gmail.com
2 Universidade Federal do Rio Grande do Sul, Porto Alegre, Brazil, juliana.marques@ufrgs.br
3 Universidade de São Paulo, São Paulo, Brazil, baseimas@usp.br
4 Universidade Federal do Rio Grande do Sul, Porto Alegre, Brazil, jose.frantz@ufrgs.br
5 Universidade Federal do Rio Grande do Sul, Porto Alegre, Brazil, roneigiusti@gmail.com

The Western Gondwana Supercontinent was product of collage stated in Early Neoproterozoic [1] of several nucleis generated during the diacronic fission of Rodinia Supercontinent ca. 1000 Ma [2]. In the meridional Brazilian shield, the Dom Feliciano Belt has a key role to shed light on the connection with the Pan-African mobile belt system during the collage. The purpose of this study is to provide new elements for unraveling the geological evolution of the Porongos Complex (PC), with focus in its northernmost region, which crops out in the central region of the Rio Grande do Sul shield. Regardless the extensive research effort over the last decades, this geological sector, the Capané Antiform (CA) has controversial tectonic models due to obliterated stratigraphic relationship caused by intense metamorphism and deformation process. Thus, new (LA-IPC-MS) U-Pb zircon ages from the CA are presented, as well as assembled with data from previous works, in an attempt to establish a jigsaw puzzle of paleogeography: merging the temporal relationship between the sequences of the Porongos belt in this area with the potential source areas in the surrounding geotectonic terranes. The CA is grouped in three sectors defined as western and eastern limbs and a central axial area. The western limb is dominated by metavolcanic sequences intercalated with metapelites with minor staurolite-garnet schists lenses. The western limb and the hinge zone have also sheets of alkaline gneiss, quartzite and metaultramafic bodies, the later interpreted as a dismembered ophiolite [3]. The eastern limb is composed mainly by metapelites, intercalated with granitic bodies, lenses of quartz mylonites and marble. The axial area presents ultramylonites, muscovite schists and quartz mylonites. Zircon ages from the meta-volcano-sedimentary sequences from both limbs revealed Paleoproterozoic, Mesoproterozoic and a significant Neoproterozoic provenance and suggested Edicarian for the maximum deposition age of the basin, in agreement to previous data from [4]. However, all mylonite samples from the central axial area provided main Paleoproterozoic peak, similar to patterns described in the Santana Fm [5]. The notorious difference among the geological features, such as distinct lithological sequences and the geochronological results, suggest that the central part of the CA represents a different terrain. The axial area of the CA can be considered a basement fragment imbricated during the tangential deformation phase of the PC. Further work is ongoing to better understand the origin of the mylonites, provenance patterns and their sources.

References:
[1] Neves et al. (1999) Episodes 22(3):155-166
[2] Fuck et al. (2008) Precambrian Research 160:108-126
[3] Marques et al. (2008) Revista Brasileira de Geociências 28:419-430
[4] Pertille et al. (2015) Journal of South American Earth Sciences 64(1):69-93
[5] Pertille et al. (2015) Journal of South American Earth Sciences 63:334-345

Relatório de desempenho acadêmico

A3. Relatório de desempenho acadêmico

Mestrando: Daianne Francis Silva da Silveira
Orientador: Juliana Charão Marques
Data de Ingresso: Março / 2015

Plano de mestrado (%)

Atividade	Semestre			
	01/2015	02/2015	01/2016	02/2016
Créditos	35%	45%	20%	-
Exame de proficiência	-	100%	-	-
Campo	50%	50%	-	-
Laboratório	75%	25%	-	-
Dissertação	-	-	50%	50%

Atividades acadêmicas (numeradas)

Atividade	Semestre			
	01/2015	02/2015	01/2016	02/2016
Participação em palestras no IG	-	-	-	-
Estágio Docência	-	1	-	-
Publicação de resumos	-	-	1	1
Publicação de artigo	-	-	-	-
Participação de exame de qualificação	-	1	-	-
Participação de defesa de tese	-	1	-	-
Treinamento Portal Periódicos CAPES	-	-	-	1
Organização de evento	-	1	-	-

- Estágio de docência em Geologia Econômica I
- Exame de qualificação do estudante Gabriel Bertolini
- Defesa de tese de Leonardo Gruber
- Organização do evento "*I Simpósio de Recursos Minerais e Energéticos*"

_____
Assinatura mestranda

_____
Assinatura orientador

Data: Março / 2017

Histórico acadêmico

Daianne Francis Silva da Silveira

266351

Lista das atividade de ensino do aluno avaliadas pelo curso.

HISTÓRICO CURSO
GEOCIÊNCIAS - Mestrado Acadêmico - 02/03/2015

Período Letivo	Código	Disciplina	Créditos	Conceito	Situação
2016/01		Estágio Docência: GEOLOGIA ECONÔMICA I	2	A	Aprovado
2016/01	GEB00101	Proveniência de Arenitos	3	C	Aprovado
2015/02	GEB00056	Cristaloquímica Aplicada	4	A	Aprovado
2015/02	GEB00057	Depósitos minerais em ambientes hidrotermais	5	A	Aprovado
2015/02	GEB00104	Petrologia e metalogenia de rochas máficas-ultramáficas	4	A	Aprovado
2015/01	GEP00048	Geoquímica das rochas graníticas	5	A	Aprovado
2015/01	GEB00102	Téc. anal. de espec. de massa e geoq. iso. aplic. a evol. manto-crosta	5	A	Aprovado
		Inglês em 22/12/2015	-	-	-

Totais

Créditos Cursados com Aprovação neste Curso:	28
Total:	28

ANEXOS – Parecer da Banca